# Heme-Utilizing Ribozymes and DNAzymes: Biological Impacts, Structural Aspects, and a Kinetic Model of Activation

**by**

**Nisreen Shumayrikh**

B.Sc., King Faisal University, 2002

Thesis Submitted in Partial Fulfillment of the
Requirements for the Degree of
Doctor of Philosophy

in the
Department of Chemistry
Faculty of Science



**SIMON FRASER UNIVERSITY**

**Fall 2017**

# Approval

**Name:** **Nisreen Shumayrikh**

**Degree:** **Doctor of Philosophy**

**Title:** ***Heme-Utilizing DNAzymes: Biological Impacts, Structural Aspects, and a Kinetic Model of Activation***

**Examining Committee:**

**Chair:** Bingyun Sun
Associate Professor

**Dipankar Sen**
Senior Supervisor
Professor

**Andrew Bennet**
Supervisor
Professor

**Erika Plettner**
Supervisor
Professor

**Tim Storr**
Internal Examiner
Associate Professor

**Ann M. English**
External Examiner
Professor
Department of Chemistry and Biochemistry
Concordia University

**Date Defended/Approved:** August 17, 2017/ Sep 28, 2017

# Abstract

Guanine-rich RNAs and DNAs that fold into guanine quadruplexes are found to complex tightly with porphyrins such as hemin [Fe(III)-heme]. The generated complex displays robust peroxidase (1 $e^-$ oxidation) as well as peroxygenase (2 $e^-$ oxidation) activity, greater than that of disaggregated heme itself. They can, thus, be regarded as heme-Utilizing DNAzymes and ribozymes. The folded DNAzymes appear to provide a unique chemical environment to the bound heme that by analogy resembles that of hemoproteins such as horseradish peroxidase (HRP) and cytochrome P450s. This work focuses on three aspects of these ribozymes and DNAzymes. First, we demonstrate that “toxic”, guanine-rich RNAs that accumulate in the cytoplasm of neurons afflicted with the familial forms of two neurodegenerative diseases: Amyotrophic Lateral Sclerosis (ALS) and Frontotemporal Dementia (FTD), and are indeed thought to be causative of those diseases, efficiently bind and activate heme. Second, we systematically investigate the special status (or not) of guanine quartets in DNA/RNA for the purpose of binding and activating heme. Specifically, we explore whether isoguanine-containing DNAs, which in the presence of certain cations (including $Na^+$, $Cs^+$ and $NH_4^+$) form isoG quintets, while in $K^+$, they form isoG quartets, can also bind and activate heme. We make the important observation that while G-quartets and iG-quintets both bind and activate heme, iG-quartets do not. Evidence from the theoretical/computational literature provides a satisfactory explanation for this observation, which in turn helps to illuminate the key structural features of nucleic acids that are necessary for binding and activating heme. Finally, we carry out fast kinetic measurements (using a stopped-flow enabled UV-vis spectrophotometer) to study the identities and formation of hydrogen peroxide-generated activated heme species within the above DNA-heme complexes. With the aid of Pro-KIV software, we perform singular value decomposition and global fitting analysis to formulate with a kinetic scheme for heme activation by these DNAzymes.

**Keywords**: Guanine G-quadruplex; DNAzyme; Ribozyme; Heme; Oxidation reactions.

## Dedication

*I dedicate this thesis to my lovely husband, Aymen Alfashkhi, my mother, father, family, and all my friends here in Vancouver.*

## Acknowledgements

I would like to express my deep gratitude to the following people for their support and help throughout my PhD research:

My wonderful husband, Aymen Alfashkhi, not only for his deep love, patience, and support, but also for being a great father taking care of my three kids while I am working for a long time in the lab. I could not have achieved this new goal in my life without him being by my side.

My supervisor, Dr. Dipankar Sen, for the great opportunity to work here in Canada, for his guidance throughout my doctoral research and advices to grow up as a scientist.

Dr. Andrew Bennet and Dr. Erika Plettner for their support and helpful inputs throughout my annual committee meetings and for allowing me to access the stopped-flow instrument in chemistry department.

Dr. Jeff Warren for his collaboration and valuable insight in solving some kinetic challenges that I had faced during my last year of the program.

I would like to also thank Dr. James McAfee and Dr. Irene Zegar from the Chemistry department at Pittsburg State University in USA for not only helping me in the admission process to SFU, but for the great time and useful discussions throughout the years I spent there. I admire them and would be thankful for their hospitality my entire life.

I would like to thank the Ministry of Education in Riyadh, Saudi Arabia and the Saudi Arabia Cultural Bureau in Ottawa, Canada for the financial support throughout my PhD research, and for their helpful instructions that facilitated our stay in Canada.

I would also like to thank Sen lab members, past and present, for sharing “hopes and fears”. Special thanks go to our research assistant, Janet Huang for being like a “mother” to us in the lab, taking care of every single issue, and for her continuous help throughout my PhD research. Also, special thanks go to Jason Grigg who had worked as a postdoc in our lab for one year and contributed to most of chapter 2 of this thesis. Also, I would like to thank friends and staff in the MBB and Chemistry departments for the helpful discussions and support.

Finally, I would like to thank all my family and relatives for their patience and encouragement from far away, and all my friends that I have met here in Vancouver for sharing with me good time and unforgettable memories. I will always be grateful for your friendship.

# Table of Contents

# List of Tables

# List of Figures

# List of Acronyms

| | |
|---|---|
| 5’-UTR | 5′- untranslated region |
| ABTS | 2,2'-azino-bis(3-ethylbenzthiazoline-6-sulphonic acid) |
| AD | Alzheimer disease |
| ALS | Amyotrophic lateral sclerosis |
| *C9orf72* | Chromosome 9 open reading frame 72 |
| CcP | Cytochrome c peroxides |
| c-*MYC* | MYC proto-oncogene, bHLH transcription factor |
| Cpd I | Compound I |
| Cpd II | Compound II |
| Cpd III | Compound III |
| Cpd0 | Compound 0 |
| CYP119 | Cytochrome P450 119 from *Sulfolobus acidocaldarius* |
| DBT | Dibenzothiophene |
| DBTO | Dibenzothiophene sulfoxide |
| DMF | *N*, *N*-Dimethylformamide |
| DNA | Deoxyribonucleic acid |
| EDTA | Ethylenediaminetetraacetic acid |
| FTD | Frontotemporal dementia |
| G4 | Guanine quadruplex |
| $H_2O_2$ | Hydrogen Peroxide |
| HEPES | 2-[4-(2-hydroxyethyl)piperazin-1-yl]ethanesulfonic acid |
| HRP | Horseradish peroxidase |
| KatG | Catalase peroxidase from *Mycobacterium tuberculosis* |
| LiP | Lignin Peroxidase |
| LPO | Lactoperoxidase |
| m-CPBA | meta-choloroperoxybenzoic acid |
| MnP | Manganease peroxidase |
| MPO | Myeloperoxidase |
| NADH | Nicotinamide adenine dinucleotide (NAD) + hydrogen (H) |
| NMM | N-Methyl Mesoporphyrin IX |
| NMR | Nuclear Magnetic Resonance |

| | |
|---|---|
| $P450_{BM3}$ | Ctochrome P450 from *Bacillus megaterium* |
| PQS | Putative Quadruplex sequences |
| PSA | Human prostate-specific antigen |
| RNA | Ribonucleic acid |
| ROS | Reactive oxygen species |
| SELEX | Systematic evolution of ligands by exponential enrichment |
| TE | Tris-EDTA buffer |
| TMPyP4 | Tetra-(N-methyl-4-pyridyl)porphyrin |
| UV | Ultraviolet light |

# Chapter 1.

# Introduction

## 1.1. Nucleic acids

The Nucleic acids, deoxyribonucleic (DNA) and ribonucleic (RNA) acid, have been known since the second half of the nineteenth century. However, it was only in the 1940s when their importance as the carrier of genetic information became clear to the scientific community. The discovery of the structure of DNA by James D. Watson and Francis Crick in 1953 gave rise to entirely new concepts and corrected the path of many established ones (1). The importance of nucleic acids became even more interesting after the discovery that they can have enzymatic functions in addition to their ability to store and transfer genetic information. The astonishing discovery of RNAs with catalytic activity *(ribozymes)* by Thomas Cech in 1982 and by Sidney Altman in 1983 was a milestone in not only our re-thinking of the biology of nucleic acids but also of primordial evolution (2, 3). This discovery of ribozymes gave rise to the "RNA World Hypothesis", which proposed that the existence of RNA might precede that of DNA and proteins and was responsible for both the genotype and phenotype of organisms in the early stage of evolution (2). Ribozymes also raised the biochemical question of the extent to which enzymes could be constructed from other biopolymers. In recent years, a technique of *in vitro* selection or SELEX (described in section 1.3.1) has enabled the investigation of not only the catalytic range of RNA, but also the remarkable catalytic possibilities of DNA (4-10). Nowadays, the study of DNA enzymes (also referred to as "catalytic DNAs", "deoxyribozymes", or "DNAzymes") has become one of central fields in nucleic acids' chemistry. This thesis reports work on the catalytic properties of DNAzymes with peroxidase and oxygenase activities discovered by Sen's lab in the late 1990s (11, 12). In this introductory unit, I would like to begin by familiarizing the reader with the basic structural aspects of DNA and RNA. Later, I will provide a detailed description of a higher-order folding structure of both

DNA and RNA, known as the G-quadruplex, which has importance for all the projects that I report in this thesis.

### 1.1.1. DNA and RNA structures

The basic repeating units in the biopolymers that are called nucleic acids (DNA and RNA) are nucleotides, which consist of three characteristic components: (1) a heterocyclic, nitrogenous base, (2) a pentose (ribose) sugar, and (3) a phosphate ester functionality. The nitrogenous bases are variants of two nitrogenous heterocycles, either a purine (adenine, guanine) or a pyrimidine (cytosine and thymine in DNA; cytosine and uracil in RNA). The base is attached to the C-1' of the sugar by a *β*-glycosidic bond. DNA contains 2-deoxy-D-ribose and RNA contains D-ribose. The structure of a nucleotide unit is shown in figure 1.1.

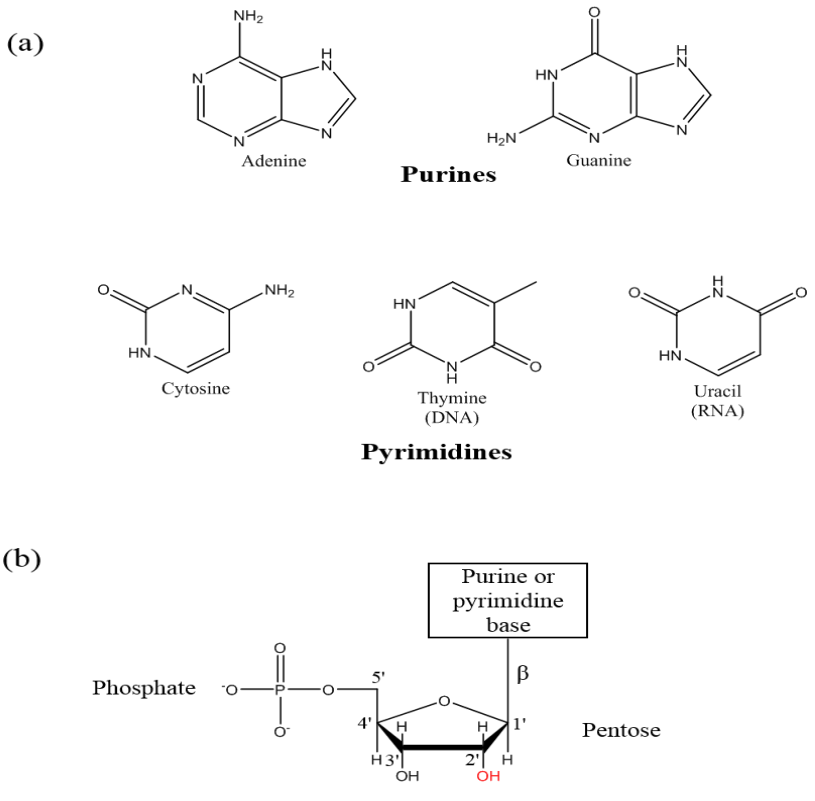


**Figure 1-1 Major purine and pyrimidine bases of nucleic acids (a). The general structure of a nucleotide unit showing the numbering convention for pentose ring (b). This is ribonucleotide. In deoxyribonucleotides the -OH group on the 2' carbon (in red) is replaced with -H.**

In nucleotides, both types of pentoses are in their β-furanose (closed five-membered ring) form. As figure 1.2 shows, the pentose ring is not planar but it occurs in what is generally described as “puckered” confirmations. The two main puckering modes are the $C_3$’-endo and $C_2$’-endo. In DNA, nucleotides can adopt both confirmations with slight differences in energy. However, in RNA, only the C3’-endo confirmation is maintained under all conditions. This can be explained as the $C_2$’-OH hydroxyl group causes steric hindrance and prohibits other puckering modes (13).

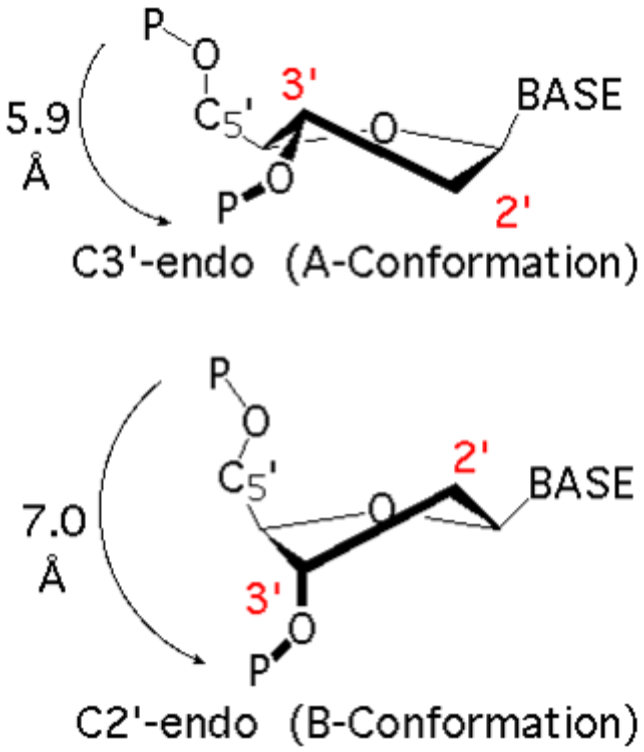


**Figure 1-2 The two main sugar pucker confirmations in nucleic acids. From (14).**

The C-3’ atom of each sugar is linked by a phosphodiester linkage to the C-5’ atom of the neighboring sugar building up the sugar phosphate backbone of DNA and RNA as shown in figure 1.3.

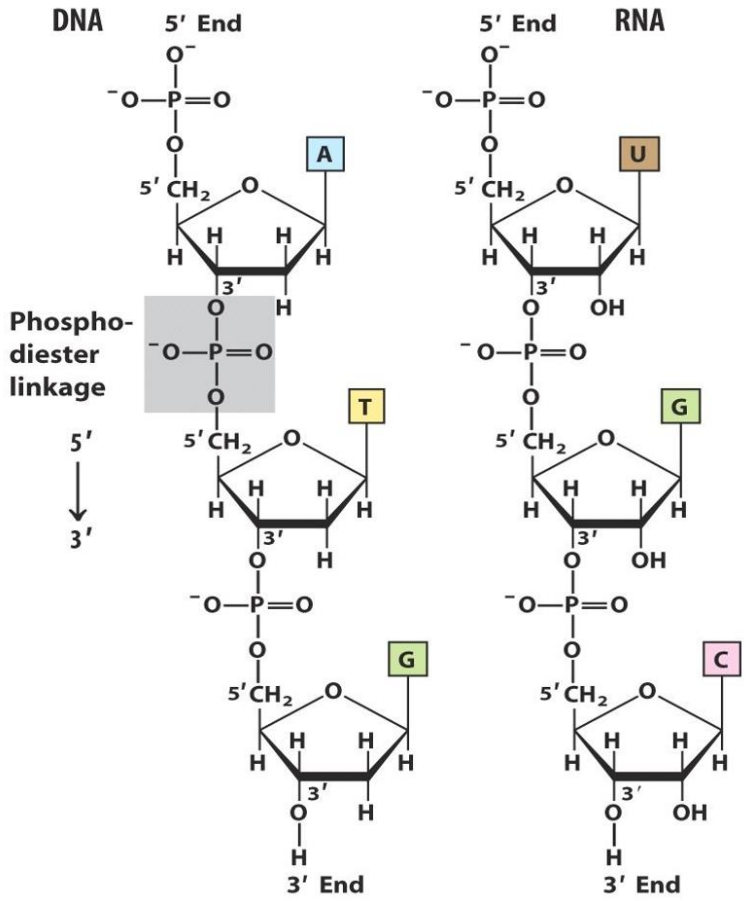


**Figure 1-3 The covalent sugar-phosphate backbone of DNA and RNA showing the phosphodiester bonds (one of which is shaded in gray) that link successive nucleotide units. Adapted from (15).**

Hydrogen bonds between bases allows a complementary association of two (and infrequently three or four) strands of nucleic acids. The most common hydrogen-bonding patterns are those defined by Watson and Crick, in which adenine bonds specifically to thymine (or uracil in RNA), and guanine bonds to cytosine, as shown below in figure 1.4. These two fundamental base pairs are dominant in double-stranded DNA and RNA.

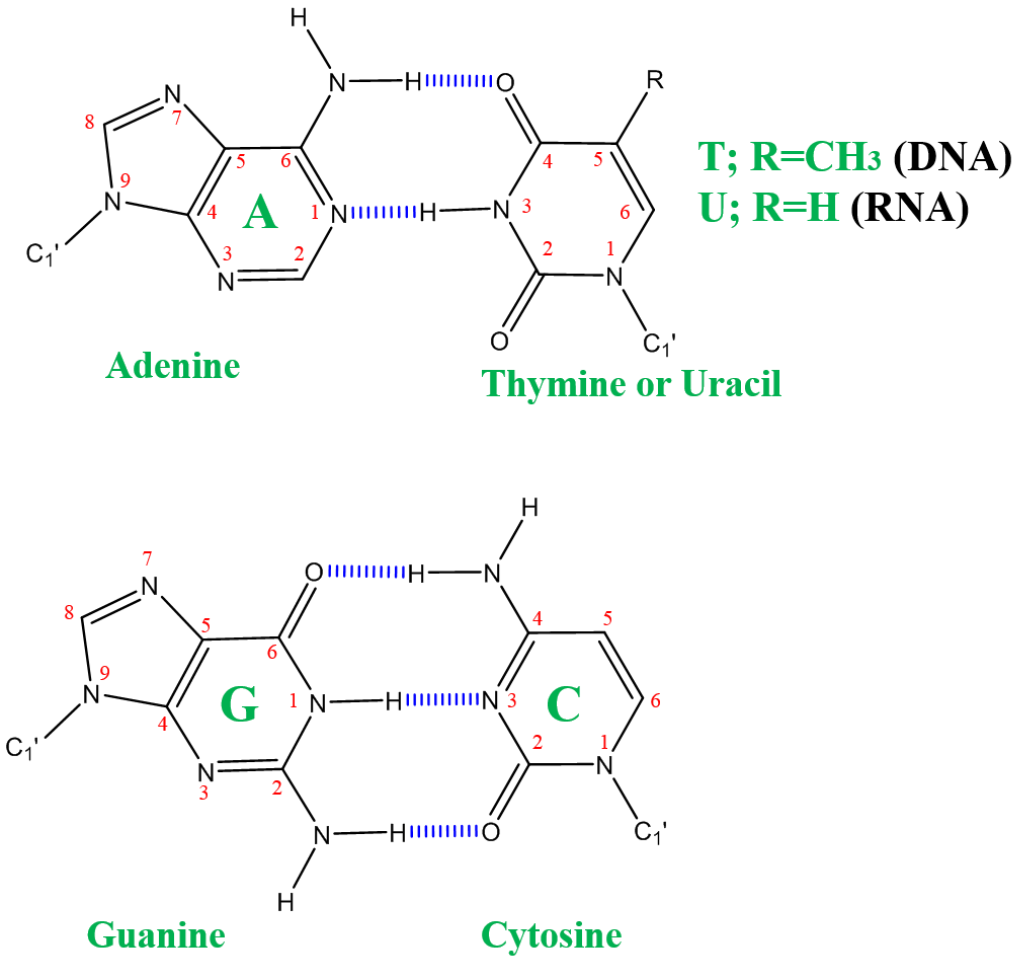


**Figure 1-4** **Hydrogen-bonding patterns in the base pairs defined by Watson and Crick. Blue dashed lines represent hydrogen bonds.**

The double helix, or “duplex”, is held together by two stabilizing forces: hydrogen bonding between the complementary base pairs described above and base-stacking interactions. The bases are naturally non-polar and have unfavorable interactions with polar solvents. In order to reduce the area exposed to the solvent, paired bases will associate and stack on each other. The stacking of the bases provides stability to the duplex through a combination of hydrophobic, electrostatic, and van der Waals forces. In canonical B-DNA form, stacking energies have been estimated to be between -9.5 and -13.2 kcal $mol^{-1}$ for GC base-pair steps, whereas an AT base-pair steps have a lower

stacking energy of about -5.4 kcal $mol^{-1}$(16). The stacked bases position themselves in such a “twisted” mode about the helical axis to avoid steric constrain.

In a duplex DNA, the strands are antiparallel means that the 5’, 3’-phosphodiester bonds run in opposite directions, and the individual nucleotides are in an *anti* glycosidic conformation. The *anti* and *syn* confirmations arise from the free rotation about the C1’-N-glycosidic bond. Purines can be both *syn* or *anti* with respect to the attached deoxyribose unit whereas pyrimidines are restricted to *anti* confirmation due to steric interference between the sugar and the carbonyl at the C2 of the pyrimidine (see figure 1.5).

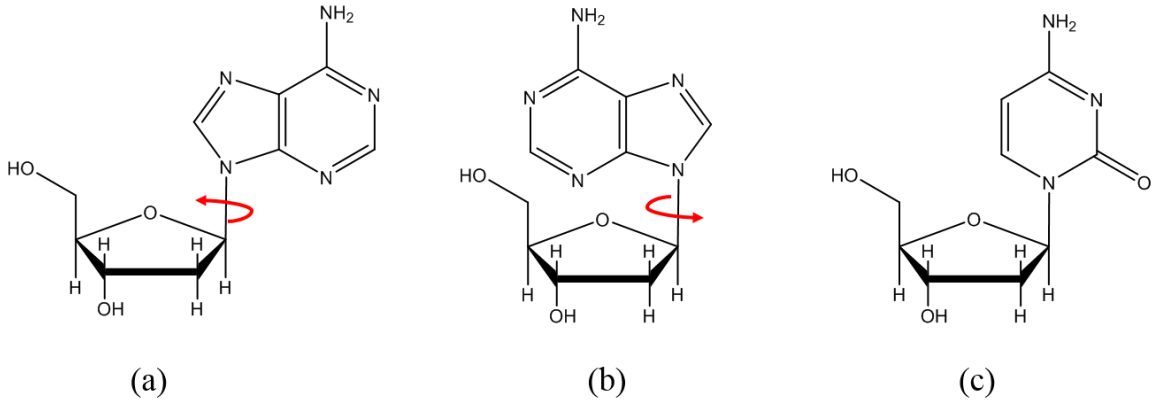


**Figure 1-5 Structural variation in DNA with regard the anti and syn confirmations. (a) anti-adenosine. (b) syn-adenosine. (c) anti-cytidine**

## 1.1.2. Fundamentals of guanine quadruplexes

Guanine quadruplexes (G-quadruplexes) have emerged as a major research topic in nucleic acids chemistry as well as biology since the discovery that guanine residues have the unique ability to self-assemble into planar molecular supramolecular arrangements known as a G-quartets. The G-quartet is a hydrogen-bonded entity formed by the cation-templated assembly of guanosines. It was first identified in 1962 as the basis for aggregation of 5’-guanosine monophosphate (17). In contrast to Watson-Crick bonding, which involves N1 and N3 of the heterocyclic rings, the G-quartet array has different type of hydrogen bonding involves the N7 position. This bonding system is known as Hoogsteen hydrogen-bonding. It allows the purines to be in the unusual *syn*

confirmation as oppose to *anti* in the Watson-Crick base pairing, and provides further stability to the G-quartet structures. In the presence of metal cations ($K^+$ or $Na^+$), DNA and RNA guanine-rich sequences can then further assemble by stacking interaction to form a variety of stable G-quadruplex structures that exhibit diverse molecularity, topologies, and strand-segment polarities depending on the exact nucleic acid sequences involved as we shall see in section (1.1.4). The base-paring pattern in the guanosine quartet, and an example of a G-quadruplex structure formed by the DNA telomeric sequence 5'-AGGG(TTAGGG)$_3$-3' is shown in figure 1.6.

While the chemical and physical properties of G-quadruplexes are fascinating on their own, studies from Blackburn (18), Cech (19), Klug (20), and Gilbert (17) laboratories in 1980s suggested that quadruplexes might in addition play important functional roles in biology. By applying the sequencing techniques, developed previously by Sanger's research laboratory in the late 1970s (21) , it was quickly realized that G-rich repetitive DNA sequences located at the end of the chromosomes, known as 'telomeres', could form higher-ordered structures and were surely implicated in chromosomal processing. Telomeres serve as the caps at the ends of chromosomes that keep the entirety of the chromosomes intact. The ground-breaking identification of telomeres and the enzyme responsible for its maintenance 'telomerase' (22) has ignited the interest in the structural arrangements of G-quadruplexes. The structure determined for the telomeric 3' overhang was of particular interest because it can help in understanding chromosomal DNA packaging and molecular self-assembly as these G-rich sequences are able to form compact, well defined and stable structural motifs. In 2002, Neidle *& et al.* (23) have determined the crystal structure of the G-quadruplexes formed by the human DNA telomeric sequence; 5'-AGGG(TTAGGG)$_3$-3' under $K^+$ salt condition (see figure 1.6). The importance of G-quadruplex nucleic acids in biology as a target for therapeutic agents or, in contrast, a source for cellular oxidative damage will be discussed in more detail in section (1.1.7).

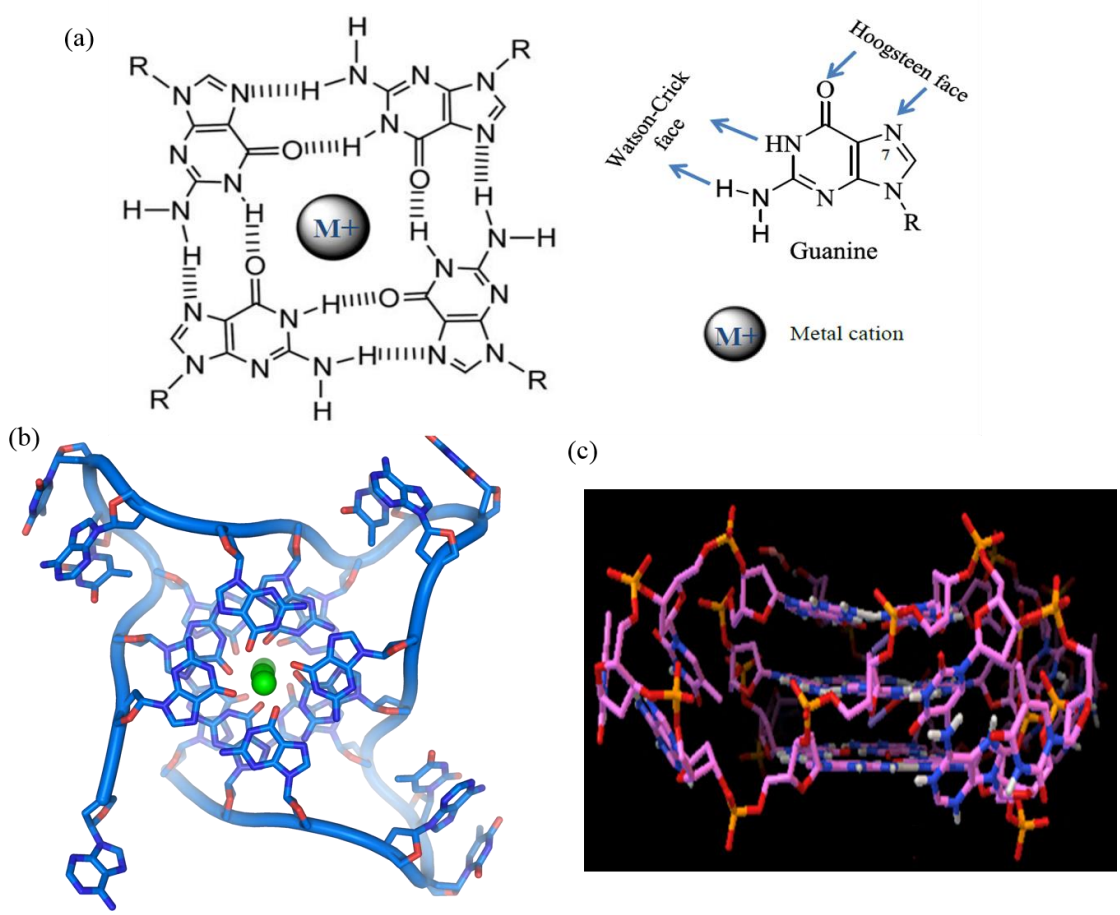


**Figure 1-6** **(a) The structure of a G-quartet showing the Hoogsteen bonding pattern. (b) Top and (c) side view of the G-quadruplex formed by 5'-AGGG(TTAGGG)3-3' telomeric sequence. The structure is derived from PBD ID 1KF1.**

### 1.1.3. G-quadruplex stabilization factors

The same stabilizing factors found in duplex structures including base stacking, hydrogen bonding, and electrostatic interactions are associated with quadruplex structures, but in G-tetrads, only guanine base stacking is considered in a G-quadruplex complex. The arrangement of the negative end of a dipole of guanine O6 carbonyl groups central to the G-quartet, though, contributes to quadruplex instability. The O6 atoms form a square planar arrangement for each tetrad with a twist of 30° and rise of 3.3 Å between each tetrad step forming a bipyramidal antiprismatic arrangement for the eight O6 atoms. Thus, these negative dipole cavities need to be stabilized by the coordination of metal cations. The choice of suitable cation, based on size and charge, significantly affect the

overall stability of the final folded quadruplex. Potassium metal ions, particularly, have the ideal characteristics of size and charge to effectively fit between G-tetrads as it is shown in figure 1.7.

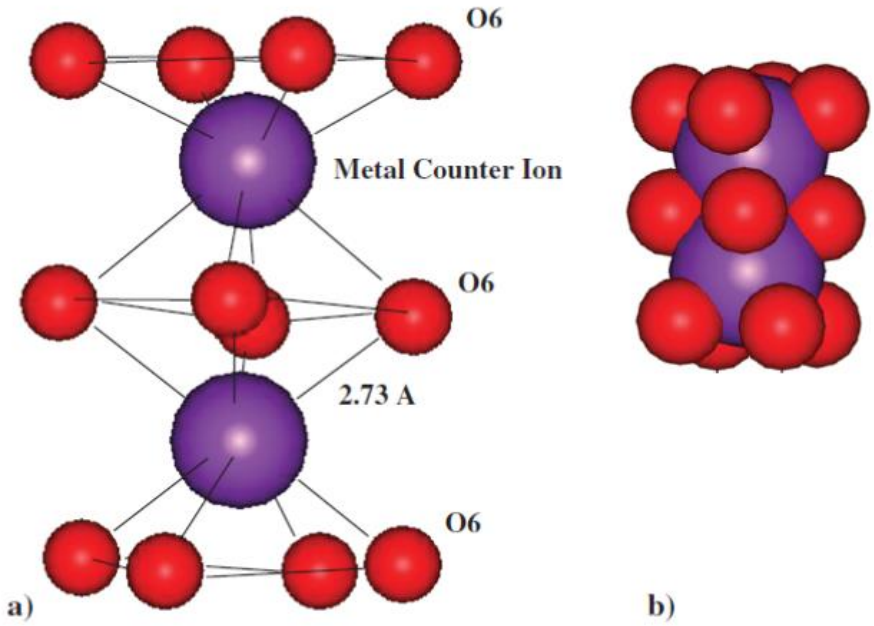


**Figure 1-7 Counter ion coordination between tetrad bases. (a) potassium metal ion (shown in purple) is coordinated between eight carbonyl oxygens with an average of 2.73 Å coordination distance. (b) A space filling model with potassium counter ions. Adapted from (24) .**

Sodium ions, with slightly smaller radii (1.16 Å compared to 1.33 Å for $K^+$), have been observed in the crystal structures to be positioned either slightly above or below the central position, closer to the tetrad planes (25). In fact, a range of cations, both monovalent and divalent, can stabilize quadruplex formation to varying degree. These ions with their various ionic radii are listed in table 1.1.

**Table 1-1 Ionic radii of quadruplex stabilizing cations.**

| Element | $K^+$ | $Na^+$ | $NH_4^+$ | $Rb^+$ | $Cs^+$ | $Li^+$ |
|---|---|---|---|---|---|---|
| Ionic radius | 1.33 | 1.16 | 1.43 | 1.66 | 1.81 | 0.9 |

Ions that coordinate effectively improve stability. A general trend in alkali ions from the most stable to least is as follows: $K^+ > Na^+ > Rb^+ > NH_4^+ > Cs^+ > Li^+$. Owing to their physiological importance, $K^+$ and $Na^+$ ions are the most extensively characterized cations with respect to their ability to stabilize G-quadruplex structures. The idea of the cation

governs the stability of one folded state over the other was first described by Sen and Gilbert as a $Na^+$ - $K^+$ switch (26). From divalent cations, Venczel and Sen have analyzed some cations and found the following order: $Sr^{2+} > Ba^{2+} > Ca^{2+} > Mg^{2+}$ (27). In general, low divalent cation concentrations initially stabilize G-quadruplexes, while increasing concentrations eventually become destabilizing.

### 1.1.4. Topology of G-quadruplexes

The formation of a quadruplex simply requires four guanine repeats to self-associate. The simplest scenario is to have DNA strands in solution containing short runs of guanine, for example: (5'-$X_n$ $G_m$ $X_n$-3'), where $X_n$ is any nucleotide of length n and $G_m$ is any number of guanines included in tetrad formation of length m. In this situation, four DNA strands self-associate to form a structure termed "intermolecular" or "tetramolecular" quadruplexes. An example of an intermolecular quadruplex is the structure that have been determined by crystallographic and NMR formed by $d(TGGGGT)_4$ (28, 29) in which the sugar phosphate backbone runs in the same direction, and all bases are in *anti* glyosidic orientation. In theory, there are four possible ways that strands containing single G-runs can self associate, However, only parallel arrangements have been observed experimentally so far. It should be noted that if the guanine is not capped by an alternative base at either 5' or 3' sides, as in d(GGGT) or d(TGGG) sequences for example, a more complicated structure can form termed "interlocked quadruplexes" (30). This structure is comprised of two stacked G-quadruplexes where the uncapped guanine tetrads from the two quadruplexes can further stack leaving the capped side oriented to the opposite direction.

More complex topologies and structures can arrange from strands containing two guanine repeats separated by non-guanine nucleotides, for example: (5'-$X_n$ $G_m$ $X_p$ $G_m$ $X_n$-3'), Where $X_p$ this time is any nucleotide of length p involved in loop formation. If two of these strands are associated, the resulted structure termed "dimeric G-quadruplexes". Both DNA and RNA sequences containing two G-runs and short nucleotides linkers can form dimeric quadruplexes, and have been reported by NMR (31-34) and crystallographic methods (35, 36). The topology of these quadruplexes depends on how the two strands connect to each other. The strands can adopt parallel or anti-parallel confirmations, and

the linking nucleotides “loop” can be diagonal, lateral (edgewise), or external (propeller) to the quadruplex.

Quadruplexes can also fold from one G-rich strand, termed “intramolecular” or “unimolecular” G-quadruplex, from the following general sequence: (5’- $X_n$ $G_m$ $X_p$ $G_m$ $X_p$ $G_m$ $X_p$ $G_m$ $X_n$-3’). The folding topologies available for the intramolecular quadruplexes are varied and more complex than those for intermolecular tetrameric or dimeric because of the extra linking nucleotides. They can be parallel, antiparallel, or hybrid mixed topology. The different quadruplex topologies are shown schematically in figure 1.8.

The linking nucleotides are crucial in determining quadruplex stability in terms of length and sequence. For example, a short loop, two nucleotides or less, will prevent diagonal loop from forming due to the distance to be covered across G-tetrad. Therefore, short linker sequences can accommodate both lateral and external loops. The nucleotides located in the loop region could be either thymines or adenines or both. The selection of thymines over adenines for connected loops affect quadruplex stability. The replacement of the TTA loop sequence in the human telomeric sequence with a run of AAA’s results in the complete destabilization of the quadruplex structure (37).

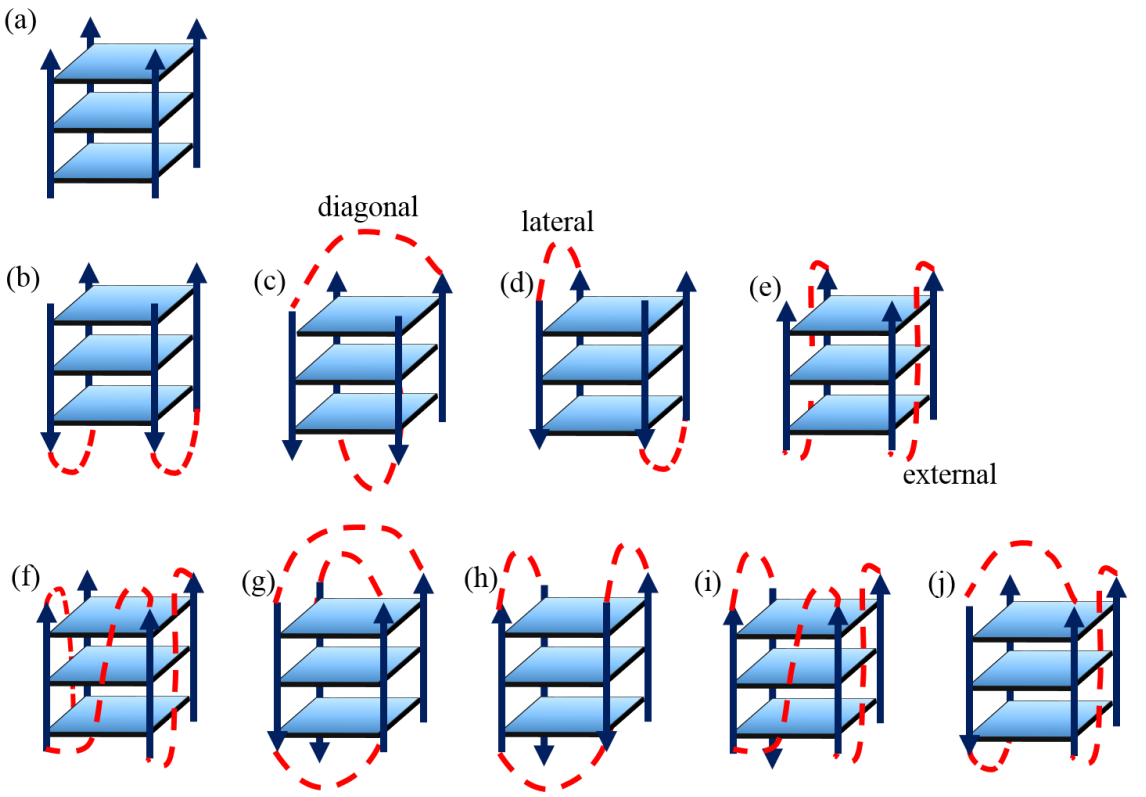


**Figure 1-8** **Schematic diagrams of various G-quadruplex topologies. Arrows indicate 5'-3' polarity. (a) intermolecular four-stranded "tetramolecular" parallel quadruplex. (b), (c), (d) and (e) intermolecular two-stranded "bimolecular" quadruplexes where in (b), (c) and (d) the strands adopt antiparallel confirmations with either diagonal or lateral loops, and (e) shows parallel confirmation with external loop. (f) intramolecular "unimolecular" parallel quadruplex. (g) and (h) unimolecular antiparallel quadruplex. (i) and (j) unimolecular mixed "hybrid" quadruplexes three strands run in parallel to each other and only one strand is antiparallel to the rest of them.**

The presence of multiple topologies within the same sequence has been observed for many quadruplex-forming sequences. For example, the human telomeric sequence d(AGGG(TTAGGG)$_3$) was shown to fold into two quite diverse folded structures: an intramolecular parallel in addition to an intermolecular bimolecular quadruplex that can adopt parallel and alternative antiparallel confirmations (38). The *Tetrahymena* telomeric sequence also folds into two different topologies depending on the numbers of G-repeats. The d(TG$_4$T$_2$G$_4$T) sequence can folds into bimolecular quadruplex with two edgewise loops, while the d(T$_2$G$_4$)$_4$ sequence forms intramolecular quadruplex (39). Interestingly,

the switching between various conformations for the same sequence can be induced by the presence of different cations and temperature. This has been shown for the human telomeric sequence as the presence of either $Na^+$ or $K^+$ has promoted and stabilized different structural forms (33, 40). Another example is from the *C-myc* promoter sequence where in high $K^+$ salt conditions, it preferentially remains in a quadruplex folded state, even in the presence of their own complementary C-rich strands. However, this is not the case under $Na^+$ salt conditions where these two folded quadruplexes unfold into their duplex DNA when presented by their complementary strands (41, 42). There are also several examples of conformational switches influenced by temperature. It has been shown that the human telomeric sequence d($UAG_3T^{br}UAG_3T$) forms an antiparallel structure below 50°, and can be converted to the parallel confirmation by increasing the temperature (33).

In summary, the structural diversity and topology of G-quadruplexes depends on a variety of factors including: the arrangements and the positions of G-runs within the sequence itself, the type and length of nucleotides linker between the guanines, type of counter ion as well as its concentration, and the temperature. Thus, the predication of a folded structure is not straightforward, and is determined by several methods and techniques as we shall see in section (1.1.6).

### 1.1.5. Thermodynamics and kinetics of quadruplex folding

In this section, we will discuss the rules that govern the formation of quadruplexes and determine their folding and stability from the point of view of thermodynamics and kinetics.

The formation of quadruplexes, regardless their types, is enthalpy driven, with an enthalpy per quartet ranging from -15 to -25 kcal $mol^{-1}$. For intramolecular quadruplexes, for example, the measured $\Delta H°$ of d($G_2T_2G_2TGTG_2T_2G_2$) sequence (thrombin binding aptamer) has a value of -19.8 kcal $mol^{-1}$ (43). Generally, the enthalpy per quartet is, as expected, more negative than the enthalpy per base pair in double-helix (44). This favorable enthalpy (very negative) is also associated with a negative (unfavorable) entropy of formation ($\Delta S°$). The measured values for $\Delta S°$ is more dependent on the stoichiometry of the associated strands and the nature and the length of the loops. Despite the negative

contribution of entropy to stability, quadruplex structures are stable under physiological conditions. In fact, most intramolecular quadruplexes have a ($\Delta G°$) < 0 at 37 °C in a buffer that mimic the intracellular conditions (near natural pH, high $K^+$ concentrations, with or without $Mg^{2+}$).

The important question that has been addressed by several laboratories was: which type of quadruplexes are the most stable? Intra-, bi-, or tetramolecular? And which conformations? Parallel or antiparallel? Lu *et al.* (45) and Petraccone *et al.* (46) have concluded that parallel structures are thermodynamically more stable than the antiparallel ones, and that tetramolecular structures are thermodynamically more stable than bimolecular ones, which in turn, are more stable than unimolecular ones. Despite that, it should be noted the comparison of stability of quadruplex structures with different molecularities is not straightforward. For example, parameters like equilibrium constant are expressed differently in the case of unimolecular, bi-, or tetramolecular (unit-less, $M^{-1}$ and $M^{-3}$ respectively). $\Delta G°$ values also might be misleading for unimolecular versus bi-, or tetramolecular structures since the number of strands (therefore the concentration) is different. A similar problem arises from comparing the association rate constants ($k_{on}$) which are expressed in $s^{-1}$, $M^{-1}$ $s^{-1}$ and $M^{-3}$ $s^{-1}$ for unimolecular, bi-, or tetramolecular quadruplexes respectively. This limitation though does not rule out the possibility of comparing other parameters. For example, it is rational to compare dissociation rate constants ($k_{off}$) expressed in $s^{-1}$ for all quadruplexes. The various G-quadruplexes exhibit very different kinetic behaviors as shown in figure (1.9). The most stable structure thermodynamically does not necessarily mean that it is kinetically favored. Venczel and Sen (27) investigated the formation of higher order structures made by the d($TGTG_3TGTGTGTG_3$) sequence. They found that there is dramatic switch in the formation of tetramolecular G4 versus bimolecular G2 structures in solution, and the G'2 bimolecular structures accumulated in $K^+$ and $Sr^{2+}$ solutions at the expense of the thermodynamically more stable G4 parallel structures.

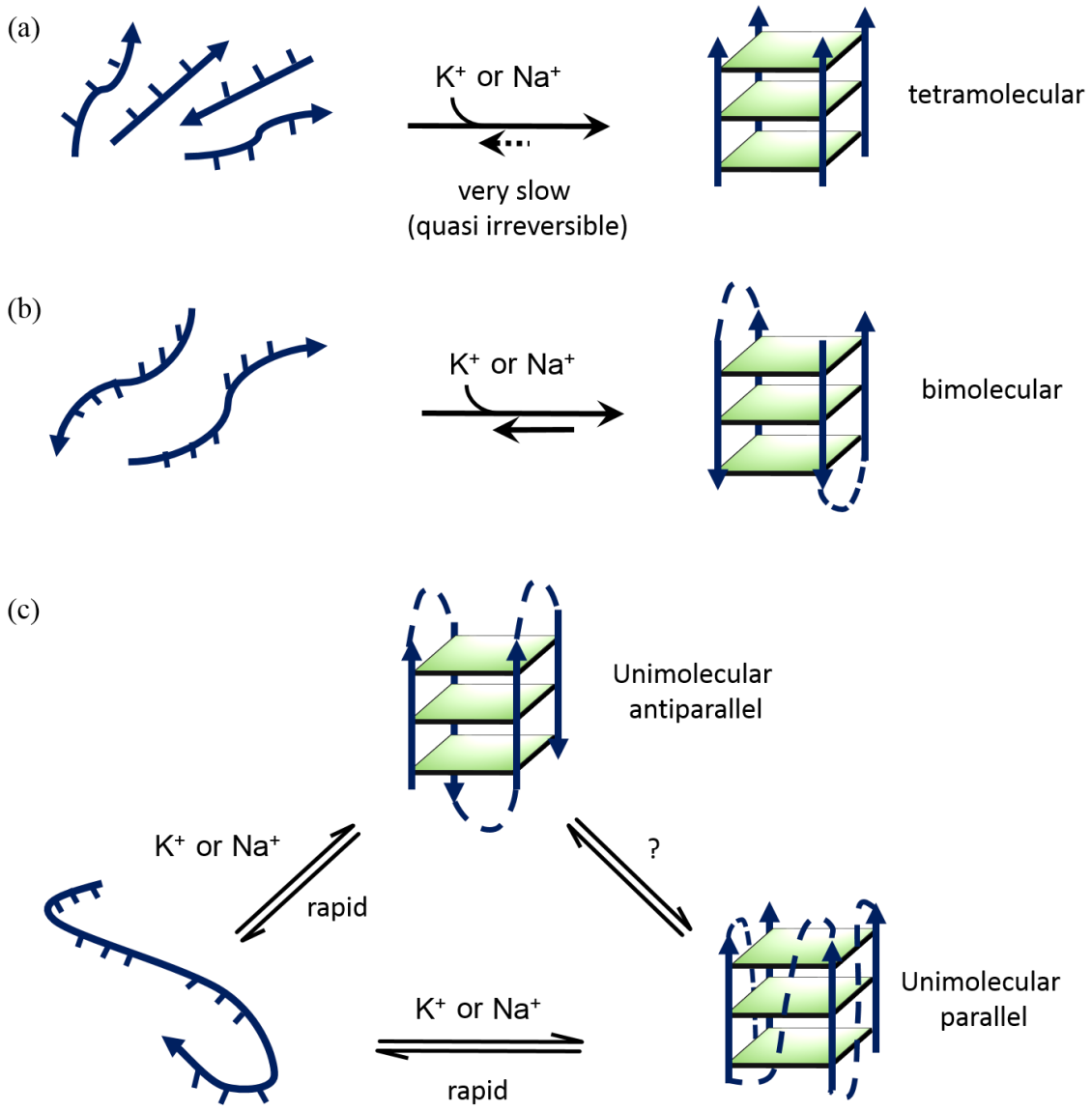


**Figure 1-9** **Summary of the different equilibria involving formation and dissociation of various G-quadruplexes. Panel (a) tetramolecular, panel (b) bimolecular, panel (c) unimolecular structures. Based on figure from (16).**

## 1.1.6. Experimental methods used in quadruplex characterization

There are number of techniques besides NMR and X-ray crystallography that have been used to study and characterize G-quadruplexes. In this section, we will explain two methods used throughout my study and that will be used in next chapters of this thesis: Circular dichroism spectroscopy (CD) and poly acrylamide gel electrophoresis.

### *1.1.6.1 Circular dichroism spectroscopy (CD)*

Circular dichroism spectroscopy (CD) was developed in the second half of the last century for determining the absolute configuration of chiral molecules (47). Nowadays, CD is a widespread technique for studying the conformational changes associated with biological macromolecules (DNA and proteins) as well as their structural disturbances by external factors. In this subsection, first, we will describe briefly the physical principles of this method, then, we explain the origin of CD signals in a G-quadruplex. Finally, we show some examples of the CD spectral features characteristic of different folding topologies of G-quadruplex structures.

CD spectrum results from a chiral molecule absorbing left and right circular polarized light differently. Circularly polarized light occurs when the direction of the electric field vector (E) rotates about its propagation direction (k). This is different from linearly polarized light which results when the direction of E is restricted to a plane perpendicular to the direction of propagation while its magnitude oscillates. A Schematic diagram displays the difference between linearly polarized light and circularly polarized light is shown in figure 1-10**,** and the basic physics behind CD is summarized in figure 1-11. The linear polarized light is passed through a Photo Elastic Modulator (PEM) that converts it into alternating left and right handed circular polarized light. The two polarization is differently absorbed, and the difference in absorption is detected with a Photo Multiplier Tube (PMT). A CD spectral feature is reported in units of absorbance or historically in unit of *Molar Ellipticity* ($\theta$) in $deg.cm^2.dmol^{-1}$.

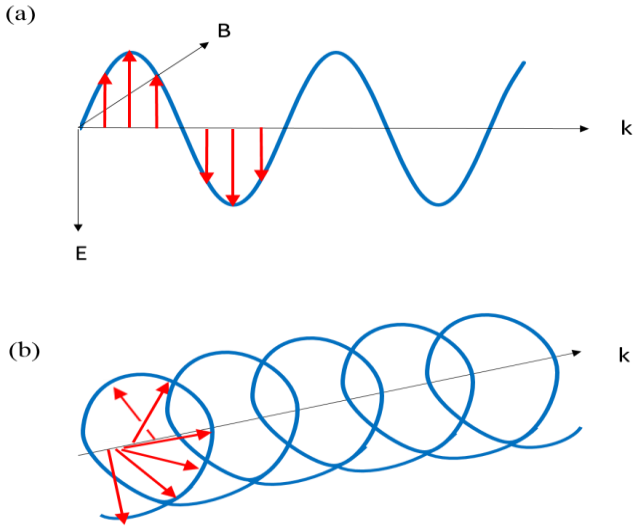


**Figure 1-10** **(a) Linearly polarized light. (b) Circularly polarized light. E is the direction of the electrical field. B is the direction of the magnetic field. k indicates the propagation direction of the transverse wave.**

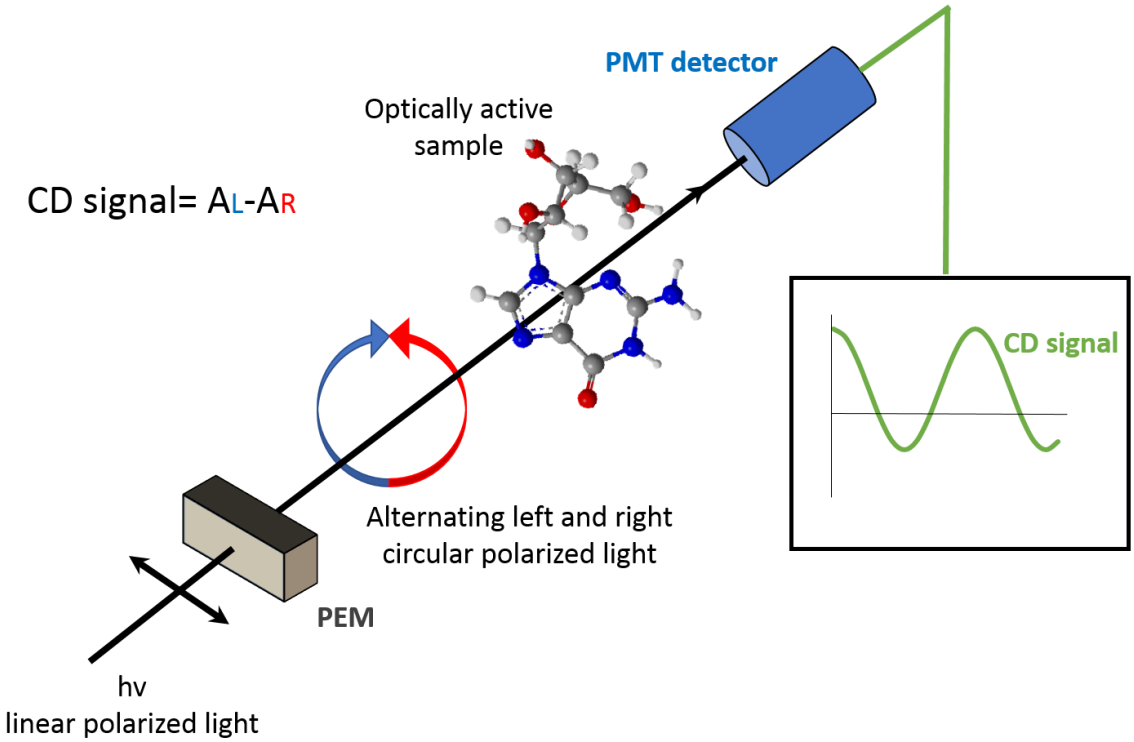


**Figure 1-11** **The principle behind circular dichroism (CD) spectroscopy.**

In general, for solutions, there is a direct correlation between the regions of absorption and CD signal. In the case of non-coupled chromophores, the shapes of CD and absorption spectra are similar, although the vibrational fine structure can be different. If two or more strongly absorbing chromophores are chirally oriented with respect to each other, one observes an exciton spectrum characterized by the presence of two bands with opposite signs, where $\lambda_{max}$ in absorption corresponds, or nearly corresponds, to zero CD intensity.

In the case of a G-quadruplex, the absorbance in the UV region with wavelength ($\lambda$) >210 nm is represented mainly by guanine nucleotides while the contribution from other nucleotides and the sugar-phosphate backbone is negligible. Guanine, in fact, is characterized by two well-isolated absorption bands due to $\pi \rightarrow \pi^*$ transitions at 279 and 248 nm (48, 49). The two transitions are roughly short and long axis polarized, respectively. In G-quadruplex structures, the stacked G-quartet units are rotated with respect to each other (see figure 1-12), and this rotation results in chiral exciton coupling between transition dipole moments in near neighbour guanines. The relative disposition of the two transition moments corresponding to the 248 nm transition of the guanine arise from two different types of G-quartet stacking (described later in text) is shown in figure 1-13 (b) as full and dotted double-head arrows. The *Rotational Strength* $R_{0a}$ of a specific electronic transition from ground state 0 to excited state *a* is proportional to the band area of the CD spectrum and can be expressed as a scalar product of the electric ($\mu_{0a}$) and magnetic ($m_{0a}$) transition dipoles of the transition (47):

$$R_{0a} = \mu_{0a} \times m_{0a}$$

Therefore, it is important that any electronic transition possess both electric and magnetic transition moments to be CD active. The magnetic moment arises from the exciton coupling of two non-coplanar electric moments (see figure (1-15). The two possible coupling modes for the two electric moments are non-degenerate and produce magnetic moments that can be either parallel or antiparallel with respect to the total electric moment. Thus, the combination of electric and magnetic moments generates either positive or negative rotational strength. The component at higher wavelength is the one that has

lower energy coupling mode. A simplified model for the origin of the positive and negative exciton couplets for different G-quartet stacking is illustrated in figure 1-15.

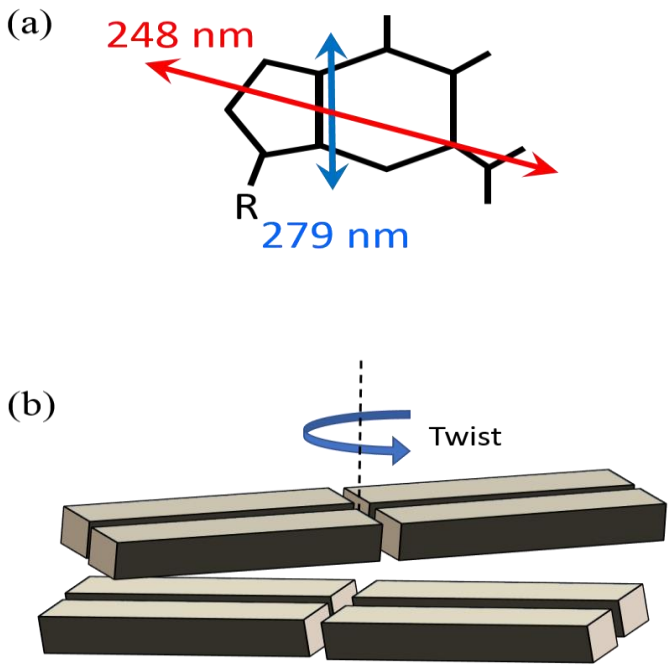


**Figure 1-12 (a) Orientation of the two significant electric transitions represented by red and blue double-head arrows of guanine (the double bonds were omitted for clarity). (b) A sketch of the chiral arrangement of two adjacent G-quartets. Each parallelepiped represents a guanine base. Based on (50).**

As we have discussed in section (1.1.4), a G-quadruplex stem may adopt either parallel, antiparallel, or mixed confirmations that vary with respect to the glycosidic bond angle *(anti* or *syn*). To have a better understanding of CD spectra of G-quadruplexes, first, we should further clarify the geometric arrangements arise from stacking of two adjacent G-tetrads. The stacking of two adjacent G-tetrads can be described by the relative polarity of Hoogsteen hydrogen bond pattern. The hydrogen bond polarity, within a single G-tetrad, is defined in the direction of hydrogen bond donor to acceptor from N2-H to N7 and from N1-H to O6. The G-quartet shows its “head” (H) side if donor to acceptor H-bonding runs clockwise, whereas the reverse side is referred as “tail” (T) (donor to acceptor H-bonding runs counter-clockwise). The two faces of G-quartet are shown in figure 1-13 (a). Accordingly, there are two classes of stacking of two neighboring G-tetrads: (i) same polarity if the stacked tetrads are oriented to be in the same direction, or (ii) opposite

polarity if the stacked tetrads are oriented to be in the opposite direction. These two classes can be further divided and referred to as *head-to-tai (anti-anti)* or *tail-to head* (*syn-syn*) belonging to same polarity "*homopolar*" and *head-to-head* (*syn-anti*) or *tail-to-tail* (*anti-syn*) belonging to opposite polarity "*heteropolar*" stacking. The homopolar and heteropolar stacking as well as the transition moments corresponding to the absorption band at 248 nm are illustrated in Figure 1-13 (b).

Figure 1-14 shows the CD spectra and the stacking arrangements of selected G-quadruplexes: $d(TGGGGT)_4$, $d(T_2G_3(T_2AG_3)_3A$, and $d(G_4T_4G_4)_2$ as typical examples of tetramolecular parallel, mixed or "hybrid" unimolecular, and bimolecular antiparallel confirmations formed by these quadruplexes.

The experimental CD spectrum of the parallel $d(TGGGGT)_4$ shown in figure 1-15 (a) is characterized by positive peak at 260 nm and negative peak at 240 nm. For the hybrid $d(T_2G_3(T_2AG_3)_3A)$, the CD spectrum is similar to the parallel case except for an additional positive peak at 290 nm (see (b) in figure 1-14). In 1998, Speda *et al* (51) compared CD spectra of different G-quadruplex structures, and proposed for the first time that the band at 290 nm is probably due to the inversion of polarity of the quartets in the hairpin structures. Inversion of polarity (from head-to-tail to head-to-head or tail-to-tail) could lead to a different arrangement of the near-neighbour transition dipole moments and consequently an oppositely-signed exciton couplet corresponding to the 250 nm transition. A few years later, Wen and Gary gave the same explanation (52). They explicitly proposed that the positive CD band near 260 nm results from the stacking of quartets of the same polarity whereas a band at longer wavelength (near 290 nm) arises from quartets stacked with alternating polarities. If the glycosidic bonds of the guanines switch between *anti* and *syn* confirmations along each strand, the G-quartet polarity also switches, while quadruplexes with all *anti* glycosidic bonds have non-alternating G-quartet polarity.

In the last example shown in Figure 1-14 (c), the bimolecular antiparallel $d(G_4T_4G_4)_2$ quadruplex is characterized by a CD spectrum that has a positive band in the region between 290 to 300 nm and a negative peak at 240 nm. This spectral difference is attributed, as mentioned above, to the consecutively stacked guanosines of distinct glycosidic bond angles (*syn-anti* and *anti-syn* steps).

The rule relating the “parallel strands” of G4-DNA to a positive CD at 260 nm and a negative one at 240 nm and “antiparallel strands” to positive CD at 290 nm and negative at 260 nm is very popular and generally adopted by research groups regardless the number of stacked G-quartets. However, the rational explanation for it had never been clarified. Furthermore, CD spectra of other high-ordered structures made out of modified DNA sequences (as we shall see in Chapter 3) is totally different than all of the above examples, so the prediction and the interpretation of such CD spectra become more challenging.

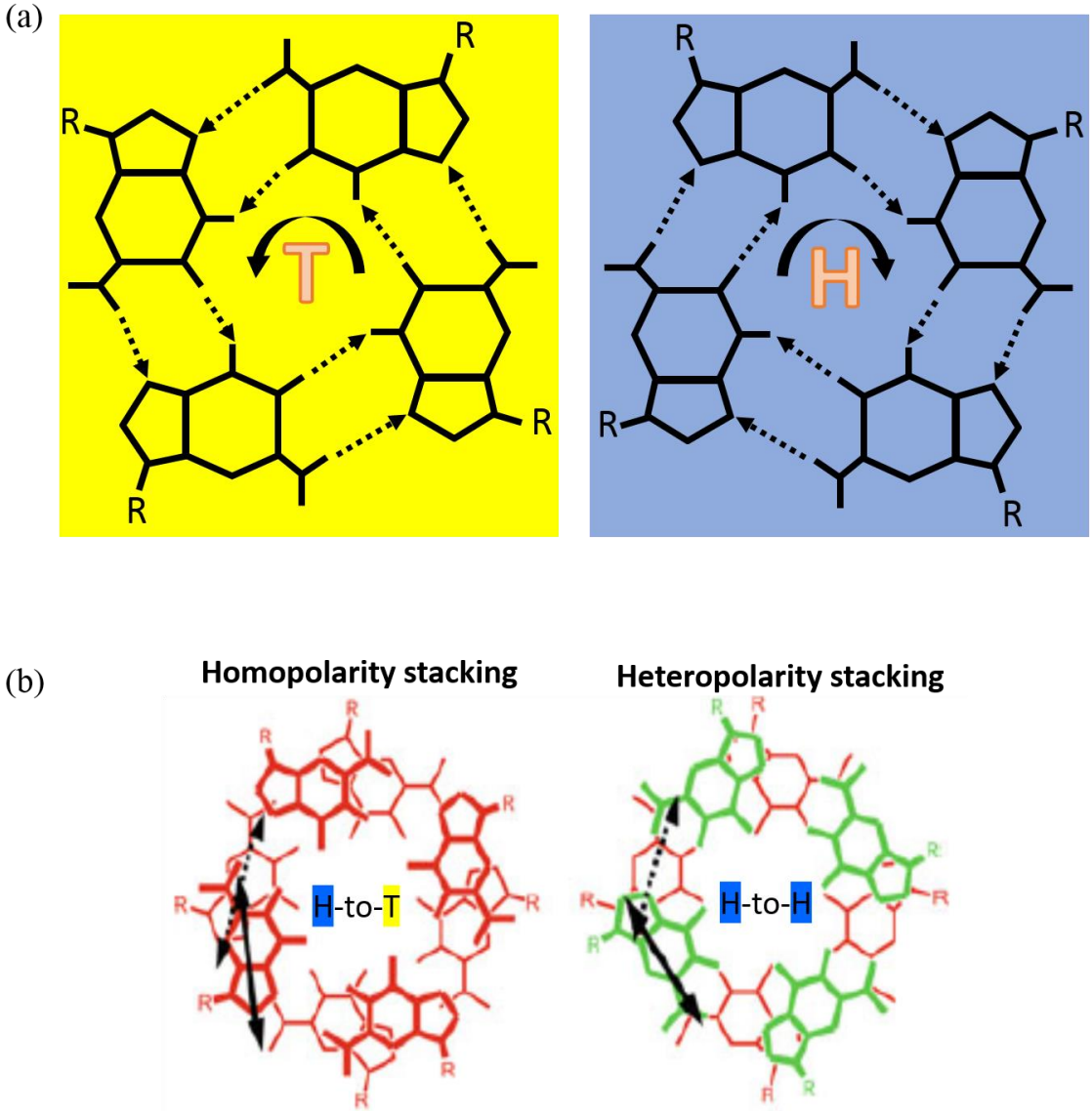


**Figure 1-13** **(a) The G-quartet head and tail faces. In head face (blue-shaded) indicated by symbol H, the donor to acceptor H-bonding runs clockwise. The reverse side is referred as tail (yellow-shaded) and indicated by symbol T where the donor to acceptor H-bonding runs counter-clockwise. (b) Top view of heteropolar and homopolar stacking of two G-quartets. The double-head arrows represent the transition moments corresponding to the absorption band at 248 nm. (b) is modified from (50).**

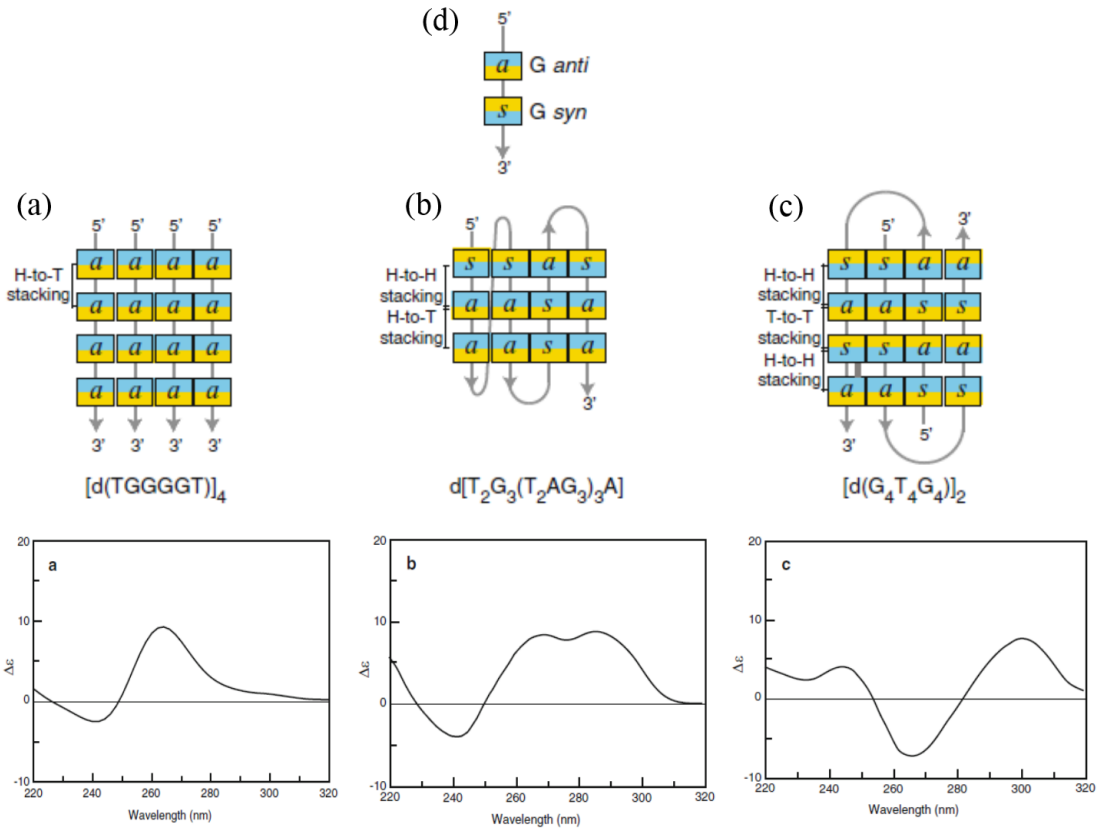


**Figure 1-14** **A sketch of the stacking arrangement of selected G-quartets made of d(TGGGGT)$_4$, d(T2G$_3$(T$_2$AG$_3$)$_3$A, and d(G$_4$T$_4$G$_4$)$_2$ and their CD spectra are shown in (a), (b) and (c), respectively. Each G residue is represented by a bi-coloured rectangle, and the head (H) and the tail (T) faces [as defined in figure (1-14)] are blue and yellow, respectively. *s* and *a* refer to the syn and anti confirmation around the glycosidic bond, respectively. the arrows represent the 5'- to -3' direction of the strand. A graphic legend is shown in (d) on top. Adapted from (50).**

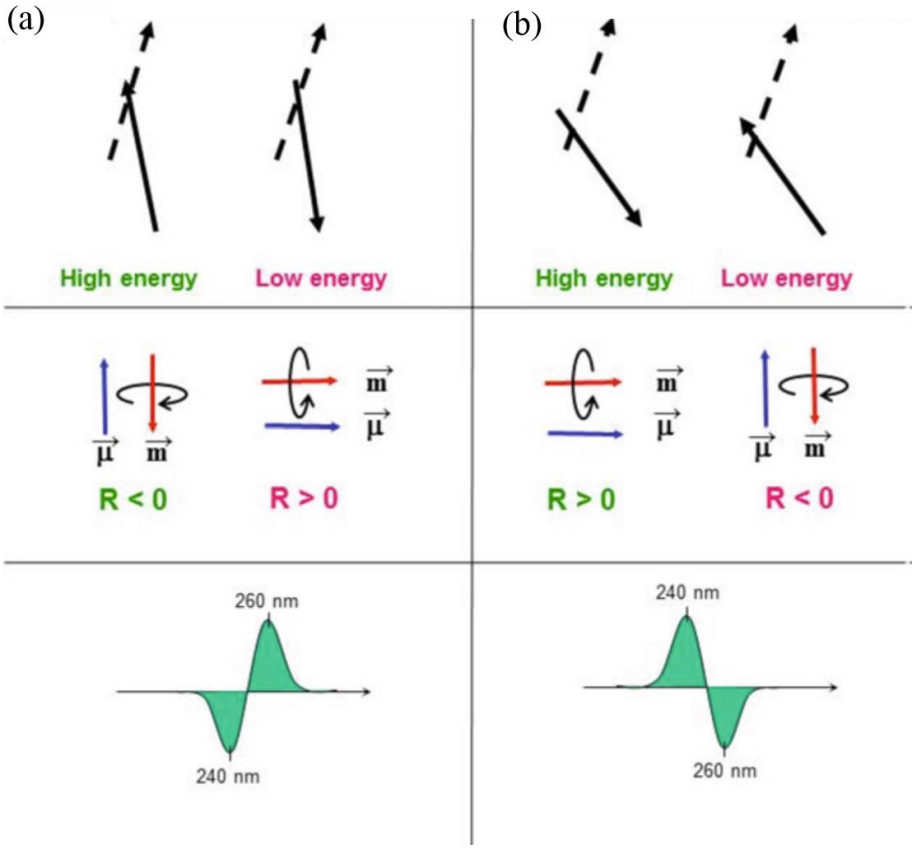


**Figure 1-15** **A model for the origin of the positive, head-to-tail (H-to-T) and negative, head-to-head (H-to-H) exciton couplets for G-quartet stacking in (a) and (b), respectively. *Top:* the arrangement of two 248 nm electric transition moments (full line: front vector; dashed line: back vector) located in two neighbouring guanines. *Middle:* the magnetic (m) and electric (μ) moments generated by the two guanines (the left panel represents the high-energy coupling in which the two electric transition moments, on *top*, sum to a total electric vector (*in blue*) pointing upward, and generated a charge rotation resulting in magnetic moment (*in red*) pointing downward, that is the antiparallel case. The parallel case with the low-energy is shown in the middle right panel. Bottom: the predicted CD spectra. Adapted from (50).**

### *1.1.6.2. polyacrylamide gel electrophoresis*

Gel electrophoresis has become an indispensable tool in the field of molecular biology. It enables the separation of nucleic acid molecules based on their size and charge using an electric field. The gel is placed in an electrophoresis chamber that is connected to a power supply. When an electric current is applied, the larger molecules move slowly through the gel while the smaller molecules move faster. Polyacrylamide gels were employed to fractionate DNA samples during the early 1970s (21). In this thesis, Polyacrylamide gels were used under native conditions to identify higher order structures as we shall see in chapter 3 in detail.

## 1.1.7 G-Quadruplexes in biology

As many guanine-rich sequences are known to form G-quadruplexes with extensive structural diversity *in vitro*, the question that arises here is how prevalent these structures are found *in vivo* within the cells, and are there any biological functions relative to their existence or locations within the genome?

Bioinformatic computational analysis of the human genome has revealed more than 300,000 sequences that have the potential to form a G-quadruplex structures; known as Putative Quadruplex Sequence or (PQS) (53), and the localization of those G-rich sequences, interestingly, is non-random as they colocalize with functional regions of the genome. These sequences are highly conserved among mammalian species and also found, with lower degree, in non-mammalian and lower organisms (54). This likely is an oversimplification as non-consensus sequences may form G-quadruplexes (55), as well as an underestimation since long runs of repeated DNA sequences are missing from the available sequence database.

The highest abundance of PQS is at telomeres. The telomeric ends of chromosomes are repetitive non-coding DNA sequences that protect the cell from deterioration, end-to-end fusion, and nuclease degradation (56, 57). In human cells, telomeric DNA consists of 5 to 8 kilobases of a double-stranded tandem repeat of the guanine-rich sequence TTAGGG with a single-stranded 3’-end overhang of 100-200 bases necessary to ensure complete chromosomal DNA replication. With each cell

division, telomeres shorten by 50-200 bases because the synthesis of the lagging strand of DNA can not replicate the 3' end overhang. Telomere shortening to a critical length negatively affects the normal growth and leads to chromosomal instability and cell death. Tumour cells, however, can avoid this through the activation of the enzyme telomerase that maintains the length of telomeres by adding the TTAGGG repeats to the 3' ends of chromosomes (58-61). Telomerase has been shown to be highly expressed and active in 85-90% of all human tumour cells (60). A prerequisite for telomerase activity is the presence of the single-stranded telomeric DNA as a primer (62). However, earlier studies (63, 64) have demonstrated that the guanine-rich telomeric sequences are able to assemble into G-quadruplex structures facilitated by the presence of monovalent cations ($Na^+$ and $K^+$) suggesting that the quadruplexes might function as a telomeric capping structure. Thus, telomere elongation could be negatively regulated *in vivo* through G-quadruplex stabilization by $K^+$ (65). Furthermore, small molecules that bind and stabilize G-quadruplexes appears to be potent telomerase inhibitors, therefore, the search of these ligands is important from a therapeutic point of view. Several recent reviews have captured the range of quadruplex-targeted ligands driven from structural-based design approaches that turn out to be potent telomerase inhibitors (25, 66, 67).

Guanine-rich sequences are also highly enriched in gene promoters implying a role for G-quadruplexes in regulating gene expression. Interestingly, PQS are more frequent in oncogenes and regulatory genes than in house keeping or tumour suppressor genes (68, 69). It has also been found that in about 3000 human genes, PQS are present in the region specifying the 5'-UTR of the encoded mRNAs and may block translation (70). The first evidence that PQS at promoter regions influence gene expression came from studies on the oncogene *c-MYC* in which it was shown that mutations of PQS or the addition of G-quadruplex stabilizing ligand such as tetra-(*N*-methyl-4-pyridyl)porphyrin (TMPyP4) affected the process of transcription *in vivo* (71). Due to the functional relationship between telomeres, oncogenes and cancer, great efforts have been devoted to find potential ligands that target G-quadruplexes to be applied in anticancer therapies (72, 73).

Besides cancers, neurological disorders are one of the main categories of human diseases that have shown an involvement of G-quadruplex motifs. This suggests G-quadruplexes can play a physiological role that is altered in disease states.

Recently, a large expansion of a GGGGCC ($G_4C_2$) hexanucleotide repeat in the first intron of the human *C9orf72* gene, was shown to fold into G-quadruplexes with distinct structures at the level of both DNA and its transcribed RNA, and has been demonstrated to cause amyotrophic lateral sclerosis (ALS) and frontotemporal dementia (FTD) (74-76). ALS is the most frequent motor neuron disease, caused by the loss of motor neurons in brain and spinal cord, resulting in progressive muscle weakness and paralysis, ultimately leading to death from respiratory failure. FTD is the second most common form of dementia in individuals younger than 65 years. It is characterized by changes in personality or language impairment, due to the progressive degeneration of the frontal and anterior temporal lobes of the brain. A number of studies have provided insight into how this repeat expansion (both RNA and DNA) may contribute to ALS and FTD including the study from our lab which will be discussed in detail in chapter 2 of this thesis.

## 1.2. Introduction to hemoproteins

Proteins containing heme, iron protoporphyrin IX (figure 1.16 a) prosthetic groups, also referred to as *hemoproteins*, are ubiquitous in nature and fulfill a stunning diversity of functions (77). In the latter part of the 20th century, there has been a tremendous amount of research on heme and hemoproteins due to the importance of heme as cofactor in key proteins and enzymes that support life. These include the following: hemoglobin and myoglobin that transport and store oxygen; cytochromes and oxidoreductases that support cellular energy generation and biosynthesis; cytochrome P450 monooxygenases that are important for drug metabolism and synthesis of endogenous substances such as lipids and steroids; peroxidases that are responsible for oxidative catalysis; and heme oxygenases that control heme degradation processes and synthesize important neuromodulators nitric oxide and carbon monoxide (77).

The heme-binding sites of all these hemoproteins are arranged as shown in figure 1.16 b. The protein provides a key “axial” coordination to the heme iron that controls the iron’s reactivity. In addition, the “distal” side of the heme contributes to the specific activity of a given hemoprotein. The iron atom can be coordinated by six ligands, but the four pyrroles of heme provide only four ligands. Therefore, the heme iron can accept two additional axial ligands. This allows heme to associate with proteins and bind to small molecules such as oxygen, nitric oxide, and carbon monoxide. The axial amino acid residue at the proximal side carries an electron rich functionality and can be histidine, methionine, tyrosine, or cysteine. Heme in proteins can be five- or six-coordinated. In the case of five-coordinated heme, then the distal site is accessible and often binds to small molecules including oxygen, nitric oxide, and carbon monoxide.

In the following sections, I will first, provide the reader with a brief view on the heme molecule itself and the versatile and fascinating roles of heme in regulating many fundamental biological processes in living organisms. Then, I focus on the catalytic properties of hemoprotein peroxidases and monooxygenases since these properties are highly related to the discovered nucleic acids the bind heme and possess similar activities; the main theme of this thesis.

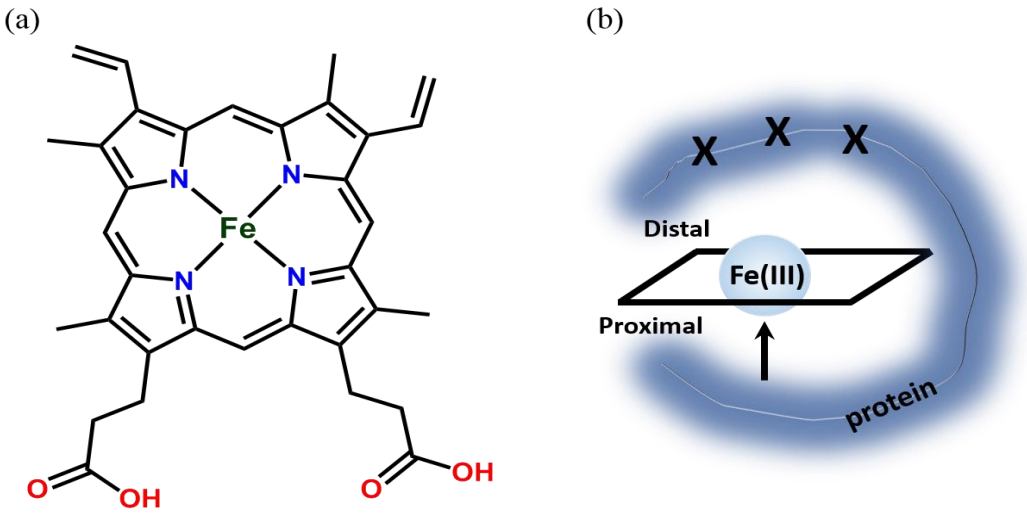


**Figure 1-16** **(a) The chemical structure of iron protoporphyrin IX. Heme is composed of a macrocycle of four pyrrole rings with four methyl groups, two vinyl groups, and two propionate groups attached. (b) A general schematic representation of the arrangement of the heme-binding site in hemoproteins (5-coordinate). The heme moiety is simplified as a parallelogram shape having the iron ion (ferric in this case) as a sphere in the middle. The key axial coordination represented by an arrow in the proximal side. The amino acid residues at the distal sites are shown as "X" symbols.**

### 1.2.1 Heme: the secret molecule of life

Heme, iron protoporphyrin IX (figure (1.16 a), is without doubt one of the most central molecules for life. The well-known example manifesting heme importance is hemoglobin; the protein that transports oxygen from the lung to all other organs and tissues in the human body. The unique oxygen-binding property of hemoglobin is due to the presence of the heme cofactor within the protein. Roughly 80% of heme in humans is made and present in the red blood cells; 15% is made and present in the liver and the rest is distributed in other tissues (78) . Heme is synthesized to a basal level to maintain proper functioning of certain proteins and enzymes that use heme as a prosthetic group. Beside serving as cofactor for many proteins, recently, scientists have discovered that heme can also serve as signaling molecule, and thereby regulate a wide array of molecular and cellular processes. For example, heme can impact the growth, differentiation, and survival

of many mammalian cells (79). Heme also was found to control basic molecular and cellular process such as protein synthesis, gene transcription, protein localization and assembly (78).

The benefit of heme is universal to all living organisms, but could it be harmful to the cells? Heme, indeed, is an essential molecule with contradictory biological functions. Recent investigations have explored the regulatory processes of free heme within cells. In fact, a satisfactory balance between availability of heme for beneficial but not toxic functions is achieved by multiple levels in regulation of metabolism, storage, and degradation of heme. However, under certain pathological conditions, this equilibrium can be distorted. Heme released from intracellular hemoproteins, if not detoxified properly by its regulatory enzymes; *heme oxygenases* (80), generates redox-active iron which leads in turn to the formation of reactive oxygen species (ROS) via the Fenton reaction (equation 1). Moreover, heme that is not bound to a functional protein as a prosthetic group, can bind to specific targets and alter their functions. This has been found explicitly in neuropathological processes. In Chapter 2, we will give an outline of heme metabolism in the brain and the contradictory roles of heme in neuronal cells.

$$Fe^{2+} + H_2O_2 \rightarrow Fe^{3+} + HO^{\bullet} + {}^{-}OH \qquad (1)$$

To fully understand the versatile roles, good or bad, of heme in living processes, it is necessary to have a clear understanding of the structure and chemistry of heme molecule. As shown in figure 1-16 (a), heme is composed of a macrocycle of four pyrrole rings. The four nitrogen atoms chelate one iron atom. The iron can be in the ferrous ($Fe^{2+}$) or ferric state ($Fe^{3+}$). In fact, the word heme is used interchangeably as a generic term to identify both ferrous and ferric forms of iron protoporphyrin IX. Correctly, however, heme refers only to the ferrous protoporphyrin IX, whereas ferric protoporphyrin IX is called hemin. When exposed to air, hemin usually is more stable than heme. Hemin has a net charge of +1 and normally exists with a counterion like chloride. In the work described in this thesis, we have used hemin (ferric protoporphyrin IX), and we will refer to it as Fe(III)-heme.

Although heme is a small molecule by molecular mass comparing to macromolecules such as proteins and nucleic acids, it is complex and chemically

multifaceted. The heme molecule contains parts that are highly hydrophobic including the porphyrin ring, the methyl, and the vinyl groups. On the other hand, heme also contains hydrophilic parts including the iron and propionate side chains. Such chemical characteristics allow heme to fit into both hydrophobic as well as hydrophilic environments; making stacking interactions with or suited in hydrophobic pockets in certain enzymes in addition to interactions through salt bridges. Moreover, the iron ion can adopt several conformations (in or out of the porphyrin plane) depending on its oxidation and electron spin states permitting heme to freely transfer electrons and interact with a wide array of molecules. The most stable and known oxidation states for iron are +2 and +3, however, less stable +4 oxidation state has been observed to form in certain catalytic intermediates in oxidation reactions as we shall see in chapter 4.

### 1.2.2 Heme and hemoproteins optical spectrum and iron spin state

The intensity and color of porphyrins are derived from the highly conjugated π electron system and a fascinating feature of porphyrins is their characteristic UV-visible spectra that consist of two distinct regions: in the near ultraviolet and in the visible region. Since we have used UV-visible (UV-vis) spectroscopic methodology in later chapters of this thesis, we thought of briefly illustrating some chemistry background behind heme optical spectra.

In the case of disaggregated heme, the most intense transition is from π ($A_{1u}$) → π* ($E_g$) which results in the Soret band at ~ 400 nm. Other weak transitions occur as well and result in α and β bands in the visible region of the spectrum. The heme optical spectrum id shown in figure 1.17.

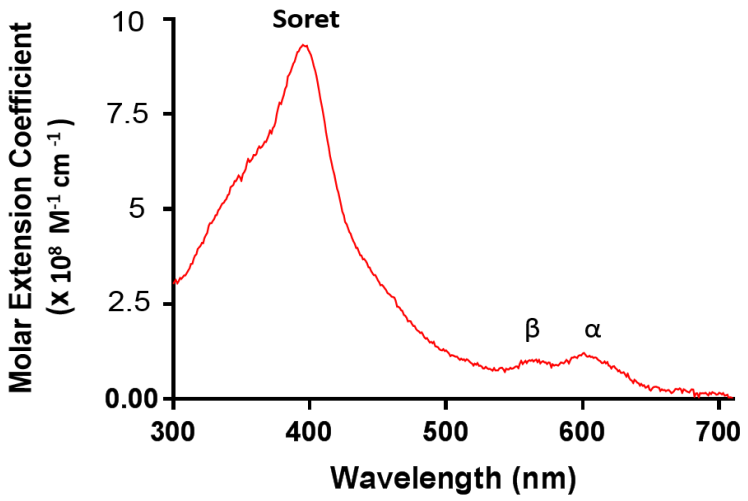


**Figure 1-17 The UV-visible spectrum of 2 μM heme indicating the position of the Soret band at 398 nm and the two visible peaks at 600 and 563 nm for α and β band respectively.**

The presence of electron-donating axial ligands in the proximal or distal sites to the heme molecule, as in hemoproteins or heme-nucleic acids complex, gives an extra coordination to the iron, thus, an additional transition can occur. This transition is attributed to charge transfer (CT) from the filled orbitals with the highest energy of the porphyrin (HOMO) to the dπ orbital of the iron. The charge transfer bands are represented as a change in the visible region of heme spectrum which we will be describing in more depth throughout the thesis. The diagram in figure 1-18 shows the energy levels for heme absorption bands. This model described by Gouterman M. (81, 82) and Doiphin (83) has successfully explained the UV-vis spectral characteristics of many hemoproteins.

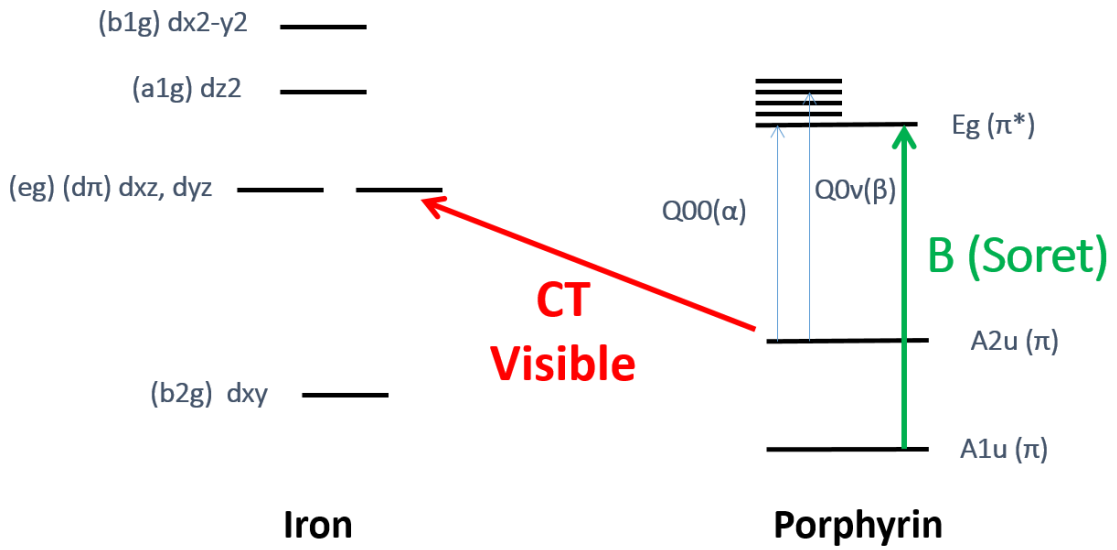


**Figure 1-18 Energy level diagram for heme absorption bands. The transition from π with A1u symmetry to π* with Eg symmetry results in Soret band (B) shown in green arrow. Charge transfer band (CT) is shown in red arrow.**

The presence of electrons in partially-filled d orbitals is a characteristic of transition metals such as iron. This property allows iron to react with ligands of electrons source such as molecular oxygen. Depending on the nature of the axial ligands; weak (small ΔE) field or strong (large ΔE) field ligands, the iron d orbitals will split differently, and this results in different iron spin states. The distribution of electrons in the d-orbitals for ferrous ($d^6$), ferric ($d^5$) and ferryl ($d^4$) iron in the octahedral ligand field as shown in figure 1-19 a**.** In the case of low-spin complex, the iron is ~ 1.9 Å with respect to the heme core whereas in high-spin complex, heme has a distorted square pyramidal geometry, with the iron pushed out (~ 0.3 – 0.5 Å) of the plane of the heme core (84). This is illustrated schematically in figure 1-19 b.

In redox reactions carried out by hemoproteins, the iron oxidation state changes from either ferrous (+2) or ferric (+3) to ferryl (+4). This oscillator between multiple oxidation states has an effect on the overall energy transitions of the complex, and this is reflected on the associated UV-Vis spectra as described in Chapter 4.

The spin state of the iron has a profound effect on the chemistry of the iron species. In biology, for example, low-spin ferric heme iron predominantly serves as redox mediator in electron-transfer proteins. This can be explained in the view of the tight conformation of the iron low-spin with two tightly bound axial ligands which prevent substrates from interacting with the metal. Therefore, the structure is little changed upon oxidation and reduction, and as a result, there is only a small reorganization energy which in turn facilitates the rate of electron transfer (85). On the other hand, high-spin ferric heme iron usually contains one ligand that is easily displaced by exogenous ligands (eg, oxygen or peroxide), allowing the heme to transport oxygen or catalyze oxidation reactions with other substrates.

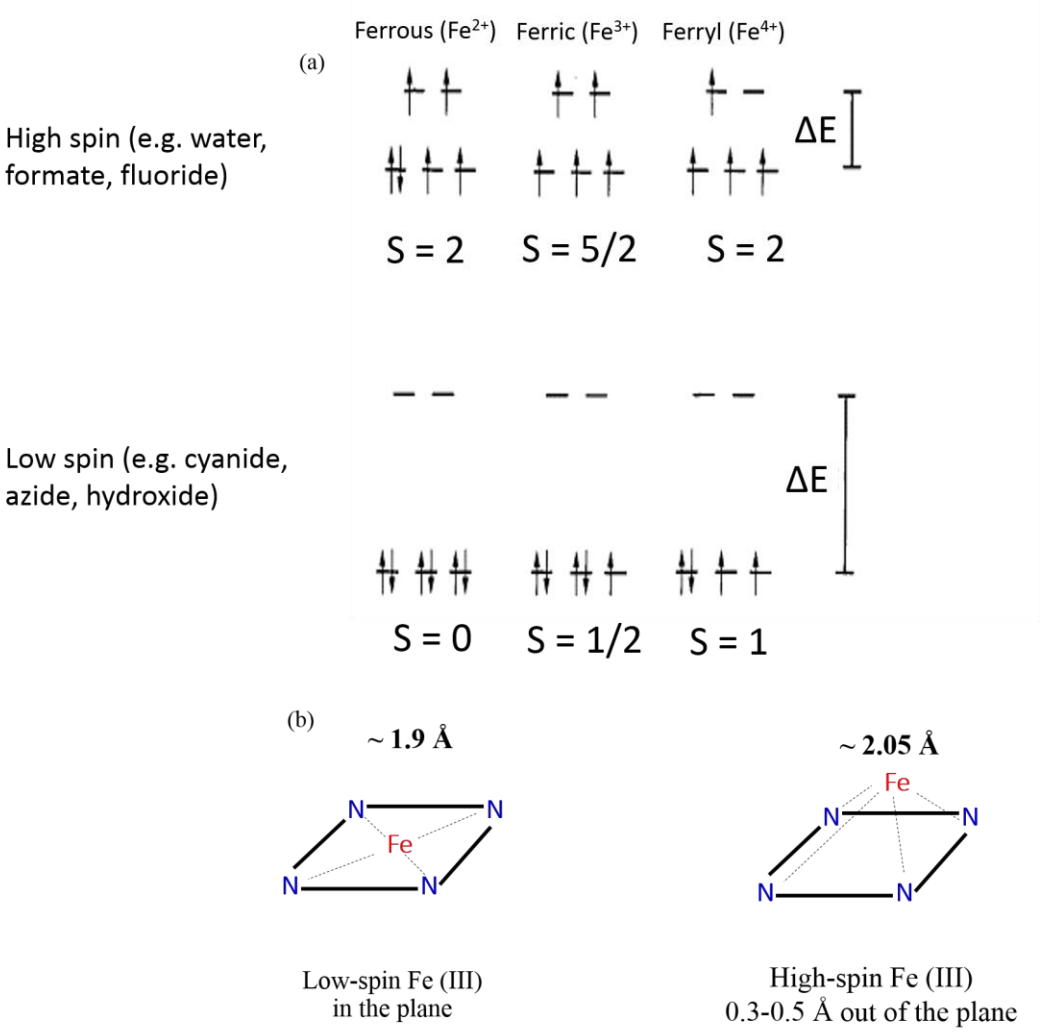


**Figure 1-19 (a) Iron spin states adapted from (85). (b) schematic representation of the effect of iron(III) spin state on the geometry of the heme core.**

### 1.2.3 Peroxidases

The hemoprotein peroxidases are ubiquitous proteins that catalyze the one-electron oxidation of various organic and inorganic substrates by peroxides, usually hydrogen peroxide ($H_2O_2$), according to the general equation (2).

$$2RH + H_2O_2 \rightarrow 2R^{\bullet+} + 2H_2O \qquad (2)$$

The most studied and best characterized of peroxidases are horseradish peroxidase (HRP) (86) and cytochrome c peroxidase (CcP) (87, 88), and more recently, enzymes like lignin peroxidase (LiP) (89) and ascorbate peroxidase (APX) (90) have been extensively investigated. In addition to these studies of plant and fungal enzymes, much work has been done on the mammalian peroxidases, particularly, myeloperoxidase (MPO) and lactoperoxidase (LPO) in terms of structure and mechanism (91)

The prosthetic heme in the resting peroxidases is in the ferric state [(FeIII)-heme]. In HRP and most peroxidases, the iron is five-coordinate, high spin with a histidine residue as the proximal iron ligand. In addition to the proximal histidine iron ligand, which in HRP is His170, in CcP His175, and in LiP His 176, there are other key amino acid residues at distal side; histidine not bound to the heme iron His42 in HRP, His52 in CcP, and His47 in LiP. A second important residue is a distal arginine (Arg38 in HRP, Arg48 in CcP, and Arg43 in LiP). These amino acid residues are important and functional during the catalytic cycle for peroxidases as follows: the proximal histidine is coordinated to the iron via imidazole functionality that helps in donating electrons to the iron “push-effect”. The distal residues play acid-base catalysis by making polar interactions that facilitate the heterolytic cleavage of the peroxide dioxygen bond “pull effect”. The push and pull effects are responsible for the formation of the catalytic intermediate known as “compound I”. This short-lived intermediate is capable of withdrawing an electron from a reducing substrate to form a second intermediate known as “compound II”. More details on the nature of theses intermediates are giving in Chapter 4. Additional residues promote the formation of compound I. In HRP, these include Asn70 on the distal side, which by hydrogen bonding to the N-H of the His42 enhances its basicity, and Asp247 on the proximal side, which by accepting a hydrogen bond from the proximal histidine increases the negative electron density on the imidazole ring and thereby, facilitating the push effect and the O-O bond

cleavage. The location of the critical catalytic residues relative to heme in the active site of HRP is shown in figure 1-20. The general sequence of push-pull effect is referred to as Poulos-Kraut mechanism (92, 93) and is illustrated in figure 1-21.

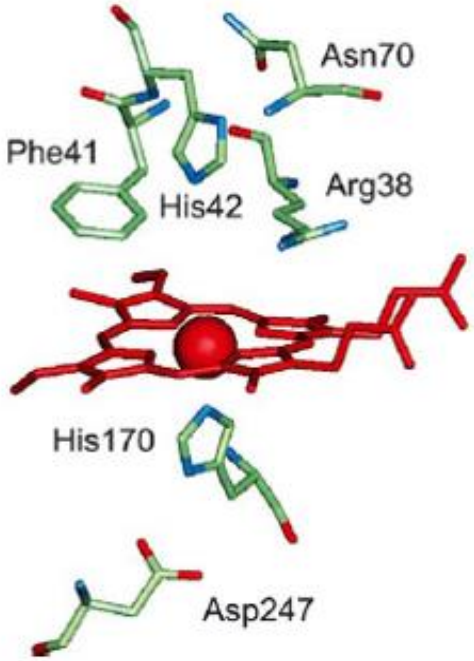


**Figure 1-20 Key amino acid residues at proximal and distal sides in the active site of HRP. Adapted from (86).**

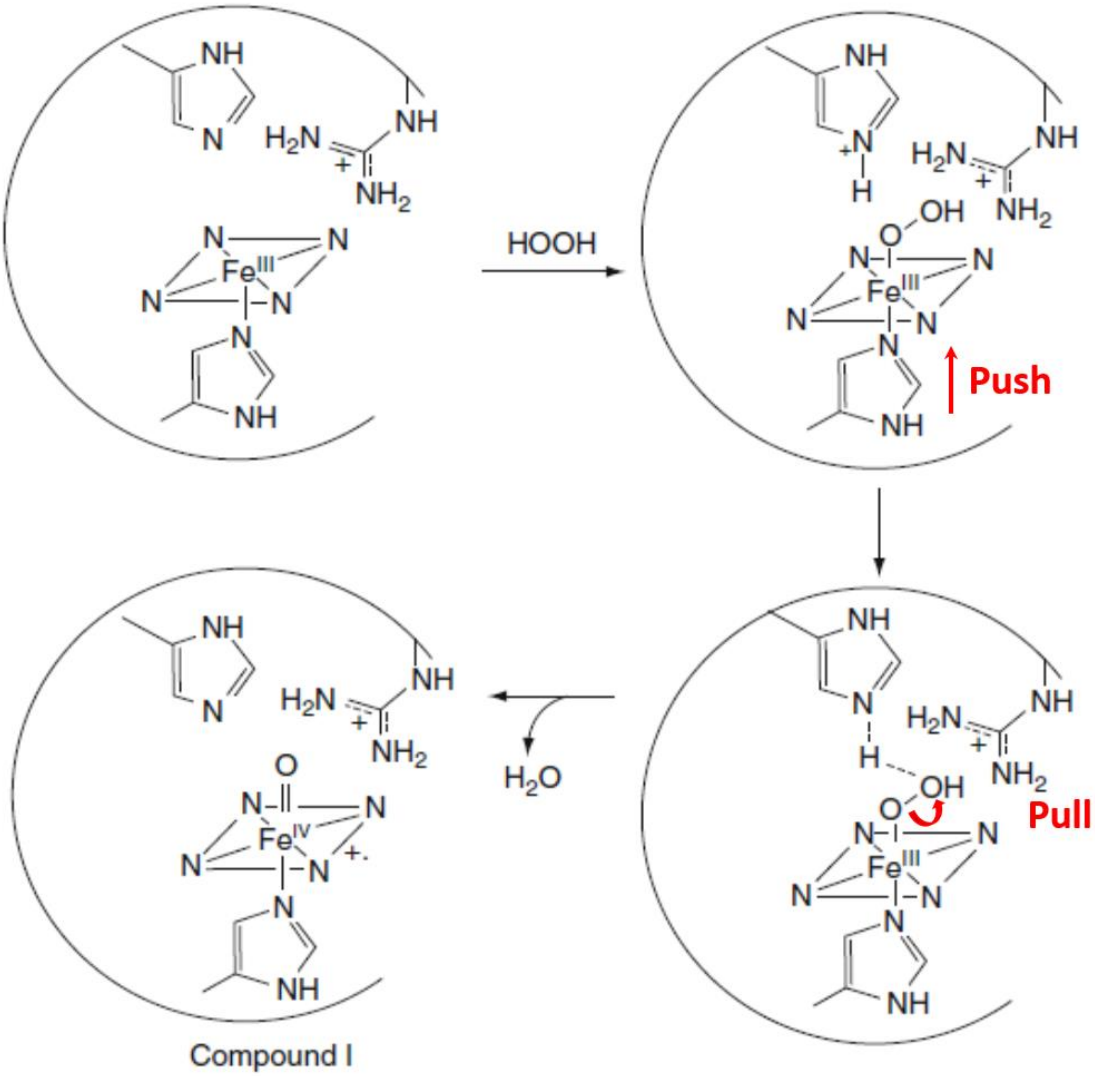


**Figure 1-21** **Schematic representation of the Poulos-Kraut peroxidase mechanism in which the conserved distal histidine serves as an acid-base catalyst that transfers a proton to the terminal oxygen after formation of the [Fe(III)-OOH] intermediate. The Arg38 at distal site helps in stabilizing the negatively charged hydroxide leaving group. The push and pull effects are indicated by red arrows. Modified from (92).**

### 1.2.4 Monooxygenases

Monooxygenases are enzymes that catalyze the insertion of a single oxygen atom from $O_2$ into an organic substrate (2-electron oxidation) according to the following equation:

$$RH_2 + O_2 \rightarrow RO + H_2O \qquad (3)$$

In order to carry out this type of reaction, these enzymes need to activate molecular oxygen to overcome its spin-forbidden reaction with the organic substrate. In most cases, monooxygenases utilize inorganic cofactors to transfer electrons to molecular oxygen for its activation. Monooxygenases typically are highly regio-, and/or enantioselective, making them attractive biocatalysts (94). Monooxygenases are classified based on the type of cofactor they require. In this section, we focus on heme-dependent monooxygenases also referred to as cytochrome P450 monooxygenases or P450s.

P450s can be found in many life forms: eukaryotes (mammals, plants, and fungi) and bacteria express a wide variety of these enzymes (95). They catalyze a wide variety of oxidation reactions. Besides epoxidations and hydroxylations, these monooxygenases are also able to perform heteroatom-dealkylations and -oxidations, oxidative deaminations, dehalogenations, dehydrogenations, dehydratations, and reductions (96). In order to catalyze these reactions, the p450s enzymes require electrons for activation of $O_2$ by the heme prosthetic group. These electrons are typically obtained from the coenzymes NADH or NADPH, but the transfer mechanism of the electrons to the heme cofactor varies.

$P450_{cam}$ (CYP101A1) is a bacterial P450 enzyme from *Pseudomonas putida* that converts 1R-(+)-camphor to 5-exo-hydroxycamphor. It is heme-thiolate ligated monooxygenase and was the first P450 whose crystal structure was solved (97). Since then, its structure has been extensively studied and it has served as a prototype for structure-function studies of the entire P450 family. The catalytic cycle for $P450_{cam}$ also holds true for the entire P450 family. In the first step, the organic substrate (XH) binds to the enzyme. Then, one electron is transferred to the heme-iron and thereby reducing it

from Fe(III) to Fe(II). Subsequently, the binding of molecular oxygen results in an oxy-P450 complex. This complex is reduced by the second electron and after a double protonation at the distal oxygen, the O-O bond is cleaved, resulting in the reactive enzyme intermediate known as compound I. This intermediate is able to insert the oxygen atom into the organic substrate and to form a product-enzyme complex. Release of the products results in the resting state enzyme with a water molecule bound as a sixth ligand of the heme. The addition of artificial oxygen donors such as peracids and peroxides to the ferric complex *in vitro* is also known to give product, likely through the formation of compound I, via a process called the “peroxide shunt pathway”. A conserved cysteine (Cys357 in P450cam) acts as the fifth ligand and is required for the activity. The catalytic cycle of P450 monooxygenases are shown in figure 1-22.

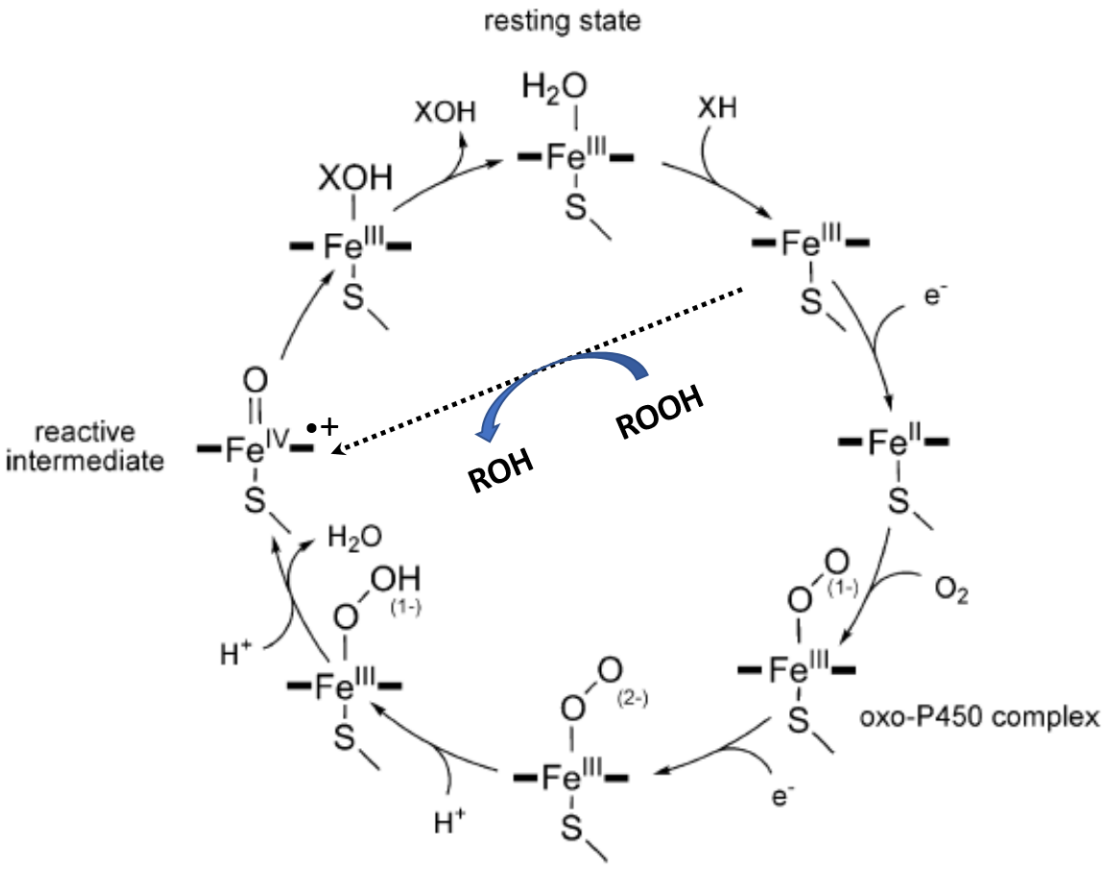


**Figure 1-22 Proposed catalytic cycle of cytochrome P450 monooxygenases. Dashed arrow indicates the shunt pathway. Modified from (98).**

Interestingly, P450 enzymes share their catalytic capabilities with certain heme-containing enzymes through the formation of the same active intermediate “compound I”, however, P450 enzymes have remarkably different nature of the active site. The proximal cysteine thiolate ligand is indispensable for compound I generation and mutation of the cysteine residue leads to loss of activity (96). Dawson and coworkers suggested that the polarizable nature of the cysteine thiolate anion ligand provides a strong ‘push’ of electron density via the heme onto the O-O bond of the ferric-hydroperoxo intermediate, thus promoting heterolytic O-O bond cleavage (96). In addition to the proximal cysteine residue, an ‘acid-alcohol’ pair that is highly conserved in almost all P450 enzymes aiding the process of oxygen activation in the distal heme pocket. The alcohol in most cases is threonine or serine and the acid can be aspartate or glutamate. In the case of P450cam, these residues are Asp251 and Thr252. The role of this acid-alcohol pair in catalysis has been investigated in several mutagenesis studies. Specifically, in $P450_{cam}$, the Thr252Ala mutant leaded to normal NADH and $O_2$ consumption but essentially no product formation (99, 100). The alcohol residue is thought to stabilize the H-bonding network in the distal pocket and controlling proton delivery to the distal oxygen of bound dioxygen complex (99-102). The acid residue, on the other hand, has an important role in electron transfer following the formation of oxyferrous intermediate. In $P450_{cam}$, the mutagenesis of Asp251 to Asn cause a strong decrease in the NADH consumption rate (103, 104). The active site of the camphor-bound oxyP450camp is shown in figure 1-23.

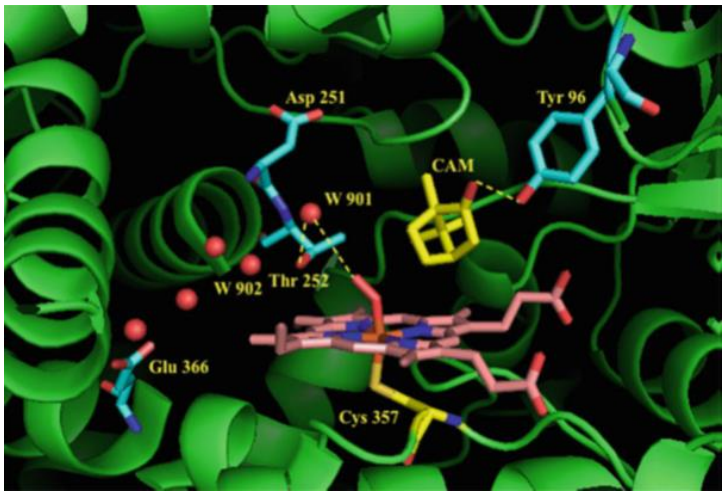


**Figure 1-23 The structure of the active site of P450 bound to camphor showing the important amino acid residues. Constructed using PDB file 1DZ8. From reference (105).**

## 1.3. A guanine-rich aptamer with oxidation activity when bound to ferric Fe(III)-heme

In the late 1990s, Sen's laboratory made the surprising discovery that guanine-rich DNAs and RNAs that fold to form G-quadruplexes (figure 1-7) bind tightly to ferric heme [Fe(III)-heme] (12). Shortly after, Sen and Travascio reported that PS2.M, a test G-rich oligonucleotide derived from *in vitro* selection (SELEX) method, as well as its RNA counterpart rPS2.M both bind heme strongly and utilize it as a cofactor, in similar fashion to hemoprotein HRP, to catalyze the one electron (1 $e^-$) peroxidation reactions (12). These observations (binding and peroxidase activity) are all in relation to the poor oxidative properties of disaggregated Fe(III)-heme on its own in aqueous solution, or in the presence of a DNA or RNA molecules that does not interact with Fe(III)-heme. Moreover, in 2010, Sen and Poon were able to show rigorously that these "heme•G-quadruplex" complexes are capable of performing the more mechanistically challenging two electrons (2 $e^-$) oxidations involving oxygen transfer to a substrate; the reactions typically catalyzed by the cytochrome P450 family *in vivo* (106). Also, these catalytic properties were found to be general and specific to G-quadruplex structures whether from genomic sequences (chromosomal telomere, promoters, UTR's region) or non-biological sequences obtained from *in vitro* selection (106, 107). Due to their catalytic activities in catalyzing oxidation reactions, these heme•G-quadruplexes derived from either DNA or RNA G-rich sequences are known nowadays as heme/G4-DNAzymes or heme/G4-ribozymes respectively.

In this section, I will start by describing the methodology that led to the discovery of such a DNA and RNA molecules with certain functions; SELEX, then summarize what is known about these heme/G4-DNAzymes and ribozymes, and this will be the gateway for laying out and framing the work described in this thesis.

### 1.3.1. SELEX

In vitro selection, or SELEX (Systematic Evolution of Ligands by EXponential enrichment), is a technique that allows the simultaneous screening of highly diverse pools "library" of different RNA and DNA molecules for performing a particular task "*aptamers*".

It was first described in 1990 (Ellington and Szostak 1990, Tuerk and Gold 1990, Robertson and Joyce, 1990). Large libraries of random sequence single-stranded oligonucleotides (whether DNA or RNA) can be thought of as a sequence-dependent folded structures with high degrees of molecular rigidity in solution. This conformational complexity of the library makes it a source of high affinity ligands for a surprising variety of molecular targets, which span from large molecules, such as proteins, to small organic molecules (108). Typically, in a SELEX experiment, a random library, up to $10^{14}$ - $10^{15}$, DNA or RNA molecules pass through a selection screen. Only a very small fraction of molecules that successfully survive is expected to be present in the initial pool. This initial low abundance can be amplified by the polymerase chain reaction (PCR). Several selection and amplification cycles are usually performed, and this results in an exponential increase in the abundance of functional sequences until they finally dominate the population. Then those functional sequences are cloned and evaluated. Figure 1-24 illustrate the steps of one round of SELEX.

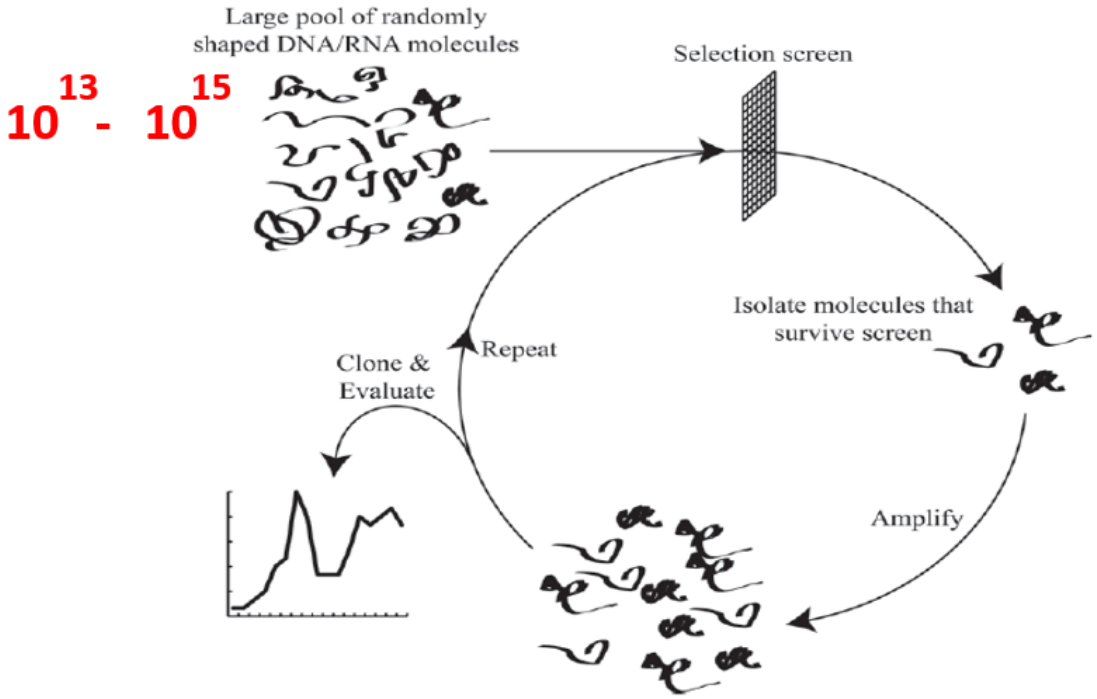


**Figure 1-24 A systematic diagram for in vitro selection (SELEX). [Adapted from (107).**

In fact, the work of Peter Schultz's group on the catalytic antibodies (109), derived to catalyze metallation reactions, inspired the Sen's lab to pose similar questions on

whether DNA/RNA molecule could be selected to catalyze the same reaction. Cochran Schultz have successfully used the distorted porphyrin *N*-methylmesoporphyrin (IX) (NMM) as a transition state analogue (TSA) to generate antibodies that catalyzed the metallation of mesoporphyrin (IX) (109). NMM mimics the presumed puckered geometry of the transition state of the porphyrin during the metallation process catalyzed by ferrochelatase; the enzyme that inserts ferrous ions into in protoporphyrin (IX) in the last step of the heme synthytic pathway. Therefore, the original and successful selection done by Sen's group was based on finding a catalytic DNA or RNA that can catalyze metallation reactions (9, 110). A subsequent study by Li and Travascio (12) on exploring a competitive inhibitor for the metallation reaction has revealed that ferric heme was an excellent one, and that was the indication for us that these G-rich DNA/RNA molecules bound to ferric heme (hemin) strongly, thus, they could be viewed as aptamers for ferric heme and not just for NMM.

A natural question raised from demonstration of tightly bound DNA/RNA-hemin complexes was: could they perhaps show any of the catalytic properties characteristic of hemoproteins? Obviously, they had not been selected for such an activity, therefore, there was no reason to think that they might. Furthermore, no biological role for putative heme-nucleic acid complexes had been hypothesized nor a stable structure of heme with DNA and RNA has been proposed up to that point. Surprisingly, though, Travascio *et al.* (1998) had showed that DNA/RNA-hemin complexes were indeed effective in catalyzing peroxidation reactions (11, 12). Details on binding and observed oxidative activity for these heme/G4-DNAzymes and ribozymes will be elaborated in the next following sections.

### 1.3.2. Binding affinity of G-quadruplexes to hemin

UV-visible spectroscopic analysis of the hemin•G-quadruplex complex shows some remarkable key differences from the spectra of hemin alone or hemin mixed with a non-hemin binding DNA or RNA (e.g., a non-G-rich unfolded single stranded) (figure 1-26). These spectroscopic features strongly resemble that of hemoproteins such as metmyoglobin and HRP (92, 111). The most prominent feature is a ~2-fold hyperchromicity and a slight (~ 5 – 6 nm) red shift of the Soret absorption band of hemin at 398 nm wavelength. Noteworthy differences are seen in the hemin visible spectrum

(480-700 nm wavelength). Fe(III) heme•G-quadruplex complex displays a more complex pattern of peaks, surprisingly reminiscent of those six-coordinate, high spin Fe(III)-hemoproteins as shown in figure 1-25. Hyperchromicity of the Soret band is usually seen as an indicator of an increased hydrophobicity of the hemin binding site (112), and the visible change is a sign that the environment around hemin became different after complexing with the G-quadruplex.

The dissociation constant ($K_d$) for the ferric heme•G-quadruplex complexes ranges from 10 nM to 1 µM as determined by examining a variety of G4-DNA and RNA structures (11, 12, 106, 107). In fact, hemin favorably binds to certain topologies of G-quadruplex structures. Travascio *et al.* (1999) has shown that the telomeric OXY4 DNA oligomer (whose structure is known to form an antiparallel G-quadruplex; as in (h) in figure 1-8 exhibit weak binding affinity compared to the parallel PS2.M and rPS2.M quadruplexes (11). Shangguan D. *& et al.* (2009) (113) carried out a broad investigation on hemin-binding, as well as peroxidation properties of a variety DNA and RNA sequences that were known to form G-quadruplexes, and they had concluded that DNAs and RNAs that fold into a parallel G-quadruplexes were the most optimal for both hemin binding and peroxidase activity. Another comprehensive series of studies by Kong and colleagues (114) has explored, in more depth, the structural characteristics (topology, loops) that a G-quadruplex requires in order to bind hemin and catalyze peroxidation. These authors elaborated that both intramolecular and multi-stranded quadruplexes were effective if their strand orientation were all parallel. The preference of parallel over antiparallel confirmation is more likely attributed to the large steric hindrance of the associated loops which obstructed the interaction between G-quartets and hemin.

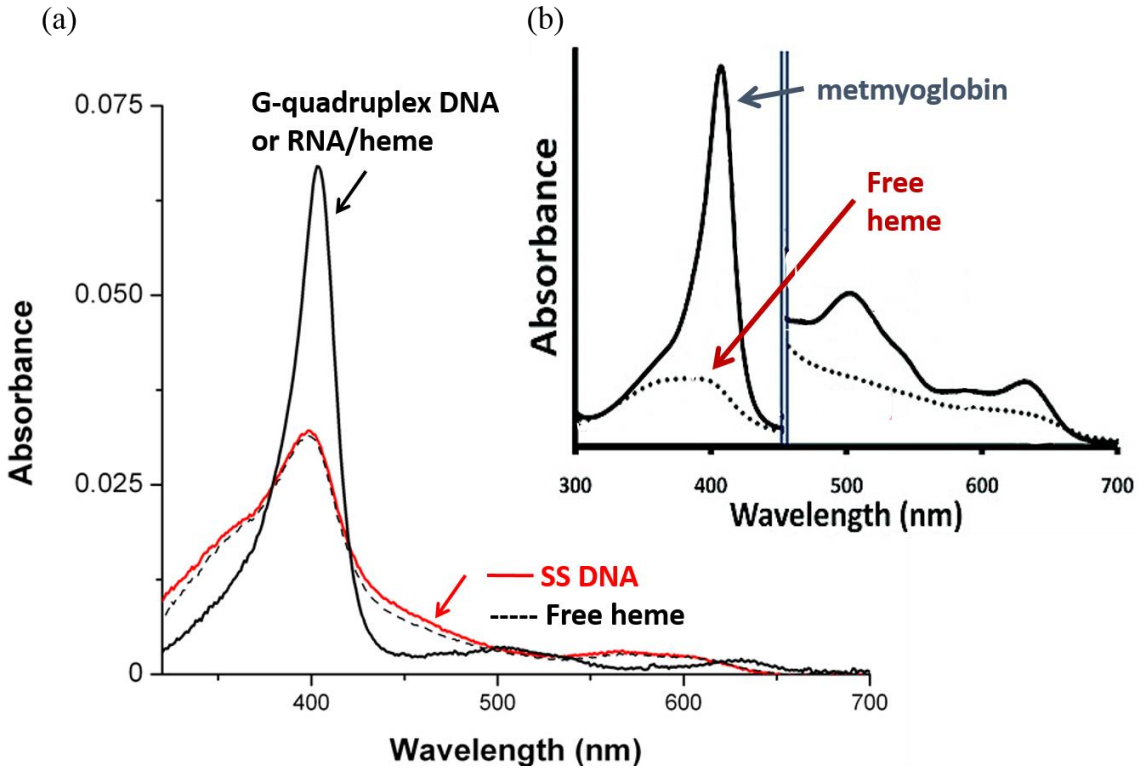


**Figure 1-25** **(a) The UV-visible absorption spectra for ferric heme•G-quadruplex complex (black line), uncomplexed Fe(III)-heme in absence of nucleic acids (dotted black line), and mixed with non-binding single stranded control DNA oligonucleotide (red line). (b) The corresponding UV-visible absorption spectra for metmyoglobin, the Fe(III)-heme bound protein (black line), and free Fe(III)-heme (dotted line). (a) and (b) were modified from (106) and (111) respectively.**

### 1.3.3. The nature of the active site of Fe(III) heme•G-quadruplex complex

The similarities in the observed spectroscopic features of those hemin-DNAzymes to that of hemoproteins led to the following question: does the G-quadruplex supply a specific axial ligand to the hemin iron? Several studies from Sen' group, including the above-mentioned UV-visible as well as electron paramagnetic resonance EPR and resonance Raman spectroscopy has postulated that the iron(III) moiety within the hemin-DNAzyme complex existed in the high-spin state and had six coordination with one of the axial ligands being water molecule (11, 12, 115).

In fact, Fe(III) hemoproteins are known to show an “alkaline transition” in their peroxidase activity which arises from the ionization of the water molecule coordinated to the sixth axial position of the hemin iron (116). Figure 1-26 illustrates this concept. Water can be exchanged relatively easily with hydrogen peroxide leading to the subsequent events of peroxidation reactions. However, deprotonation of this bound water to a hydroxide ion leads to a much slower exchange with peroxide and as a result a decline in peroxidase activity. For example, Fe(III)-hemoglobin which exhibits peroxidase activity has a $pK_a$ value of 8.3 (12, 115).

By way of comparison, hemin-PS2.M and hemin-rPS2.M complexes have $pK_a$ values of 8.7 and 8.6 respectively while the uncomplexed disaggregated hemin shows $pK_a$ of 3.4 - 4 (12, 115). The disparity between the alkaline transition $pK_a$ values of uncomplexed hemin and the hemin-DNAzyme provides insight into the superior catalysis displays by the complex at or near neutral pH. In uncomplexed hemin, the bound water is deprotonated at pH 7, thus, the resultant hydroxide complex exchanges poorly with $H_2O_2$. On the other hand, the hemin-DNAzymes, similarly to hemoproteins, has water that is not deprotonated and associated with fast exchange with peroxide; leading to the steps of peroxidation reactions.

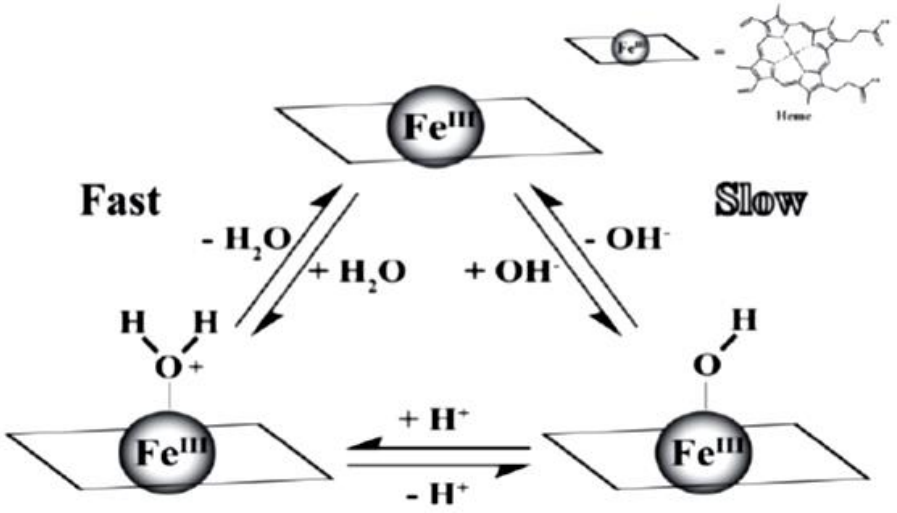


**Figure 1-26 The alkaline transition for hemoproteins. Adapted from (107).**

Beside our group, Sen's lab, there are number of studies that shed the light on the nature of the active site of hemin•G-quadruplexes. Most notably, a series of studies by Yamamoto's group in Japan in which they characterized the interaction between heme and the biologically relevant vertebrate telomeric DNA sequence; d(TTAGGG) by $^{1}$H NMR spectroscopy. The solution structure of this motif sequence has been shown to form intermolecular parallel G-quadruplexed DNA in the presence of $K^{+}$ (117). Yamamoto & *et al.* (117-119) found that heme binds specifically to the 3' terminal G-quartet of this DNA through π-π stacking interactions between the porphyrin and the quartet surfaces. In addition, a water molecule was found under the iron, and is housed in a hole provided by the G-quartet at the proximal side. Although it was not mentioned clearly in their studies, what interest us the most is whether or not this water molecule is indeed providing the iron with electron density via its oxygen atom; playing the same role of proximal histidine or cystine residues in hemoproteins during heme activation. Or is it simply the stacking interaction between the porphyrin and the G-quartet what gives the "push effect"? Further studies need to be done to address these ambiguities.

Another key mechanistic factor was the effect of having nitrogenous buffers in the catalyzed reactions by the hemin•G-quadruplex complexes. Travascio had carefully examined a variety of buffers in her studies on the catalyzed (in the presence of hemin•G-quadruplex) versus uncatalyzed (hemin alone or in presence of non-binding sequence) reactions and found that both, catalyzed and background reactions, were accelerated by the presence of nitrogenous buffer such as Tris, HEPES-ammonium and collidine (12). A hypothesis was that the nitrogenous buffer played the acid-base roles that distal residues within hemoproteins active sites typically play in activating hydrogen peroxide.

In 2007, Rojas *et al.* reported a forward exploration of the potential of PS2.M-hemin complex to catalyze the peroxidation of a variety of substrates in enantio-specific and /or regio specific manner (120). They also examined the relative effectiveness of oxidants other than $H_2O_2$ for PS2.M-hemin activation. These authors reported that in addition to hydrogen peroxide, bulkier oxidants such as t-butyl hydroperoxide and cumene hydroperoxide were also effective at activating the hemin-DNAzyme (120). Moreover, they had shown that not only PS2.M-hemin can oxidize a broad range of substrate; remarkable finding was that with certain phenolic substrates, including *L*- and *D*-tyrosine, *N*-acetyl-*L*-

tyrosine, and hydroxycinnamic acid but also, the rate enhancements were superior to those of horseradish peroxides (120). A key finding of these authors was that although the hemin-DNAzyme showed some regioselectivity with regard the substrates that it oxidized, it showed no enantioselectivity (120). This is consistent with what the Sen lab found in 2010 during the investigation of the $2e^-$ oxidation catalytic capabilities (see section 1.3.4) of not only hemin aptamers, but also genomic DNA and RNA sequences that are postulated to form G-quadruplexes *in vivo* (106). These findings have identified a substantial difference between the hemin-utilizing DNAzymes/ribozymes and hemoproteins; most of protein hemoenzymes show significant enantioselectivity (121). The absence of enantioselectivity in the nucleic acid-hemin complexes suggest relatively "open" active sites for them. However, more sophisticated active sites can be built around the hemin. This innovated approach was shown by Willner *et al.* to improve the catalytic activities of the hemin-DNAzyme (122). In Willner's study, the hemin-DNAzyme was conjugated, by either the 5'- or 3'- end to a catalytic unit (dopamine binding aptamer DBA); aiming to control the enantioselectivity for hemin-DNAzymes. The resulting conjugates "termed apzymes" have shown an enhancement in the catalytic function compared to the wild-type hemin-DNAzyme. Also, they have shown enantioselective oxidation of chiral substrates (122).

A schematic hypothetical picture of the generally Fe(III)-heme-utilizing nucleic acids is shown in figure 1-27.

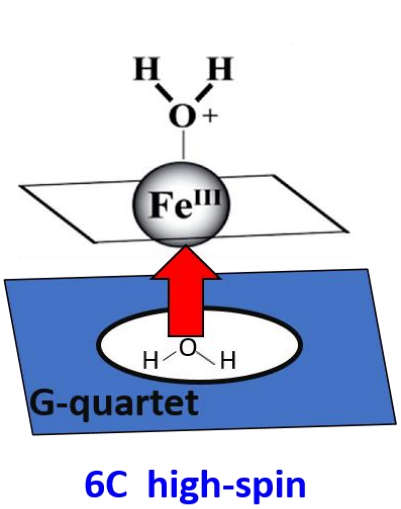


**Figure 1-27 A schematic representation of the hemin-DNAzyme. Ferric heme and the terminal G-quartet are shown as parallelograms. The red arrows toward the iron center indicates possible coordination that provides electron density to the iron center.**

### 1.3.4. Oxidation activities of the hemin-DNAzymes and ribozymes

Travascio *et al.* (12) investigated whether PS2.M-hemin and rPS2.M-hemin were capable of accelerating a peroxidase reaction relative to hemin alone or hemin mixed with a control DNA that did not complex with it. Hydrogen peroxide was used to activate the hemin, and a standard chromogenic substrate, ABTS [2.2'-azido-bis(3-ethylbenzothiazoline-6-sulfonic acid] was used as the substrate [see figure 1-28 a]. Remarkably, both aptamer-hemin complexes showed significantly higher peroxidase activity than the two controls. Observed velocity ($V_{obs}$) of PS2.M-hemin under the most optimal conditions was ~ 250-fold grater than that of hemin alone, and was superior to that of previously reported catalytic antibodiy-hemin complex (109).

In addition to chromogenic substrates, Herman O. Sintim & *et al.* (123) identified a variety of non-fluorescent molecules that can be oxidized by the hemin•G-quadruplexes into fluorescent products (fluorogenic compounds) including Tyramine and 10-acetyl-3,7-dihydroxyphenoxazine (Amplex red) [see figure 1-28 b].

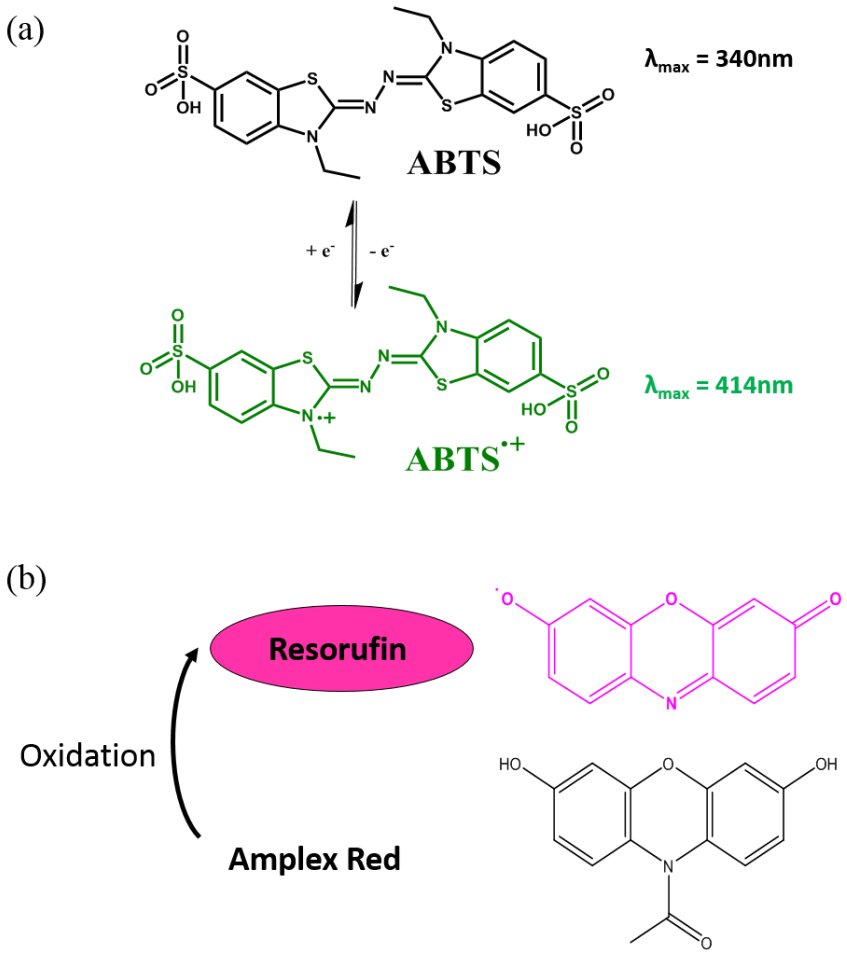


**Figure 1-28** **The oxidation of the chromogenic and fluorogenic substrates used in this study. (a) the oxidation of ABTS to $ABTS^{\bullet+}$ radical; a green-colored product that has maximum absorbance at 414 nm. (b) The oxidation of amplex red to resorufin; a pink-colored product that has excitation and emission maxima of approximately 571 nm and 585 nm.**

In 2010, we began to investigate whether other known reactions of hemoproteins, such as 2-electron oxidations, could also be catalyzed by hemin-DNAzymes or ribozymes Natural peroxidases, such as HRP, oxidize a variety of substrates and appear not to require substrate binding close to their activated hemin; simply collision of the substrates with the edges of activated hemins is sufficient and enables electron transfer between hemin and substrate within these peroxidases (124). DNA/RNA -hemin complexes, too, catalyze the peroxidation of a wide variety of structurally distinct substrates, therefore and by analogy, it is also likely that DNAzymes and ribozymes carry out 1-electron oxidations by enabling collisions of the substrate with their activated moieties.

Catalysis of 2-electron, “oxygen transfer” reactions, however, are intrinsically more challenging for these DNAzymes and ribozymes. Given the significant evidence for the “open or exposed” active sites within DNA/RNA-hemin complexes (figure 1-27), it was worth testing to see if these hemin-complexes would be able to catalyze oxygen transfer reactions. Figure 1-29 (a) shows schematically two alternative mechanisms by which monooxygenases and peroxygenases are though to transfer oxygen to substrates: by a direct, one step, or by oxygen rebound, two steps oxygen transfer mechanisms (125-127). The oxygen rebound mechanism involves two successive 1-electron oxidations. For both mechanisms, however, in order to transfer the ferryl oxygen atom to the substrate, either the substrate is bound already to the active site (eg. Camphor is bound to the active site of $P450_{cam}$) or at least prolonged localization of the substrate close to the activated hemin is required. Poon *et al.* (106) have shown three classic oxygen transfer reactions could be catalyzed by a variety of DNA/RNA-hemin complexes. These reactions are summarized in figure 1-29 (b) and include: the oxidation of a heteroatom, in this case sulfur (thioanisole to its sulfoxide), oxidation of an electron-rich alkene (indole) and a less electron-rich alkene (styrene) to various products. He found that all three substrates were readily oxidized to the expected products with kinetics in each case being comparable to those of hemoproteins (106). The use of $^{18}O$-labeled $H_2O_2$ revealed that the oxygen atom transferred to form thioanisole sulfoxide and styrene oxide came from the added $H_2O_2$ (rather than dissolved oxygen, for instance) (106). Hammett analysis of the kinetics of thioanisole sulfoxide formation, however, could not distinguish clearly between the one-step or two-step mechanisms of catalysis (106). One distinctive feature of these 2-electron oxidations was the lack enantioselectivity as judged by the generation of racemic thioanisole sulfoxide (106). This is consistent with the earlier findings of Rojas *et al.* (120). The fact that these hemin-DNAzymes/ribozymes catalyze both one- and two-electron oxidations efficiently, and appear to have relatively open and accessible active sites, they somewhat resemble microperoxidases (128) in these two aspects. Therefore, the studies from microperoxidases may demonstrate useful structural and mechanistical information leading to better understanding of these hemin-containing DNAzymes and ribozymes.

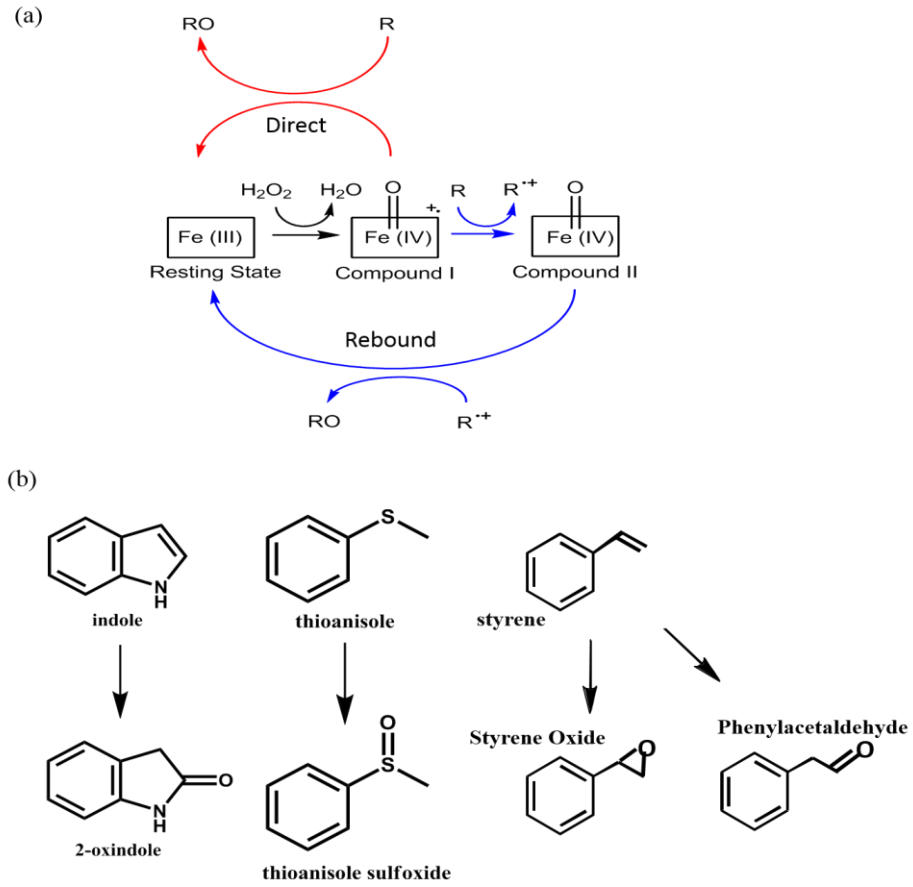


**Figure 1-29 (a) The peroxygenase (oxygen transfer; 2-electrom oxidation) catalytic cycle. The blue arrows show the two-step rebound mechanism and the red arrow indicate the direct oxygen insertion mechanism. (b) The substrates and products for the peroxygenase activity displayed by various hemin•G-quadruplex complexes. Based on reference (106).**

A novel activity was identified by Willner *et al.* (129) for these hemin•G-quadruplex complexes in which they reported that these DNAzymes can mimic the activity of NADH oxidase under aerobic conditions The NADH oxidase catalyzes the oxidation of NADH by $O_2$ with concomitant formation of $H_2O_2$. Figure 1-30 schematically illustrates this new activity for hemin-DNAzymes through the oxidation of Amplex red.

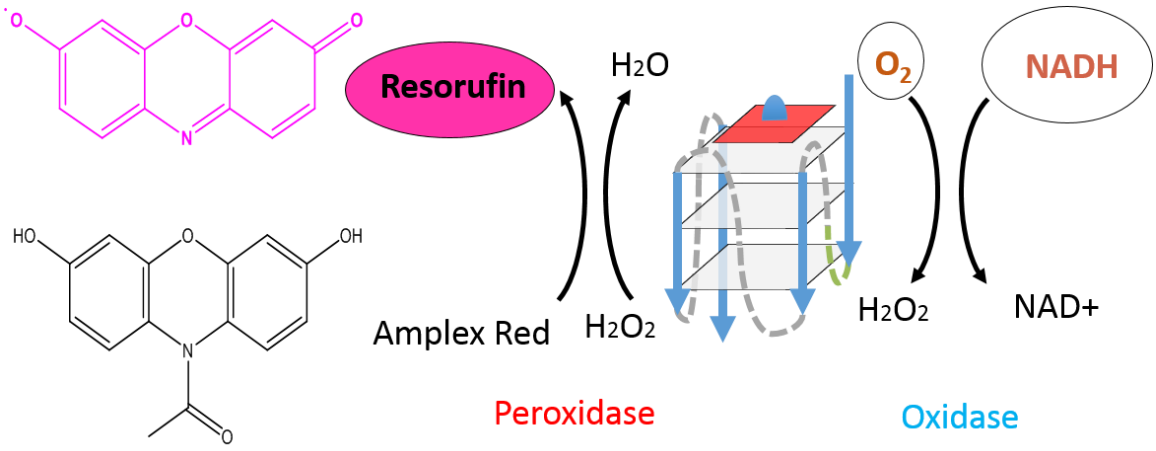


**Figure 1-30 The NADH oxidase activity; hemin•G-quadruplex complex (in the middle) catalyzes the oxidation of NADH by $O_2$ into $NAD^+$ and $H_2O_2$ respectively, and the associated oxidation of Amplex red into Resorufin.**

All these catalytic functions of hemin•G-quadruplex have found a versatile practical utility including chemical sensing using colorimetry, electrochemistry, and bioelectronics and the construction of molecular devices (130). An interesting different kind of utility that is typically associated with HRP is immunohistochemistry. Thirstrup and Baird (131) compared the relative tissue immuno-staining properties of PS2.M-hemin and HRP. These authors covalently linked the porphyrin and DNA, then used the conjugate for successful staining for the prostate-specific antigen (PSA) in human prostate tissue sections.

Among all these practical applications, though, what attracts us the most is the possible implications for hemin-DNAzymes and ribozymes in biology. The formation of RNA and DNA G-quadruplexes *in vivo* is a subject of significant current research interest: for example, a DNA G-quadruplex has been implicated in the pilin antigenic variation in *Neisseria gonorrheae* (132), and a diversity of mammalian DNA and RNA sequences ranging from oncogene promoters to chromosomal telomeres have also been postulated to form G-quadruplexes *in vivo* (133). On the basis of the oxidative catalysis of hemin-DNAzymes/ribozymes, we believe that such an activity could play regulatory roles in certain disease states as we shall see in chapter one of the thesis.

## 1.4. Thesis overview

The central theme of this thesis focuses on exploring the catalytic properties of hemin-DNAzyme/ribozymes with respect to three aspects; in biological, structural, and mechanistical matters.

Atamna *et al*. (134) state that in the cell, amino acids, peptides, and proteins are believed to transiently bind or “sequester” the newly synthesized heme. The pool of this transiently bound heme is referred to as “regulatory heme”. Given the evidence here of folded RNAs and DNAs that strongly bind heme, the likelihood of intracellular sequestering agents for regulatory heme including guanine-rich RNAs and DNAs. Regarding the deleterious effect of heme activation *in vivo*, a particularly interesting observation has been reported; that in Alzheimer’s disease patients, the toxic agent of the disease; amyloid-β peptide, both sequesters and binds heme (134, 135). Given this, it is possible to imagine that certain disease states accumulate an overabundance of guanine-rich transcripts in the cell. Such RNAs may then, in similar way to amyloid-β peptide, serve to sequester heme away from its optimal utilization in the cell, as well as promote harmful oxidative reactions that damage the cell.

In fact, the expansion of a $(G_4C_2)_n$ repeat within the human *C9orf72* gene has been causally linked to a number of neurodegenerative diseases, most notably familial amyotrophic lateral sclerosis (ALS) and frontotemporal dementia (FTD). Recent studies have shown that the repeat expansion alters gene function in many ways, disrupting the gene’s normal cellular roles and introducing toxic gain of function at the level of both DNA and RNA (74-76). $(G_4C_2)_n$ DNA, as well as the RNA transcribed from it, are found to fold into four-stranded G-quadruplex structures. It has been shown that the toxicity of the RNA G-quadruplexes, often localized in intracellular RNA foci, lies in their ability to sequester many important RNA binding proteins (136).

In Chapter 2, we propose that a distinct toxic property of such RNA and DNA G-quadruplexes from the *C9orf72* gene may arise from their ability to bind and oxidatively activate cellular heme. We showed that G-quadruplexes formed by both $(G_4C_2)_4$ RNA and DNA not only complex tightly with Fe(III)-heme but also enhance its intrinsic peroxidase and oxidase propensities. By contrast, the antisense $(C_4G_2)_4$ RNA and DNA neither bind

ferric heme nor influence its oxidative activity. Curiously, the ability of *C9orf72* DNA and transcripts to bind and activate heme mirror similar properties that have been reported for the Aβ peptide and its oligomers in Alzheimer's disease neurons. It is therefore conceivable that *C9orf72* RNA G-quadruplex tangles play roles in sequestering intracellular heme and promoting oxidative damage in ALS and FTD analogous to those proposed for Aβ peptide and its aggregates in Alzheimer's Disease. Given that neurodegenerative diseases in general are characterized by mitochondrial and respiratory malfunctions, the role of *C9orf72* DNA and RNA in heme sequestration as well as its inappropriate activation in ALS and FTD neurons may warrant examination.

Chapter 3 describes specific methodology as we wished to determine how heme/G4-DNAzymes structurally replicate the catalytic properties of hemoproteins. Towards this objective, we asked the following questions: does the nucleic acid matrix supply all the important proximal side coordination to the hemin iron ion? Is it possible that binding to any large aromatic surface, like a G-quartet, in itself activates hemin? Or that a G-quartet provides a specific interaction or coordination?

In this chapter, we investigated whether G-quadruplexes were strictly required for heme activation or whether related multistranded DNA/RNA structures such as isoguanine (iG) quadruplexes and pentaplexes could also bind and activate heme. We found that iG-pentaplexes did indeed bind and activate heme comparably to G-quadruplexes; however, iG-quadruplexes did not. Earlier structural and computational studies had suggested that while the geometry of backbone unconstrained, iG-quintets templated by cations such as $Na^+$ or $NH_4^+$ was planar, that of iG-quartets deviated from planarity (137-140). We hypothesize that the binding as well as activation of heme by DNA or RNA is strongly supported by the planarity of the nucleobase quartet or quintet that interacts directly with the hemin.

In Chapter 4, we investigated spectroscopically the reaction of hydrogen peroxide ($H_2O_2$) with ferric heme/G4-DNAzyme in presence or in absence of substrate. The goal was to identify possible transient intermediates forming and leading to the robust observed catalysis (1 e- peroxidation) as well as (2 e- preoxygenation) reactions. Preliminary EPR studies done by Travascio *et al*. on the reaction of the hemin-PS2.M complex without the

addition of substrate had revealed the formation of an organic radical that exhibit single EPR signal (115). Moreover, EPR spin-trapping experiments using nitroso spin trap (t-nitrosobutane MNP) indicated that a radical likely formed on the PS2.M nucleotides and not on the hemin group (115). In support of this, chemical-probing (footprinting) experiments on the reaction of hemin-PS2.M (115) as well as other hemin•G-quadruplex complexes with $H_2O_2$ as well as stronger oxidizing agent m-CPBA have shown guanines forming at the external quartets underwent oxidation to a base that is cleavable by piperidine treatment.

Peroxidases and monooxygenases produce a reactive intermediate, Compound I, whose reactions are controlled by the protein environment. First reported in the 1940s in peroxidase enzymes; Compound I formed rapidly from the reactions of ferric enzymes with hydrogen peroxide and other oxygen atom donors such as peracids (141). Because of the interrupted aromaticity of the porphyrin π-cation radical, Classic compound I is characterized by a Soret absorption band of diminished intensity compared to the Soret transitions of other heme states. The most thoroughly characterized Compound I is from horseradish peroxides, which is well established to be ferryl centre coupled to a porphyrin π-cation radical (92). However, in several peroxidases, most notably cytochrome c peroxidase, the initial species observed after addition of hydrogen peroxide to the ferric enzyme has a ferryl centre associated with an aromatic amino acid radical; a tryptophan radical in the case of Cytochrome c peroxidase. This state presumably results from a transient Compound I that oxidized the nearby aromatic amino acid residue. For cytochrome c peroxidase, this derivative will be named Compound I' to distinguish it from the classic Compound I, the porphyrin-based radical cation (142). With fully aromatic porphyrin ring, the extinction coefficient of the Soret band of Cytochrome c peroxidase Compound ES is undiminished and looks like compound II; a second intermediate results from 1-electron reduction step of Compound I, and characterized as a ferryl heme without a poprphyrin π-cation radical. Numerous other heme-containing peroxidase and globin proteins have been found to form Compound I'-like derivatives with either tyrosyl or tryptophanyl radicals in conjunction with the ferryl heme center. Compound I'-like heme state have been reported for myoglobin (143), P450cam (144, 145), as well as for the H42L horseradish peroxidase mutant (146).

On the basis of hemoprotein literature, and Travascio's work, we wished to further investigate the possibility of the formation of any of these intermediates (compound I, Compound I', or compound II) with the aid of rapid scan stopped-flow spectroscopy and the Pro-KIV software available from applied photophysics. Our data reveals that the activated species in heme/G4-DNAzymes is equivalent to Compound I'-like species formed during hemoproteins' oxidation reactions consisting of a ferryl Fe(IV)=O porphyrin and a protein radical site. In the system of hemin-DNAzyme, the radical site is more likely to be on a guanine base, thus, the activated intermediate can be described as ferryl Fe(IV)=O porphyrin coupled to a guanine cation radical.

Finally, in Chapter 5, I summarized and suggested some future directions regards the heme/G4-DNAzymes and ribozymes system.

# Chapter 2.

# Expanded hexanucleotide repeat RNA and DNA from the neurodegenerative disease-linked *C9orf72* gene Binds heme and enhance its oxidative activity

The work described in this chapter is a collaboration with Dr. Jason Grigg who is now a Postdoctoral Fellow in Dr. Michael Murphy's lab at University of British Columbia. He had worked for my doctoral supervisor, Dr. Dipankar Sen, at Simon Fraser University, as a Postdoctoral Fellow for one year. Most of the data shown here was his work and I helped in data analysis including fitting the binding curves and calculating the dissociation constants. Also, I performed some of the Amplex red oxidation reactions by heme/G4-DNAzymes; particularly the ones initiated by $H_2O_2$ and molecular oxygen that are shown in figure 2-6. This work has been published and can be found in:

Grigg, J. C., Shumayrikh, N., & Sen, D. (2014), PLoS One, 9(9), e106449. doi:10.1371/journal.pone.0106449

## 2.1 Introduction

Amyotrophic lateral sclerosis (ALS or Lou Gehrig's Disease) and frontotemporal dementia (FTD) are both serious and significant neurological diseases that appear to have familial forms as well as arising sporadically within populations (147). Recently, an abnormal expansion of a repeating GGGGCC sequence in the DNA of the *C9orf72* gene was identified in patients with the familial forms of these diseases, but also in a proportion of patients with the sporadic diseases (74, 76, 147). This repeat expansion has also been reported in the brains of certain patients of depressive pseudodementia (148), Huntington disease (149), hippocampal sclerosis dementia (150), and non-fluent aphasia (151). A number of studies have provided insight into how this repeat expansion, at the level of both RNA and DNA, may contribute to ALS and FTD. A circular dichroism and NMR study by Fratta *et al.* (152) showed that the 'minimal' repeat sequence [r-$(G_4C_2)_3G_4C$, termed ''C9Gru''] from *C9orf72* RNA forms an intramolecular, parallel-stranded, G-quadruplex fold

in the presence of $K^+$ ions. A subsequent study by Reddy *et al.* (153) showed that longer repeats of $r(G_4C_2)_4$ could also form irregular intermolecular multimers, which were proposed to correspond to intranuclear RNA foci observed in ALS neurons. Most recently, a broad-ranging study by Haeusler *et al.* (154) defined a conceptual framework in which multiple roles for this hexanucleotide repeat expansion in disease were invoked. Working with DNA and RNA oligomers corresponding to various pieces of the repeat, Haeusler et al. (154) showed that both the DNA and RNA form highly stable G-quadruplex folds (133, 155, 156). It was proposed that both gain-of-function and loss-of-function toxicity could be linked to repeat expansion within *C9orf72*, at the level of gene (DNA) as well as transcript (RNA). Loss of function at the DNA level could be manifested in poor transcription of *C9orf72*, owing to formation of G-quadruplexes in the gene itself. Loss of function at the RNA level likely occurs from a dearth of the *C9orf72* gene product, owing to inefficient translation of repeat expanded transcripts folded into stable G-quadruplexes. Gain of function can be contemplated at the level of G-quadruplex-folded *C9orf72* transcripts: (i) sequestering essential RNA-interacting binding proteins, including splicing factors such as ASF/SF2 and hnRNPA1, and nucleolin (see figure 2-1); and (ii) from the potential synthesis of toxic dipeptides from the repeat GGGGCC motifs within the transcript (154, 157). Most notably, Haeusler *et al* (154) reported a deep proteomic analysis of the cellular proteins sequestered away by the *C9orf72* transcript-containing RNA foci. There were 288 proteins identified in the pull-downs, including nucleolin and heterogeneous nuclear ribonucleoprotein (hnRNP) U, which showed specificity for the G-quadruplex. G-quadruplexes provide excellent binding surfaces for a variety of large- and small-molecule ligands (158, 159).

Our lab first showed that the ubiquitous cellular cofactor, ferric heme [Fe(III)-protoporphyrin IX], binds tightly to some but not all G-quadruplexes (10, 12) with dissociation constant ($K_d$) values as low as 10 nM (107). The most remarkable property of such G-quadruplex•heme complexes (invariably containing parallel or partially parallel stranded quadruplexes), however, is that the DNA/RNA activates the bound heme for enhanced oxidative activity frequently to the levels of heme-utilizing proteinaceous enzymes such as peroxidases, peroxygenases, and monooxygenases (11, 12, 107). In the presence of low concentrations of oxidizing agents such as hydrogen peroxide, or molecular oxygen aided by cellular reducing agents such as NADH (129) or ascorbate, G-

quadruplex•heme complexes catalyze robust one-electron (peroxidase) as well as two-electron (peroxygenase and monooxygenase) oxidation reactions (106). In the following introductory sections, we will provide the reader, first, with some information on *C9orf72* gene, and second on heme disturbances pertinent to neuronal cells followed by chapter overview.

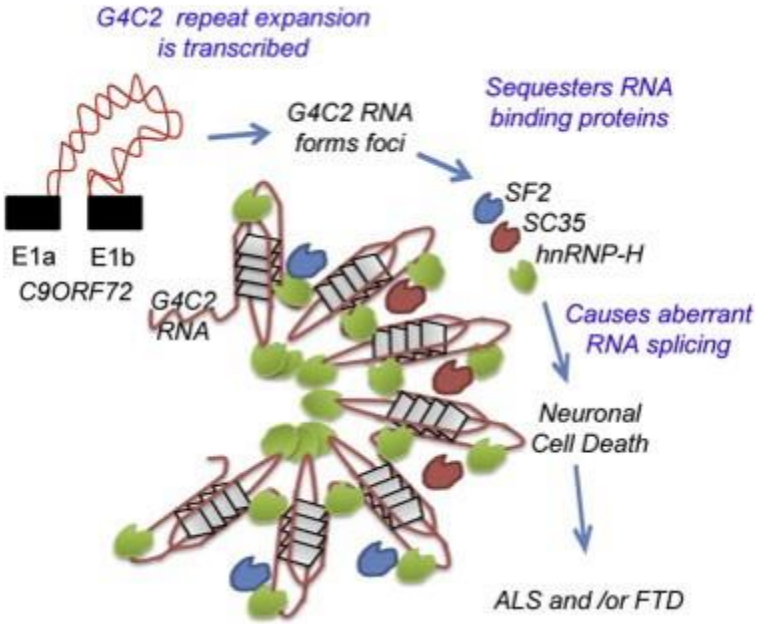


**Figure 2-1 A graphical illustration shows $G_4C_2$ RNA toxicity and protein sequestration disrupting RNA processing and contributing to neurodegeneration. Adapted from (160).**

### 2.1.1 *C9orf72*

*C9orf72* is a protein which in humans is encoded by the gene *C9orf72 (chromosome 9 open reading frame 72)*. The human *C9orf72* gene is located on the short (p) arm of chromosome 9 open reading frame 72, from base pair 27, 546, 542 to base pair 27,573, 863. Its cytogenetic location is at 9p21.2 see figure (2.2). The protein is found in many regions of the brain, in the cytoplasm of neurons as well as in presynaptic terminals. This area is important for sending and receiving signals between neurons. The mutation of *C9orf72* gene is a hexanucleotide repeat expansion of the six string of nucleotides GGGGCC (161). In a healthyl person, there are few repeats of this hexanucleotide, typically less than 20-30, but in people with the mutation, the repeat can occur in the order of hundreds and this is known as the hexanucleotide repeat expansion mutation (162).

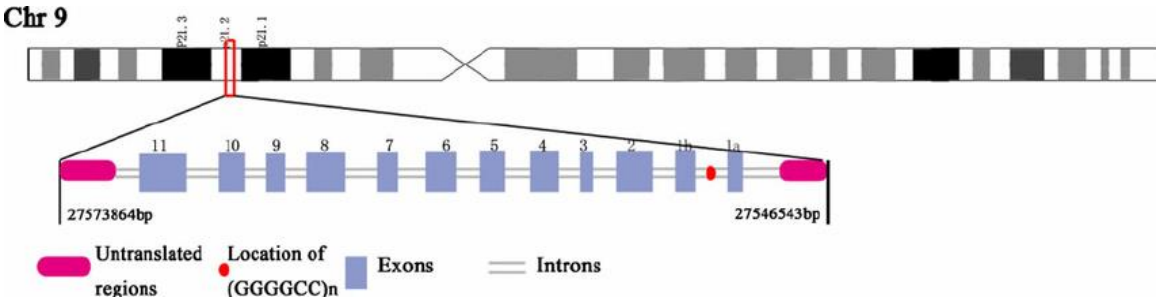


**Figure 2-2 Cytogenetic location of *C9orf72* gene; 9p21.2 which is the short (p) arm of the chromosome 9 at position 21.2. Adapted from (163).**

### 2.1.2 Heme disturbances relevant to neuronal cells

The biosynthesis and regulation of heme in the brain itself has received more attention now since many critically important oxidative biotransformation and signaling processes occur there. The brain has lower, but significant heme content than the liver (table 2-1), but has a higher metabolic rate and higher affinity for oxygen than liver tissue (164). Because of its high rate of oxygen consumption and its high content of polyunsaturated fatty acids, the brain exhibits increased vulnerability to oxidative stress.

One of the neurodegenerative disorder connected with heme deficiency in the brain is Alzheimer's disease (AD). AD is an age-related disorder characterized by synaptic loss and neuronal cell death and manifested clinically by progressive cognitive dysfunction and memory loss (165). The pathological hallmarks of AD are the aggregation of amyloid-β- peptide; formation of neurofibrillary tangles and selective synaptic and neuronal loss in the brain regions involved in learning and memory. Elevated lipid peroxidation in the brain of AD patients reflects induction of oxidative stress (166), which then causes secondary effects such as protein modification, oxidation, and conformational changes (167). Disruption in the metabolism of iron as well as iron-induced oxidative stress has been postulated to play a role in the pathogenesis of AD [reviewed by Altamura and Muckenthaler (168)]. Heme is a common factor linking several perturbations in AD, including those associated with iron metabolism, mitochondrial complex IV, heme oxygenase, and bilirubin. Atamna and colleagues showed that chemical-induced heme deficiency results in a selective decrease in mitocondireal complex V that leads to oxidative stress in neuronal cell lines and primary hippocampal neurons (169), and

suggested that functional deficiency of heme, and also storage of heme a, particularly, causes mitochondrial and neuronal decay of aging (170).

The metabolic consequences resulting from heme deficiency seemed similar to that in dysfunctional neurons in patients with AD and following work demonstrated heme binding to amyloid-β (135, 171). Interaction of heme with amyloid-β *in vitro* was examined further and confirmed by spectral analysis which outlined the possible mechanism of heme depletion due to binding to amyloid-β (171). Furthermore, the differential affinity of heme binding to human and rodent amyloid-β peptide was reported and the authors suggested that this explains the susceptibility of human to AD (135). Homodimerization of amyloid precursor protein and amyloid-β has been also reported previously as a factor implicated in the amyloidogenic pathway of AD (172). Howlett and co-workers reported the inhibitory effect of heme on amyloid-β aggregation as well as amelioration of amyloid-β aggregation-dependent cell toxicity *in vitro* (173). On the other hand, the heme-amyloid-β complex has a peroxidase activity in *vitro* that may contribute to the neurotoxicity in the cytopathology of the disease (174). Sequestration of heme in these complexes may result in functional heme deficiency and cause mitochondrial dysfunction.

**Table 2-1 Comparison of heme concentrations in mouse brain fractions, kidney, and liver. From (78).**

| Tissue | Heme content | |
|---|---|---|
| | *pmol/mg tissue* | *% of liver value* |
| Liver | 7.09 ± 0.78 | 100 ± 11 |
| Kidney | 2.68 ± 0.38 | 37.7 ± 5.3 |
| Brain olfactory bulb | 2.81 ± 0.13 | 39.6 ± 1.8 |
| Brain cortex | 2.35 ± 0.58 | 33.1 ± 8.2 |
| Brain subcortical white matter | 2.27 ± 0.03 | 32 ± 0.4 |

## 2.2 Chapter Overview

ALS and neurodegenerative diseases in general are characterized, among other things, by (a) respiratory/mitochondrial dysfunction, and (b) general oxidative stress. It has recently been reported that the Aβ peptide, thought to be the causal agent of Alzheimer's disease, both binds and activates heme towards oxidative activity (134, 175). These remarkable observations have led to proposals that sequestration of heme by Aβ peptide tangles may, on one hand, constitute a ''loss of function'' for cellular respiratory/mitochondrial activity, but also an oxidative ''gain of function'' by way of Aβ-bound heme activation (175). Given that in *C9orf72*-impacted diseases both the DNA and RNA corresponding to the hexanucleotide repeat expansion fold into G-quadruplexes, we investigated whether such G-quadruplexes also binds heme, concomitantly activating the bound heme towards accelerated oxidative activity.

## 2.3 Materials and methods

### 2.3.1 Materials

All DNA and RNA oligonucleotides were purchased from University Core DNA Services (University of Calgary), purified with standard desalting and gel purification methods. Sequences are listed in Table 2-2. Oligos were dissolved in 10 mM Tris-EDTA buffer (10 mM Tris pH 7.5, 0.1 mM ethylenediaminetetraactetate (EDTA)) and frozen at 20°C until needed. Hemin was purchased from Frontier Scientific (Logan, UT, USA). Amplex red was purchased from (Santa Cruz Biotechnology Inc., Dallas, TX, USA). All other chemicals were purchased from Sigma-Aldrich.

**Table 2-2 Oligonucleotide sequences used in this study. RNA sequences have an ''r'' prefix and DNA sequences have a ''d'' prefix.**

| Name | Sequence |
|---|---|
| $r(G_4C_2)_4$ | 5' – GGGGCCGGGGCCGGGGCCGGGGC – 3' |
| $r(C_4G2)_4$ | 5' – GGCCCCGGCCCCGGCCCCGGCCCC – 3' |
| $d(G_4C2)_4$ | 5' – GGGGCCGGGGCCGGGGCCGGGGC – 3' |
| $d(C_4G2)_4$ | 5' – GGCCCCGGCCCCGGCCCCGGCCCC – 3' |
| CatG4 | 5' – TGGGTAGGGCGGGTTGGGAAA – 3' |

### 2.3.2 Circular dichroism spectroscopy of $r(G_4C_2)_4$ and $d(G_4C_2)_4$ repeats in presence of potassium salt

DNA and RNA solutions (25 µM) were prepared in 25 mM Tris, pH 7.5. Samples were heated at 95°C for 5 minutes, removed from heat and allowed to cool to room temperature. CD spectra were obtained using a Jasco J-810 CD spectrometer with a 1 mm pathlength cuvette at 21 °C. Scans were recorded over the 200–320 nm wavelength range and averaged from three scans recorded at a scan rate of 100 nm/min with a 1 nm bandwidth. Potassium chloride was added directly from a stock solution to the sample in question. The sample was then incubated at 21°C until equilibrium had been reached and no further change in the spectrum was observed (~10 minutes).

### 2.3.3 UV-Vis heme binding assay

UV/Vis spectra were obtained using a Cary 100 UV/Vis spectrophotometer. Hemin stock solutions were freshly prepared at 10 mM in 0.1 M potassium hydroxide. Hemin was diluted to 0.5 µM in 40 mM HEPES-$NH_4OH$, pH 8.0, 20 mM KCl, 1% dimethyl formamide (DMF), 0.05% Triton X-100. Quadruplex DNA or RNA (25 µM) was prepared in the same buffer by heating at 95 °C for 5 minutes and cooling to room temperature. Hemin solutions were titrated with RNA and DNA (0–20 µM) and allowed to incubate for at least one hour at 20 °C before recording spectra. Dissociation constants ($K_d$) were determined using the following equation as described by Wang *et. al* (176):

$$[DNA]_0 = K_d\,(A - A_0)/(A_\infty - A) + [P_0]\,(A - A_0)/(A_\infty - A_0).$$

Where $[DNA]_0$ is the initial concentration of DNA; $[P_0]$ is the initial concentration of monomeric heme; $A_\infty$, $A_0$, and A represent heme absorbance at saturation DNA concentrations, in absence of DNA, and in presence of variable DNA concentrations respectively.

### 2.3.4 ABTS peroxidation assay

Quadruplex solutions were prepared as described for the heme binding experiments, in two buffers: 40 mM HEPES, pH 8.0, 20 mM potassium chloride, 1% N,N-

dimethylformamide, 0.05% Triton X-100 ($NH_4OH$-HEPES buffer); and, 25 mM Tris-Cl, pH 8.0, 20 mM potassium chloride, 1% N,N-dimethylformamide (DMF), 0.05% Triton X-100 (Tris buffer). Peroxidase reactions were set up with 10 µM DNA/RNA G-quadruplex, 0.1 µM heme, 1 mM 2,2'-azino-bis(3-ethylbenzothiazoline-6-sulphonic acid) (ABTS) and 0-5 mM hydrogen peroxide. The reaction was initiated by addition of varying amounts of peroxide and monitored by following absorbance at 414 nm.

### 2.3.5 Oxidase activity assay

Quadruplex solutions were prepared as described for the heme binding experiments, in 40 mM HEPES-$NH_4OH$, pH 8.0, 20 mM potassium chloride, 1% DMF, 0.05% Triton X-100. Reactions were performed in the same buffer supplemented with 10 µM DNA/RNA G-quadruplex and 1 µM heme. Amplex red was added to 0.1 mM, and the solutions were incubated at room temperature for 30 minutes. Reductant [1 mM reduced β-nicotinamide adenine dinucleotide (NADH), 1 mM ascorbate] or 0.1 mM hydrogen peroxide were then added to the sample and incubated in the dark, at room temperature. Samples were photographed at intervals from 0–24 hrs. To verify that the color changes observed were a result of resorufin production, final absorption spectra were recorded on a Cary 100 UV/Vis spectrophotometer.

## 2.4 Results

### 2.4.1 $(G_4C_2)_4$ but not $(C_4G_2)_4$ DNA and RNA fold into G-quadruplexes in the presence of $K^+$ ions

Circular dichroism was used to investigate secondary structure formation by the four oligonucleotides, $d(G_4C_2)_4$, $r(G_4C_2)_4$, $d(C_4G_2)_4$, and $r(C_4G_2)_4$**.** Figure 2.3 shows the data. The CD spectrum of each oligonucleotide, at 25 µM concentration, was examined in solution in 25 mM Tris, pH 7.5 (grey lines, Figure 2-3), as well as in 25 mM Tris, pH 7.5, 100 mM KCl (black lines, Figure 2-3). Panels B and D show that both $r(C_4G_2)_4$ and $d(C_4G_2)_4$ give CD spectra that do not change upon the addition of potassium, suggesting their likely single-stranded/Watson-Crick duplex composite structures are unchanged with or without KCl. Panels A and C, however, show that both $r(G_4C_2)_4$, and $d(G_4C_2)_4$ show characteristic

features of G-quadruplex formation. Thus, r($G_4C_2$)$_4$ shows an enhanced positive peak at 260 nm and a negative peak at ~240 nm. These are consistent with its forming a parallel-stranded quadruplex, consistent with earlier reports (152-154), and also with the requirement that RNA G-quadruplexes be parallel-stranded. The DNA oligomer, d($C_4G_2$)$_4$, shows a major positive peak at 295 nm and a lesser one at 260 nm, as well as a negative peak at ~235 nm. Such a spectrum is consistent with the formation of a conformer mixture of G-quadruplexes of both antiparallel (positive peak at 295 nm) and parallel (positive peak at 260 nm) strand orientation. The formation of such a conformer mixture is consistent with the known polymorphism of DNA G-quadruplexes, whereby the formation of a given fold is acutely sensitive to DNA sequence, concentration, as well as to salt identity and concentration. In a recent study Haeusler *et al.* (154) reported that d($G_4C_2$)$_4$, at a much lower DNA concentration (4 μM) than the 25 μM used in this study formed primarily an antiparallel quadruplex; however, they also found that the CD spectra of oligomers in the series d($G_4C_2$)$_n$, where n = 3, 6, or 10, gave $K^+$-generated parallel/antiparallel conformer mixtures with composite CD spectra similar to that shown in figure 2-3, panel A. Our data and those of Haeusler *et al.*(154), are therefore not mutually inconsistent.

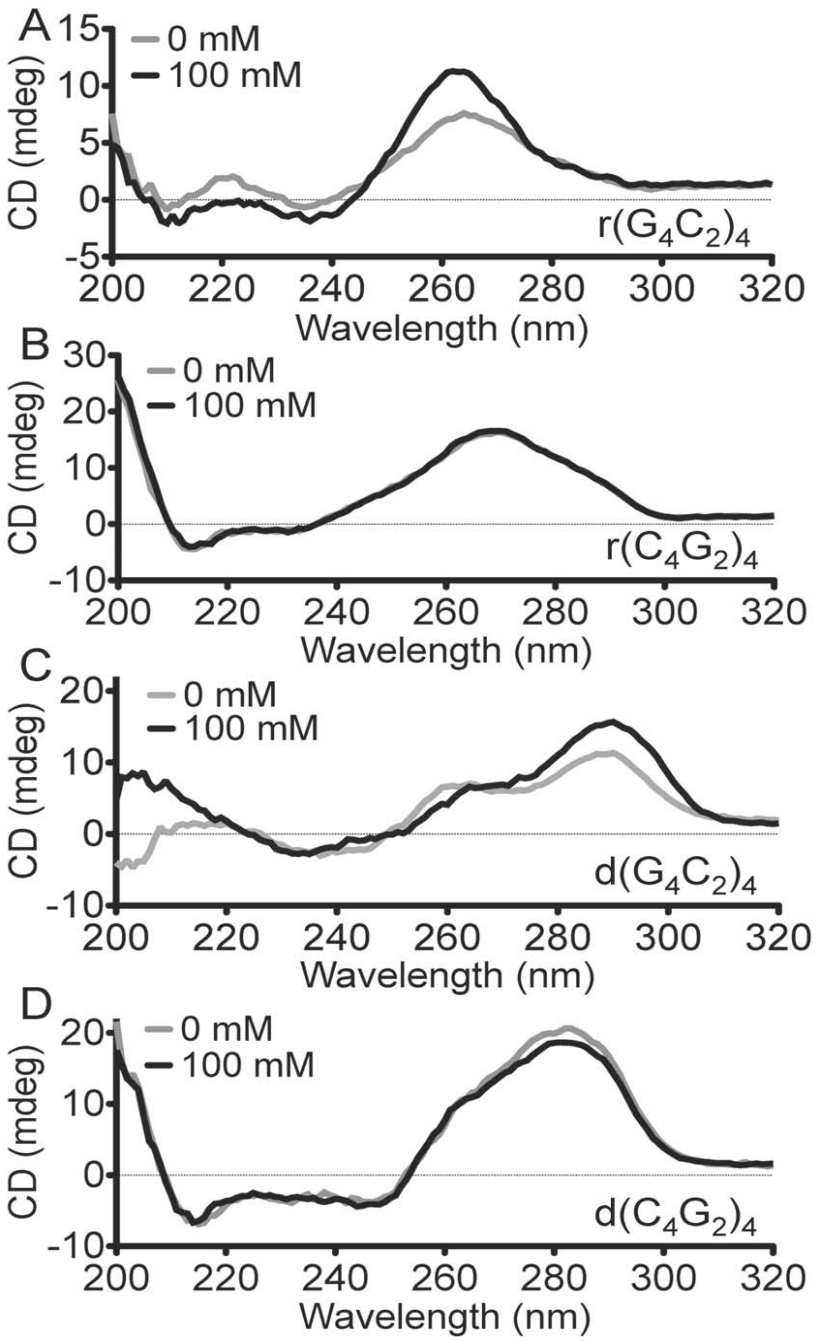


**Figure 2-3** **G-repeat expansion RNA and DNA form G-quadruplexes in the presence of potassium. UV Circular Dichroism spectra of (A) $r(G_4C_2)_4$, (B) $r(C_4G_2)_4$, (C) $d(G_4C_2)_4$, and (D) $d(C_4G_2)_4$ in 25 mM Tris, pH 7.5, in the presence of either 0 mM or 100 mM KCl.**

### 2.4.2 G-quadruplexes formed by $d(G_4C_2)_4$ and $r(G_4C_2)_4$ bind heme

We carried out UV-vis spectroscopy experiments to investigate whether, in the presence of $K^+$, the four oligonucleotides, $d(G_4C_2)_4$, $r(G_4C_2)_4$, $d(C_4G_2)_4$, and $r(C_4G_2)_4$, bind heme. We in the Sen lab, and others, had previously reported that many G-quadruplexes, particularly those with parallel or mixed parallel/antiparallel strand orientations, complexed strongly with heme (107, 177, 178). The salient spectroscopic characteristics of heme binding by G-quadruplexes (in experiments in which a fixed heme concentration is titrated with increasing concentrations of G-quadruplex) are (a) a large hyperchromicity as well as red-shift (from 398 nm to 402–404 nm) of the dominant Soret absorption peak of the heme, and (b) characteristic changes in the heme visible spectra. Cumulatively, these features of G-quadruplex•heme complexes strongly resemble the spectroscopic features of the bound heme within natural hemoenzymes such as metmyoglobin and horseradish peroxidase (HRP) (12). Figure 2-4, panels A–D, show the effect of titrating 0–20 mM of $d(G_4C_2)_4$, $r(G_4C_2)_4$, $d(C_4G_2)_4$, or $r(C_4G_2)_4$ into a buffered HEPES-$NH_4OH$ solution (pH 8.0) with 0.5 mM heme and 20 mM $K^+$. A known parallel G-quadruplex forming DNA, CatG4 (5′-TGG GTA GGG CGG GTT GGG AAA-3′), was separately examined as a positive control, under identical conditions (panel E). It is evident that $d(G_4C_2)_4$, $r(G_4C_2)_4$, as well as CatG4 (panels A, B, and E) show the Soret peak hyperchromicity and red-shift features that are indicative of heme-binding by these oligonucleotides. The plots in panel F of Figure 2 reveal that the repeat expansion RNA oligonucleotide, $r(G_4C_2)_4$, binds heme with a dissociation constant, $K_d$, of 3 μM. $d(G_4C_2)_4$ also binds heme, albeit with a weaker affinity than its RNA counterpart. This was expected because $d(G_4C_2)_4$ forms antiparallel or mixture hybrid G4 structures while $r(G_4C_2)_4$ forms a parallel G4 structure, as discussed in section 2.4.1. By comparison, the known parallel-stranded DNA G quadruplex, CatG4, binds heme strongly ($K_d$ < 0.5 μM). In contrast to the above three G-rich oligonucleotides the two cytosine-rich oligonucleotides, $d(C_4G_2)_4$ and $r(C_4G_2)_4$, show none of the characteristic spectroscopic features of heme binding.

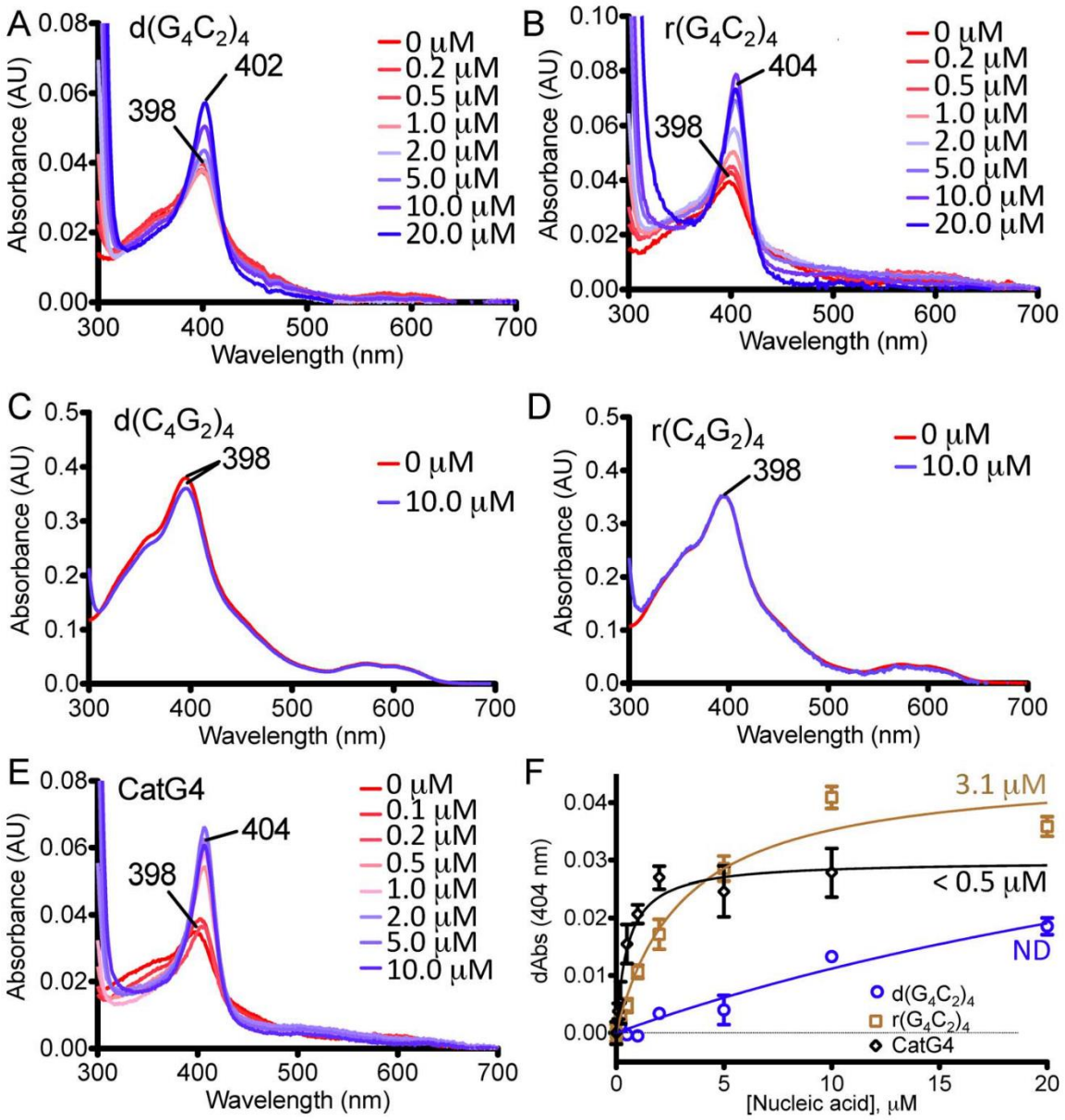


**Figure 2-4** **G-repeat expansion RNA and DNA bind heme. UV-visible spectroscopy of fixed concentrations of heme (0.5 μM) titrated and equilibrated with progressively increasing concentrations of DNA/RNA. (A) $d(G_4C_2)_4$, (B) $r(G_4C_2)_4$, (C) $d(C_4G_2)_4$, (D) $r(C_4G_2)_4$, (E) CatG4. Panel F shows plots of $A_{404nm}$ from each of the plots shown in (A)–(E), as functions of the DNA/RNA concentration.**

### 2.4.3 Complexes of heme with $d(G_4C_2)_4$ and $r(G_4C_2)_4$ show enhanced peroxidase activity

Our original discovery that some G-quadruplexes complexed strongly with heme (10, 12) came with an unexpected corollary: such complexes showed a $10^2$–$10^3$-fold, G-quadruplex-enhanced, peroxidase (one-electron oxidation) activity over the low intrinsic peroxidase activity of monomeric heme. In the presence of micromolar to millimolar concentrations of hydrogen peroxide and a chromogenic reducing substrate, such as 2,2′-azino-bis(3-ethylbenzothiazoline-6-sulphonic acid) (ABTS), heme•G-quadruplex complexes show vigorous oxidation of the colorless ABTS to generate the green $ABTS^{\bullet+}$ radical cation species. This specifically G-quadruplex-enhanced peroxidase activity of the bound heme requires only a buffered solution containing $K^+$ ions; however optimal activity is enabled by the presence, in addition to $K^+$ , of $NH_4^+$ (12) or intracellular amines such as putrescine, spermidine or, especially, spermine (179). Figure 2-5 plots the measured peroxidase activities of heme (reported as $k_{obs}$ values), in the presence of the four *C9orf72*-related oligomers, as functions of hydrogen peroxide concentration. Figure 2-5, panel A, shows peroxidation rates in the optimal buffer (10 mM DNA/RNA and 0.1 μM heme in 40 mM HEPES-$NH_4OH$, pH 8.0, 20 mM potassium chloride, 1% DMF, 0.05% Triton X-100). Under these conditions, it can be seen that heme in the two C-rich oligomers [$r(C_4G_2)_4$ and $d(C_4G_2)_4$] solutions show no detectable peroxidase activity. Heme complexed with the two G-rich oligomers, $r(G_4C_2)_4$ and $d(G_4C_2)_4$, however, both show substantial peroxidase activity; the DNA•heme complex greater than the RNA•heme complex. Figure 2-5, panel B, shows the peroxidation activities of the above DNA/RNA•heme complexes in the potassium-only buffer solution (25 mM Tris-Cl, pH 8.0, 20 mM KCl, 1% DMF, 0.05% Triton X-100). Here, too (though the overall peroxidation rate constants are lower than in the optimal HEPES-$NH_4$ buffer) the same qualitative patterns are observed; the C-rich oligomers do not activate the heme towards peroxidase activity, whereas the G-rich oligomers do. Interestingly, in the Tris/potassium buffer the G rich oligomers, $r(G_4C_2)_4$ and $d(G_4C_2)_4$, activate their complexed heme moiety to approximately the same degree. It is worth mentioning here that although the RNA•heme complex exhibited stronger binding affinity than the DNA version, the peroxidase activity of the latter found to be greater in HEPES-$NH_4OH$ buffer. Ammonium ions not only help stabilizing the G4 structures, but also promote the acid-base catalysis; leading to the cleavage of the O-O hydroperoxide

complex. Overall, the data shown in figure 2-5 A suggest that the acid-base catalysis played by $NH_4^+$ using the DNA•heme complex is more effective than in the case of the RNA•heme complex.

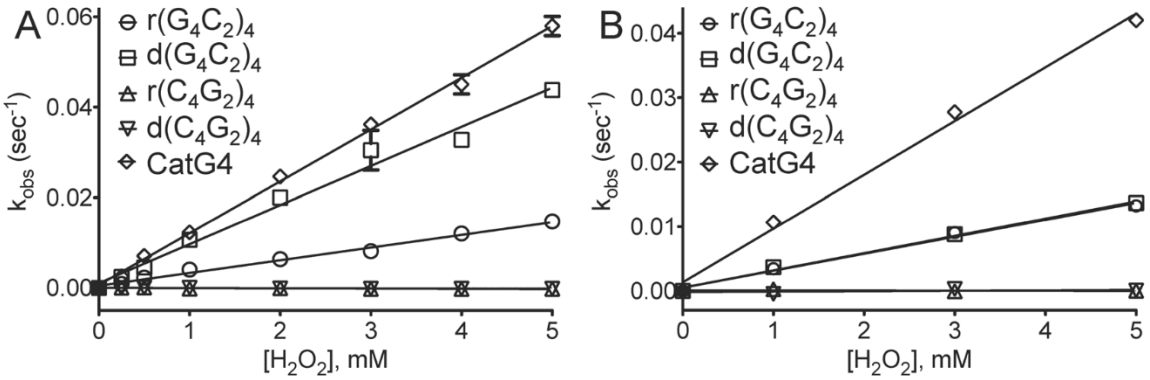


**Figure 2-5** ***C9orf72*** **repeat DNA and RNA catalyze peroxidase reactions. $k_{obs}$ values for peroxidation reactions made up of 10 mM DNA/RNA, 0.1 µM heme, 1 mM ABTS and varied hydrogen peroxide concentrations from 0-5 mM. Panel A reactions were carried out in HEPES-$NH_4$ buffer (40 mM HEPES, pH 8.0, 20 mM potassium chloride, 1% N,N dimethylformamide, 0.05% Triton X-100); and, Panel B reactions were carried out in Tris buffer (25 mM Tris-HCl, pH 8.0, 20 mM potassium chloride, 1% N,N-dimethylformamide, 0.05% Triton X-100).**

### 2.4.4 $d(G_4C_2)_4$•heme and $r(G_4C_2)_4$•heme complexes also display enhanced oxidase activity

The above peroxidase activity displayed by the heme complexes of $r(G_4C_2)_4$ and $d(G_4C_2)_4$ depends on the availability of hydrogen peroxide. However, some G-quadruplexes complexed with heme have also been reported to display an oxidase activity, whereby they can harness ambient dioxygen ($O_2$) gas in the presence of the cellular reductant, nicotine adenine dinucleotide (NADH) (129). NADH oxidase catalyzes the oxidation of NADH by $O_2$ with the concomitant formation of $H_2O_2$ (180). The present system consists of reduced nicotinamide adenine dinucleotide (NADH), heme/G-quadruplex, and Amplex Red as a reporter dye. Under aerobic conditions, NADH is oxidized to $NAD^+$, while Amplex Red is oxidized to Resorufin (see figure 1-31). Willner & *et al.* suggested a mechanism for the DNAzyme-catalyzed oxidation of NADH according to the scheme shown in figure 2-6.

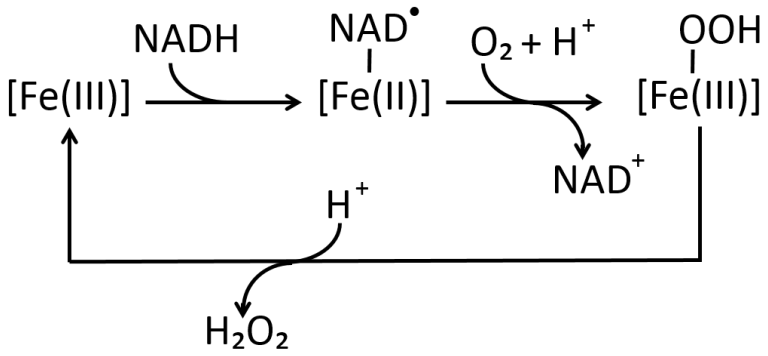


**Figure 2-6 Suggested mechanism for the heme/G4-DNAzyme catalyzing the oxidation of NADH. Based on (129).**

We investigated whether the *C9orf72* repeat expansion-linked DNA and RNA sequences were capable of utilizing heme and ambient oxygen to manifest an oxidase activity. We also investigated whether a different cellular reductant, ascorbate, could take the place of NADH in this reaction. A particularly sensitive means for monitoring oxidase reactions is via the oxidative deacetylation of a fluorogenic substrate, Amplex Red, to a bright pink product; resorufin. Figure 2-6, panel A, shows time-lapse photographs of reactions containing Amplex Red, 10 µM oligonucleotide and 1 µM heme in $NH_4$-HEPES buffer containing potassium chloride (*vide infra*) supplemented with 1 mM of ascorbate or NADH, or 0.1 mM hydrogen peroxide as a control. In reactions containing $r(G_4C_2)_4$ and $d(G_4C_2)_4$, or the control DNA G-quadruplex, CatG4, colour appears rapidly (1 min) in the presence of hydrogen peroxide, and within 90 min - 20 hrs in the presence of NADH or ascorbate. No colour is seen in these DNA solutions in the absence of any added reductant (labeled as ‘‘None’’). In reactions incorporating the C-rich oligonucleotides, $r(C_4G_2)_4$ and $d(C_4G_2)_4$, or in a solution where no oligonucleotide is present, no resorufin colour develops in the reactions containing NADH, ascorbate, or no added reductant; and, appears relatively slowly (1–90 min) with hydrogen peroxide. That the observed pink colour in all of the above experiments does correspond to resorufin is confirmed in the spectra shown in figure 2-6, panel B (the resorufin absorption peaks at 570 nm).

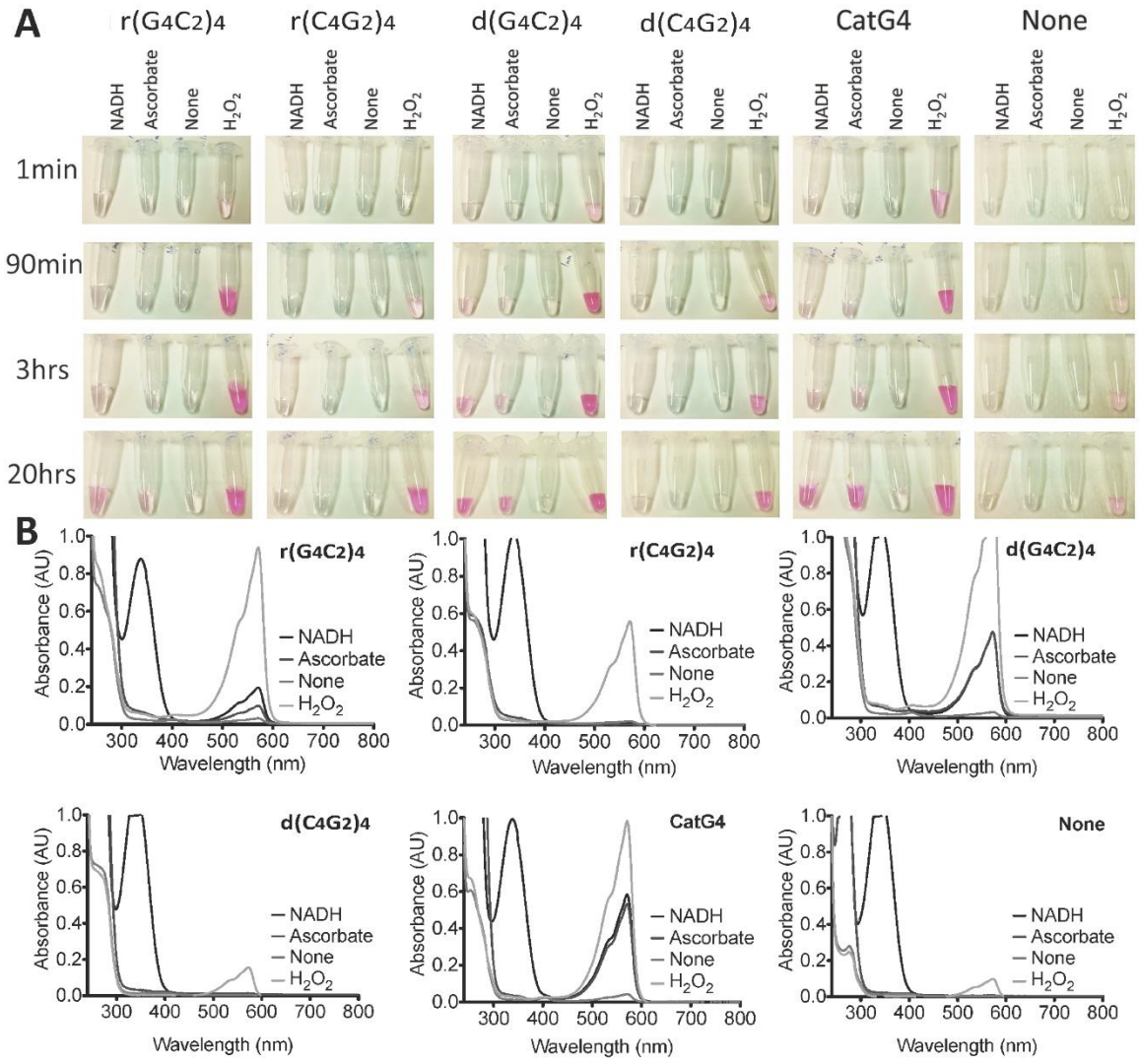


**Figure 2-7** ***C9orf72*** **repeat DNA and RNA catalyze oxidase reactions with NADH and ascorbate. (A) A photographic record of the oxidase activity of different DNA/RNA solutions in the presence of heme. Amplex Red oxidation to resorufin produces an intense pink color. Each solution containing DNA/RNA (10 μM) and heme (1 μM) was incubated with 1 mM Amplex Red in the presence of NADH or Ascorbate (1 mM), the absence of a reductant or hydrogen peroxide (0.1 mM). (B) UV/Vis spectra for samples from panel A at 24 hrs showing characteristic spectra for resorufin ($\lambda_{max}$ ~570 nm).**

## 2.5 Discussion

A major underpinning of the postulated gain of function by the repeat expanded *C9orf72* gene in familial ALS and FTD is the formation of G-quadruplexes by the G-rich transcript. It has been convincingly shown that RNA G quadruplexes and their aggregates, as found in the intracellular RNA foci, are efficient binders of a variety of cellular proteins, and likely serve to sequester away such proteins from their natural functions within the cell. Here, we hypothesize an additional pair of ‘‘gain of function’’ attributes for such RNA G-quadruplexes in ALS, FTD, as well as the other diseases linked to the repeat expansion of the *C9orf72* gene (154). In this study, we have shown that G quadruplexes formed by both the RNA and the single-stranded, ‘‘sense’’ strand of DNA from the *C9orf72* repeat expansion (a) bind heme with sufficient affinity to possibly sequester heme away from key cellular (chiefly, mitochondrial and respiratory) functions; and (b) these RNA and DNA G-quadruplexes serve to chemically activate the bound heme towards catalyzing oxidative reactions, using either hydrogen peroxide or naturally dissolved oxygen as oxidant. Both the G-quadruplex mediated sequestration and activation of heme reported herein occur under physiologically plausible conditions, in terms of solution components, salt, temperature and pH. Furthermore, the neurons from a broad spectrum of neurodegenerative diseases have been found to be significantly enriched with reactive oxygen species (ROS), including hydrogen peroxide, relative to unaffected neurons (181, 182). Thus, repeat expansion RNA/DNA-sequestered heme may threaten the local cellular environment of ALS and FTD neurons with enhanced oxidative damage. Indeed, this is the first proposal of a role in human disease for the heme binding and activating propensities of G-rich nucleic acids. It has been estimated that in normally functioning human cells there exist, 300,000 DNA motifs potentially capable of folding to G-quadruplexes (183). However, whatever proportion of these actually do fold to G-quadruplexes may play a constitutive role in the normal trafficking of, especially, regulatory heme (175) from the mitochondria to other loci within the cell. By contrast, the profuse generation of RNA transcripts from the hexanucleotide-expanded *C9orf72* gene in ALS and FTD neurons, which has been observed to cause the assembly and persistence within the cytosol of aggregated RNA tangles and foci, may supply significantly higher numbers of heme-binding and –activating sites within these cells. As a rule, iron dysfunction and respiration defects appear to be common features of neurodegenerative diseases. Heme

constitutes 95% of functional iron in the human body (184). Jeong *et al*. (185) have reported that dysregulation of iron homeostasis leads to ALS progression in a mouse model for the disease. Deterioration of mitochondrial function, with concomitantly lowered availability of hemes b, c-c1, and a-a3 have also been reported in an ALS yeast model system by Gunther *et al.* (186). Regarding oxidative damage, there is a strong body of evidence that oxidative damage may play a role in the pathogenesis of neuronal degeneration in both sporadic and familial ALS (187). The frequent association of a defective form of superoxide dismutase (SOD) with ALS itself can lead to high levels of intracellular hydrogen peroxide. Liu *et al.* (188). showed that mice transfected with a defective ALS-linked human SOD gene had heightened intracellular concentrations of hydrogen peroxide and hydroxide radical relative to superoxide. Curiously, the above-described binding as well as activation of heme by RNA and DNA G-quadruplexes from the *C9orf72* gene may find a curious parallel with the observed affinity for heme shown by the monomer and aggregates of the Aβ peptide, causative agents of Alzheimer's disease. Work by Atamna and colleagues has demonstrated altered metabolism of heme found in the brains of Alzheimer's Disease patients and heme activation by monomeric Aβ peptide as well as its oligomeric aggregates (134, 135, 175, 189). Indeed, these authors have claimed a significant role for the sequestration and activation of heme in the overall Alzheimer's disease. Aβ has been found to bind two molecules of heme, with $K_d$ values of ~7 and ~3 μM, respectively (190). These numbers are remarkably similar to our own measured $K_d$ value of 3.1 μM for the binding of heme to $r(G_4C_2)_4$. It is therefore conceivable that the Aβ peptide and the *C9orf72*-derived G-quadruplex RNA play equivalent roles in heme sequestration and activation in Alzheimer's Disease and in Familial ALS and FTD, respectively. How strong is the peroxidase activity of heme•G-quadruplex complexes? A study by Klibanov and colleagues (120). found that while a commonly used (but non-biological) substrate such as ABTS was oxidized notably more slowly by heme•G-quadruplexes than by horseradish peroxidase, for certain substrates such as phenolic compounds (for instance, tyrosine, and by extension tyrosine-containing peptides and proteins) heme•G-quadruplexes were superior oxidizing catalysts relative to horseradish peroxidase. Thus, the oxidative damage potential of putative heme•G-quadruplex complexes within cells is by no means negligible.

## 2.6 Chapter conclusion

In this work, we have explored the properties of primarily monomeric, intramolecular folds of the $d(G_4C_2)_4$ and $r(G_4C_2)_4$ oligonucleotides. Longer repeats of these same sequences have been shown to form, additionally, into large, parallel-stranded G-quadruplex aggregates (153, 154). It has been suggested that the RNA foci observed in the neurons of ALS and FTP patients may correspond structurally to these larger G-quadruplex aggregates (153, 154). Based on earlier observations we fully expect that the larger, irregular aggregates also bind and activate heme. Recently, G-quadruplex aggregates whose formation has been promoted by spermine, have been shown to display superior peroxidation properties relative to their unaggregated counterparts, besides enjoying enhanced longevity for the active heme moiety within the aggregation milieu (179). Could it be feasible to prevent or interfere with the heme binding and activation properties of the *C9orf72* RNAs, as well as, potentially, other intracellular toxic RNAs that may participate in disease processes? Pearson and coworkers recently reported the interesting observation that a cationic porphyrin, 5,10,15,20- tetra(N-methyl-4-pyridyl) porphyrin (TMPyP4), which is known to be an excellent binder of G-quadruplexes as well as of other DNA and RNA folds, sufficiently altered the structure of $r(G_4C_2)_n$ quadruplexes to impact on the latters' ability to sequester away cellular proteins (191). To date, a very large number of G-quadruplex binding small molecule ligands have been reported in the literature (158, 159, 192). It is possible that the identification of a ligand, or ligands, that interfere with heme binding to RNA G-quadruplexes, may contribute positively to therapeutic strategies aimed at neurodegenerative diseases such as ALS and FTD.

# Chapter 3.

# Heme activation by DNA: isoguanine pentaplexes, but not quadruplexes, bind heme and enhance its oxidative activity

Many Thanks to Janet Huang who helped me mainly in designing as well as running the gel electrophoresis experiments described in this chapter. This work has been published and can be found in:

Shumayrikh, N., Huang, Y. C., & Sen, D. (2015). Nucleic Acids Res, 43(8), 4191-4201. doi:10.1093/nar/gkv266

## 3.1 Introduction

G-quadruplexes make up a family of folded structures formed by single-stranded and guanine-rich DNAs and RNAs (133, 155, 156, 193). Sequences known to fold to G-quadruplexes under physiological conditions can be of genomic origin or entirely artificial, including many aptamers obtained from *in vitro* selection (133, 155, 156, 193) out of random-sequence DNA/RNA libraries. In G-quadruplex, guanines from one to four distinct DNA or RNA strands hydrogen bond together in Hoogsteen fashion, to form guanine base quartets. G-quadruplexes are polymorphic, showing diverse strand molecularities, orientations/topologies, as well as forming both inter- and intra-stranded folds. Wholly parallel, antiparallel, as well as combination strand orientations have been described for DNA G-quadruplexes; RNA G-quadruplexes typically adopt a parallel strand orientation. Of the physiological cations, $K^+$, and to a lesser extent, $Na^+$, specifically support the formation and stabilization of G-quadruplexes. They do so by complexing to multiple guanine keto functionalities, either within a given G-quartet or between successive G-quartets (194). Other cations known to support G-quartet formation include $Rb^+$, $NH_4^+$, $Sr^{2+}$, $Ba^{2+}$ and $Pb^{2+}$. However, cations such as $Mg^{2+}$ and $Ca^{2+}$ do not specifically stabilize G-quartets, though they do stabilize G-quadruplexes via general electrostatic stabilization (26, 194).

Isoguanine (2-oxo-6-aminoguanine) is a natural but noncanonical purine mutagenic nucleobase that results from spontaneous oxidative stress of adenine (195). It exhibits unique self-association properties compared to its isomer, guanine, and results in formation of different higher order DNA structures. A number of recent papers, by Chaput and Switzer (196) and by others (137-140, 197-201), have probed the structure and properties of intermolecular multi-stranded complexes formed by isolated iG nucleosides, as well as by iG-containing single-stranded DNAs. While the difference between guanine and isoguanine only involves the transportation of the carbonyl and amino groups, it has been found that in the presence of specific cations (e.g. $Na^+$, $Rb^+$, $Cs^+$, $NH_4^+$, $Sr^{2+}$), the iG nucleosides form cation-templated iG-quartets or quintets (196, 202). In the case of the DNA oligomers, parallel-stranded iG-pentaplexes are formed (and held together by iG quintets) in solutions of most of the above cations; however, in $K^+$ solutions, especially at 0 °C, iG-containing oligonucleotides form a parallel-stranded iG-quadruplex (held together by iG quartets) (196). Figure 3-1 shows the structures of (i) a G-quartet, (ii) an iG-quintet, (iii) and an iG-quartet.

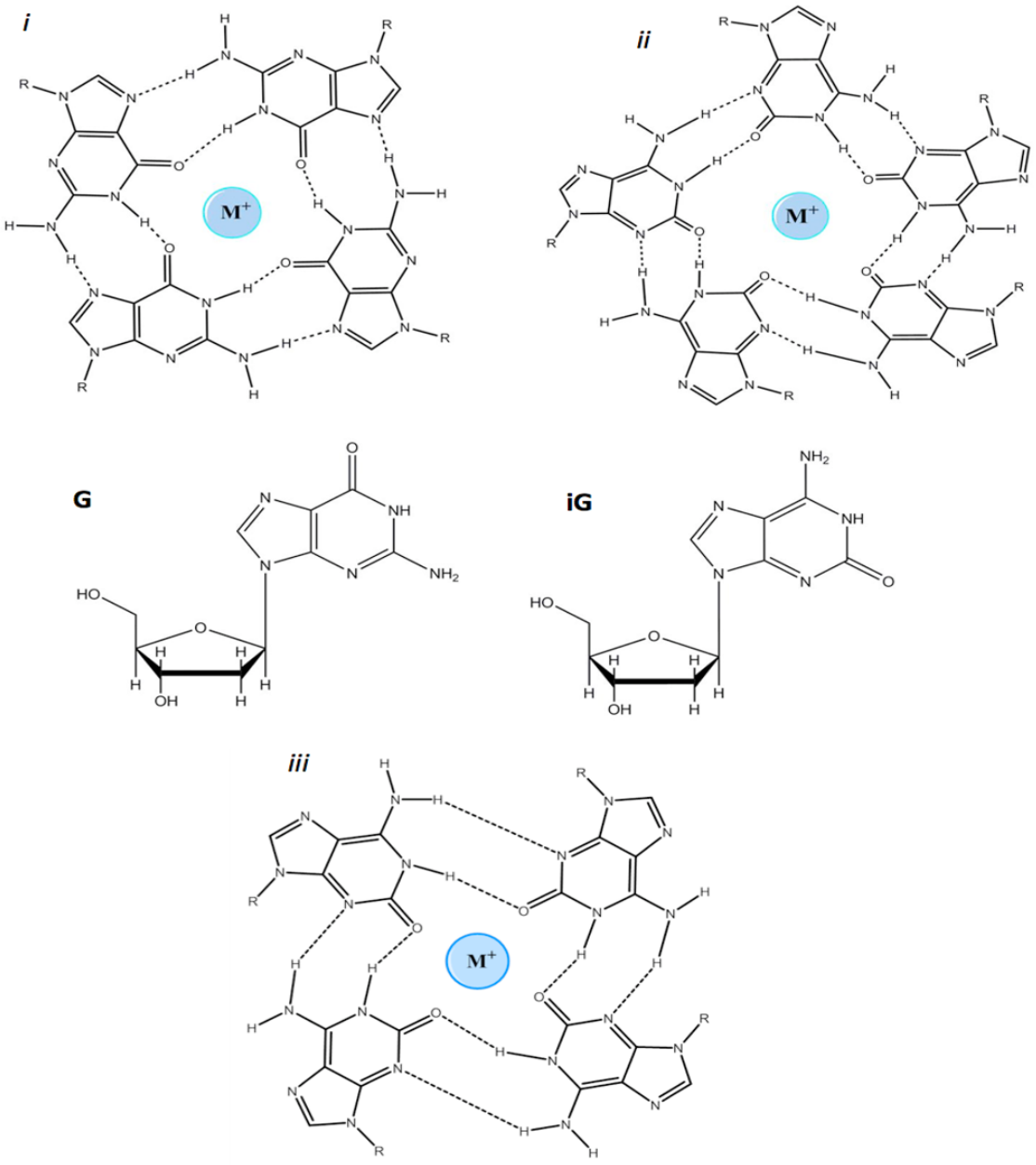


**Figure 3-1** **Chemical structures of 2'-deoxyguanosine (G), 2'-deoxyisoguanine (iG), guanine quartet (i), isoguanine quintet (ii), and isoguanine quartet (iii).**

## 3.2 Chapter overview

In spite of a large literature on G-quadruplex–heme complexes and their oxidative properties, many structural and mechanistic features of these systems remain incompletely characterized. The following are known to date: (i) heme molecules in these complexes are end-stacked upon rather than intercalated into G-quadruplexes (203); (ii) in the catalytically active complexes the heme iron is in a six-coordinate, high spin state (12, 115); and (iii) there appears to be a requirement for an extended π-surface such as the guanine quartets of a G-quadruplex provide. To date, neither duplexes nor folds other than G-quadruplexes formed by DNA and RNA have been shown to bind or activate heme.

We therefore wished to investigate what specific features of G-quadruplexes (and their component G-quartets) were necessary for heme binding and activation. Toward that end, we identified higher order structures formed by DNA containing the naturally occurring but non-genetic nucleobase; isoguanine (iG). We carried out a variety of spectroscopic and chemical experiments to, first, assemble and characterize iG-qudruplexes and pentaplexes, in order to investigate their heme-binding and activating properties, relative to standard G-quadruplexes.

## 3.3 Materials and methods

### 3.3.1 Materials

All DNA oligomers were purchased from the University Core DNA Services (University of Calgary) and size-purified by denaturing gel electrophoresis. Isoguanine phosphoramidite was purchased from Glen Research; Fe(III)-heme (hemin) from Frontier Scientific; and $\gamma$-$^{32}$P ATP was from PerkinElmer Life and from Analytical Sciences (33 μl, 185 Mbq; 6000 Ci/mmol). T4 polynucleotide kinase was from New England BioLabs Inc. (10,000 units/ml). All other chemicals and reagents were purchased from Sigma Aldrich. DNA sequences used in this study were shown in table 3-1

**Table 3-1 DNA sequences used in this study. iG is isoguanine base.**

| Name | Sequence |
|---|---|
| d($T_8G_4T$) | 5' – TTTTTTTTGGGGT – 3' |
| d($T_4G_4T$) | 5' – TTTTGGGGT– 3' |
| d($T_8iG_4T$) | 5' – TTTTTTTTiGiGiGiGT – 3' |
| d($T_4iG_4T$) | 5' – TTTTiGiGiGiGT– 3' |

### 3.3.2 Preparation of G-quadruplexes, iG-quintaplexes, and iG-quadruplex

Relevant DNA oligonucleotides were denatured at 100 °C for 3 minutes in TE [10-mM Tris, pH 7.5, 0.1 mM ethylenediaminetetraacetic acid (EDTA)] buffer, followed by cooling on ice. 80 nanomoles of DNA were then incubated in 25 mM Tris-HCl, pH 7.5, supplemented with 500 mM potassium, sodium, ammonium, or cesium chloride, at 25°C for 24 hours. In experiments where multi-strand complexes were made by the mixing of two differently sized oligonucleotides, 5'-$T_4iG_4T$-3' was mixed with 5'-$T_8iG_4T$-3' (or 5'-$T_4G_4T$-3' with 5'-$T_8G_4T$-3') in 1:1 molar ratios. For the preparation of the iG-quadruplex from 5'-$T_8iG_4T$-3', that oligonucleotide was incubated in 25 mM Tris-HCl, pH 7.5, supplemented with 500 mM potassium chloride, at 0°C, for 24 hours.

In order to visualize the multi-strand complexes after gel electrophoresis, the oligonucleotides were 5'-labelled using γ-$^{32}$P-ATP using standard kinase procedure; The 5'- radiolabeling was performed in 20 µl reaction mixture with 4 pmol of DNA, 2 µL of 10X T4 kinase buffer (70 mM Tris-HCl, 10 mM $MgCl_2$, 5 mM Dithiothreitol, pH 7.6), 5 µCi of [γ-$^{32}$P] ATP, and 10 units of T4 polynucleotide kinase. The mixture was then gently vortexed and centrifuged followed by incubation at 37℃ for 30 minutes. The reaction was stopped by adding 2 ul of 0.5 mM EDTA pH 8.0 followed by size purification through 12% denaturing polyacrylamide gel and 50 mM TBE (Tris/boric acid/EDTA) pH 8.0 as running buffer. Samples were heated in denaturing loading dye; (gel-loading dye contains 95% formamide and the dyes xylene cyanole FF and bromophenol blue), at 100℃ for 2 minutes prior to electrophoresis. Isolated bands were eluted using crush and soak method in TE buffer overnight at 4℃. The samples were then centrifuged for 10 min and 300 ul from the eluted DNA was carefully removed and added to new tube. The radiolabelled pallets then

were recovered by ethanol precipitation, and used to prepare the G4-DNA complexes by mixing the corresponding hot pellet with 80 nmol of cold DNA followed by incubation in buffer supplemented with salt as described above.

### 3.3.3 Circular dichroism spectroscopy of G-quadruplexes and iG-quintaplexes under varying salt conditions and iG-quadruplex under potassium salt condition

Circular dichroism (CD) experiments were carried out in a JASCO J-810 Spectropolarimeter at 25 °C, using 0.05 cm path-length cuvettes. CD spectra were recorded both in the absence and presence of hemin. The final concentration of any given DNA multi-stranded complex was 10 µM, in 40 mM Tris-HCl, pH 8.0, 1% dimethylformamide (DMF), 0.05% Triton X-100. The final concentration of hemin was 0.5 µM. Spectra were recorded between 200 and 320 nm, and were averaged from three scans. CD measurements were also carried out at 0 °C on the iG-quadruplex, assembled in a $K^+$ buffer (see above). For experiments on the iG-quadruplex, in which NaCl and $NH_4Cl$ salts (to 20 and 35 mM final concentrations) were added post-assembly, incubation with the added salts was carried out for 24 hrs at 25° C. The CD spectra were then recorded for such solutions.

### 3.3.4 Native acrylamide gel electrophoresis

DNA complexes were prepared as described above and analyzed by electrophoresis through 20% acrylamide native gels, run at 4 °C in 100 mM TBE buffer, pH 8.0. For iG containing DNA oligomers incubated with $K^+$, the samples were analyzed in a gel, run at 4 °C, in 100mM TBE buffer, pH 8.0, supplemented with 5 mM KCl. The gels were exposed to phosphorous screens (Amersham Biosciences) for various times (3–5 hrs), at 4 °C, and the exposed screens were scanned in a Molecular Dynamics Typhoon 9410 Variable Mode Imager, to visualize radiolabeled bands. The gel images were then analyzed using either ImageQuant 5.2 (GE Healthcare) or ImageJ (NIH) software.

### 3.3.5 Heme binding assay

Heme-binding by all multi-stranded DNA complexes was monitored in a Varian Cary 300 bio UV-visible spectrophotometer, at 25 ± 1° C, using 10 mm quartz cuvette. A 5 mM hemin stock was prepared in DMF and stored in the dark at −20 °C. Hemin was freshly diluted to 0.5 µM from the stock into the reaction buffer [40-mM Tris-HCl pH 8.0, 1% DMF, 0.05% Triton X-100] containing multi-stranded DNA complexes at final concentrations of 0.2–20 µM, with either no further salt added (negative controls) or appropriate salt solutions (NaCl, $NH_4Cl$, etc.) added to final concentrations of 20 mM. Spectra were collected from 200 to 800 nm wavelength.

### 3.3.6 Calculation of binding constant

Absorbance data from titration experiments were used to construct saturation binding curves by plotting absorbance changes in the Soret band (404 nm) as a function of DNA concentration. Dissociation equilibrium constants ($K_d$) were obtained by fitting the binding isotherm using nonlinear regression (OriginLab 9) with the following equation described by Wang *et al.* (176): $[DNA]_0 = K_d(A-A_0)/(A_\infty-A) + [P_0](A-A_0)/(A_\infty-A_0)$, where $[DNA]_0$ is the initial concentration of DNA, $[P_0]$ is the initial concentration of monomeric hemin (the concentration of hemin was calculated using $\varepsilon_{398}$ = 80,000 $M^{-1}$ $cm^{-1}$). $A_\infty$ indicates maximum hemin absorbance and $A_0$ the initial absorbance in the absence of DNA.

### 3.3.7 Peroxidase activity measurement

ABTS [2,2’ azino-bis (3-ethylbenzothiazoline-6-sulfonic acid] was used as the oxidizable, chromogenic substrate. Peroxidation reaction was monitored by following the appearance of the oxidized $ABTS^{\bullet+}$ radical cation product, which absorbs light at 414 nm. For these assays, the final hemin concentration was 0.1 µM, in reaction buffer [40 mM Tris- HCl, pH 8.0, 20 mM of XCl (where X is $Na^+$, $K^+$, $Cs^+$ or $NH_4^+$), 1% DMF (v/v), 0.05% Triton X-100 (w/v)]. The ‘no salt’ reactions were monitored in reaction buffer itself, with no XCl added. The final concentrations of ABTS and of the multi-stranded DNA complexes were 5 mM and 20 µM, respectively. Reactions were initiated with the addition of 1 mM

$H_2O_2$ and were followed at 25 °C. Peroxidase activity was measured also at 0 °C for the iG-quadruplex and its controls.

## 3.4 Results

### 3.4.1 CD characterization of multi-stranded DNA complexes

To generate G- and iG-mediated DNA strand-multimers, d($T_8G_4T$) and, separately, d($T_8iG_4T$) were first incubated in the buffered chloride solutions of various cations. The complexes formed by these strands, initially monitored by native gel electrophoresis, were then characterized using CD spectroscopy. CD is an excellent reporter of the strand orientations of such multiple-stranded DNA assemblies, although it does not provide the strand molecularities/stoichiometries of any such complexes. Figure 3-2 (left) shows the CD spectra of what are clearly G-quadruplexes formed by d($T_8G_4T$), in the presence of well-known G-quadruplex-promoting cations ($Na^+$, $K^+$, $NH_4^+$). All spectra show a strong positive peak at 260 nm and a negative peak at ~245 nm; in all these cases, parallel-stranded G-quadruplexes are being formed. Incubations in $Cs^+$, however, show only a modest amplitude enhancement over that of single-stranded d($T_8G_4T$) (without any added salt). Figure 3-2 (right) shows spectra for d($T_8iG_4T$), incubated in the presence of the same set of cations, above. Here, two different kinds of spectra can be seen. In $Na^+$, $Cs^+$ and $NH_4^+$ solutions, maxima are seen at 275 nm (minor) and 310 nm (major), with a minimum at ~245 nm. These spectra correspond to parallel-stranded iG pentaplexes, in agreement with earlier data by Pierce *et al.* (202). By contrast, in the $K^+$ solution, the CD spectra are quite distinct, with a positive peak at ~295 nm and a strong negative at ~310 nm. These latter CD features have been proposed to correspond to an iG-quadruplex (202).

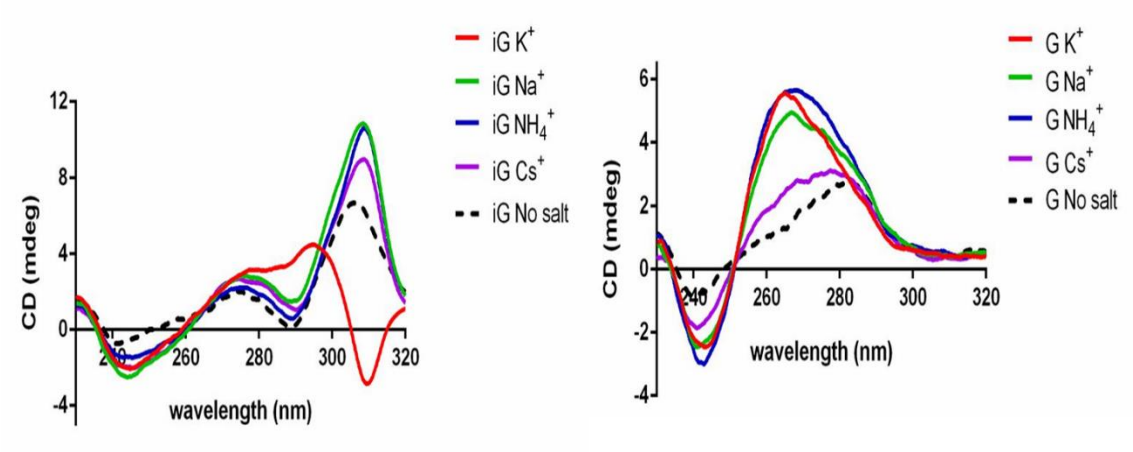


**Figure 3-2 Circular dichroism (CD) spectra of the products of incubation of 5'-$T_8G_4T$ ('G') and of 5'-$T_8iG_4T$ ('iG'), in buffered solutions containing, variously, 20 mM of NaCl, KCl, $NH_4Cl$, CsCl or no added salt.**

### 3.4.2 Native gel analysis of strand stochiometries of iG-pentaplexes and quadruplexes

To investigate the strand stoichiometries of complexes formed by d($T_8G_4T$) and d($T_8iG_4T$) in the different salt solutions, strand-mixing experiments were carried out. The number of strands in a multi-stranded DNA complex can be precisely determined by counting the total number of such complexes formed from mixtures containing two single stranded DNAs (each with the identical $G_4$ or $iG_4$ motif but of different overall strand length) (26, 196). Because strand multimers formed in such a mixing experiment would have different molecular weights (and, correspondingly, different electrophoretic mobilities), the formation of *n* multistranded complexes would indicate a strand molecularity of *(n−1)* for the complex. Figure 3-3a shows that co-incubation (at 25 °C) of 1 mM d($T_4iG_4T$) with 1 mM d($T_8iG_4T$), in solutions of 0.5 M $Na^+$, $Cs^+$ and $NH_4^+$, respectively, gives rise to a total of six closely spaced product bands of low electrophoretic mobility in each case. This indicates that these complexes are strand pentaplexes. In contrast, incubation of the d($T_4G_4T$)/d($T_8G_4T$) with 0.5 M $K^+$ gives rise to the expected five bands, corresponding to G-quadruplexes formed by these oligonucleotides. The results of $K^+$-promoted formation of strand multimers, at different temperatures, from a mixture of d($T_4iG_4T$) and d($T_8iG_4T$) are shown in Figure 3-3b. Here, the temperature of incubation determines which product

is obtained. In a 0 °C incubation, five product bands are seen, consistent with the formation of iG-quadruplexes only; while the 25 °C incubation gives rise to a more complex pattern of bands, indicating the formation of both iG-quadruplexes and iG-pentaplexes (196).

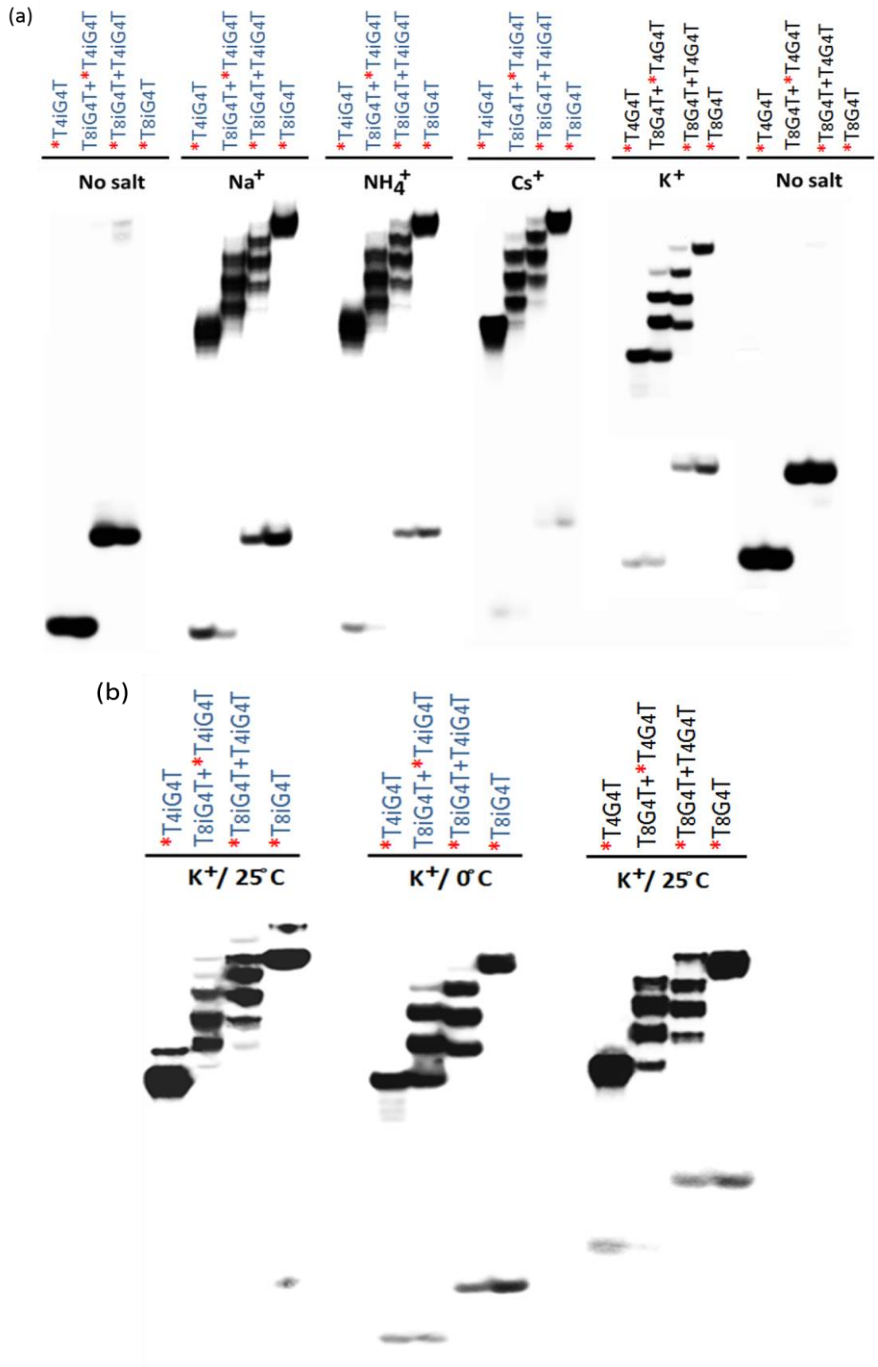


**Figure 3-3** **Native gel electrophoresis analysis of the multi-stranded products formed from incubation, with specific salt solutions, of 1:1 molar mixtures of 5'-$T_4G_4T$ and 5'-$T_8G_4T$ (labeled in black); or 5'-$T_4iG_4T$ and 5'-$T_8iG_4T$ (labeled in blue). Oligomers marked with a red asterisk are 5'-$^{32}$P-labeled; those not so marked are not radiolabeled. (a) Incubations carried out at 25° C. (b) Incubations carried out at 25 °C versus 0 °C.**

### 3.4.3 Heme binding by iG-pentaplexes, iG- and G-quadruplexes

Do these various multi-stranded DNA complexes bind heme? In the case of G-quadruplexes, key UV-vis spectroscopic features indicative of heme-binding are well established (12); upon titration of a fixed concentration of monomeric heme with increasing concentrations of G-quadruplex, the following spectral features are seen: (i) a ~2-fold hyperchromicity and modest red-shift (from ~398 nm to 402–404 nm) of the heme's Soret absorption peak, and (b) characteristic changes in the heme's visible spectrum resemble these of hemoprotein enzymes like metmyoglobin (6-coordinate) and HRP (5-coordinate). Figure 3-4 shows the spectra of 0.5 µM hemin, dissolved in a buffer [40 mM Tris-HCl, pH 8.0, 1% dimethylformamide (v/v) and 0.05% Triton 100X (w/v)], supplemented with, variously, 20-mM final concentrations of KCl, NaCl, $NH_4Cl$ or CsCl. Figure 3-4 shows the spectra of monomeric heme, either in the absence of added DNA ('heme alone') or in the presence of 10 µM of $d(T_8iG_4T)_5$ ['iG $Na^+$', 'iG $NH_4^+$' and 'iG $Cs^+$']; $d(T_8iG_4T)_4$ ['iG $K^+$']; and $d(T_8G_4T)_4$ ['G $K^+$', 'G $Na^+$', 'G $NH_4^+$' and 'G $Cs^+$']. Inspection of the spectra of the $Na^+$, $NH_4^+$ and $Cs^+$ solutions shows that titration of 'both' the isoguanine pentaplex $d(T_8iG_4T)_5$ and the guanine quadruplex $(T_8G_4T)_4$ to heme generates the classic signatures for heme–DNA complex formation (*vide infra*). In all cases, the red shift of the Soret band is observed, although the magnitude of Soret band hyperchromicity is somewhat variable. For instance, in $NH_4^+$ solution, G-quadruplex binding elicits a larger Soret hyperchromicity relative to iG-pentaplex binding, however, that trend is reversed in $Na^+$ solution. In $Cs^+$ solution, titration of heme with either the G-quadruplex or iG-pentaplex shows relatively modest changes in the UV-vis spectra; nevertheless, the changes seen are consistent with heme–DNA complex formation. Moreover, presence of iG-pentaplexes templated in $Na^+$, $NH_4^+$, and $Cs^+$ changes the heme visible spectrum similarly to that of their G-quadruplex counterparts. Overall, the UV-vis spectra of heme/iG-pentaplex and heme/G-quadruplex complexes are relatively alike, and therefore parallel conclusion can be drawn that the environment around the heme is similar and is also 6-coordinate for heme/iG-pentaplexes. The most interesting results, however, are observed in $K^+$ solutions. The G-quadruplex, $d(T_8G_4T)_4$, binds heme, as defined by the spectral changes. However, addition of the iG-quadruplex, $d(T_8iG_4T)_4$, to the heme (even at a quadruplex: heme ratio of 20:1) does not change the heme UV-vis spectrum at all. Such a lack of spectral change suggests that $d(T_8iG_4T)_4$ does not bind heme or does so with a very low affinity. To determine binding

affinities, titration of a fixed concentration (0.5 µM) of heme with various DNA multistrand complexes was carried out. Figure 3-5 shows UV-vis spectra of the heme titrated with 0–20 µM G-quadruplex, $d(T_8G_4T)_4]$, and 0–20 µM iG-pentaplex, $d(T_8iG_4T)_5]$, both in $Na^+$ buffer. Dissociation constants ($K_d$) values calculated were 3.22 ± 0.43 and 1.28 ± 0.05 µM, respectively. Figure 3-6 shows that in $K^+$ buffer, titration with 0 – 20 µM G-quadruplex $[d(T_8G_4T)_4]$ yields a $K_d$ value of 7.89 ± 0.96 µM, whereas titration with even 70 µM iG quadruplex $[d(T_8iG_4T)_4]$ results in no discernable spectral change, consistent with a lack of heme binding to the iG-quadruplex.

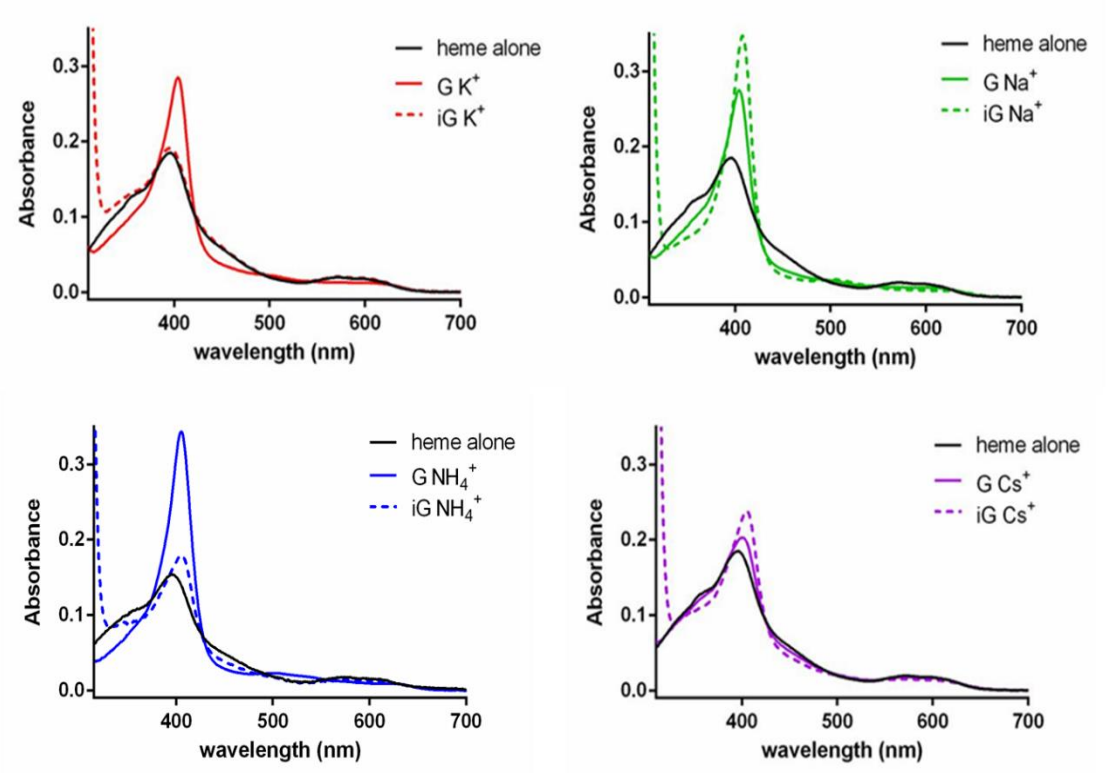


**Figure 3-4** **UV-vis spectra of 0.5 µM solutions of monomeric heme, following incubation with specific multi-stranded complexes formed by 5'-$T_8G_4T$ ('G') and by 5'-$T_8iG_4T$ ('iG') in buffered solutions containing, respectively, NaCl, KCl, $NH_4Cl$ and CsCl.**

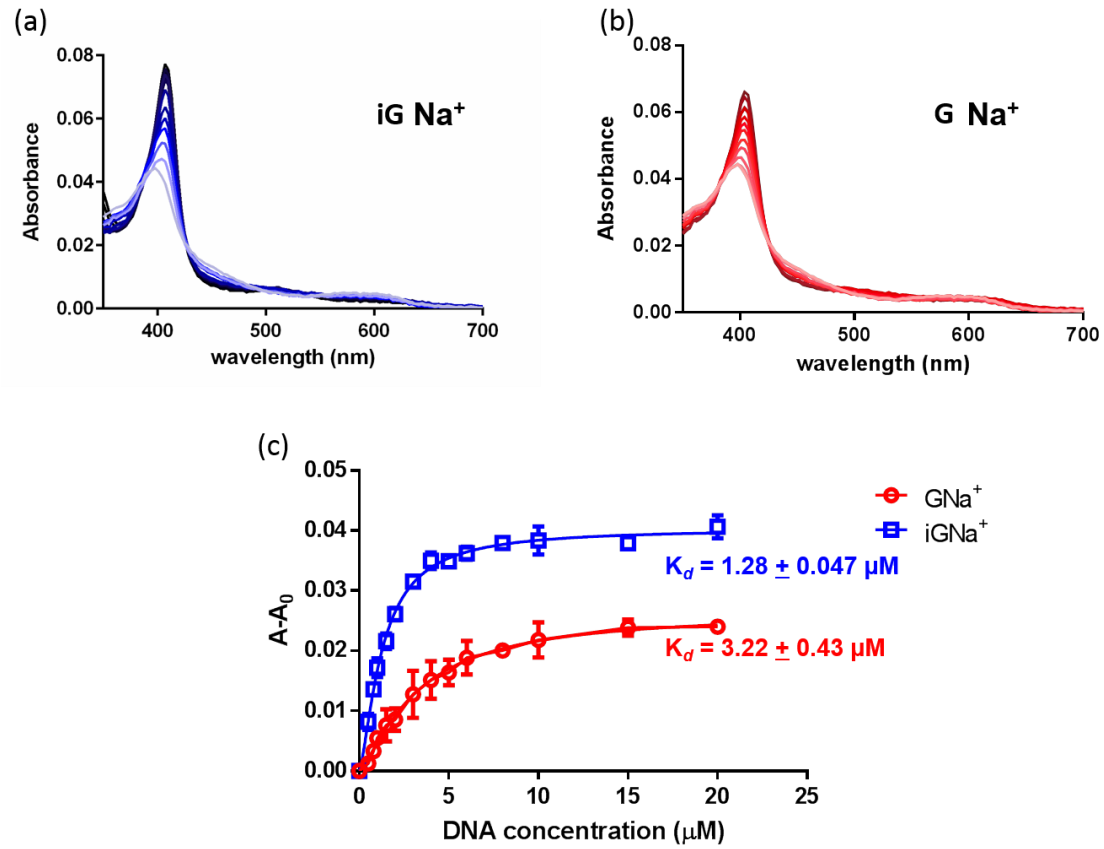


**Figure 3-5** **UV-vis spectra of 0.5 μM heme titrated with 0-20 μM multi-stranded DNA structures in a $Na^+$ buffer solution (40 mM Tris-HCl, pH 8.0, 20 mM NaCl, 1% DMF, 0.05% Triton X-100), at 25 °C. Titrations were carried out with a: the iG-pentaplex, $d(T_8iG_4T)_5$; and, b: the G-quadruplex, $d(T_8G_4T)_4$. c: Plots of $A-A_0$ at 404 nm plotted against [multi-stranded DNA], to generate binding isotherms, and dissociation equilibrium constants ($K_d$) derived from them.**

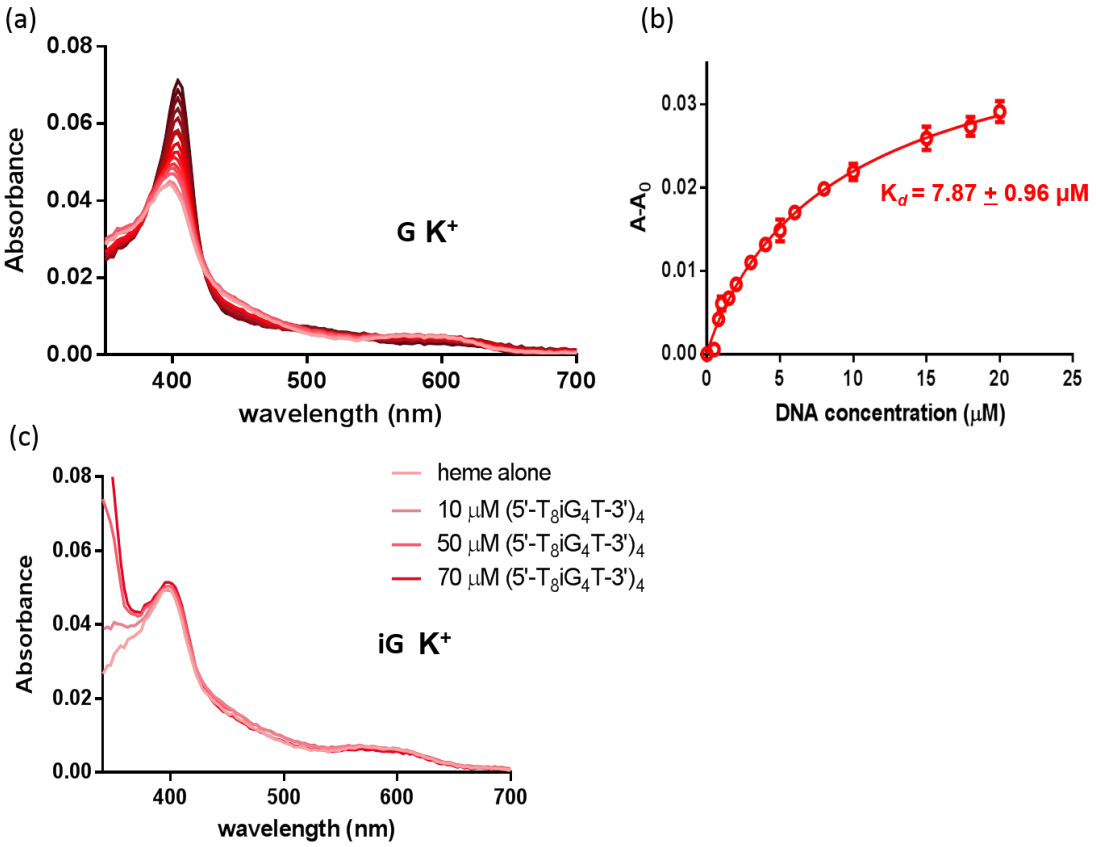


**Figure 3-6** **UV-vis spectra of 0.5 μM heme titrated with multi-stranded DNA structures in a $K^+$ buffer solution (40 mM Tris-HCl, pH 8.0, 20 mM KCl, 1% DMF, 0.05% Triton X-100), at 25 °C. a: Titrations were carried out with the G-quadruplex, $d(T_8G_4T)_4$, 0-20 μM. b: Plot of A-$A_0$ at 404 nm plotted against $[d(T_8G_4T)_4]$, to generate a binding isotherm, and the dissociation equilibrium constants ($K_d$) calculated from it. c: Plot of titration of 0.5 μM heme with 10-70 μM iG-quadruplex, $d(T_8iG_4T)_4$.**

To ensure that heme binding under these experimental conditions does not grossly change the structure of the DNA quadruplexes and pentaplexes, CD spectra of the multi-stranded structures, with and without added heme, were recorded. Figure 3-7 shows that in no case is a substantial change in the CD spectrum seen following the addition of heme.

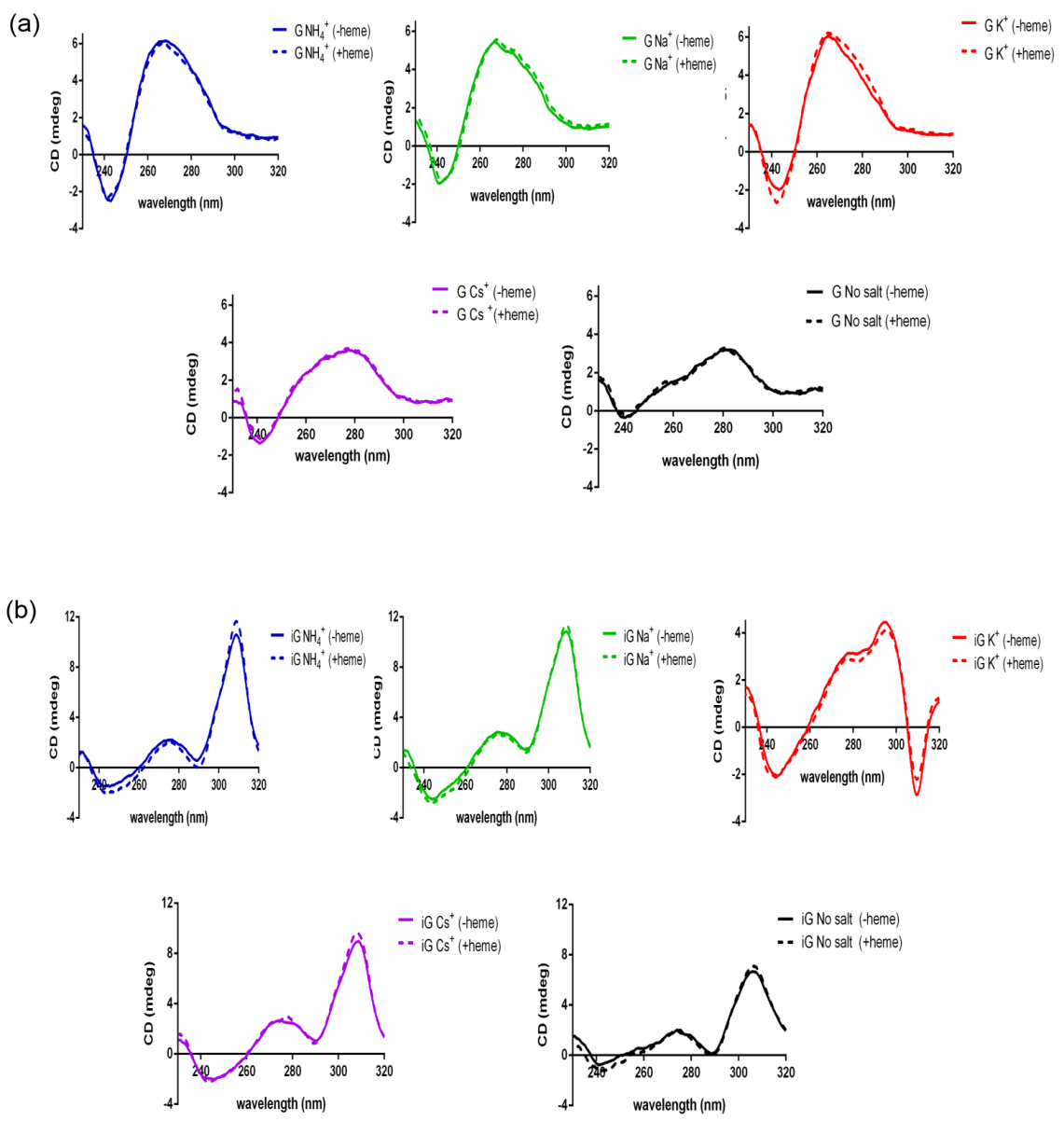


**Figure 3-7** **Circular dichroism spectra, in the absence and presence of 0.5 μM heme of: (a) G-quadruplexes formed by d($T_8G_4T$) (G $NH_4^+$/$Na^+$/$K^+$/$Cs^+$) and of the single stranded DNA itself (G No salt), and (b) iG-pentaplexes formed by d($T_8iG_4T$) (G $NH_4^+$/$Na^+$/$Cs^+$), iG-quadruplex formed by d($T_8iG_4T$) (G $K^+$), and of the single stranded DNA itself (G No salt).**

### 3.4.4 ABTS peroxidase activity of heme in presence of excess of iG-pentaplexes, G-quadruplexes, or iG-quadruplex

The peroxidase activity of proteinaceous heme enzymes, as well as of heme–DNA complexes, is conveniently monitored using hydrogen peroxide and a chromogenic substrate such as ABTS [2, 2'-azino bis (3-ethylbenzothiazoline-6-sulfonic acid]. The raw data for ABTS oxidation by the various heme–DNA complexes are shown in Figure 3-8 while Figure 3-9 plots the observed rate constants ($k_{obs}$) obtained from those kinetic data. Here, 'G' refers to data obtained from heme in solution with excess G quadruplex, whereas 'iG' refers to corresponding data from excess iG-quadruplex and iG-pentaplex. It can be seen that in the $Na^+$, $Cs^+$ and $NH_4^+$ buffers, heme–G-quadruplex complexes ('G') show comparable oxidative behavior to heme– iG-pentaplex complexes ('iG'). In the $K^+$ buffer, the oxidative activity of the heme–G-quadruplex complex ('G') is comparable to those measured in $Na^+$, $NH_4^+$ or $Cs^+$ buffers; however, that of heme in the presence of excess iG-quadruplex shows only background activity. This is consistent with the observation, above, that the iG-quadruplex does not bind heme. Cumulatively, these data highlight an unexpected set of observations that (i) while both G-quadruplexes and iG-pentaplexes appear to manifest structural features capable of binding and activating heme, (ii) the iG-quadruplex, at least in a $K^+$ buffer, does not present those features.

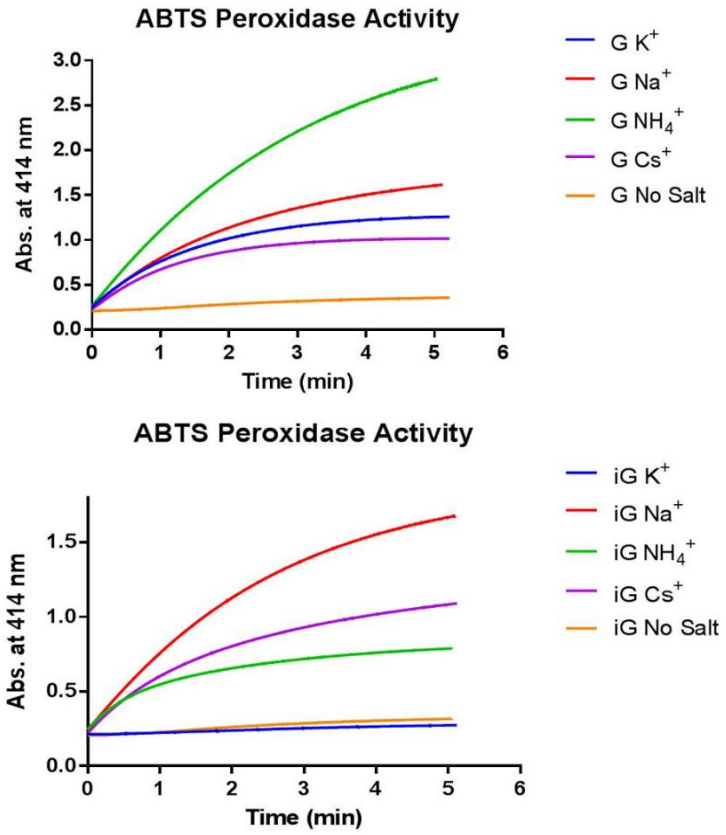


**Figure 3-8** **ABTS peroxidation as a function of time. Reactions solutions contained heme (0.1 µM), in reaction buffer containing 20 mM of XCl (where X is $Na^+$, $K^+$, $Cs^+$, or $NH_4^+$). The "no salt" reactions were monitored in reaction buffer itself, with no XCl added. ABTS was at 5 mM and multi-stranded DNA at 20 µM, respectively. Reactions were initiated, at 25 °C, with the addition of 1 mM $H_2O_2$.**

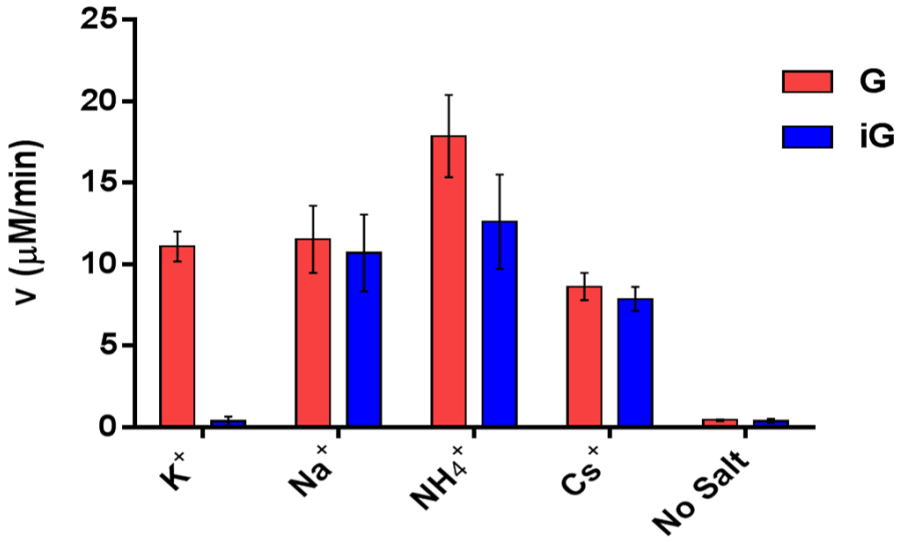


**Figure 3-9** **Peroxidase activity of 0.1 μM solutions of heme, in the presence of 20 μM multi-stranded product of either 5'-$T_8G_4T$ ('G') or 5'-$T_8iG_4T$ ('iG'), formed in buffered solutions of, respectively, NaCl, KCl, $NH_4Cl$ and CsCl. Plotted are mean values, obtained from three independent experiments, of the reaction velocities of oxidation of the chromogenic substrate, ABTS, in the presence of 1 mM $H_2O_2$. Error bars indicate one standard deviation from the mean.**

### 3.4.5 The iG-quadruplex does not support peroxidase activity at different temperatures, or in the presence of $Na^+$ or $NH_4^+$

We wished to probe the effect of temperature on the structural stability of the $K^+$ buffer-generated iG-quadruplex, as well as on the latter ability to bind and activate heme at different temperatures. Thus, the $K^+$-generated iG-quadruplex, formed at 0 °C, was stored at 25 °C for 7 days. Figure 3-10 a**,** upper, shows that this prolonged storage at 25 °C does not alter the CD spectrum of this multi-stranded structure. Therefore, the iG-quadruplex, once formed, does not readily disintegrate or reassemble as an iG-pentaplex, at least at 25 °C. Figure 3-10 a**,** lower, shows that solutions of 0.1 μM heme in the presence of either 10 μM of $K^+$-generated iG-quadruplex or 40 μM of the single-stranded d($T_8iG_4T$) oligonucleotide ('No salt') show only baseline levels of peroxidase activity, both at 0 °C and 25 °C, whereas the $K^+$ generated conventional G-quadruplex, under equivalent experimental conditions, shows peroxidase activity at both 0 °C and 25 °C. With regard to the inability of the iG-quadruplex to bind or activate heme, we explored whether the $K^+$ cation might play some inhibitory role. We had earlier shown that with G-quadruplex–heme

complexes, cations such as $Na^+$, $K^+$ and $NH_4^+$ played a 2-fold role: first, the cations were necessary for the formation and stability of the G-quadruplex itself; however, $NH_4^+/NH_3$ (as well as other nitrogenous base/conjugate acid systems, such as collidine/collidinium$^+$) also substantially enhanced the peroxidase activity of G-quadruplex–heme complexes by means of general acid-base catalysis (12). We therefore investigated whether the addition of $NH_4^+$ or $Na^+$ ions to pre-existing $K^+$-generated iG-quadruplex/heme solutions led to any enhancement of peroxidase activity. Figure 3-10 b, left, plots the ABTS peroxidation $k_{obs}$ values for heme•G-quadruplex complexes, in buffered 20 mM KCl solutions that have been supplemented with 20 or 35 mM of either NaCl or $NH_4Cl$. It can be seen that while NaCl supplementations do not notably change the $k_{obs}$ values, the addition of $NH_4Cl$ does lead to enhancements of the $k_{obs}$ values, as expected. However, addition of either $Na^+$ or $NH_4^+$ to the iG-quadruplex/heme solution does not improve on the background levels of peroxidase reaction (Figure 3-10 b, right). To investigate the continuing structural integrity, or not, of the two DNA quadruplexes upon the addition of $NH_4^+$ or $Na^+$ ions, CD spectroscopy was carried out. Figure 3-11 shows CD spectra of both the G-quadruplex and iG-quadruplex, prior to as well as following addition of $Na^+$ or $NH_4^+$. Changes in the CD spectra of either quadruplex are minimal upon addition of $Na^+$. With $NH_4^+$, the amplitudes of the spectra change somewhat but the overall shape of each spectrum is maintained, suggesting that no gross rearrangement of structure occurs for either DNA quadruplex. The above experiments contribute incremental evidence that the inability of the iG-quadruplex to enhance the peroxidase activity of heme lies in some structural property of the iG-quadruplex, which renders it a poor binding site for heme.

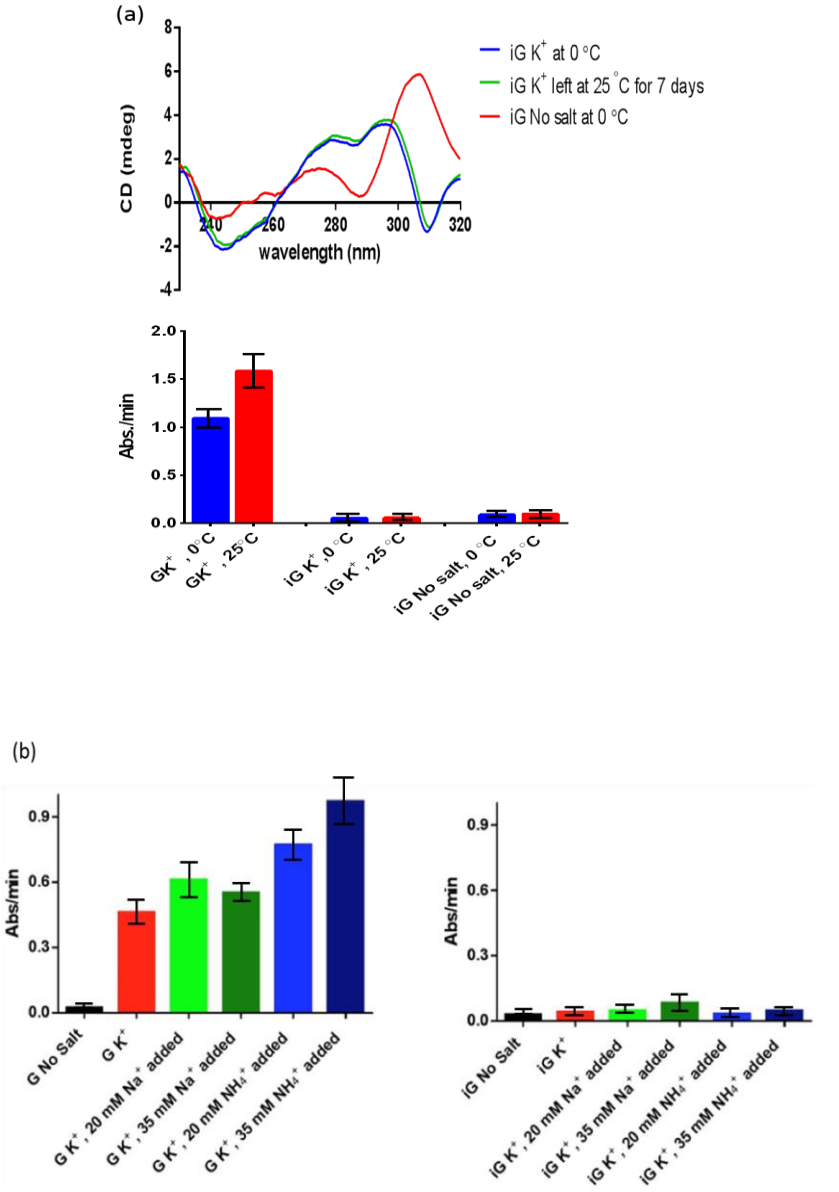


**Figure 3-10** **(a) Upper: Circular dichroism spectra of $K^+$ buffer-generated iG-quadruplex at 0 °C, as well as following incubation at 25 °C for 7 days. The spectrum of the single-stranded 5'-$T_8iG_4T$ ('no salt') at 0 °C is shown for comparison. Lower: Peroxidase activity of heme in the presence of excess iG-quadruplex, at 0 °C and 25 °C, compared to that of heme in the presence of excess G-quadruplex, also at 0 °C and 25 °C. (b) Peroxidase activity (reported as absorbance/min) of 0.1 μM heme in the presence of 20 μM of the $K^+$-generated G-quadruplex, (5'-$T_8G_4T)_4$ (left), and of 20 μM $K^+$-generated iG-quadruplex, (5'-$T_8iG_4T)_4$ (right). Shown in red in either graph is the activity observed in $K^+$ buffer alone. Bars shown in green and blue map activity observed in $K^+$ buffers supplemented with $Na^+$ and $NH_4^+$, respectively.**

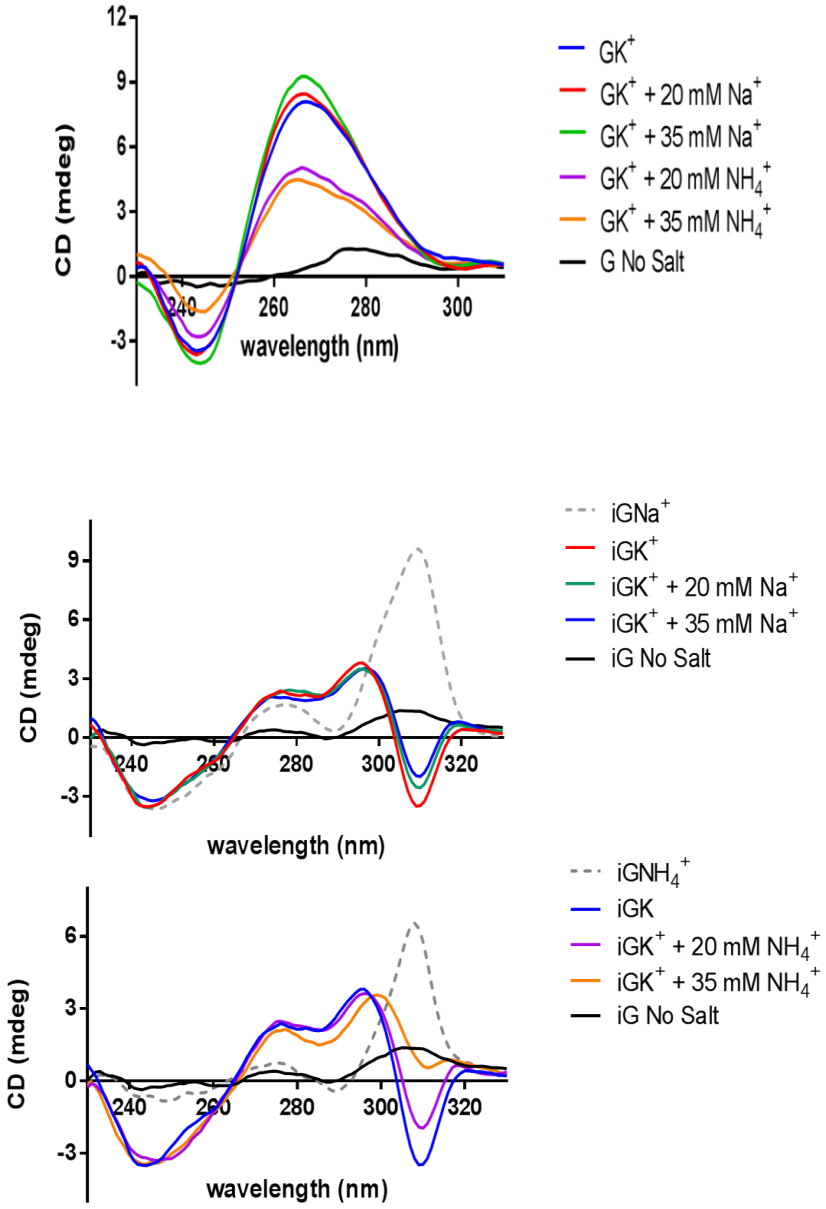


**Figure 3-11** **Upper: Circular dichroism spectra of the G-quadruplex, $d(T_8G_4T)_4$, formed in $K^+$ buffer ("GK"), and, following the addition of different concentrations of NaCl and $NH_4Cl$, as indicated. Middle and bottom: Circular dichroism spectra of the iG-quadruplex, $d(T_8iG_4T)_4$, formed in $K^+$-buffer ("iGK"), and, following the addition of different concentrations of NaCl and $NH_4Cl$, as indicated. "iGNa" indicates, for reference, the CD spectrum of the iG-pentaplex, $d(T_8iG_4T)_5$, formed in $Na^+$ buffer.**

## 3.5 Discussion

Early studies on the formation of cation-templated structures formed by iG nucleosides and iG-containing DNA strands were both structural and computational (138, 140, 197, 198, 200, 201). Seela *et al.*(199, 200, 204) demonstrated the formation of tetra-stranded complexes by d($T_4iG_4T_4$). DFT calculations by Meyer *et al.* (140, 198) compared iG base quartets and quintets (lacking sugar-phosphate backbones) formed in the presence of $Na^+$, $K^+$, $Rb^+$ ions and found that, in general, the quintets had relatively planar structures, whereas the quartets deviated from planarity. Even so, G-quintets templated by $K^+$ and $Rb^+$ were calculated to be planar; however, those templated by $Cs^+$ were not expected to be planar (140). Brodbelt *et al.* (202) combined ESI-mass and CD spectroscopy experiments with *ab initio* calculations to further examine the influence of the annealing cation, and reported that while G-quadruplex formation was strongly dependent on the identity of that cation, iG-pentaplexes were templated by a variety of cations (with the notable exception of $K^+$, which favored the formation of iG-quartets from a combination of kinetic and thermodynamic factors) (196, 202). The only experimentally determined high-resolution structure reported to date is from a nuclear magnetic resonance study, by Feigon *et al.*, of a DNA iG-pentaplex formed by 5'-$TiG_4T$ (137). However, even in this Cs+-templated structure, the 5'-most of the four consecutive G-quintets has an almost planar structure, although the remaining three iG-quintets do indeed deviate significantly from planarity, as predicted (137). Based on the above suggestive, albeit not conclusive, studies on the relative planarity of iG-quintets and iG-quartets, we hypothesize that our own observed lack of heme binding by the iG-quadruplex (as well as satisfactory heme binding by iG-pentaplexes) relates to the relative planarity of iG quintets within $Na^+$ and $NH_4^+$-templated DNA iG-pentaplexes, and to deviation from such planarity of iG-quartets within $K^+$ templated DNA iG-quadruplexes. Further high-resolution structural studies, especially on the iG-quadruplex, will clearly be required to throw light on this hypothesis.

## 3.6 Chapter conclusion

In this study, we have shown unequivocally that the G-quartet is not the only nucleic acid 'surface' suitable for the dual property of heme binding and activation. The iG-quintet appears to function just as well, promising much for the potential future use of iG-pentaplexes in bioanalytical chemistry. An important question in this regard would be the relative chemical stability of iG-pentaplex DNA, compared to G-quadruplex DNA, in the presence of reactive oxygen species generated by DNA-activated heme and oxidants such as $H_2O_2$. An important experimental priority will be to determine, precisely, the relative chemical stabilities of the distinct DNA multi-strand structures. A higher durability of iG-pentaplexes under oxidative conditions would surely encourage their use over G quadruplexes in practical applications.

An important question regarding the mechanism by which heme is activated by DNA, that remains to be fully elucidated is the following: is a large and planar surface, capable of π-stacking, sufficient to (a) bind and also (b) activate heme? In this study, heme binding and activation properties have been found to be tightly linked, inasmuch as activation necessitates binding. But are the two necessarily linked? It is conceivable that there exist DNA/RNA folded motifs that are capable of binding heme without activating it. We hypothesize that the 'hole' at the center of both G-quartets and iG-quintets is an important structural feature for the activation, though not necessarily for the binding of heme. We had earlier reported, on the basis of UV-vis (12) and EPR (115) data, that in a G-quadruplex bound heme (at physiological pH) the iron moiety was a six-coordinate, high-spin species. Such a 6-fold coordination of the iron necessarily implies the presence of an axial ligand in the direction of the G quartet/iG-quintet upon which the heme is stacked. We propose that the presence of this yet unidentified axial ligand requires the central hole provided by G-quartets and iG-quintents, but not necessarily by other, extended base-paired structures in DNA and RNA that lack this structural feature. Further experiments need to be done to test this hypothesis.

# Chapter 4.

# Spectroscopic and rapid kinetic investigations of the oxidation of the ferric heme/G4-DNAzyme by hydrogen peroxide: insights into the higher oxidation activated species

## 4.1 Introduction

Guanine-rich RNAs and DNAs that fold into guanine quadruplexes are found to complex tightly with porphyrins such as hemin [Fe(III)-heme]. The generated complex displays robust peroxidase (1 $e^-$ oxidation), oxygen transfer (2 $e^-$ oxidation) as well as NADH oxidase activities greater than that of disaggregated heme itself. Thus, they are known as heme-utilizing DNAzymes and ribozymes. The folded DNAzymes appear to provide a unique chemical environment to the heme that by analogy resembles that of hemoproteins such as horseradish peroxidase (HRP) and cytochrome P450s. As discussed in Chapter 1 of this thesis, UV-Vis spectroscopy and EPR analysis has indicated that the heme iron centre is a hexacoordinated high-spin species in which the distal site is occupied by water molecule and the proximal site has an axial ligand whose identity is still not clearly defined to date (12, 115). Recent $^1$H NMR studies by Yamamoto *et al*. showed that the ferric heme is sandwiched between the terminal 3' end of two G-quadruplex complexes of the folded human telomeric sequence (5'-TTAGGG-3') (203). A subsequent NMR study by the same lab has analyzed the interaction of ferrous heme [Fe(II)-CO] adduct to G-quadruplex formed by human telomeric sequence (5'-TTAGGG-3') (119). Through the analysis of the NMR results, together with theoretical consideration, they have concluded that the heme ($Fe^{2+}$) axial ligand trans to CO in the complex is a water molecule ($H_2O$) as the likely proximal ligand to the iron centre (119). However, is a water molecule on its own sufficient to provide the iron with the needed electron density that would explain the intrinsic binding and catalytic behavior observed for the heme/G4-DNAzymes? Does the availability of a structure like G-quadruplex contribute (either directly or indirectly) to both binding and oxidative activity through a specific proximal

coordination from the amine or the carbonyl functional groups? The answer to these questions has not been explicitly stated in these NMR studies.

DNAzymes with peroxidase-like activity have recently attracted great interest and become part of numerous practical applications in many areas of science ranging from chemistry to biology to medicine due to many advantages of nucleic acids over conventional protein enzymes, such as thermal stability, low cost, and simpler preparation. These applications include biosensing, bioelectronics, molecular machines, electrocatalysis, and immunohistology. Willner and co-workers (205, 206) reported a chemiluminescence approach for a target DNA detection using luminol/$H_2O_2$ system with DNAzymes with peroxidase-like activity. The application of gold nanoparticles (Au-NPs) has also been reported for the amplified detection of DNA or telomerase activity (207). Other applications include the determination of metal cations such as $Ag^+$, $K^+$, $Hg^{2+}$, $Pb^{2+}$ or $Cu^{2+}$ (208, 209), and amplified detection of small molecules such as adenosine (210), cocaine and adenosine 5′-monophosphate (AMP) (211) and proteins such as lysozyme (212) or thrombin (213). Assays for telomerase or methyltransferase activity, which are potential targets in anticancer therapy, have been also demonstrated (214) (215).

The interesting question that remains unclear to date with these heme/G4-DNAzymes is what activated heme species within them are responsible for the observed 1 $e^-$ and 2 $e^-$ oxidation reactions known to be catalyzed by them. With most hemoproteins, the classic “compound I” is known to be the initial active intermediate species, and it is formed rapidly from the reactions of ferric enzymes with hydrogen peroxide and other oxygen atom donors such as peracids. Compound I is a ferryl oxo-species in which the iron has a formal (+5) oxidation state, but owing to the delocalization of one oxidizing equivalent upon the porphyrin ring itself, its dominant electronic resonance form is a ferryl centre with (+4) oxidation state coupled to a porphyrin π- radical cation. The most thoroughly characterized “classic compound I” is from horseradish peroxidase (141, 216, 217). The well-known classical peroxidation catalytic cycle of hemoproteins is shown in figure 4-1. In this cycle, $H_2O_2$ withdraws 2 electrons from ferric ($Fe^{III}$) hemoprotein thereby producing a ferrylporphyrin radical cation ($Fe^{IV}$=OPor•+), compound I. Then, compound I is capable of withdrawing one electron from a reducing substrate $AH_2$ to generate Compound II; a second intermediate described as ferryl heme with an iron that has (+4)

oxidation state without the radical cation ($Fe^{IV}$=OPor). Finally, compound II pulls another electron from the substrate to produce the product and reform the original resting state of the hemoprotein.

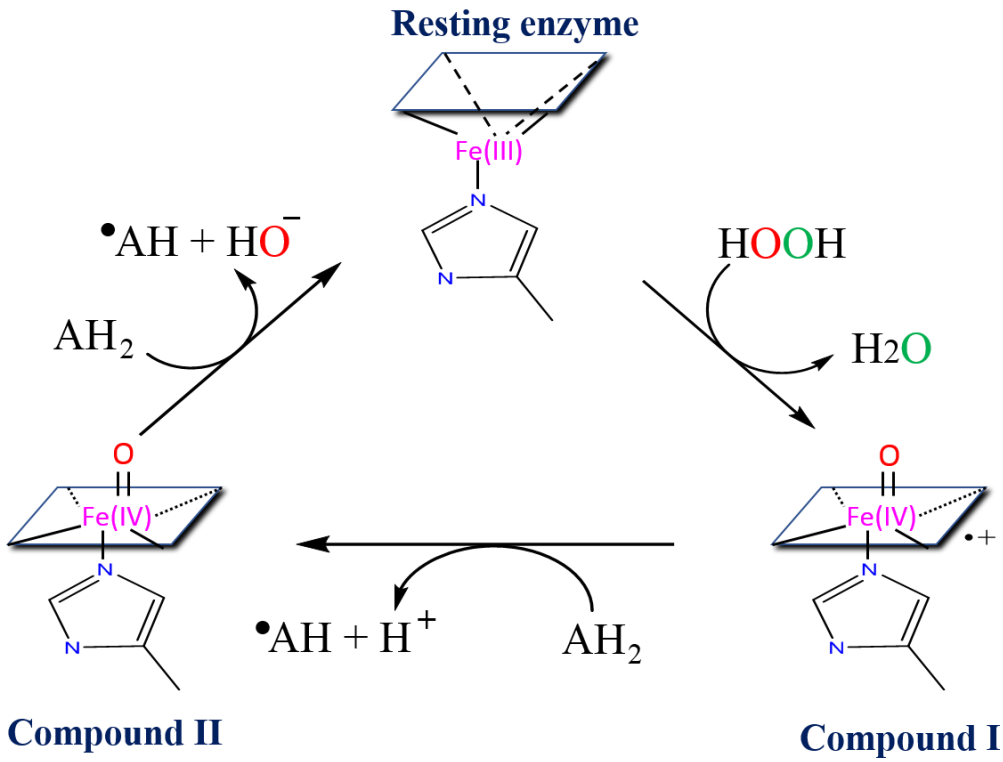


**Figure 4-1 The Nature of the High-Valent Complexes in the Catalytic Cycles of Hemoproteins.**

Curiously, in several peroxidases, most notably cytochrome c peroxidase, the initial species observed after addition of hydrogen peroxide to the ferric enzyme is not a classic compound I; here, the ferryl centre is associated with an aromatic amino acid (rather than porphyrin) radical cation (142, 218-220). This species, will be referred to as compound I' rather than the old known name used in hemoprotein literature; compound ES. This state presumably arises from a transiently formed Compound I that oxidized the nearby aromatic amino acid side chain via an electron transfer process.

A number of other heme-containing peroxidase and globin proteins have been found to form Compound I'-like derivatives with either tyrosyl or tryptophanyl radicals in conjunction with the ferryl heme center. Compound I'-like heme state have been reported

for myoglobin (143, 221), bovine catalase (222), turnip peroxidase (223), prostaglandin-H synthase (224-228), various catalases (222, 229-231), as well as for the Phe172Tyr and H42L horseradish peroxidase mutants (146, 232).

UV-vis spectroscopy is an excellent tool by which one can study these above various activated species. Classic compound I and compound II are easily distinguishable from each other by their own distinct spectroscopic features. Compound I from HRP is characterized by a Soret absorption band of diminished intensity compared to the Soret transitions of other heme states. On the other hand, with fully aromatic porphyrin ring, the extinction coefficient of the Soret band of cytochrome c peroxidase Compound I' is undiminished and looks like compound II (233). Moreover, the visible region of the spectrum provides valuable information about the spin state of the iron (85).

Interestingly, a previous EPR study conducted in our lab in collaboration with Grant Mauk's lab at the University of British Columbia, found that the reaction of the heme•G-quadruplex complex with $H_2O_2$ led to the formation of an organic radical that exhibited a simple singlet EPR signal. This intermediate was described as a carbon centred radical adduct, most likely on a guanine base (115). In support of this, chemical foot-printing studies using $H_2O_2$ (115) and other oxidizing agents such as m-CPBA in absence of reducing substrates have shown that the G-quadruplex underwent preferential oxidative cleavage at specific guanines.

The UV-vis spectroscopic characteristics of heme•G-quadruplex complexes is well-known since our lab reported them back in 1998 (12). Owing to the complexation with the G-quadruplex, the heme Soret band exhibits hyperchromicity, red shift of ~ 5-6 nm, and a visible spectrum that looks like those of hemoproteins such as metmyoglobin and HRP. In order to have some insights into the reaction mechanism, Travascio *et al*. (115) looked at changes in UV-vis absorption spectrum upon treatment of the heme•G-quadruplex (PS2.M-heme) complex with $H_2O_2$ in the absence or in the presence of a reducing substrate H2Q (hydroquinone). Travascio *et al*. found that the amplitude of the Soret band of the heme/G4-DNAzyme was protected in the presence of H2Q whereas it progressively decayed in absence of H2Q and exhibited some features for which a "Compound I-like species" was proposed to form (115). A subsequent detailed study

performed by Wang *et al*. in 2009 (178) and Shangguan and co-workers in 2011 (234) elaborated several mechanistic features of these heme/G4-DNAzymes. First, it was found that peroxidase activity was dependent on $H_2O_2$ but not on ABTS substrate concentration. This result indicates a different reaction mechanism for heme/G4-DNAzymes compared to HRP for which activity increases with ABTS concentration (178). Second, the heme/G4-DNAzyme showed broader substrate specificity than HRP due to its "open" catalytic centre, which agreed with what has been reported from our lab and Klibanov's study (106, 120). Furthermore, the main reason for its inactivation was demonstrated to be the degradation of the bound heme rather than the destruction of the G-quadruplex within the DNAzyme (234). Travascio's, Wang's, and Shangguan's data, though, were limited to UV-visible absorption spectra that were accumulated as a function of time every 1 min following the addition of peroxide. Herein, we used stopped-flow rapid-scan fast spectroscopy in order to explore the spectra of the activated species formed by heme/G4-DNAzymes during the early stages of the oxidation reactions to see what correspondences might be found with the spectra of corresponding hemoproteins. For example, does the DNAzyme operate via a classic "compound I" (with the heme iron in a formal oxidation state of +5)? Does it go through compound II (with the heme iron in a formal oxidation state of +4?) What other intermediates are involved after the heme/G4-DNAzyme becomes inactive? And what is the scheme of activation and deactivation of these heme-utilizing DNAzyme? The stopped-flow experiments should reveal valuable information about how a nucleic acid bound to heme supports the oxidant-dependent activation of the heme relative to hemoproteins that do a similar thing. Moreover, understanding the catalytic cycle is helpful information for improving G4/heme DNAzyme design, for a broader range of analytical and therapeutic applications.

## 4.2 Chapter overview

Considering the above findings, we wished to carry out fast kinetic measurements in a stopped-flow enabled UV-vis spectrophotometer to reveal the spectroscopic and kinetic features of intermediates generated in the oxidation reactions carried out by G4/heme system. We therefore collected datasets generated by rapid single mixing experiments in which the ferric Fe(III) DNAzyme was mixed with hydrogen peroxide in the

presence or absence of a reducing substrate; dibenzothiophene (DBT). Upon oxidation, DBT generates dibenzothiophene sulfoxide (DBTO) (see figure 4-2). The advantage of using DBT as a substrate of choice is that the UV-vis spectra of both DBT and DBTO don't overlap with those of heme or of various heme activated species (both DBT and DBTO absorb in the region between 300 – 360 nm). However, DBT is a substrate that has poor solubility in water (20 µM). Fortunately, the catalysis of the heme/G4-DNAzyme operates well in a mixture of aqueous/organic solvents (235), and this enabled us to include methanol in the reaction buffer to enhance the solubility of DBT (see Experimental and Results section).

Robust fitting and global analysis of the multivariate datasets was performed using the pro-KIV (Pro-Kineticist IV) software developed for analysis of time-dependent spectra generated by the Applied Photophysics SX stopped-flow spectrometer. A detailed description of the software's criteria can be found in the Experimental and Results sections.

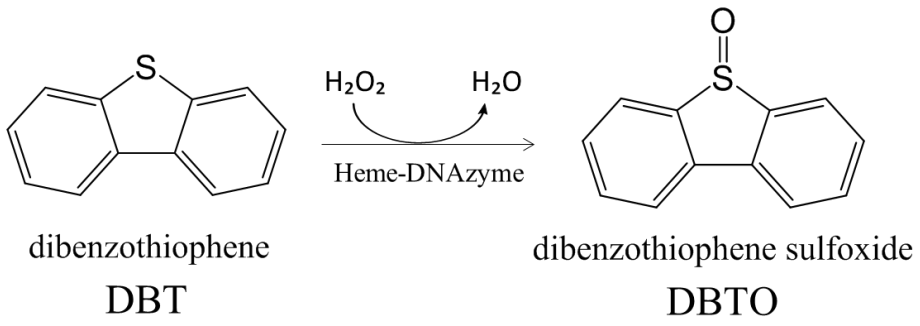


**Figure 4-2 The oxidation of dibenzothiophene to dibenzothiophene sulfoxide.**

## 4.3 Materials and methods

### 4.3.1 Materials

DNA oligonucleotide (CatG4); [5' -TGG GTA GGG CGG GTT GGG AAA - 3'], and (BLD); [5'- AAT ACG ACT CAC TAT ACT-3'] were used for this study and purchased from the University Core DNA Services (University of Calgary), purified by gel purification and standard desalting methods. The oligonucleotides were dissolved in 10 mM Tris-EDTA

buffer (10 mM Tris pH 7.5, 0.1 mM EDTA and frozen at -20 °C until needed. The G-quadruplex folded structure was prepared by incubating the oligonucleotide in the reaction buffer (40 mM HEPES-$NH_4OH$, 20 mM KCl, 1% DMF, 25% methanol, 0.05 % Triton, pH 8.0). Hemin was purchased from Frontier Scientific (Logan, UT, USA). Dibenzothiophene (DBT) was purchased from Santa Cruz Biotechnology Inc., Dallas, TX, USA. A stock of 10 mM DBT was prepared in methanol and stored at 4 °C. All other chemicals were purchased from Sigma-Aldrich.

### 4.3.2 Stopped-flow Spectroscopy

All experiments were performed using the SX20 stopped flow spectrophotometer from Applied Photophysics, using a 2 mm path-length cell and a standard 20 µl cell volume. The dead time of the stopped flow using this cell was determined to be 1 ms. Detection of a time-resolved spectra at multiple wavelengths was achieved with an Applied Photophysics Photodiode Array Accessory (PDA), capable of an integration speed of 1.4 ms per scan. Time-resolved spectra were recorded in 180 - 740 nm spectral range, and 1000 spectra were collected within a scan period of 200 sec. The sample handling unit of the instrument was fitted with a water bath to provide temperature control of the stopped-flow experiments. All experiments were performed at 21 °C.

### 4.3.3 Single mixing experiments

Two solutions of the G-quadruplex-forming oligonucleotide (CatG4) and unfolded oligonucleotide (BLD), as a negative control, were prepared in 2X reaction buffer (80 mM HEPES-$NH_4OH$, pH 8.0, 40 mM KCl, 2% DMF, 50% methanol, 0.1 % Triton-100X). The two solutions were allowed to incubate at room temperature for 10 min for proper DNA folding in case of CatG4. Then, heme was added to both solutions followed by another 10 min incubation. For the solutions containing substrate, DBT was added last. Hydrogen peroxide solutions were diluted freshly from the stock. The mixture of heme, DNA, and DBT (if present or absent) was added to stopped-flow syringe (A), and the peroxide solutions were added to the second syringe (B). The components in solution A were mixed with peroxide in B in a 1:1 mixing ratio. The final concentrations in the optical observation cell after mixing became as follows: 7 µM heme, 50 µM DNA in the reaction buffer (40 mM

HEPES-$NH_4OH$ pH 8.0, 20 mM KCl, 1% DMF, 25% methanol, 0.05 % Triton-100X). The final concentration of DBT after mixing became 100 µM. Hydrogen peroxide concentrations were 0.007, 0.5, and 100 mM.

### 4.3.4 Description of the software and treatment of the kinetic data

The experimental traces recorded from 300 nm to 740 nm were exported as glb file extensions and processed by Pro-KIV Global Analysis Software. Singular value decomposition (SVD) was performed, by which the data matrix was decomposed into 3 matrices with the form of:

$$Y= U . S . V^T$$

Each column of the U matrix represents the time evolution of the reaction. U is a matrix of column vectors where each column is an eigenvector in the time domain. $V^T$ is a matrix of column vectors where each column is an eigenvector in the wavelength domain. S is a diagonal matrix with the singular values S. Each element of S represents the contribution of the corresponding basis spectra to the observed data.

SVD analysis can be viewed as a reduced representation of the data matrix as an ordered set of basis spectra and corresponding time dependent amplitudes as well as their singular values in descending order. It should be noted that SVD output is completely abstract and has no physical or chemical meaning (abstract factor analysis) (236, 237). However, the SVD application aids the analysis in speeding up the subsequent numerical calculations and reduce noise in the dataset.

The SVD output then is analyzed by global optimization of the provided reaction parameters using the Marquardt-Levenberg algorithm (238). The reaction scheme is input in to the Analysis Equations window as successive steps. Compiling the model generates the rate parameters associated with each step of the entered scheme. The spectrum of the starting material (the ferric DNAzyme) as well as the DBT and the DBTO were collected under the same experimental conditions, averaged, and saved as a single spectrum, then fed into the software as known spectra. Hydrogen peroxide was included in the reaction scheme but not incorporated into the regression analysis and was assigned

as a colourless species. In order to run the analysis, the concentrations of each of the starting materials (heme/G4-DNAzyme, $H_2O_2$, and DBT) were entered, with an initial estimate given for each rate constant. This value was used as the “first guess” for the rate constant by the analysis process. The more accurate this initial estimate the fewer iterations would be needed in the analysis process. Upon completion, rate constants, component spectra, and their corresponding concentration profiles could be displayed. The calculated rate constants obtained from the software analysis were reported as the mean attained from three replicate experiments with their standard deviation errors.

The software also calculates the wavelength residual plots, which illustrate the global accuracy of the selected model. Any systematic deviation (as opposed to random noise) in the residual suggests that a significant true spectral event has been missed or not accounted for (see results section). A second assessment of the fit validity can be made by inspecting the calculated spectra. If a model is satisfactory in terms of residual plots, then the calculated spectra must make chemical sense in terms of their shape and sign. Negative extinction spectra can arise when the rate parameters are assigned to individual steps in the wrong order. A judgment can then be made by the user based on the experimental conditions or other evidence in order to modify the rate constants, swap their orders, or adjust them by increasing or decreasing their values, to see the effect on the resultant residual plot. Figure 4-3 represents supporting chart showing the order of steps by which the analysis process is accomplished.

In this work, a number of models as well as values of rate parameters have been tested in order to achieve reasonable calculated spectra and residual plots. Also, to test the robustness of our hypothesized model, one individual step was systematically removed from the scheme, followed by re-performing the analysis and inspection of the residual plots (see the Results section).

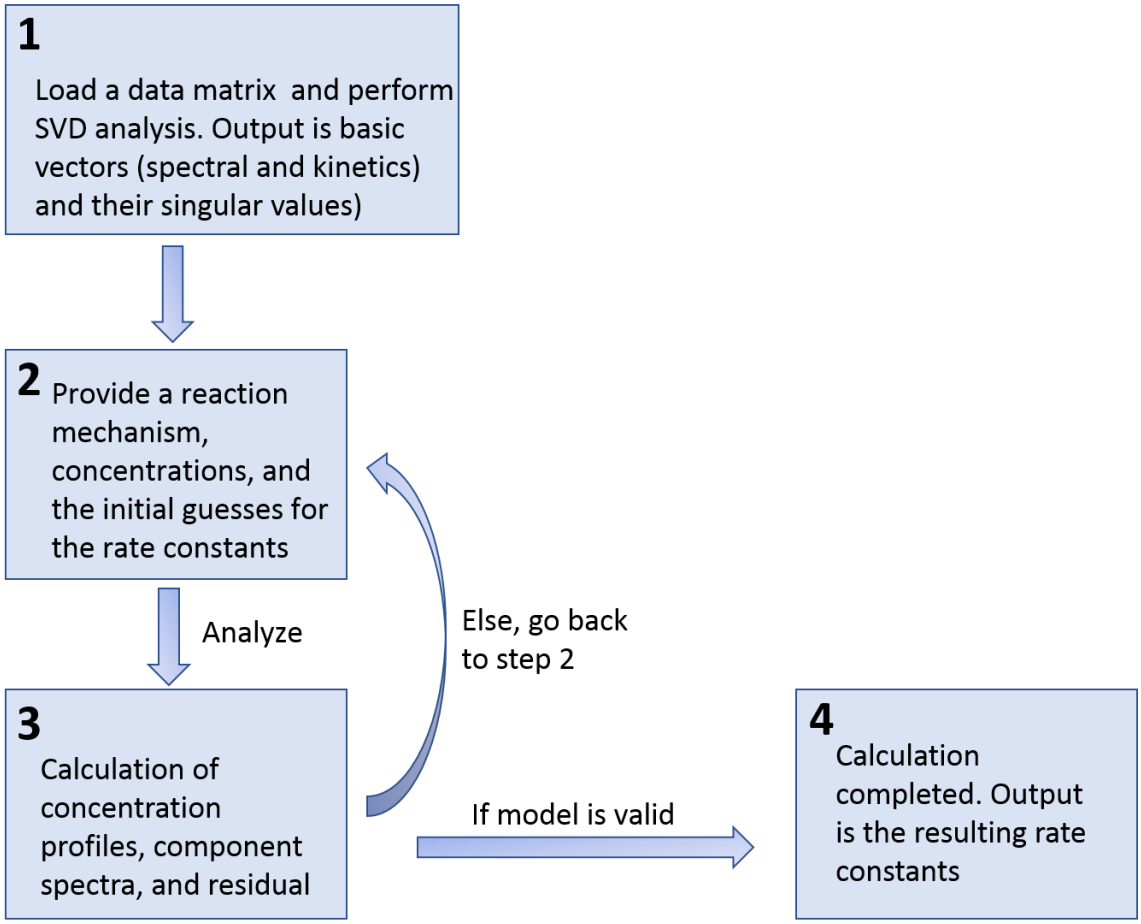


**Figure 4-3 Schematic representation of steps flow during the fitting process by Pro-KIV software.**

## 4.4 Results

### 4.4.1 Determination of the experimental conditions for the oxidation of DBT to DBTO

To ensure completeness of heme binding by the folded G-quadruplex, we have managed these experiments so that the concentration of DNA used was ~7 fold greater than that of heme. Under these conditions, 99% of the heme is bound as calculated based on the dissociation constant ($K_d$) of the complex (12, 239). Also, we have used a concentration of heme (7 µM) to enable observation of highly reactive intermediates if they

formed. However, we first investigated the concentration of $H_2O_2$ that would allow optimal detection of any catalytically active heme intermediates.

We began by testing the possibility of generating the catalytic active intermediates of heme/G4-DNAzyme under the conditions of high excess peroxide concentrations. The detection of high-valent intermediates (Compounds I and I') has been reported in the literature for ferric native and mutant sperm whale and horse heart metmyoglobins (metMbs) in the absence of any reducing substrate and under conditions of high $H_2O_2$ concentration (up to 50 -100 mM of $H_2O_2$ to 5 µM enzyme) (143, 240). In fact, previous comparison of absorbance parameters ($\lambda_{max}$ and εM) of different hemoprotein complexes in terms of Soret maxima, D, and E charge transfer bands revealed that metmyoglobin closely resembles our heme/G4-DNAzyme in terms of its UV-Vis spectrum (12). Therefore, we first tried similar experimental conditions to those used in the study of metmyoglobin for the detection of any active intermediate. The spectral changes we observed at high hydrogen peroxide concentration, however, were complicated because of the extensive heme degradation (bleaching) that occurred (see figure 4-4). Heme bleaching has been also observed for hemoproteins, particularly at higher peroxide or peracid concentrations (241-247). As can be seen from figure 4-4, upon reaction with 100 mM $H_2O_2$ the following spectroscopic characteristics were observed: (i) a sharp and progressive loss of the Soret peak, (ii) the visible region became featureless, and (iii) a new band in the far visible region centred at ~ 670 nm appeared. These spectroscopic features are reminiscent of those of rat liver heme oxygenase, treated with a single equivalent of hydrogen peroxide, which yielded enzyme-bound ferric verdoheme (248). It has also been reported that the oxidative decay product of horseradish peroxidase presents a similarly diminished intensity of the Soret band (proportional to the loss of peroxidase catalytic activity) and the appearance of a new signal at 670 nm. In the case of HRP, this compound was named p670 and was determined to be verdoheme [see figure 4-4] (249, 250). Correspondingly, it is very likely that the species formed with the heme/G4-DNAzyme under high hydrogen peroxide concentration are comparable to those accumulating in hemoproteins from the heme degradation process. Our experimental observation is also consistent with the results of Shangguan *et al*. where the main cause of heme/G4 deactivation is the destruction of the heme molecule and that heme/G4 DNAzyme is extremely sensitive to $H_2O_2$ even compared to hemoproteins such as HRP

(234). Such high sensitivity is understandable in view of the higher predicted solvent accessibility of the heme centre in the heme/G4-DNAzyme's "open active site" and the lack of protection from surrounding groups within heme/G4 complex such as typically found in hemoproteins. Heme destruction at high hydrogen peroxide concentrations therefore hindered the study of intermediates formation in the heme/G4-DNAzyme.

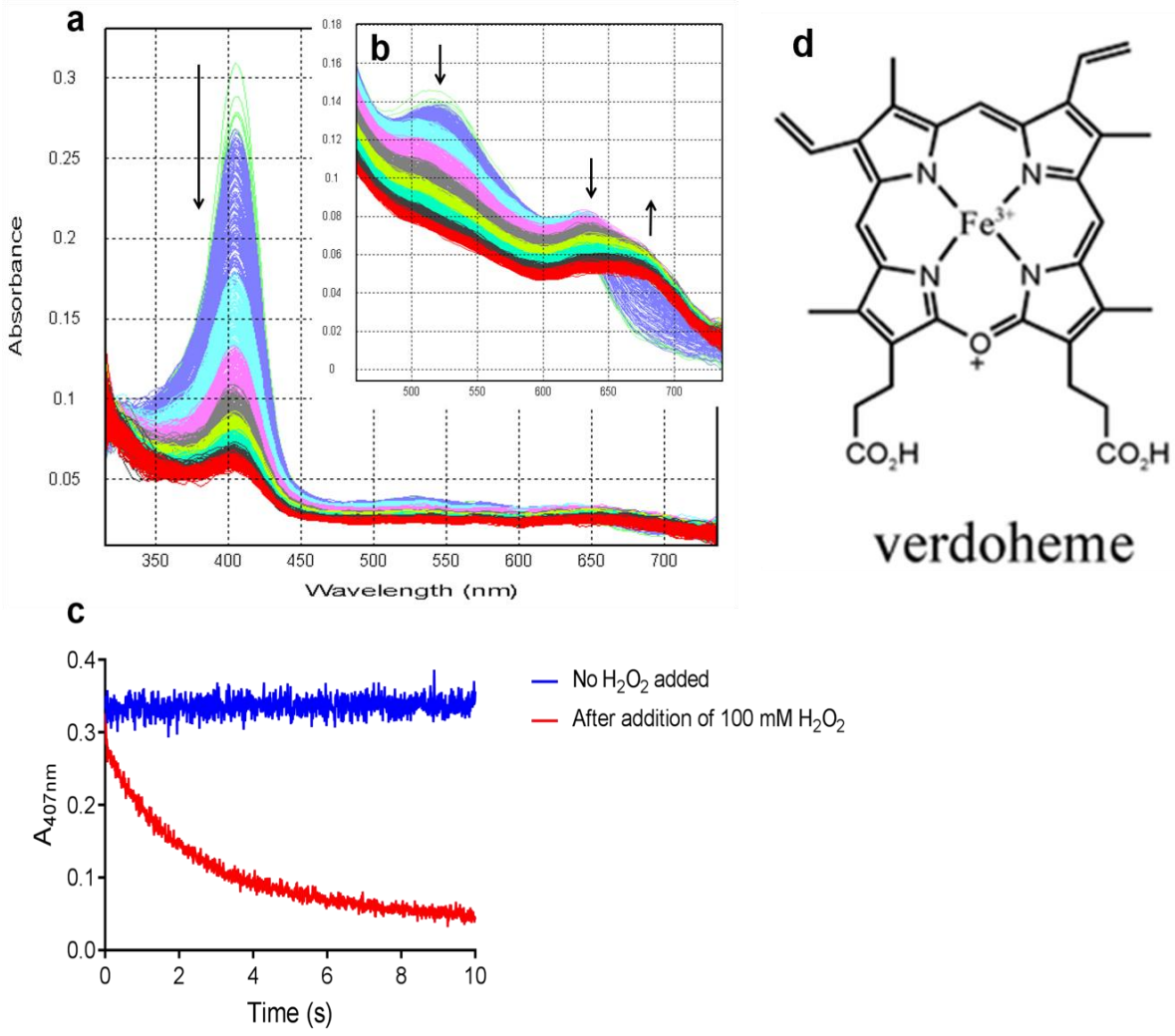


**Figure 4-4** **Spectral change induced in the reaction of heme/G4-DNAzyme with 100 mM $H_2O_2$ in absence of substrate at pH 8.0, 21 °C followed over 10 seconds. (a) Soret region, (b) visible region, and (c) graph of the change in absorbance at the Soret wavelength (407 nm). 7 µM (a) or 15 µM (b) of heme/G4-DNAzyme was used for the measurements on a stopped-flow rapid-scan system. (d) the structure of verdoheme.**

A stochiometric concentration of $H_2O_2$ (7 µM) relative to the heme concentration of the heme/G4-DNAzyme was used next, to see if activated species could be detected under this low $H_2O_2$ concentration. Stochiometric addition of hydrogen peroxide to hemoprotein enzymes has been reported for HRP, and was indeed sufficient for the detection of Compound I in a stopped flow measurement (251, 252). However, in our case the data obtained using 7 µM DNAzyme and 7 µM hydrogen peroxide showed no change

in the spectrum of heme/G4 complex in either the Soret peak or the visible region over short timescales (10 sec) (see figure 4-5). This finding was in agreement with previous reports that at least 40-200 equivalents of peroxide were required for heme/G4-DNAzyme to observe significant changes in the optical spectrum over a longer time-frame (~ 3-5 min) (115, 234). This requirement for high $H_2O_2$ concentrations is, however, understandable in view of the large dissociation constant of $H_2O_2$ (~ 3 mM) for the heme/G4 complex (12, 115). This follows that perhaps the O-O bond breakage of the peroxide is not effective under these stoichiometric conditions. Or that the activated species forms, but does not accumulate to a detectable level to be spectrally observed.

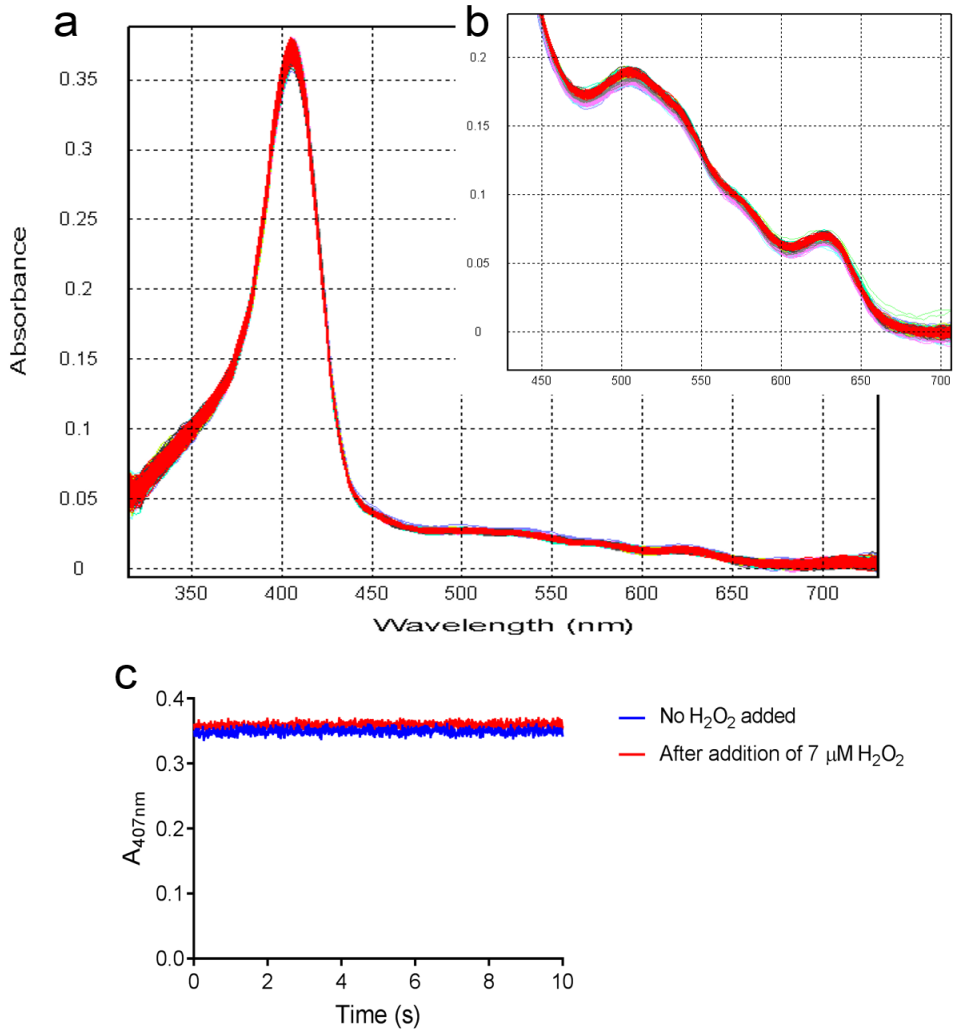


**Figure 4-5** **Spectral change induced in the reaction of heme/G4-DNAzyme with 7 μM $H_2O_2$ in absence of substrate at pH 8.0, 21 °C followed over 10 seconds. (a) Soret region, (b) visible region, and (c) graph of the change in absorbance at the Soret wavelength (407 nm). 7 μM (a) or 15 μM (b) of heme/G4-DNAzyme was used for the measurements on a stopped-flow rapid-scan system.**

Based on the above observations, we decided to; (i) use modest "intermediate" hydrogen peroxide concentrations, and to (ii) use a "guide" reducing substrate that produced an oxidized product which could be monitored independently from the features of the heme spectra. With such a substrate, in principle one can monitor the catalytic reaction in terms of spectral changes in the Soret, as well as the visible spectrum, in addition to observing the conversion of substrate to product and the time required for

achieve that oxidation. DBT was a good choice for us for multiple reasons: (i) this reaction proceeds via 2-electron oxidation (oxygen transfer to a thioether to form a sulfoxide), known to be catalyzed efficiently by heme/G4-DNAzymes as previously shown by Poon and Canale (106, 235); (ii) Both DBT and DBTO absorb in the 300 - 360 nm spectral region (see figure 4-6), which does not overlap with the absorbance of heme and so simplifies our experimental analysis. In the 300 - 360 nm region, DBTO shows one absorbance peak, at 334 nm, while DBT has two, at 322 and 310 nm. The peak at 310 nm would be overwhelmed by the DNA absorbance after mixing DBT with a solution containing the DNAzyme, so it was excluded from the analysis. (iii) Given the poor solubility of DBT in aqueous solutions, we took advantage of the previous demonstration that heme/G4 activity in certain organic solvent-water mixtures even surpasses the activity of most catalytic hemoproteins; indeed, methanol was found safe to use, both to enhance the solubility of DBT and in maintaining the structure of the G-quadruplex (235). Therefore, 25% methanol (found to be enough to solubilize DBT up to 200 µM) was included into the reaction buffer described in the experimental section.

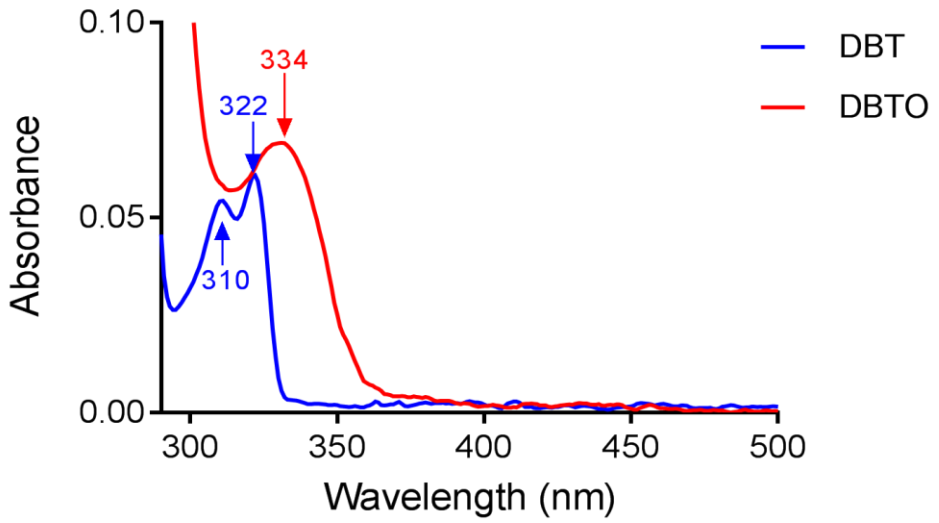


**Figure 4-6** **The absorption spectrum of 50 µM of DBT (blue trace) and DBTO (red trace) in the region of 300 – 360 nm. The samples were prepared in 1X buffer containing 25% methanol [HEPES-$NH_4OH$ pH 8.0, 20 mM KCl, 1% DMF, 0.05% Triton X-100, 25% methanol] and scanned in a Varian Cary 300 bio UV-visible spectrophotometer, at 21 ± 1° C. baseline was obtained using the 1X buffer as a blank.**

To check if the presence of DBT in the reaction solution would change the spectrum of the G4/heme complex, UV-vis scans, shown in figure (4-7), were carried out in the 300 -740 nm range from heme complexed with DNA G-quadruplex either in the presence or absence of DBT. The data show no change in the DNAzyme's spectrum in either the Soret or visible region.

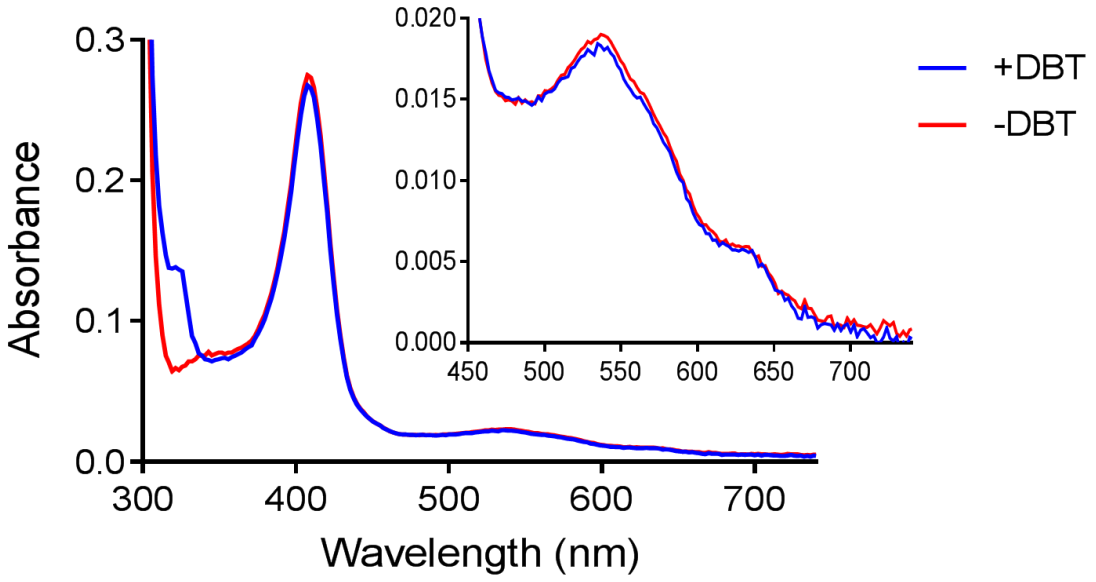


**Figure 4-7 Ferric(III)-DNAzyme UV-Vis spectrum in the presence (blue trace) and absence (red trace) of DBT. Scans were taken in 1 X reaction buffer [40 mM HEPES-$NH_4OH$, pH 8.0, 20 mM KCl, 1% DMF, 0.05% Triton 100-X containing 25% methanol].**

We found that 0.5 mM hydrogen peroxide is sufficient to induce a spectral change of the heme/G4 complex (7 µM) and, at the same time, quantitatively convert DBT to DBTO (approximately 80 -89 % conversion) in ~45 seconds (see figure 4-8). Peroxidase catalyzed sulfoxidation of DBT has been reported using HRP, lignin peroxidase (LiP), and cytochrome c, albeit under extreme conditions (such as the addition of a high concentration of hydrophilic organic solvents, and/or an extremely high concentration of $H_2O_2$). For those hemoproteins, despite the use of such severe conditions, the reaction efficiency was very low (253-255). For example, HRP was reported to oxidize DBT to DBTO with an activity of ~20 pmol/min/nmol of the enzyme at 5 mM $H_2O_2$ (254). Subsequently, DBT oxidation was attempted using HRP, LiP, and MnP in aqueous solutions containing 30% methanol or less with 0.1 – 1 mM $H_2O_2$; however, no reaction

was observed, suggesting that the solubility of DBT substrate affected the reaction efficiency and that conformational changes and/or partial denaturation of those enzymes might be involved in the access of the relatively bulky DBT to the active site (253). On the other hand, microperoxidase MP-11, a heme-containing octapeptide obtained from proteolytic digestion of cytochrome c (256), was reported to be more efficient in catalyzing the sulfoxidation of DBT (with an activity of 8.7 nmol/min/nmol of MP-11 at only 30 μM $H_2O_2$ in a reaction mixture containing 30% methanol) (128). Wariishi *et al.* attributed this effective catalysis to the vacancy of the distal side of the heme within MP-11, which allows the ferryl-oxy core of MP-11 to react with bulky substrates. The property of an open active site is also available in our heme/G4-DNAzyme, so it was expected that the heme/G4 system is also capable of catalyzing the sufoxidation with high efficiency. In this study, we have found that, Indeed, heme/G4 catalyzed the oxidation of DBT to DBTO with an activity of 13 nmol/min/nmol of the DNAzyme.

Interestingly, hemoproteins are also known to catalyze the oxidation of sulfoxides to sulfones. The generation of sulfone was reported for HRP using optimized conditions in monophasic organic media containing 25% (v/v) acetonitrile, HRP 0.06 IU/ml, DBT 0.267 mM, pH 8.0, at 45°C, and DBT:$H_2O_2$ molar ratio of 1:20 using a stepwise peroxide addition (257). The stepwise optimization of the reaction conditions, mainly related to the use of the peroxide, allowed a threefold increase on DBT oxidation by HRP; ~ 60% of DBT in total was converted into dibenzothiophene sulfoxide (12%) and dibenzothiophene sulfone (46%). In the case of heme/G4-catalyzed reaction, however, no sulfone was detected by HPLC or MS (235) suggesting that the enzyme is converted to the inactive state before it can catalyze the further oxidation of sulfoxide to sulfone.

### 4.4.2 Single mixing experiment in the presence or absence of DBT

The time dependent spectral changes upon mixing the DNAzyme with 0.5 mM $H_2O_2$ at 21 °C were recorded from 300 to 742 nm over 200 seconds either in the presence or absence of DBT. The data are shown in figure 4-8 a. Several spectral changes were observed: first, in the presence of DBT, the Soret band was stable for the first ~25-30 seconds of the reaction, followed by a slow decay in amplitude; whereas in the absence of DBT, only progressive loss of Soret intensity was observed (figure 4-8 b). Second, in

the absence of DBT, there is an increase in intensity at ~ 630 nm but a decrease at 570 and 530 nm intensities. Third, a new additional peak starts to appear at 502 nm as the reaction progress until 200 sec regardless the presence or absence of DBT. The conversion of DBT to DBTO was monitored by following the disappearance of the peak at 322 nm and the appearance of the one at 334 nm. Two additional observations can be made from the time-dependent spectral change of DBT to DBTO: (i) the oxidation reaction is completed by ~45 sec with (ii) an isosbestic point at 327 nm is noticed (see figure 4-10).

The stopped-flow single mixing experiments were also applied to “uncatalyzed” reactions in presence of a non-G-quadruplex-forming oligonucleotide “BLD”. These data are shown in figure 4-9. For the uncatalyzed reactions, the difference in the Soret decline in the case where DBT is present or absent is noticeable suggests some degree of a slow background catalysis (see figure 4-9 b).

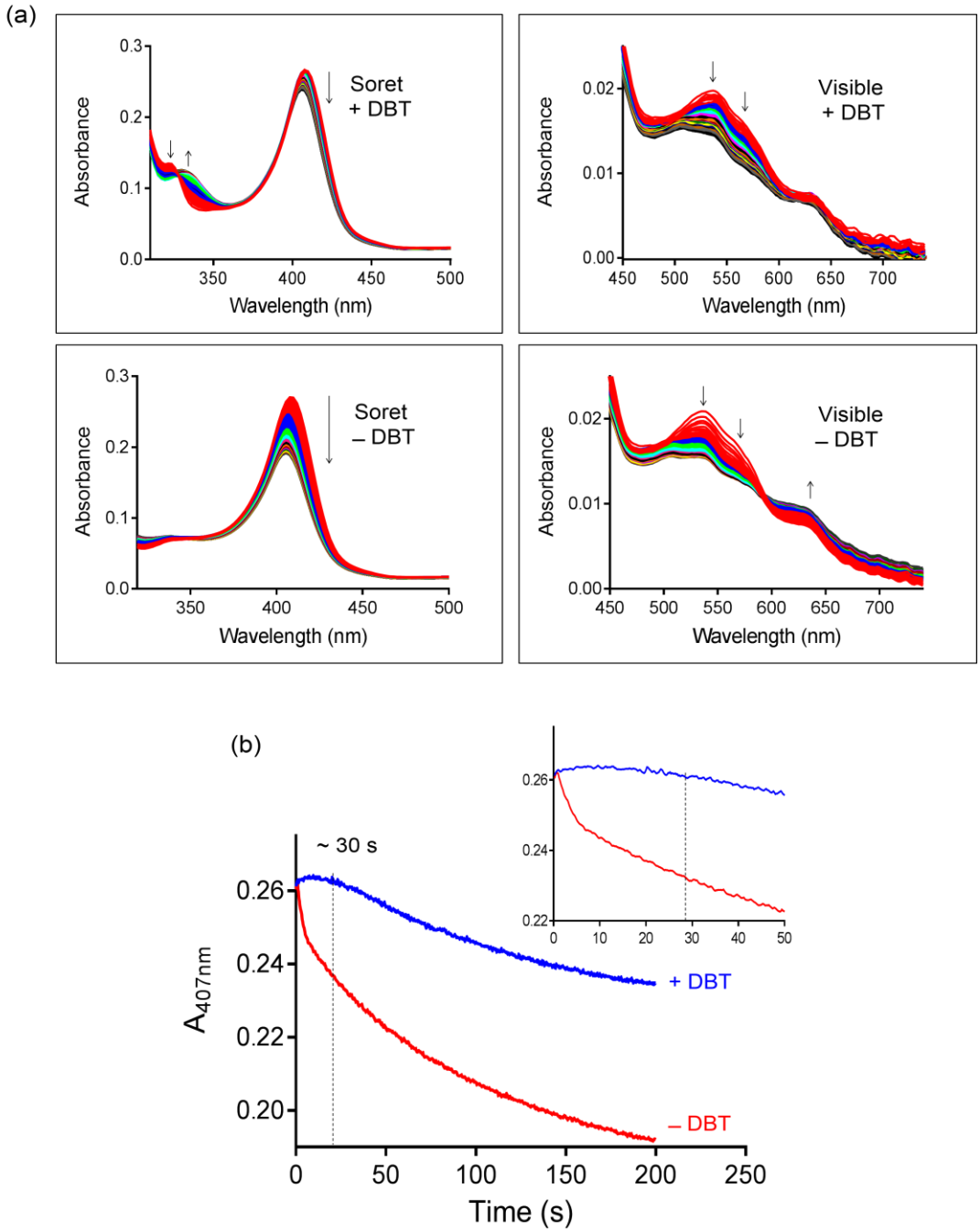


**Figure 4-8** **(a)Time dependent spectral changes in Soret (left) and visible (right) in the presence (top) or absence (bottom) of DBT for the reactions catalyzed by heme/G4-DNAzyme. Data were collected over a scan period of 200 sec. Arrows indicate the direction of the absorbance change with time. (b) a graph demonstrates the time dependent changes of the absorbance at the Soret wavelength ($A_{407}$).**

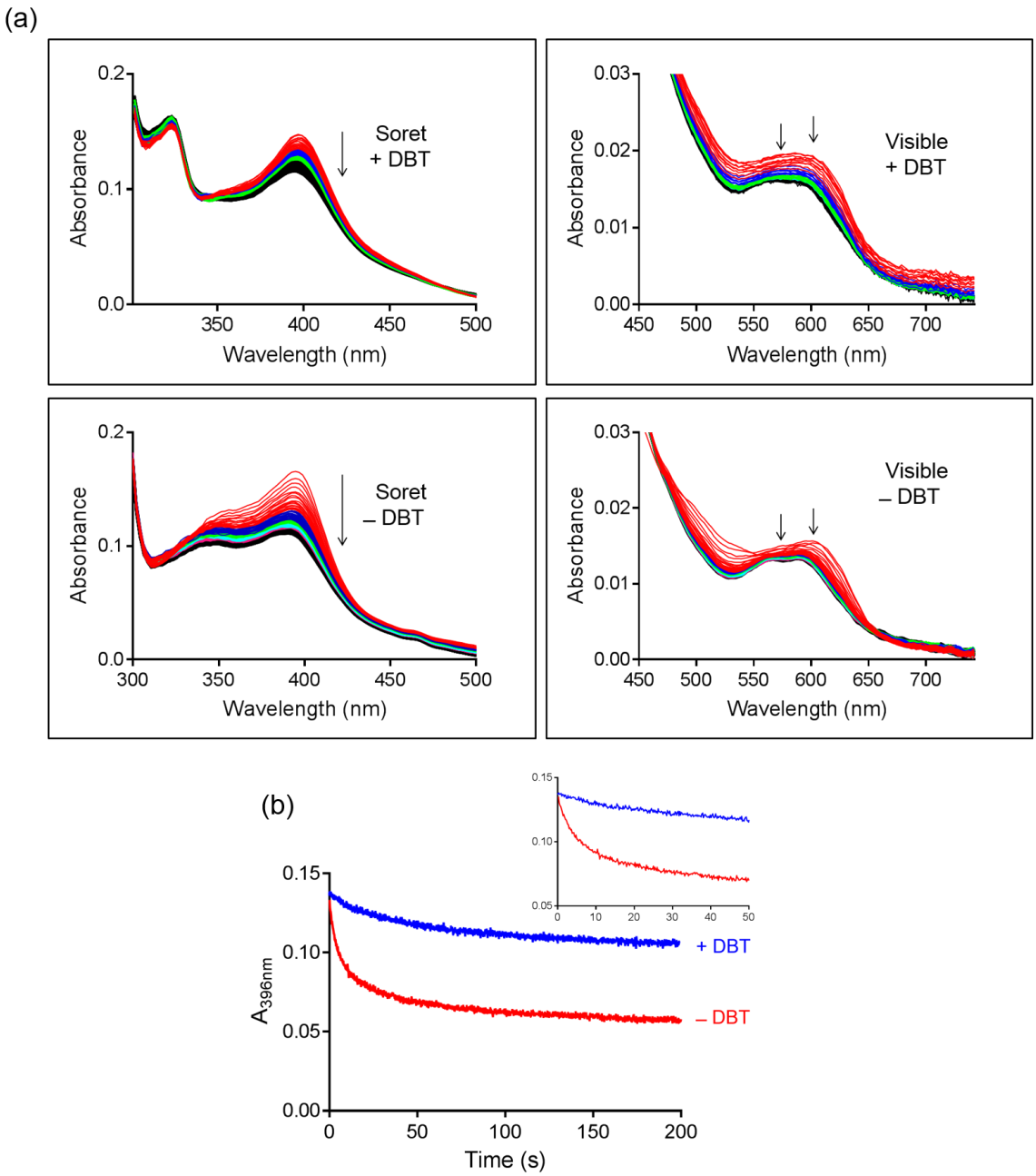


**Figure 4-9** **(a)Time dependent spectral changes in Soret (left) and visible (right) in the presence (top) or absence (bottom) of DBT for the uncatalyzed reactions using BLD oligonucleotide. Data were collected over a scan period of 200 sec. Arrows indicate the direction of the absorbance change with time. (b) a graph demonstrates the time dependent changes of the absorbance at the Soret wavelength ($A_{396}$).**

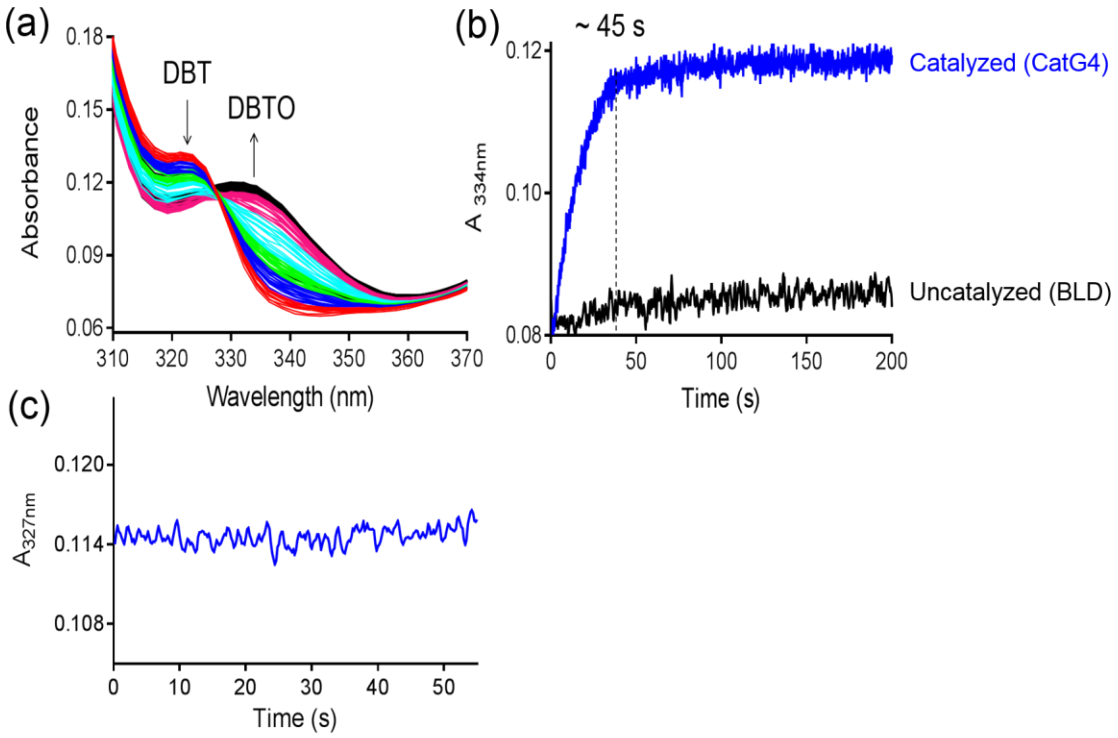


**Figure 4-10 (a) The time dependent spectral change in the region (310-370 nm) indicating the formation of DBTO from DBT. (b) The corresponding time profile change in absorbance of DBTO at 334 nm for the catalyzed (blue) and the uncatalyzed (black) reactions. (c) Time profile absorption change at 327 nm.**

In the presence of the reducing substrate DBT, the Soret band of the heme is unchanged for ~ 30 sec [see figure (4-8 a and 4-8 b)]. This is likely arising from a reaction of the active heme species with DBT to produce DBTO, followed by the heme/G4-DNAzyme recovery step. This is also consistent with the time profile of DBTO fast production within the first 30 sec of the reaction (figure 4-10 b). However, the time profile for formation of DBTO (figure 4-10 b) indicates that the reaction is over by ~ 45 sec. The presence of DBT prior the addition of hydrogen peroxide offers a degree of protection to the heme/G4-DNAzyme; preventing the process of heme degradation. This protection, after the addition of $H_2O_2$ lasts for 30 sec, then a competing process begins. This competing process conceivably involves a second molecule of $H_2O_2$ and the active intermediate to generate a product that leads to the irreversible deactivation of the heme/G4-DNAzyme, and this what corresponds to the subsequent decay of the Soret band (figure 4-8 b).

In absence of DBT, the sharp decline of the Soret band within the first ~2 sec (figure 4-8 b) probably signifies the time required for the formation of the active intermediate. This is followed by continuous decay of the Soret peak; a sign of heme being degraded. In peroxidases, in absence of reducing substrate, a second molecule of $H_2O_2$ could serve as a reducing substrate that could either restore the ground state of the enzyme or generate reactive oxygen species, which in turn leads to modification of the heme prosthetic group and form verdohemoprotein as a final product (258-260).

In order to deconvolute the spectra associated with each species involved, and to obtain rate constants, the collected datasets shown in figure (4-8 a) and (4-9 a) were reduced by SVD as described in the Methods section, then processed by the global fitting routine. Based on the above remarks regarding the changes in the Soret band in the presence or absence of DBT, the datasets were fit to the models described in the scheme shown in figure 4-11. In this scheme, when DBT is present [shown in figure 4-11 (a)] the ferric(III)-DNAzyme (denoted E) reacts with $H_2O_2$ to produce the active intermediate C, which then reacts with the substrate S (DBT) to produce the product SO (DBTO) and re-forms the resting enzyme. These two processes describe the early stage of the reaction (0-30 seconds). After the substrate is almost consumed, the competing reaction of C and $H_2O_2$ leading to heme degradation (product denoted as “P”) becomes prominent. The same model was proposed for the case where DBT is absent except for the step of the DNAzyme recovery [see figure 4-11 (b)].

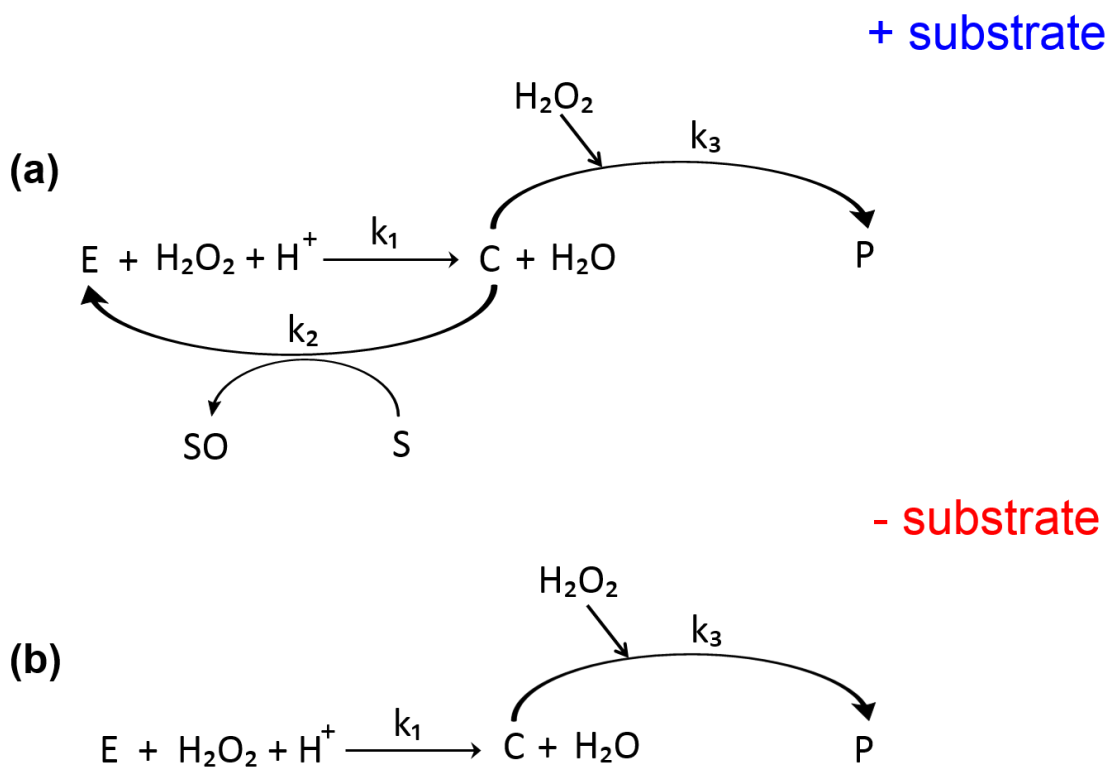


**Figure 4-11 The model of activation and deactivation of the heme/G4-DNAzyme. (a) The scheme in the presence of substrate (DBT) showing the catalytic turnover of the enzyme described by the second order rate constant $k_2$. (b) The scheme in the absence of substrate showing the route of deactivation described by $k_3$.**

The deconvolved spectra of each species: E, C, and P, are shown in figure 4-12. The data demonstrate that the ferric(III)-DNAzyme converted to species C which exhibits an undiminished and slightly blue-shifted Soret (~2 nm) with the following spectroscopic features: Soret at 405, and visible peaks at 530, 582, 633 and a shoulder at ~506 nm. Then, the spectrum of species C changes to P with the Soret peaking at 406, and visible peaks at 500, 533, 580, and 631 nm. The spectroscopic characteristics of species E, C, and P are summarized in table 4-1.

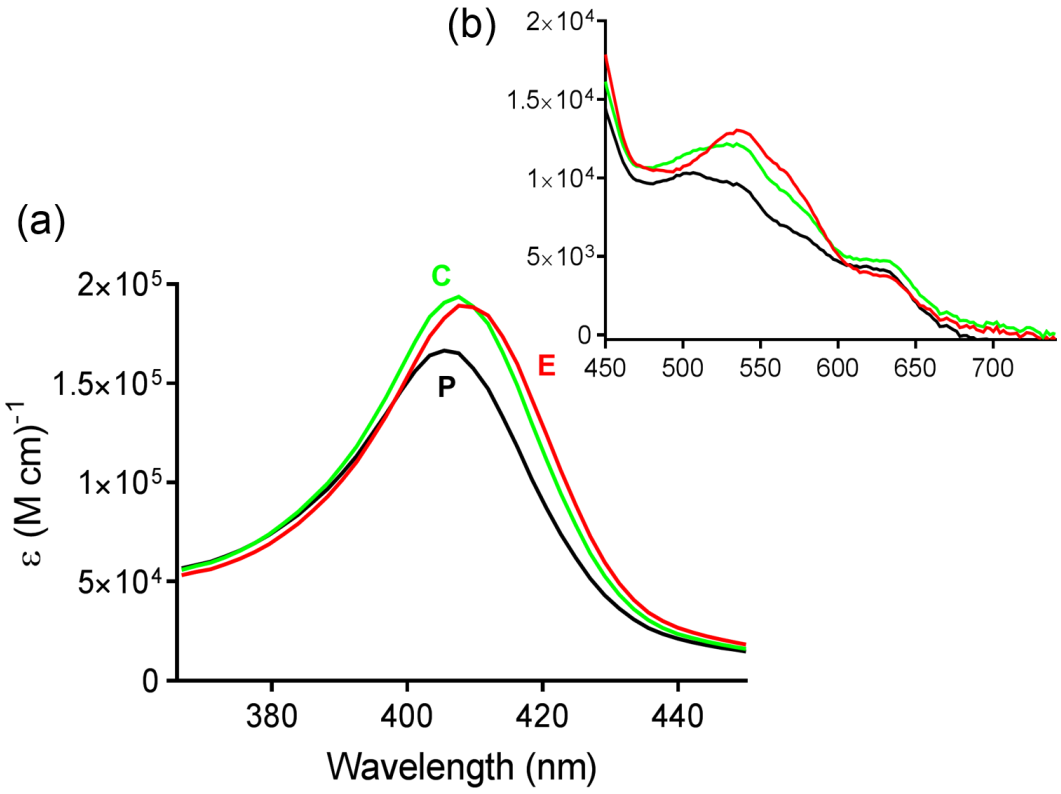


**Figure 4-12** **Deconvolved spectra for the catalyzed reaction. (a) Soret region of the spectrum; heme/G4-DNAzyme (red), activated species C (green), and the product leading to heme degradation P (black). (b) Visible region.**

| Heme enzyme | Axial ligand | radical position | Soret $\lambda_{max}$ (nm) | Visible peaks $\lambda_{max}$ (nm) | References |
|---|---|---|---|---|---|
| HRP H42L mutant | His170 | Not reported | 404 | 495, 540, 576, 640, ~600 | (146) |
| Metmyoglobin | His93 | Trp14 | 421 | 551, 586 | (143) |
| Cytochrome c peroxidase | His175 | Trp191 | 419 | 530, 560<br>(530, 560, 632)* | (261)<br>(262) |
| P450cam | Cys357 | Tyr96 or Tyr75 | 406 | 537, 571 | (144, 145) |
| Heme/G4 DNAzyme | G4?<br>$H_2O$? | Guanine | 407 | ~506, 530, 582, 633 | [this work] |

**Table 4-1 Comparison of Compound I' absorption parameters of different heme enzyme complexes. The asterisk beside Cytochrome c peroxidase visible peaks indicates that this data was obtained from single crystal microspectrophotometry experiment from (262). All other parameters were based on stopped-flow experiments.**

In comparison with hemoproteins, the DNAzyme's active intermediate in general manifests the spectroscopic characteristics of a compound I', such as reported for many hemoproteins. These include an undiminished Soret amplitude as well as a defining set of visible peaks (see table 4-1). The central difference between Compound I' and classic Compound I is that the former has an oxidizing equivalent radical cation on an amino acid residue rather than on the porphyrin core as in the latter. Several studies have indicated that a tryptophan radical is formed on reaction of cytochrome c peroxidase with $H_2O_2$ (142, 220, 233). A tyrosine-centred radical was also reported in the case of $P450_{cam}$ (144, 145). Compound I' has also been reported for metmyoglobin (143, 263). Interestingly, a Compound I' was reported to be formed in a site-directed mutant of HRP enzyme, in which the polar distal histidine His42 was mutated to leucine (H42L mutant) (146). Our stopped-flow study is in agreement with Travascio's earlier EPR study (115), that revealed an EPR signal obtained by reacting the heme/G4 (heme-PS2M) complex with $H_2O_2$ to those obtained from cytochrome c peroxidase and metmyoglobin. The question then becomes: what does the active species look like in a heme-utilizing nucleic acid enzyme? The evidence suggests that it is a species resembling the various Compound I' found in hemoproteins. Then, where might the radical cation that is the second oxidizing equivalent

within the ferryl-oxo species of the DNAzyme be hosted? It is well-known that guanine (G) has the lowest oxidation potential of the four DNA bases, and is therefore the most readily oxidized (264) to a guanine radical cation (G•+) (see figure 4-13). It is highly plausible, therefore, that a heme/G4 complex's activated species is a ferryl-oxo species coupled to a guanine radical cation (Fe(IV)=O G•+).

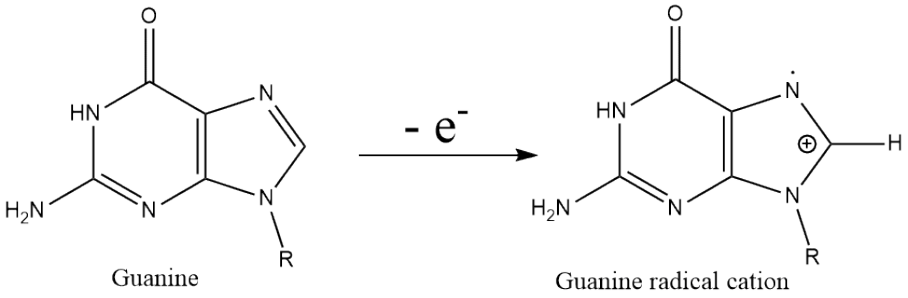


**Figure 4-13 The oxidation of guanine base to guanine radical cation.**

### 4.4.3 The kinetics of DBT sulfoxidation

The concentration profiles that resulted from global fitting to the model shown in scheme 4-3, in the cases of (+DBT) and (-DBT), are shown in Figure 4-14. The concentration differences over ~ 45 sec of species E and C of the case where DBT is present and of the case where it is absent are mainly due to step 2 (described by $k_2$) in the proposed scheme (see scheme 4-11). In the presence of DBT, the decay of the DNAzyme (E) and the formation of the activated species (C) had biphasic behavior: rapid decay of E and formation of C in the first ~900 ms followed by a slower change in concentration over time. The activated species, C, starts to decay after 30 sec, consistent with competition with the heme degradation reaction. In the absence of DBT, a rapid and continuous decay observed for E associated with rapid formation of C. Figure 4-14 c and d shows the concentration profiles of DBT to DBTO conversion for the catalyzed and the uncatalyzed reactions respectively. It can be clearly seen from figure 4-14 c and d that the heme/G4-DNAzyme accelerated the oxidation of DBT to DBTO relative to the uncomplexed heme "in presence of a single stranded oligonucleotide".

The second order rate constants obtained from the global fit are summarized in table 4-2. It should be noted that the various values of $k_1$ (describing the formation of the activated species) and of $k_3$ (describing the heme degradation process) are mutually

consistent, suggesting that they define the same steps whether in absence or in presence of DBT. Also, the rate enhancement (described by $k_2$) for the catalyzed reaction in the presence of DBT was found to be 100-fold greater than that of the uncatalyzed reaction confirming a role for the G-quadruplex in catalyzing the conversion of DBT to DBTO. Interestingly, In the case where DBT is present, the rate of formation of the "catalytic species" (described by $k_1$) for the catalyzed reaction was found to be 20-fold that of the uncatalyzed reaction. The protection of the Soret band in the presence of DBT is also observed in the uncatalyzed reaction suggesting some sort of heme activation happening probably through a formation of "Compound I-like species". However, the nature of the activated species formed during the activation of heme in the uncatalyzed reaction is not explicitly clear to us. Another important observation, here, is regarding the heme degradation process described by $k_3$. Shangguan *et al*. claimed that the binding to G4 might have accelerated the degradation of heme (234). They based this assumption on the fact that the decrease of the Soret band of G4/heme complex (89%) is much higher than that of free heme (13%). Here, we found that the heme degradation step is not affected by binding to G4.

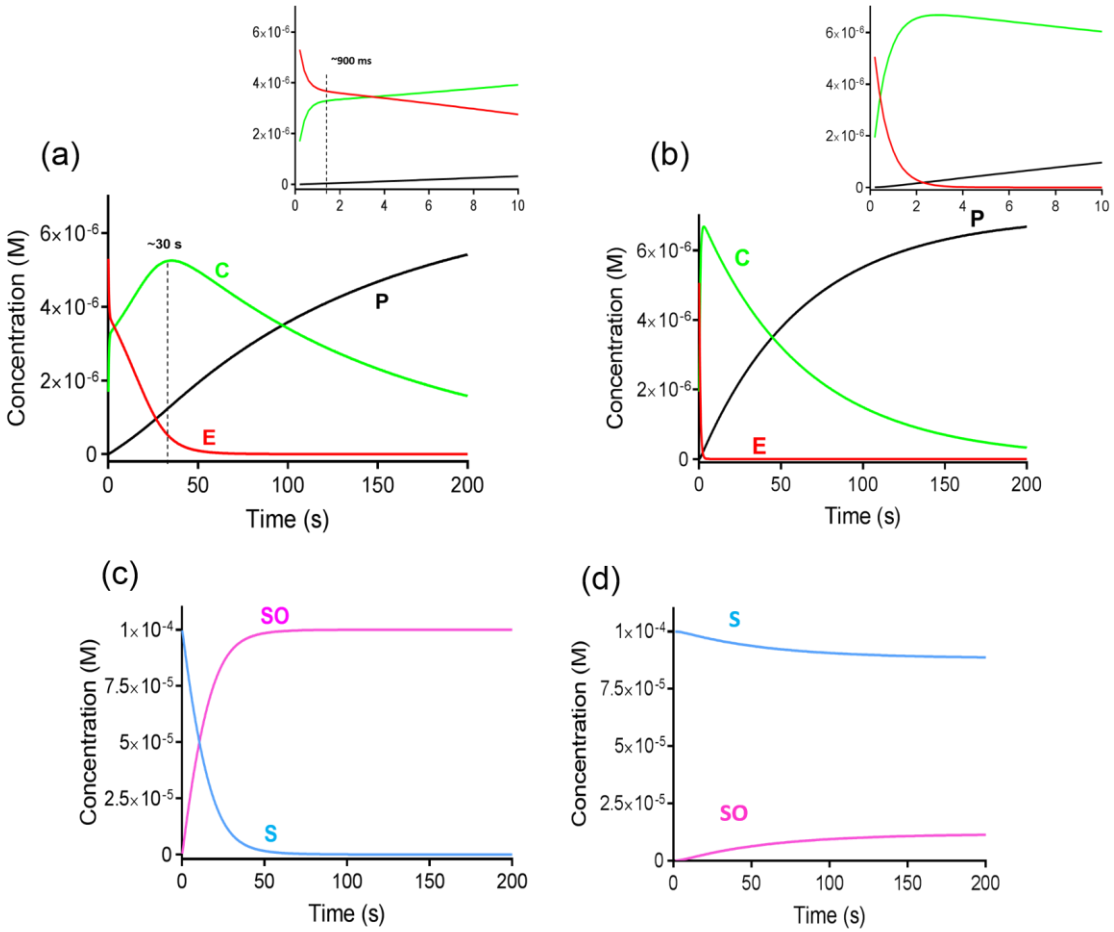


**Figure 4-14** **Concentration profiles for the catalyzed reaction in the presence of DBT (a) and in absence of DBT (b). The heme/G4-DNAzyme E (red trace), intermediate C (green trace), and intermediate P (black trace) are shown over 200 sec. (c) and (d) show the concentration profiles for the DBT (blue) and DBTO (pink) for the catalyzed and the uncatalyzed reaction, respectively.**

**Table 4-2 Second order rate constants describing the oxidation of DBT to DBTO. Rate constants $k_1$, $k_2$, and $k_3$ (see figure 4-11) are reported as the mean of 3 replicate experiment with their standard deviation.**

| Rate constants ($M^{-1}$ $s^{-1}$) | Catalyzed racations | | Uncatalyzed reactions | |
|---|---|---|---|---|
| | + DBT | – DBT | + DBT | – DBT |
| $k_1$ | $(4.9 \pm 2.8) \times 10^3$ | $(3.4 \pm 0.5) \times 10^3$ | $(2.6 \pm 0.9) \times 10^2$ | $(3.3 \pm 0.4) \times 10^2$ |
| $k_2$ | $(23 \pm 8) \times 10^3$ | - | $(3.2 \pm 0.6) \times 10^2$ | - |
| $k_3$ | $21 \pm 4$ | $27 \pm 3$ | $47 \pm 7$ | $30 \pm 5$ |

It would be interesting to relate the rate constants found in our study to hemoproteins known to oxidize DBT substrate or perform sufoxidation reactions. Unfortunately, the Wariishi *et al*. (128) study on the oxidation of DBT by microperoxidase did not report rate constants. Abraham spector *et al.* (247), though, have determined the second order rate constant for the reaction of MP-11 with $H_2O_2$ to be $3.5 \times 10^3$ $M^{-1}$ $s^{-1}$ at 25 °C, in agreement with other studies (247, 265-267). By analogy to HRP, the observed spectral changes resulting from the reaction of MP-11 and $H_2O_2$ was attributed to the formation of a peroxidatic intermediate analogous to peroxidase Compound I (containing a high valent iron-oxo ferryl moiety (FeIV=O) and a π-radical cation localized on the protoporphyrin ring (247, 268). On the other hand, Hui-Chun Yeh *et al*. (268) have performed a stopped-flow kinetic study of peroxidation reactions using $H_2O_2$ and microperxidase-8 at 25 °C in the presence of several substrates. Theses authors have reported the rate constants of reducing compound I to the resting enzyme by ABTS, aniline, and ferrocyanide to be $4.08 \times 10^5$, $4.68 \times 10^4$, and $4.03 \times 10^4$ $M^{-1}$ $s^{-1}$ respectively. Interestingly, these values are comparable to this of the heme/G4 system ($k_2 = 2.3 \times 10^4$ $M^{-1}$ $s^{-1}$), despite the difference in the type of the oxidation reactions and the active intermediate observed in the two cases. On the other hand, cytochrome c peroxidase, known to mediate the oxidation reaction via the formation of a Trp-191 radical cation-based compound I (Compound I'), has higher rate constant of formation of Compound I' from $H_2O_2$ than the heme/G-DNAzyme determined to be $3.4 \times 10^7$ $M^{-1}$ $s^{-1}$ at 25 °C (269). The formation of Compound I' from cytochrome c peroxidase and $H_2O_2$ at 25 °C has been also reported by other parallel studies; $4.5 \times 10^7$ $M^{-1}$ $s^{-1}$ (270) and $2.7 \times 10^7$ $M^{-1}$ $s^{-1}$ (271).

It would be more appropriate, however, to compare the rate constants obtained in our study on the heme/G4-DNAzyme to those of hemoproteins known to perform sulfoxidation. The monooxygenation of thioanisole by Compound I was reported by Ishimura *et al*. for sperm whale metmyoglobin and horse heart metmyoglobin, with rate constants of 27.3 x $10^3$ and 30.3 x $10^3$ $M^{-1}$ $s^{-1}$, respectively (143). Interestingly, it has been reported that ~ 30% of the peroxide O-O bond-breaking reaction in sperm whale metmyoglobin occurs via homolytic cleavage compared to 100% heterolytic cleavage in peroxidases (218, 272). These mechanisms are discussed in section 4.5.1. Ishimura *et al.* determined the values corresponds to the rate constants for the homolytic and heterolytic cleavages of $H_2O_2$ to be 4.9 x $10^2$ and 1.8 x $10^2$ $M^{-1}$ $s^{-1}$ for sperm whale metmyoglobin and 3.9 x $10^2$ and 1.1 x $10^2$ $M^{-1}$ $s^{-1}$ for horse heart metmyoglobin respectively. These latter values, though, were not experimentally determined but they were obtained based on rate equation assumptions (see reference (143) for details). Nevertheless, these values clearly indicate that the homolytic cleavages indeed proceeded at significant rates, which were of a comparable order of magnitude as that of the heterolysis. Our obtained $k_1$ value is larger than both values of homolytic and heterolytic breakage (~ 10-fold and ~ 30-fold higher than that of sperm whale metmyoglobin and ~ 12-fold and ~ 50-fold that of horse heat metmyoglobin), respectively. More experiments are still needed to check for the true mechanism (see Discussion section); however, the faster $k_1$ value for the formation of the activated species within the heme/G4-DNAzyme compared to ferric myoglobin might be explained in the view of the stability of the activated species formed in the two cases.

### 4.4.4 Residual plots

To probe the validity of our proposed model, we looked at the associated wavelength residual plots. Residuals are the results of subtracting the calculated data from the measured data. They represent an informative gauge to the quality of the fit as we explained earlier in the experimental section. The obtained residuals obtained from fitting the above model showed no systematic deviations; a sign of an appropriate fit. As a further check, one kinetic step was systematically removed from the model, rate constants values were fixed for the included steps, and datasets were reanalyzed followed by inspecting the effect on the residuals. Interestingly, removing any of the steps from the model

generated asymmetric residuals. These data are shown in figures 4-15 for + DBT and – DBT models.

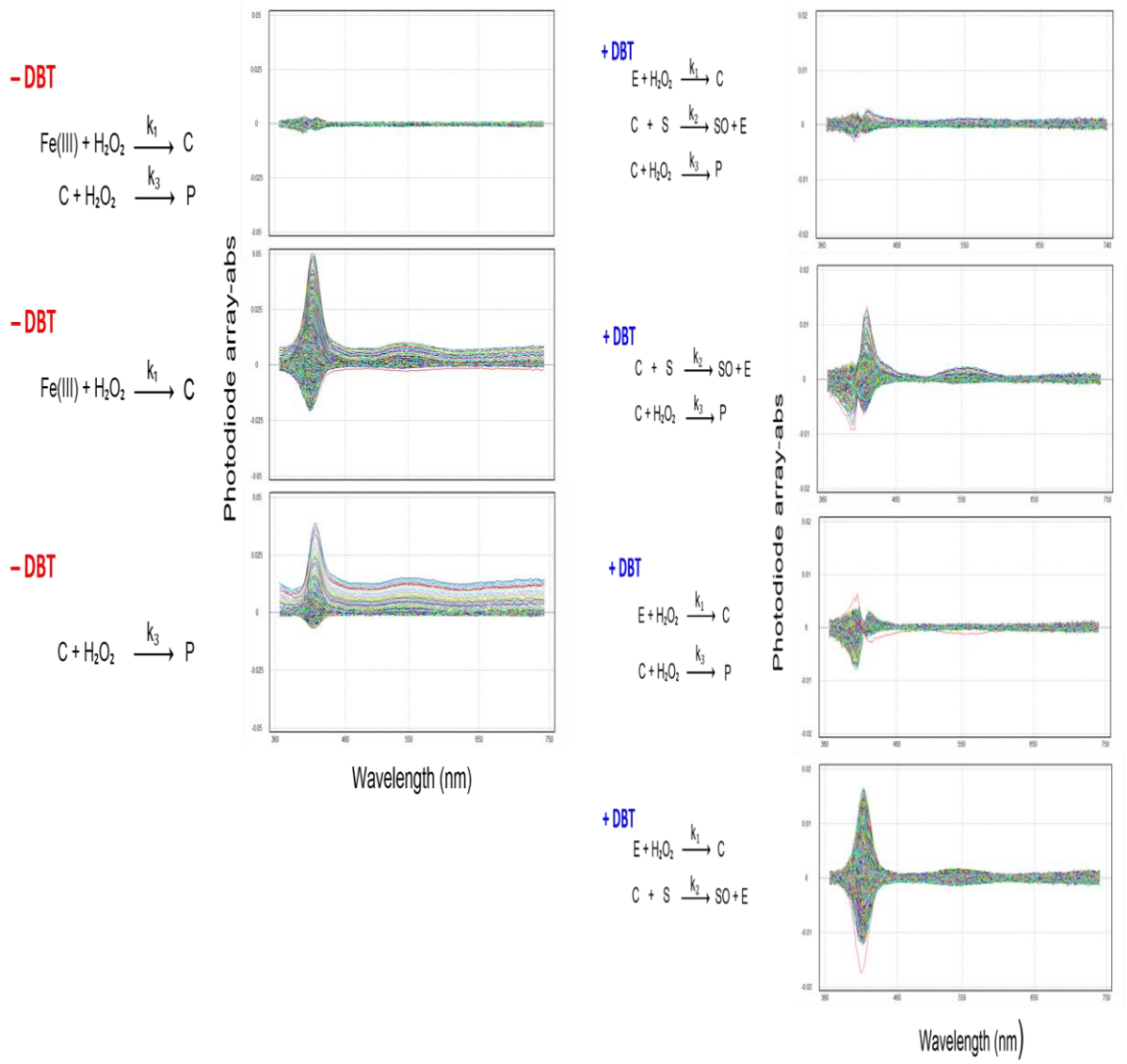


**Figure 4-15 Residual plots are shown as a function of wavelength. Right and left panels represent residual plots from + DBT and -DBT datasets, respectively. The complete model and the ones with the omitted step is shown next to the plots.**

## 4.5 Discussion

### 4.5.1 Heterolytic vs homolytic cleavage of the O-O bond of the hydroperoxide complex

Various studies on hemoproteins have suggested two mechanisms by which compound I'-type is generated [see figure 4-16]. The first mechanism involves a transitory porphyrin radical cation that forms by heterolytic cleavage of the O-O bond present in the ferric hydroperoxide intermediate [Fe(III)-OOH] formed by complexation of the peroxide anion to the heme iron atom. The formation of a classic compound I [Fe(IV)=OPor•+] is followed by an electron transfer process that oxidizes a nearby amino acid residue to generate the lowest energy structure possible. Schunemann, Jung, and colleagues tried unsuccessfully to trap $P450_{cam}$ compound I by rapid-mixing/freeze-quench methods (273-277). Instead, they observed a ferryl heme centre combined with a tyrosine radical cation (Compound I') that has been also reported by Spolitak *at el.* (144). However, the formation Fe(IV)=O Por•+ species has been reported for CYP119 (278, 279) and $P450_{BM3}$ (280) using singular value decomposition and spectral deconvolution methods. Spolitak *et al*. (144) more extensively examined the formation of the classic compound I form in $P450_{cam}$ as a function of pH, temperature, and oxidizing agents. They found that while $P450_{cam}$ compound I formation was optimal with the m-CPBA oxidant at 25 °C and pH 7.4, and Compound I' forms best at 3 °C and pH 6.2 (144). The $P450_{cam}$ studies, however, suffered from the onset of heme bleaching after about 50 -100 ms owing to secondary reactions of the ferryl species with the excess peracid present. Nevertheless, their results have confirmed that compound I from $P450_{cam}$ is a sufficiently potent oxidant to react with either Tyr96 or Tyr75 to form Cpd I'-like species (144, 145, 281). With regard to the heme/G4 system, evidence form our lab has shown that the best oxidizing agent to be used with these heme/G4-DNAzymes is $H_2O_2$. Other strong oxidizing agents (eg; sodium hypochlorite/bleach or m-CPBA) were found to be efficient in not only accelerating the process of heme bleaching but also promoting the oxidation of "free" uncomplexed heme. Furthermore, the significant level of the heme degradation, indicated by the heme Soret band decay, when using 2- ,5-, and 10-fold of excess of m-CPBA over the DNAzyme concentration prevents detection of Compound I or Compound I' in the stopped-flow experiments. We are going to examine the effect of temperature as well as the pH under

the same experimental condition described in section 4.3.3 to see whether the classic Compound I [Fe(IV)=OPor•+] is detectable.

The second mechanism of formation of Compound I' species involves homolytic cleavage of the O-O bond, by which a species like compound II [Fe(IV)=OPor] and hydroxyl radicals are formed. This mechanism has been proposed by Thorneley *et al*. (146) for the HRP H42L mutant, in which a mutation of the polar, distal histidine to nonpolar leucine was found to promote the homolytic cleavage of the O-O bond, giving rise to a novel type of compound I with a protein based radical cation (Compound I') located more than 10 Å away from the iron observed instead of the normally-detected compound I with wild-type HRP. These authors reported the spectrum of a Compound I' at 13 sec and further confirmed the formation of such a species by EPR and kinetic studies (146). They proposed a mechanism whereby Compound I' is formed from [Fe(IV)=OPor] and •OH via 1 $e^-$ transfer process.

It is the polarity of the heme's distal residues that governs the type of O-O cleavage in a hemporotein. In fact, in peroxidase-catalyzed reactions, the O-O bond of the [Fe(III)-OOH] intermediate, also known as compound 0, is known to be cleaved in heterolytic fashion (93). For this cleavage, in addition to histidine's role in acid-base catalysis, a positive charge on an arginine residue present on the heme's distal side (Arg-38 in HRP and Arg-48 in CcP) has been suggested to assist the heterolysis (141). On the other hand, hydrophobic residues such as Phe-43 and Val-68 occupy the distal space in metMb, resulting in the lack of amino acid residues analogous to Arg of peroxidases, thus, homolytic cleavage can occur.

Applying the above observations to the heme-nucleic acid catalyst highlight some common arguments. The homolytic cleavage-based mechanism is at odds with earlier data from our lab, in which Travascio *et al*. showed that the presence of nitrogenous buffers enhanced the peroxidation of ABTS by the heme-nucleic acid catalysts (12). Based on these outcomes, the acid-base catalysis which should boost the heterolytic cleavage, seen here, was ascribed to the nitrogenous buffering agents in the reaction solution. Moreover, her spin-trapping EPR experiments failed to detect •OH radicals in the reaction of the heme-PS2M complex with $H_2O_2$ (115). In support of this, our unpublished data on

ABTS peroxidation carried out under a condition where hydroxyl radical scavengers; *N*, *N'*-dimethylthiourea [DMTU] and nitrotetrazolium blue [NBT] were present, at 10-fold higher concentration than heme/G4-DNAzyme resulted in no inhibition of the initial rate of $ABTS^{\bullet+}$ formation over 10 min. Our inability to detect any Fe(IV)=OPor•+ species does not rule out the O-O homolytic cleavage mechanism which perhaps is occurring. In fact, evidence that supports the homolytic cleavage was observed in a previous spin trapping EPR experiment, in which it was shown that heme-PS2M complex degrades t-Bu-OOH by scission of the O-O bond in a homolytic fashion to yield *tert*-butyloxyl radicals as the primary radical species (282). However, parallel spin-trapping studies with $H_2O_2$ indicated that the free radical detected upon reactions of the PS2M-heme complex was either a tertiary or secondary carbon-centered radical, likely localized on the PS2M G4-oligonucleotide (115). Overall, the EPR data indicated that the O-O bond must be cleaved in order to generate these radical species, however, further experiments are needed to clearly determine the correct mechanism of O-O bond cleavage. For example, Wonwoo Nam *et al*. (283) performed interesting experiments while studying the electronic effect of porphyrin ligands on the heterolytic versus homolytic O-O bond cleavage of the hydroperoxides. They studied catalytic epoxidations of cyclohexene by various iron(III) porphyrin complexes containing electron-withdrawing and -donating substituents on the phenyl groups at the meso positions of the porphyrin ring. In addition, various imidazoles were introduced as axial ligands to investigate the electronic effect of axial ligands on the pathways of hydroperoxide O-O bond cleavage. The hydroperoxide O-O bonds were found to be significantly affected by the electronic nature of the iron porphyrin complexes (i.e., electronic properties of porphyrin and axial ligands). Electron-deficient iron porphyrin complexes showed a tendency to cleave the hydroperoxide O-O bond heterolytically, whereas electron-rich iron porphyrin complexes cleaved the hydroperoxide O-O bond homolytically (283). On the other hand, a binding study by Yamamoto *et al*. (119) on some chemically modified porphyrins differing in the numbers trifluoromethyl ($CF_3$), $CH_3$, and $C_2H_5$ side chains to the parallel G-quadruplex DNA (formed from a single repeat sequence of the human telomere, d(TTAGGG) showed that the measured association constant values ($K_a$) of binding to heme were unaffected by these modifications (119). It would be interesting to investigate what effect those peripheral heme modifications have on peroxidation (1 $e^-$) as well as the (2 $e^-$) oxygen transfer oxidation reactions catalyzed by

these DNAzymes. Results that should throw light on the key requirements of hetero- versus homolytic O-O bond breakage.

### 4.5.2 Direct vs rebound oxygen transfer

Another mechanistic perspective worth considering is that for protein heme enzymes that catalyze 2-electron oxidations, two contrasting mechanisms [reviewed in (284)], have been proposed: a direct transfer of oxygen from compound I to the substrate and two successive 1-electron oxidations that proceed via a substrate radical intermediate. The latter mechanism is called “oxygen rebound”. Poon *et al*. (106) analyzed the mechanism of thioanisole sulfoxidation based on a Hammett analysis of para-substituted thioanisoles, containing net electron-donating (methyl and methoxy) or -withdrawing (nitro and chloro) groups. Specifically, the log of the initial oxidation rate (v) was plotted against a Hammett substituent constant-- either σ, which is based on an equilibrium ionization process, or σ+, which is based on the rates for a carbenium ion forming reaction. log v values were found to correlate with the electron-donating power of the substituent (- 0.7 ± 0.07 in the σ+ plot and - 0.96 ± 0.12 in the σ plot), and both are consistent with a buildup of positive charge in the oxidation transition state. However, The correlations between the σ+ and σ substituent constants with the initial rates of the para-substituted substrates are not significantly different, and therefore not enough to permit a definitive mechanistic conclusion to be made (106). A following experiment by the same authors involved an $^{18}O$ labeling experiment using $^{18}O$-$H_2O_2$, that showed that the oxygen in the thioanisole sulfoxide was quantitatively $^{18}O$. This last observation suggests that thioanisole does not transiently come in contact with the catalytic core of heme/G4 complex, but must be positioned near the ferryl-oxygen for sufficient time for quantitative oxygen atom transfer to take place. This indicates that perhaps direct oxygen insertion mechanism was indeed operational for the heme/G4-DNAzyme (see figure 4-16). In my stopped-flow study, the presence of spectral isosbestic point across the conversion of DBT to DBTO is not in itself sufficient to prove the direct oxygen insertion mechanism as there is the possibility of rapid formation and decay of the $DBT^{\bullet+}$ transition state intermediate. We would like to apply the$^{18}O$-$H_2O_2$ labeling experiment on DBT sulsoxidation to further inspect the direct vs rebound mechanisms.

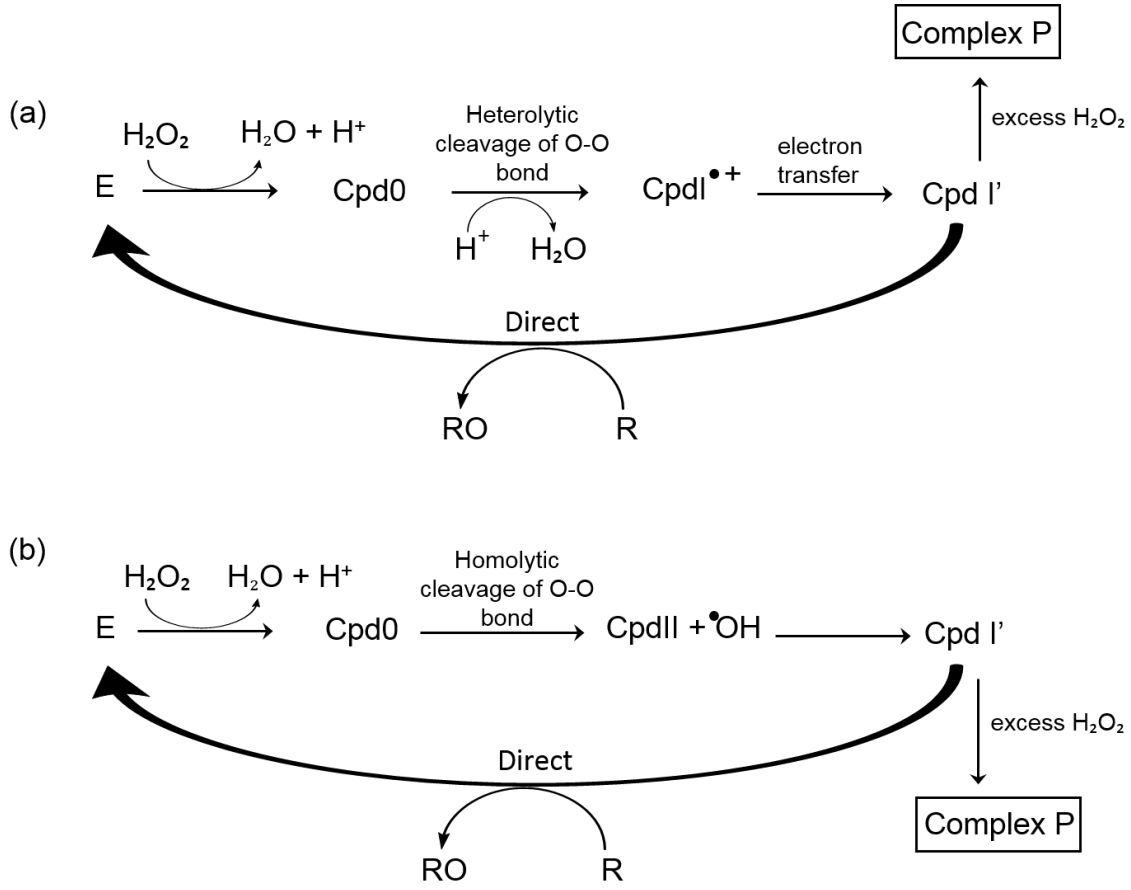


**Figure 4-16 Proposed mechanism for Compound l' (denoted as Cpd l') formation by heterolytic (a) or hemolytic (b) cleavage of the O-O bond. Complex P denoted the product leading to heme degradation.**

### 4.5.3 What other intermediate species are generated in the reaction of heme/G4-DNAzyme with $H_2O_2$?

If the mechanism of direct oxygen transfer for the (2 $e^-$) oxidation reactions catalyzed by these heme/G4-DNAzymes is true, that would exclude the formation of a compound II [Fe(IV)=OPor] species. However, compound II should form theoretically in reactions involving one electron oxidation (1 $e^-$) (e.g oxidation of ABTS). The study of Shangguan *et al*. did not detect the spectroscopic characteristics of compound II, but this was explained in terms of such an intermediate rapidly reacting with the reducing substrate or with $H_2O_2$ to form a third intermediate leading to heme degradation (234). A similar example of with a hemoprotein was that of KatG (Mycobacterium tuberculosis), where Chouchance *et al*. (285) concluded that compound I could be reduced to the ferric enzyme by isoniazid, ascorbate, or potassium ferrocyanide, but no compound II could be detected in any case.

An intermediate leading to the heme destruction pathway, known as compound III, is a peroxy-Fe(III)-porphyrin free radical [Fe(III)-$OO^{\bullet-}$]. Compound III (Cpd III) of peroxidases was first reported by Keilin and Mann in the reaction of HRP with a large excess of $H_2O_2$ (286), and it is known to be formed by several routes. A competition between an electron-donor substrate and $H_2O_2$ can either restore the ground state or form compound III (243, 260). An alternative mechanism proposed by Grant Mauk *et al*. (287) involves a reaction of compound I with an excess of $H_2O_2$ to produce superoxide anion-cpd III. Further reaction of cpd III with $H_2O_2$ generates hydroxyl radicals which in turn react irreversibly to inactivate the heme; most likely via the formation of verdohemoprotein as a final product. Cpd III is analogous to oxyhemoglobin and oxymyoglobin, since the latter both contain low-spin heme iron with His and dioxygen in the fifth and sixth ligand positions, respectively. Equivalent species have been detected in other hemoproteins, such as cytochrome c (288) cytochrome c peroxidase (289), lignin peroxidase (290), bovine liver catalase (291), and manganese peroxidase (292). The optical spectrum of Cpd III from HRP A2 generated by the addition of 500 mM excess of $H_2O_2$ has a Soret maximum at 416 nm and secondary maxima at 540, 580, and 665 nm (293). Comparably, we propose here that the active intermediate reacts with excess $H_2O_2$ in absence or presence of limiting reducing substrate to form a Cpd III-like intermediate (spectrum P in

figure 4-12), that in turn leads to chemical modification of the heme prosthetic group. A detailed mass spectroscopy analysis is required to check this hypothesis.

### 4.5.4 Is the classic compound I [Fe(IV)=OPor•+] actually forming in the reaction of heme/G4-DNAzyme with $H_2O_2$?

If Compound I' is forming via a heterolytic cleavage mechanism in these heme/G4-DNAzymes, as in mechanism a shown in figure 4-16, then a question can be posed: why are we not detecting the high-valent ferryl oxo species coupled to porphyrin radical cation (the "classic Cpd I")? In fact, several systems, in addition to $P450_{cam}$, have been shown to form protein radical species as a result of ferryl porphyrin π-cation radical intermediates being reduced by nearby easily oxidizable amino acid residues. In some cases, there is no observed porphyrin π-cation radical, probably because it does not accumulate to a detectable level, or is only seen transitorily. The classic example is that of the reaction of cytochrome c peroxidase with $H_2O_2$ to form Cpd I', where a Fe(IV)=O is formed with the second oxidizing equivalent residing on a tryptophan residue as a stable tryptophanyl radical cation; no Cpd I is seen (294-297). However, in the W191F mutant form of CcP, a transient porphyrin π-cation radical is seen, but with a half-life of only 14 ms (decays with a rate constant of 51 $s^{-1}$) (219, 298, 299). In that regard, it would be interesting to test other DNA-forming G-quadruplexes or other heme-binding structures like isoguanine pentaplexes which also exhibit peroxidase activity as described in chapter 3, to see if any of these enable us to see a classic compound I rather than Compound I'.

When Compound I' forms in Cytochrome $P450_{cam}$, the radical cation is located either on Try96 or Try75. These residues are the closest to the heme iron centre, with distances of 7.4 Å and 7.6 Å respectively. Thus, they are suitable candidates for oxidation and radical cation formation (145). Curiously, in heme/G4-DNAzymes the likely distance between the bound heme porphyrin and the uppermost G-quartet of the G-quadruplex should be similar to the typical π-π stacking distance of a base-pair in duplex DNA (3.4 Å) (300). It would therefore, in principle, be even easier for Cpd I to be reduced by a guanine base to form Cpd I', and this is perhaps what makes it challenging to detect the ferryl porphyrin π-radical cation in the heme/G4-DNAzyme. Interestingly, within GG and GGG clusters of either duplexes or G-quadruplexes, guanine oxidation potentials are even lower

than for an isolated guanine base (301); a fact that may also complicate the task of trapping the classic Cpd I . The guanine radical cation (G•+) in such DNA structures can be formed either by direct oxidation of specific guanines by a large variety of oxidants (264), or indirectly via hole (radical cation) migration through guanine stacks (302-304).

Guanine radical cations are susceptible to a degree of reaction with water and with dissolved oxygen to give guanine oxidation products such as 8-oxoguanine which can be further oxidized to (264, 305). However, we believe that this is prevented during the DNAzyme's turn over cycle by the presence of sufficient amount of reducing substrates. However, footprinting data using $H_2O_2$ as well as m-CPBA in the absence of any reducing substrate showed a band corresponding to a piperidine-cleavable oxidized guanine product (115). Burrows *et al.* (264) identified a number of guanine oxidation products observed from G-quadruplex-folded human telomeric sequence with four different oxidant systems: riboflavin photosensitization, carbonate radical generation, singlet oxygen, and the copper Fenton-like reaction. Interestingly, the final guanine oxidation products were found to depend on the type of oxidation system used as well as on the topology of the G-quadruplex structures. It would be beneficial for us to determine the structure of the guanine oxidation product by mass spectroscopy as this can suggest a pathway of the G-quadruplex oxidation by the heme/$H_2O_2$ or heme/m-CPBA systems.

### 4.5.5 Can an amino acid-based compound I catalyze oxygen transfer reactions via direct oxygen insertion mechanism?

The catalytic action of classic peroxidases as well as cytochrome p450 monooxygenases is mediated by the two-electron oxidized species in which the iron is oxidized to ferryl [Fe(IV)=O] coupled to a porphyrin radical cation. In cytochrome c peroxidase, the main catalytic species is generated when the second electron is removed from Trp-191 amino acid residue to generate the ferryl [Fe(IV)=O] and a protein radical. A protein radical-type activated species was also reported for ferric myoglobin and HRP H42L mutant. Both types of these high-valent iron compounds were found to be essential intermediates in the peroxidation reactions involving 1 e- electron transfer (143, 146). However, the question to be raised here: if the second oxidizing electron is localized on an amino acid residue [compound I'], can it participate in the 2 e- oxygen transfer reactions

as the ferryl porphyrin-based radical cation? And if yes, by which mechanism; direct or rebound?

In fact, cytochrome c peroxidase “CcP” was found to have a unique peroxygenase activity which does not conflict with its peroxidase function because of its open active site relative to classic peroxidases. Specifically, Ortiz de Montellano *et al.* (306) reported that CcP can oxidize thioanisole to the racemic sulfoxide. Moreover, incubation of thioanisole with CcP and [$^{18}$O] $H_2O_2$ followed by mass spectroscopic analysis of the sulfoxide indicated that all of the sulfoxide oxygen derives from the peroxide, suggesting a direct oxygen insertion. These results are similar to what Poon *et al.* reported in the Sen lab for the heme/G4-DNAzyme in which the source of oxygen in thioanisole sulfoxide was quantitatively from $H_2O_2$ (106).

Additionally, Ortiz de Motellano *et al.* (307) investigated whether the protein radical intermediate generated from ferric myoglobin plays roles in the epoxidation of styrene. They found that the time-dependent decrease of the epoxidation rate was proportional to the rate of decay of the protein radical, as measured by parallel EPR experiments, confirming the inference that the protein radical is involved in the epoxidation reaction. Poon *et al.* also showed that the heme/G4-DNAzyme can catalyze the epoxidation of styrene and that 73% of the oxygen of styrene oxide is derived from $H_2{}^{18}O_2$ (106).

Together, these results indicated that a ferryl [Fe(IV)=O]/protein radical pair can be coupled to achieve two-electron oxidation. Likewise, we propose that the Fe(IV)=O]/guanine radical cation pair is the activated species within the heme/G4-DNAzyme, and is capable of catalyzing the 2-electron oxygen transfer reactions. We also believe that the power of the heme/G4-DNAzyme as a catalytic system, that proves comparably efficient to evolved hemoproteins, comes from the fact of a delocalization process of the radical cation that is possible within a G-quadruplex stack, offering significant stability to the formation of a ferryl oxo species conjugated to a guanine radical cation. The hypothetical picture of the active, “delocalized” compound I’ species formed by a heme/G4-DNAzyme is shown in figure 4-17.

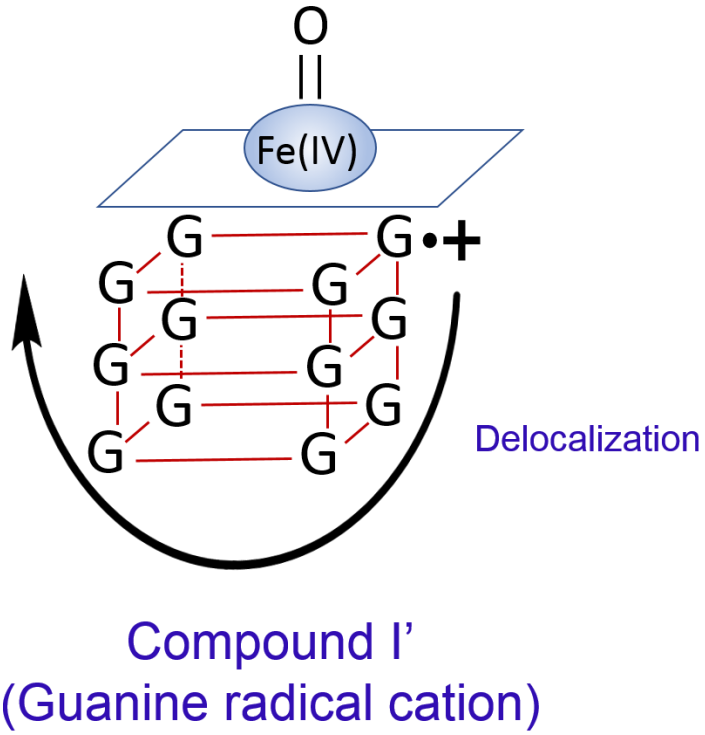


**Figure 4-17** **A schematic representation of Compound I' in heme/G4 DNAzymes. The arrow indicates the process of radical cation delocalization.**

## 4.6 Chapter conclusion

In this work, a novel type of active intermediate, defined as [Fe(IV)=OG•+], within the catalytic cycle of heme-utilizing DNAzymes has been proposed. Spolitak *et al.* have shown that the ferryl-oxo species with tyrosine radical (CpdI') formed by the reaction of Fe(III) $P450_{cam}$ with m-CPBA can participate in peroxidase reactions, as can Cpd I (144). However, they doubted that this protein radical form can carry out the hydroxylation reactions on hydrocarbons probably because of the unproperly positioned substrates (144, 145). In that regard, we have shown, so far, that heme-DNAzyems and ribozymes can carry out a variety of oxidation activities including peroxidation, oxygen transfer, as well as NADH oxidase activity. The remaining challenging activity that we would like to see for these heme/G4 systems is the C-H bond activation. From a structural point of view, we think that hydroxylation is possible even with a Cpd I'-type intermediate in a heme•G-quadruplex-based enzyme that has an open active site. The only challenge here may come from the lack of a well-developed substrate binding site in the heme•G-quadruplex-based enzyme. Aromatic substrates such as dibenzothiephene, indole, styrene, ABTS, and Amplex Red likely form transient, Michaelis-like complexes with the DNAzyme to enable their oxidation. But, potentially poorly binding substrates, like aliphatic hydrocarbons, may not localize near the active site for sufficient time to enable their oxidation. Nevertheless, linking such hydrocarbon substrates to the DNA sequence by an appropriate linker is feasible and may localize these difficult substrates in closer proximity to the active site. We believe that this would encourage aliphatic C-H bond activation. These experiments are currently in progress in our lab.

# Chapter 5

# Conclusion

## 5.1 Conclusion and outlook

The discovery of the catalytic capability of nucleic acids continues to fascinate the scientific community in diverse perspectives. In this thesis, we have covered three areas related to heme-utilizing DNAzymes and ribozymes from biological, structural, and mechanistical point of view.

In recent years, compelling evidence has been gathered on the occurrence of G-quadruplexes *in vivo*, as well as of their likely role in many cellular processes and in key human diseases. Genomic elements implicated in forming G-quadruplexes in *vivo* include telomeres, oncogenic and other gene promoters, ribosomal genes, immunoglobulin switch regions and various repetitive satellite sequences. In particular, it has been shown that telomeric DNA sequences, when folded into G-quadruplexes in *vitro*, inhibit the enzymatic action of the telomere-extending enzyme, telomerase. *In vivo*, telomerase over-expression is a characteristic of the overwhelming majority of human cancers. Recently, massive expansion of a $(G_4C_2)_n$ repeat within the human *C9orf72* gene has been found to be causal of certain neurodegenerative diseases, notably, familial amyotrophic lateral sclerosis and frontotemporal dementia. $(G_4C_2)_n$ DNA, as well as the RNA transcribed from it, forms G-quadruplexes. It has been proposed that the RNA G-quadruplexes, localized as intracellular RNA foci in affected cells, behave in a toxic fashion, sequestering many important RNA binding proteins as well as heme. Our *in vitro* studies, in chapter 2, have revealed that both DNA as well as the RNA transcribed from it, of the sequence $(G_4C_2)_4$ bind heme and enhance its oxidative activity. As a result, we proposed that these tangles may be toxic to the cells; playing roles that by analogy resemble those proposed for amyloid-β peptide tangles in Alzheimer disease. Recently, our lab showed that the G-quadruplex-heme DNAzyme can tag itself with the reactive substrate biotin tyramide through intrinsic peroxidase activated biotinylation *in vitro* (308). This technique could also

be used for the visualization or pulldown of intracellular G-quadruplexes. We are currently investigating this *in vivo*.

In chapter 3, we have shown that the G-quadruplexes are not the only DNA folds capable of the dual functions of binding to and enhancing heme oxidative activity. Isoguanine pentaplexes do so to some extent. An interesting outcome revealed by this study was that while Isoguanine pentaplexes are capable of both functions, isoguanine quartet, found to form in certain conditions, is not. We have concluded that the planarity of the π-surface upon which heme stacks, not maintained in iG-quartet, is a structural requirement for both binding and oxidative activity. The isoguanine base can form as a product of oxidative damage to DNA and has been shown to cause mutation (195). However, no evidence exists on the presence of pentaplex structures in the cell. Nevertheless, these structures could potentially be used in practical applications in which they can be used as an output device for detecting small molecules via a colorimetric signal activated by the binding of the analyte, which in turn enables the binding and activation of heme. One interesting experiment would be to compare the resistance of the heme/iG-pentaplex and the heme/G-quadruplex structures against oxidative damage by $H_2O_2$ or m-CPBA. If heme/iG-pentaplexes are more stable that heme/G-quadruplexes (whether the stability of heme moiety or the DNA itself), then, that will provide a system for the detection of a Compound I porphyrin radical cation. We plan to carry out these experiments in the future.

Finally, in Chapter 4, we have performed a stopped-flow analysis on the reaction of heme/G4-DNAzyme with hydrogen peroxide in the presence or absence of reducing substrate; dibenzothiophene. Our data suggested a formation of a unique type of activated species; Compound I', and it is defined in this study as ferryl-oxo species coupled to guanine cation radical [Fe(IV)=OG•+]. We have also proposed a kinetic scheme of activation and deactivation by these nucleic acids-based enzymes. Our study should provide helpful information for improving heme\G4-DNAzymes for a broader range of applications. There are a number of experiments, though, that need to be accomplished to solidify the hypothesis of the formation of this unique activated species as well as other mechanistic aspects of the oxygen transfer oxidation. First, we wish to further investigate the sufoxidation of DBT to DBTO by a [$^{18}O$] $H_2O_2$ labelling experiment followed by mass

spectroscopic analysis to see if the oxidation is quantitative, as with thioanisole. Also, we need to perform the stopped-flow analysis under low temperature (4 °C or lower) in the presence and absence of DBT to see what effect of temperature would have on the kinetics of sufoxidation, and if these would help in the detection of the classic Compound I [Fe(IV)=OPor•+]. Other methods to confirm the formation of the ferryl iron complex and a guanine radical cation would include: X-ray crystallography, X-ray absorption fine structure (EXAFS), magnetic susceptibility, electron nuclear double resonance (ENDOR), Magnetic circular dichroism (MCD), Mössbauer spectroscopy, and resonance Raman spectroscopy (RRS).

Although our knowledge, so far, about the properties as well as the wide range of applications of this unique system of “heme-Utilizing DNAzymes and ribozymes” has progressed significantly over the past 10 years, some structural and mechanistical aspects remain unclarified. The G-quadruplex within these DNAzymes and ribozymes appears to offer a hydrophobic binding pocket to the heme molecule, however, it is not yet fully clear what part-- “if there is”-- of DNA or RNA contributing to axial liganding of the heme iron center that is characteristic of protein heme enzymes. So far, there is no crystal structure for the heme complexed with a G-quadruplex. This can be an area of investigation that we hope to accomplish in the future.

Further directions in this field will explore the nature and the extent of other porphyrins usage for nucleic acid-mediated catalysis in more depth. Moreover, we are interested in exploring other types of oxidation reactions that can be catalyzed by the heme/G4-DNAzymes or ribozymes; mainly, the aliphatic, unactivated (C-H) bond activation known to be catalyzed by cytochrome P450 enzymes. Our laboratory is actively considering all these avenues of research.

# References


1. Watson JD, Crick FH. Molecular structure of nucleic acids; a structure for deoxyribose nucleic acid. Nature. 1953;171(4356):737-8.

2. Altman S. An overview of the RNA world: for now. Biological chemistry. 2007;388(7):663-4.

3. Cech TR. Ribozymes, the first 20 years. Biochemical Society transactions. 2002;30(Pt 6):1162-6.

4. Breaker RR, Joyce GF. A DNA enzyme that cleaves RNA. Chem Biol. 1994;1(4):223-9.

5. Breaker RR, Joyce GF. A DNA enzyme with Mg(2+)-dependent RNA phosphoesterase activity. Chem Biol. 1995;2(10):655-60.

6. Carmi N, Shultz LA, Breaker RR. In vitro selection of self-cleaving DNAs. Chem Biol. 1996;3(12):1039-46.

7. Cuenoud B, Szostak JW. A DNA metalloenzyme with DNA ligase activity. Nature. 1995;375(6532):611-4.

8. Joyce GF. In vitro evolution of nucleic acids. Current opinion in structural biology. 1994;4:331-6.

9. Li Y, Geyer CR, Sen D. Recognition of anionic porphyrins by DNA aptamers. Biochemistry. 1996;35(21):6911-22.

10. Li Y, Sen D. A catalytic DNA for porphyrin metallation. Nature structural biology. 1996;3(9):743-7.

11. Travascio P, Bennet AJ, Wang DY, Sen D. A ribozyme and a catalytic DNA with peroxidase activity: active sites versus cofactor-binding sites. Chem Biol. 1999;6(11):779-87.

12. Travascio P, Li Y, Sen D. DNA-enhanced peroxidase activity of a DNA-aptamer-hemin complex. Chem Biol. 1998;5(9):505-17.

13. Chary KVR, Govil G. Structure and Dynamics Of Nucleic Acids. In: Chary KVR, Govil G, editors. NMR in Biological Systems: From Molecules to Humans. Dordrecht: Springer Netherlands; 2008. p. 247-90.

14. Lu XJ, Olson WK. 3DNA: a versatile, integrated software system for the analysis, rebuilding and visualization of three-dimensional nucleic-acid structures. Nature protocols. 2008;3(7):1213-27.

15. David L. Nelson MMC. Lehninger Principles of Biochemistry New York 2005.

16. Müller S. Quadruplex Nucleic Acids. Edited by Stephen Neidle and Shankar Balasubramanian. Angewandte Chemie International Edition. 2008;47(16):2914-.

17. Gellert M, Lipsett MN, Davies DR. Helix formation by guanylic acid. Proc Natl Acad Sci U S A. 1962;48:2013-8.

18. Henderson E, Hardin CC, Walk SK, Tinoco I, Jr., Blackburn EH. Telomeric DNA oligonucleotides form novel intramolecular structures containing guanine-guanine base pairs. Cell. 1987;51(6):899-908.

19. Williamson JR, Raghuraman MK, Cech TR. Monovalent cation-induced structure of telomeric DNA: the G-quartet model. Cell. 1989;59(5):871-80.

20. Sundquist WI, Klug A. Telomeric DNA dimerizes by formation of guanine tetrads between hairpin loops. Nature. 1989;342(6251):825-9.

21. Sanger F, Coulson AR. The use of thin acrylamide gels for DNA sequencing. FEBS letters. 1978;87(1):107-10.

22. Blackburn EH, Greider CW, Szostak JW. Telomeres and telomerase: the path from maize, Tetrahymena and yeast to human cancer and aging. Nature medicine. 2006;12(10):1133-8.

23. Parkinson GN, Lee MP, Neidle S. Crystal structure of parallel quadruplexes from human telomeric DNA. Nature. 2002;417(6891):876-80.

24. Quadruplex Nucleic Acids. Stephen Neidle SB, editor. Cambridge, UK: RSC publishing 2006.

25. Mergny JL, Mailliet P, Lavelle F, Riou JF, Laoui A, Helene C. The development of telomerase inhibitors: the G-quartet approach. Anti-cancer drug design. 1999;14(4):327-39.

26. Sen D, Gilbert W. A sodium-potassium switch in the formation of four-stranded G4-DNA. Nature. 1990;344(6265):410-4.

27. Venczel EA, Sen D. Parallel and antiparallel G-DNA structures from a complex telomeric sequence. Biochemistry. 1993;32(24):6220-8.

28. Laughlan G, Murchie AI, Norman DG, Moore MH, Moody PC, Lilley DM, et al. The high-resolution crystal structure of a parallel-stranded guanine tetraplex. Science (New York, NY). 1994;265(5171):520-4.

29. Phillips K, Dauter Z, Murchie AI, Lilley DM, Luisi B. The crystal structure of a parallel-stranded guanine tetraplex at 0.95 A resolution. Journal of molecular biology. 1997;273(1):171-82.

30. Krishnan-Ghosh Y, Liu D, Balasubramanian S. Formation of an interlocked quadruplex dimer by d(GGGT). J Am Chem Soc. 2004;126(35):11009-16.

31. Crnugelj M, Hud NV, Plavec J. The solution structure of d(G(4)T(4)G(3))(2): a bimolecular G-quadruplex with a novel fold. Journal of molecular biology. 2002;320(5):911-24.

32. Phan AT, Modi YS, Patel DJ. Two-repeat Tetrahymena telomeric d(TGGGGTTGGGGT) Sequence interconverts between asymmetric dimeric G-quadruplexes in solution. Journal of molecular biology. 2004;338(1):93-102.

33. Phan AT, Patel DJ. Two-repeat human telomeric d(TAGGGTTAGGGT) sequence forms interconverting parallel and antiparallel G-quadruplexes in solution: distinct topologies, thermodynamic properties, and folding/unfolding kinetics. J Am Chem Soc. 2003;125(49):15021-7.

34. Smith FW, Lau FW, Feigon J. d(G3T4G3) forms an asymmetric diagonally looped dimeric quadruplex with guanosine 5'-syn-syn-anti and 5'-syn-anti-anti N-glycosidic conformations. Proc Natl Acad Sci U S A. 1994;91(22):10546-50.

35. Haider SM, Parkinson GN, Neidle S. Structure of a G-quadruplex-ligand complex. Journal of molecular biology. 2003;326(1):117-25.

36. Horvath MP, Schultz SC. DNA G-quartets in a 1.86 A resolution structure of an Oxytricha nova telomeric protein-DNA complex. Journal of molecular biology. 2001;310(2):367-77.

37. Risitano A, Fox KR. Stability of Intramolecular DNA Quadruplexes: Comparison with DNA Duplexes. Biochemistry. 2003;42(21):6507-13.

38. Seenisamy J, Rezler EM, Powell TJ, Tye D, Gokhale V, Joshi CS, et al. The dynamic character of the G-quadruplex element in the c-MYC promoter and modification by TMPyP4. J Am Chem Soc. 2004;126(28):8702-9.

39. Wang Y, Patel DJ. Solution structure of the Tetrahymena telomeric repeat d(T2G4)4 G-tetraplex. Structure (London, England : 1993). 1994;2(12):1141-56.

40. Rujan IN, Meleney JC, Bolton PH. Vertebrate telomere repeat DNAs favor external loop propeller quadruplex structures in the presence of high concentrations of potassium. Nucleic Acids Res. 2005;33(6):2022-31.

41. Hatzakis E, Okamoto K, Yang D. Thermodynamic stability and folding kinetics of the major G-quadruplex and its loop isomers formed in the nuclease hypersensitive element in the human c-Myc promoter: effect of loops and flanking segments on the stability of parallel-stranded intramolecular G-quadruplexes. Biochemistry. 2010;49(43):9152-60.

42. Mathad RI, Hatzakis E, Dai J, Yang D. c-MYC promoter G-quadruplex formed at the 5'-end of NHE III1 element: insights into biological relevance and parallel-stranded G-quadruplex stability. Nucleic Acids Res. 2011;39(20):9023-33.

43. Mergny JL, Phan AT, Lacroix L. Following G-quartet formation by UV-spectroscopy. FEBS letters. 1998;435(1):74-8.

44. Pilch DS, Plum GE, Breslauer KJ. The thermodynamics of DNA structures that contain lesions or guanine tetrads. Current opinion in structural biology. 1995;5(3):334-42.

45. Lu M, Guo Q, Kallenbach NR. Thermodynamics of G-tetraplex formation by telomeric DNAs. Biochemistry. 1993;32(2):598-601.

46. Petraccone L, Erra E, Esposito V, Randazzo A, Mayol L, Nasti L, et al. Stability and structure of telomeric DNA sequences forming quadruplexes containing four G-tetrads with different topological arrangements. Biochemistry. 2004;43(16):4877-84.

47. Berova N, Di Bari L, Pescitelli G. Application of electronic circular dichroism in configurational and conformational analysis of organic compounds. Chemical Society reviews. 2007;36(6):914-31.

48. Clark LB. Electronic Spectra of Crystalline Guanosine: Transition Moment Directions of the Guanine Chromophore. Journal of the American Chemical Society. 1994;116(12):5265-70.

49. Fülscher MP, Serrano-Andrés L, Roos BO. A Theoretical Study of the Electronic Spectra of Adenine and Guanine. Journal of the American Chemical Society. 1997;119(26):6168-76.

50. Randazzo A, Spada GP, da Silva MW. Circular dichroism of quadruplex structures. Topics in current chemistry. 2013;330:67-86.

51. Gottarelli G MS, Spada GP The use of CD spectroscopy for the study of the self-assembly of guanine dereivative. Enantiomer 1998;3:429-38.

52. Wen J-D, Gray DM. The Ff Gene 5 Single-Stranded DNA-Binding Protein Binds to the Transiently Folded Form of an Intramolecular G-Quadruplex. Biochemistry. 2002;41(38):11438-48.

53. Huppert JL, Balasubramanian S. Prevalence of quadruplexes in the human genome. Nucleic Acids Res. 2005;33(9):2908-16.

54. Frees S, Menendez C, Crum M, Bagga PS. QGRS-Conserve: a computational method for discovering evolutionarily conserved G-quadruplex motifs. Human Genomics. 2014;8(1):8-.

55. Schiavone D, Guilbaud G, Murat P, Papadopoulou C, Sarkies P, Prioleau MN, et al. Determinants of G quadruplex-induced epigenetic instability in REV1-deficient cells. The EMBO journal. 2014;33(21):2507-20.

56. Blackburn EH. Telomeres: no end in sight. Cell. 1994;77(5):621-3.

57. Zakian VA. Telomeres: beginning to understand the end. Science (New York, NY). 1995;270(5242):1601-7.

58. Harley CB, Villeponteau B. Telomeres and telomerase in aging and cancer. Current opinion in genetics & development. 1995;5(2):249-55.

59. Bryan TM, Cech TR. Telomerase and the maintenance of chromosome ends. Current opinion in cell biology. 1999;11(3):318-24.

60. Kim NW, Piatyszek MA, Prowse KR, Harley CB, West MD, Ho PL, et al. Specific association of human telomerase activity with immortal cells and cancer. Science (New York, NY). 1994;266(5193):2011-5.

61. de Lange T. Activation of telomerase in a human tumor. Proceedings of the National Academy of Sciences of the United States of America. 1994;91(8):2882-5.

62. Lingner J, Hughes TR, Shevchenko A, Mann M, Lundblad V, Cech TR. Reverse transcriptase motifs in the catalytic subunit of telomerase. Science (New York, NY). 1997;276(5312):561-7.

63. Williamson JR. G-quartet structures in telomeric DNA. Annual review of biophysics and biomolecular structure. 1994;23:703-30.

64. Feigon J, Koshlap KM, Smith FW. 1H NMR spectroscopy of DNA triplexes and quadruplexes. Methods in enzymology. 1995;261:225-55.

65. Zahler AM, Williamson JR, Cech TR, Prescott DM. Inhibition of telomerase by G-quartet DNA structures. Nature. 1991;350(6320):718-20.

66. Han FX, Wheelhouse RT, Hurley LH. Interactions of TMPyP4 and TMPyP2 with Quadruplex DNA. Structural Basis for the Differential Effects on Telomerase Inhibition. Journal of the American Chemical Society. 1999;121(15):3561-70.

67. Cairns D, Anderson RJ, Perry PJ, Jenkins TC. Design of telomerase inhibitors for the treatment of cancer. Current pharmaceutical design. 2002;8(27):2491-504.

68. Huppert JL, Balasubramanian S. G-quadruplexes in promoters throughout the human genome. Nucleic Acids Res. 2007;35(2):406-13.

69. Eddy J, Maizels N. Gene function correlates with potential for G4 DNA formation in the human genome. Nucleic Acids Research. 2006;34(14):3887-96.

70. Bugaut A, Balasubramanian S. 5′-UTR RNA G-quadruplexes: translation regulation and targeting. Nucleic Acids Research. 2012;40(11):4727-41.

71. Siddiqui-Jain A, Grand CL, Bearss DJ, Hurley LH. Direct evidence for a G-quadruplex in a promoter region and its targeting with a small molecule to repress c-MYC transcription. Proceedings of the National Academy of Sciences. 2002;99(18):11593-8.

72. Balasubramanian S, Hurley LH, Neidle S. Targeting G-quadruplexes in gene promoters: a novel anticancer strategy? Nat Rev Drug Discov. 2011;10(4):261-75.

73. Patel DJ, Phan AT, Kuryavyi V. Human telomere, oncogenic promoter and 5′-UTR G-quadruplexes: diverse higher order DNA and RNA targets for cancer therapeutics. Nucleic Acids Research. 2007;35(22):7429-55.

74. Renton Alan E, Majounie E, Waite A, Simón-Sánchez J, Rollinson S, Gibbs JR, et al. A Hexanucleotide Repeat Expansion in C9ORF72 Is the Cause of Chromosome 9p21-Linked ALS-FTD. Neuron. 2011;72(2):257-68.

75. Majounie E, Renton AE, Mok K, Dopper EGP, Waite A, Rollinson S, et al. Frequency of the C9orf72 hexanucleotide repeat expansion in patients with amyotrophic lateral sclerosis and frontotemporal dementia: a cross-sectional study. The Lancet Neurology. 2012;11(4):323-30.

76. DeJesus-Hernandez M, Mackenzie Ian R, Boeve Bradley F, Boxer Adam L, Baker M, Rutherford Nicola J, et al. Expanded GGGGCC Hexanucleotide Repeat in Noncoding Region of C9ORF72 Causes Chromosome 9p-Linked FTD and ALS. Neuron. 2011;72(2):245-56.

77. K. W. Bock GHE, L. G. Israels, G. S Marcks, F. De. Matteis, J. D. Maxwell, U. A. Meyer, H. L., Rayner, H. L. Remmer, S. Sassa, B. A. Schacter, C. H. Tait, T. R. Tephly, D. P. Tschudy. Heme and hemoproteins: Springer science and business media 2012. 452 p.

78. Li Z. Heme biology, The secret life of heme in regulating diverse biological processes World scientific 2011.

79. Mense SM, Zhang L. Heme: a versatile signaling molecule controlling the activities of diverse regulators ranging from transcription factors to MAP kinases. Cell research. 2006;16(8):681-92.

80. Unno M, Matsui T, Ikeda-Saito M. Structure and catalytic mechanism of heme oxygenase. Natural product reports. 2007;24(3):553-70.

81. Gouterman M. Study of the Effects of Substitution on the Absorption Spectra of Porphin. The Journal of Chemical Physics. 1959;30(5):1139-61.

82. Gouterman M. Spectra of porphyrins. Journal of Molecular Spectroscopy. 1961;6:138-63.

83. Dolphin aD. Porphyrins. Academic, New York 1979;4(Part B):197-256.

84. P STaS. Iron in Biochemistry and Medicine Academic Press, New York 1974;1.

85. Burdon CAR-EaRH. Free radical damage and its control Elsevier; 1994.

86. Veitch NC. Horseradish peroxidase: a modern view of a classic enzyme. Phytochemistry. 2004;65(3):249-59.

87. Smulevich G, Mauro JM, Fishel LA, English AM, Kraut J, Spiro TG. Heme pocket interactions in cytochrome c peroxidase studied by site-directed mutagenesis and resonance Raman spectroscopy. Biochemistry. 1988;27(15):5477-85.

88. Finzel BC, Poulos TL, Kraut J. Crystal structure of yeast cytochrome c peroxidase refined at 1.7-A resolution. The Journal of biological chemistry. 1984;259(21):13027-36.

89. Piontek K, Smith AT, Blodig W. Lignin peroxidase structure and function. Biochemical Society transactions. 2001;29(Pt 2):111-6.

90. Shigeoka S, Ishikawa T, Tamoi M, Miyagawa Y, Takeda T, Yabuta Y, et al. Regulation and function of ascorbate peroxidase isoenzymes. Journal of experimental botany. 2002;53(372):1305-19.

91. Furtmuller PG, Zederbauer M, Jantschko W, Helm J, Bogner M, Jakopitsch C, et al. Active site structure and catalytic mechanisms of human peroxidases. Archives of biochemistry and biophysics. 2006;445(2):199-213.

92. de Montellano PRO. Catalytic Mechanisms of Heme Peroxidases. In: Torres E, Ayala M, editors. Biocatalysis Based on Heme Peroxidases: Peroxidases as Potential Industrial Biocatalysts. Berlin, Heidelberg: Springer Berlin Heidelberg; 2010. p. 79-107.

93. Poulos TL, Kraut J. The stereochemistry of peroxidase catalysis. The Journal of biological chemistry. 1980;255(17):8199-205.

94. Torres Pazmino DE, Winkler M, Glieder A, Fraaije MW. Monooxygenases as biocatalysts: Classification, mechanistic aspects and biotechnological applications. Journal of biotechnology. 2010;146(1-2):9-24.

95. Nelson DR, Koymans L, Kamataki T, Stegeman JJ, Feyereisen R, Waxman DJ, et al. P450 superfamily: update on new sequences, gene mapping, accession numbers and nomenclature. Pharmacogenetics. 1996;6(1):1-42.

96. Sono M, Roach MP, Coulter ED, Dawson JH. Heme-Containing Oxygenases. Chemical reviews. 1996;96(7):2841-88.

97. Poulos TL, Finzel BC, Gunsalus IC, Wagner GC, Kraut J. The 2.6-A crystal structure of Pseudomonas putida cytochrome P-450. The Journal of biological chemistry. 1985;260(30):16122-30.

98. Denisov IG, Makris TM, Sligar SG, Schlichting I. Structure and chemistry of cytochrome P450. Chemical reviews. 2005;105(6):2253-77.

99. Imai M, Shimada H, Watanabe Y, Matsushima-Hibiya Y, Makino R, Koga H, et al. Uncoupling of the cytochrome P-450cam monooxygenase reaction by a single mutation, threonine-252 to alanine or valine: possible role of the hydroxy amino acid in oxygen activation. Proc Natl Acad Sci U S A. 1989;86(20):7823-7.

100. Martinis SA, Atkins WM, Stayton PS, Sligar SG. A conserved residue of cytochrome P-450 is involved in heme-oxygen stability and activation. Journal of the American Chemical Society. 1989;111(26):9252-3.

101. Shimada H, Watanabe Y, Imai M, Makino R, Koga H, Horiuchi T, et al. The Role of Threonine 252 in the Oxygen Activation by Cytochrome P-450 cam: Mechanistic Studies by Site-directed Mutagenesis. Studies in Surface Science and Catalysis. 1991;66:313-9.

102. Raag R, Martinis SA, Sligar SG, Poulos TL. Crystal structure of the cytochrome P-450CAM active site mutant Thr252Ala. Biochemistry. 1991;30(48):11420-9.

103. Vidakovic M, Sligar SG, Li H, Poulos TL. Understanding the Role of the Essential Asp251 in Cytochrome P450cam Using Site-Directed Mutagenesis, Crystallography, and Kinetic Solvent Isotope Effect. Biochemistry. 1998;37(26):9211-9.

104. Gerber NC, Sligar SG. A role for Asp-251 in cytochrome P-450cam oxygen activation. The Journal of biological chemistry. 1994;269(6):4260-6.

105. Schlichting I, Berendzen J, Chu K, Stock AM, Maves SA, Benson DE, et al. The catalytic pathway of cytochrome p450cam at atomic resolution. Science (New York, NY). 2000;287(5458):1615-22.

106. Poon LC, Methot SP, Morabi-Pazooki W, Pio F, Bennet AJ, Sen D. Guanine-rich RNAs and DNAs that bind heme robustly catalyze oxygen transfer reactions. J Am Chem Soc. 2011;133(6):1877-84.

107. Sen D, Poon LC. RNA and DNA complexes with hemin [Fe(III) heme] are efficient peroxidases and peroxygenases: how do they do it and what does it mean? Crit Rev Biochem Mol Biol. 2011;46(6):478-92.

108. Gold L, Polisky B, Uhlenbeck O, Yarus M. Diversity of oligonucleotide functions. Annual review of biochemistry. 1995;64:763-97.

109. Cochran AG, Schultz PG. Antibody-catalyzed porphyrin metallation. Science (New York, NY). 1990;249(4970):781-3.

110. Li Y, Sen D. Toward an efficient DNAzyme. Biochemistry. 1997;36(18):5589-99.

111. Culbertson DS, Olson JS. Role of heme in the unfolding and assembly of myoglobin. Biochemistry. 2010;49(29):6052-63.

112. Slama-Schwok A, Lehn JM. Interaction of porphyrin-containing macrotetracyclic receptor molecule with single-stranded and double-stranded polynucleotides. A photophysical study. Biochemistry. 1990;29(34):7895-903.

113. Cheng X, Liu X, Bing T, Cao Z, Shangguan D. General peroxidase activity of G-quadruplex-hemin complexes and its application in ligand screening. Biochemistry. 2009;48(33):7817-23.

114. Kong DM, Yang W, Wu J, Li CX, Shen HX. Structure-function study of peroxidase-like G-quadruplex-hemin complexes. The Analyst. 2010;135(2):321-6.

115. Travascio P, Witting PK, Mauk AG, Sen D. The peroxidase activity of a hemin--DNA oligonucleotide complex: free radical damage to specific guanine bases of the DNA. J Am Chem Soc. 2001;123(7):1337-48.

116. Antonini E, & Brunori, M. Hemoglobin and myoglobin in their reactions with ligands. Amsterdam: North-Holland1971.

117. Saito K, Tai H, Fukaya M, Shibata T, Nishimura R, Neya S, et al. Structural characterization of a carbon monoxide adduct of a heme-DNA complex. Journal of biological inorganic chemistry : JBIC : a publication of the Society of Biological Inorganic Chemistry. 2012;17(3):437-45.

118. Shibata T, Nakayama Y, Katahira Y, Tai H, Moritaka Y, Nakano Y, et al. Characterization of the interaction between heme and a parallel G-quadruplex DNA formed from d(TTGAGG). Biochim Biophys Acta. 2017;1861(5 Pt B):1264-70.

119. Yamamoto Y, Kinoshita M, Katahira Y, Shimizu H, Di Y, Shibata T, et al. Characterization of Heme-DNA Complexes Composed of Some Chemically Modified Hemes and Parallel G-Quadruplex DNAs. Biochemistry. 2015;54(49):7168-77.

120. Rojas AM, Gonzalez PA, Antipov E, Klibanov AM. Specificity of a DNA-based (DNAzyme) peroxidative biocatalyst. Biotechnology letters. 2007;29(2):227-32.

121. van Rantwijk F, Sheldon RA. Selective oxygen transfer catalysed by heme peroxidases: synthetic and mechanistic aspects. Current opinion in biotechnology. 2000;11(6):554-64.

122. Golub E, Albada HB, Liao WC, Biniuri Y, Willner I. Nucleoapzymes: Hemin/G-Quadruplex DNAzyme-Aptamer Binding Site Conjugates with Superior Enzyme-like Catalytic Functions. J Am Chem Soc. 2016;138(1):164-72.

123. Nakayama S, Sintim HO. Biomolecule detection with peroxidase-mimicking DNAzymes; expanding detection modality with fluorogenic compounds. Molecular bioSystems. 2010;6(1):95-7.

124. Ator MA, Ortiz de Montellano PR. Protein control of prosthetic heme reactivity. Reaction of substrates with the heme edge of horseradish peroxidase. The Journal of biological chemistry. 1987;262(4):1542-51.

125. Baciocchi E, Lanzalunga O, Malandrucco S, Ioele M, Steenken S. Oxidation of Sulfides by Peroxidases. Involvement of Radical Cations and the Rate of the Oxygen Rebound Step. Journal of the American Chemical Society. 1996;118(37):8973-4.

126. Kobayashi S, Nakano M, Kimura T, Schaap AP. On the mechanism of the peroxidase-catalyzed oxygen-transfer reaction. Biochemistry. 1987;26(16):5019-22.

127. Su J, Groves JT. Direct detection of the oxygen rebound intermediates, ferryl Mb and NO2, in the reaction of metmyoglobin with peroxynitrite. J Am Chem Soc. 2009;131(36):12979-88.

128. Ichinose H, Wariishi H, Tanaka H. Effective oxygen transfer reaction catalyzed by microperoxidase-11 during sulfur oxidation of dibenzothiophene. Enzyme and microbial technology. 2002;30(3):334-9.

129. Golub E, Freeman R, Willner I. A hemin/G-quadruplex acts as an NADH oxidase and NADH peroxidase mimicking DNAzyme. Angew Chem Int Ed Engl. 2011;50(49):11710-4.

130. Kosman J, Juskowiak B. Peroxidase-mimicking DNAzymes for biosensing applications: a review. Analytica chimica acta. 2011;707(1-2):7-17.

131. Thirstrup D, Baird GS. Histochemical application of a peroxidase DNAzyme with a covalently attached hemin cofactor. Analytical chemistry. 2010;82(6):2498-504.

132. Cahoon LA, Seifert HS. An alternative DNA structure is necessary for pilin antigenic variation in Neisseria gonorrhoeae. Science (New York, NY). 2009;325(5941):764-7.

133. Lipps HJ, Rhodes D. G-quadruplex structures: in vivo evidence and function. Trends in cell biology. 2009;19(8):414-22.

134. Atamna H, Boyle K. Amyloid-beta peptide binds with heme to form a peroxidase: relationship to the cytopathologies of Alzheimer's disease. Proc Natl Acad Sci U S A. 2006;103(9):3381-6.

135. Atamna H, Frey WH, 2nd, Ko N. Human and rodent amyloid-beta peptides differentially bind heme: relevance to the human susceptibility to Alzheimer's disease. Archives of biochemistry and biophysics. 2009;487(1):59-65.

136. Lee YB, Chen HJ, Peres JN, Gomez-Deza J, Attig J, Stalekar M, et al. Hexanucleotide repeats in ALS/FTD form length-dependent RNA foci, sequester RNA binding proteins, and are neurotoxic. Cell reports. 2013;5(5):1178-86.

137. Kang M, Heuberger B, Chaput JC, Switzer C, Feigon J. Solution structure of a parallel-stranded oligoisoguanine DNA pentaplex formed by d(T(iG)4 T) in the presence of Cs+ ions. Angew Chem Int Ed Engl. 2012;51(32):7952-5.

138. Gu J, Wang J, Leszczynski J. Iso-guanine quintet complexes coordinated by mono valent cations (Na+, K+, Rb+, and Cs+). J Comput Chem. 2007;28(11):1790-5.

139. Gu J, Leszczynski J. Isoguanine Complexes: Quintet versus Tetrad. The Journal of Physical Chemistry B. 2003;107(27):6609-13.

140. Meyer M, Steinke T, Suhnel J. Density functional study of isoguanine tetrad and pentad sandwich complexes with alkali metal ions. J Mol Model. 2007;13(2):335-45.

141. Dunford HB. Heme Peroxidases. New York Wiley-VCH 1999.

142. Bonagura CA, Bhaskar B, Shimizu H, Li H, Sundaramoorthy M, McRee DE, et al. High-resolution crystal structures and spectroscopy of native and compound I cytochrome c peroxidase. Biochemistry. 2003;42(19):5600-8.

143. Egawa T, Shimada H, Ishimura Y. Formation of compound I in the reaction of native myoglobins with hydrogen peroxide. The Journal of biological chemistry. 2000;275(45):34858-66.

144. Spolitak T, Dawson JH, Ballou DP. Reaction of ferric cytochrome P450cam with peracids: kinetic characterization of intermediates on the reaction pathway. The Journal of biological chemistry. 2005;280(21):20300-9.

145. Spolitak T, Dawson JH, Ballou DP. Rapid kinetics investigations of peracid oxidation of ferric cytochrome P450cam: nature and possible function of compound ES. Journal of inorganic biochemistry. 2006;100(12):2034-44.

146. Rodriguez-Lopez JN, Lowe DJ, Hernandez-Ruiz J, Hiner AN, Garcia-Canovas F, Thorneley RN. Mechanism of reaction of hydrogen peroxide with horseradish peroxidase: identification of intermediates in the catalytic cycle. J Am Chem Soc. 2001;123(48):11838-47.

147. Van Langenhove T, van der Zee J, Van Broeckhoven C. The molecular basis of the frontotemporal lobar degeneration-amyotrophic lateral sclerosis spectrum. Annals of medicine. 2012;44(8):817-28.

148. Bieniek KF, van Blitterswijk M, Baker MC, Petrucelli L, Rademakers R, Dickson DW. Expanded C9ORF72 hexanucleotide repeat in depressive pseudodementia. JAMA neurology. 2014;71(6):775-81.

149. Hensman Moss DJ, Poulter M, Beck J, Hehir J, Polke JM, Campbell T, et al. C9orf72 expansions are the most common genetic cause of Huntington disease phenocopies. Neurology. 2014;82(4):292-9.

150. Pletnikova O, Sloane KL, Renton AE, Traynor BJ, Crain BJ, Reid T, et al. Hippocampal sclerosis dementia with the C9ORF72 hexancleotide repeat expansion. Neurobiology of aging. 2014;35(10):2419.e17-.e21.

151. Mignarri A, Battistini S, Tomai Pitinca ML, Monti L, Burroni L, Ginanneschi F, et al. Double trouble? Progranulin mutation and C9ORF72 repeat expansion in a case of primary non-fluent aphasia. Journal of the neurological sciences. 2014;341(1-2):176-8.

152. Fratta P, Mizielinska S, Nicoll AJ, Zloh M, Fisher EMC, Parkinson G, et al. C9orf72 hexanucleotide repeat associated with amyotrophic lateral sclerosis and frontotemporal dementia forms RNA G-quadruplexes. Scientific Reports. 2012;2:1016.

153. Reddy K, Zamiri B, Stanley SY, Macgregor RB, Jr., Pearson CE. The disease-associated r(GGGGCC)n repeat from the C9orf72 gene forms tract length-dependent uni- and multimolecular RNA G-quadruplex structures. The Journal of biological chemistry. 2013;288(14):9860-6.

154. Haeusler AR, Donnelly CJ, Periz G, Simko EA, Shaw PG, Kim MS, et al. C9orf72 nucleotide repeat structures initiate molecular cascades of disease. Nature. 2014;507(7491):195-200.

155. Sen D, Gilbert W. Formation of parallel four-stranded complexes by guanine-rich motifs in DNA and its implications for meiosis. Nature. 1988;334(6180):364-6.

156. Wu Y, Brosh RM, Jr. G-quadruplex nucleic acids and human disease. The FEBS journal. 2010;277(17):3470-88.

157. Taylor JP. Neurodegenerative diseases: G-quadruplex poses quadruple threat. Nature. 2014;507(7491):175-7.

158. Balasubramanian S, Hurley LH, Neidle S. Targeting G-quadruplexes in gene promoters: a novel anticancer strategy? Nature reviews Drug discovery. 2011;10(4):261-75.

159. Monchaud D, Teulade-Fichou MP. A hitchhiker's guide to G-quadruplex ligands. Organic & biomolecular chemistry. 2008;6(4):627-36.

160. Lee Y-B, Chen H-J, Peres João N, Gomez-Deza J, Attig J, Štalekar M, et al. Hexanucleotide Repeats in ALS/FTD Form Length-Dependent RNA Foci, Sequester RNA Binding Proteins, and Are Neurotoxic. Cell reports. 2013;5(5):1178-86.

161. Bigio EH. C9ORF72, the new gene on the block, causes C9FTD/ALS: new insights provided by neuropathology. Acta Neuropathologica. 2011;122(6):653-5.

162. Fong JC, Karydas AM, Goldman JS. Genetic counseling for FTD/ALS caused by the C9ORF72 hexanucleotide expansion. Alzheimer's Research & Therapy. 2012;4(4):27-.

163. Liu Y, Yu JT, Zong Y, Zhou J, Tan L. C9ORF72 mutations in neurodegenerative diseases. Molecular neurobiology. 2014;49(1):386-98.

164. Buerk DG, Saidel GM. A Comparison of Two Nonclassical Models for Oxygen Consumption in Brain and Liver Tissue. In: Silver IA, Erecińska M, Bicher HI, editors. Oxygen Transport to Tissue — III. Boston, MA: Springer US; 1978. p. 225-32.

165. Raff MC, Whitmore AV, Finn JT. Axonal self-destruction and neurodegeneration. Science (New York, NY). 2002;296(5569):868-71.

166. Subbarao KV, Richardson JS. Iron-dependent peroxidation of rat brain: a regional study. Journal of neuroscience research. 1990;26(2):224-32.

167. Pamplona R, Dalfo E, Ayala V, Bellmunt MJ, Prat J, Ferrer I, et al. Proteins in human brain cortex are modified by oxidation, glycoxidation, and lipoxidation. Effects of Alzheimer disease and identification of lipoxidation targets. The Journal of biological chemistry. 2005;280(22):21522-30.

168. Altamura S, Muckenthaler MU. Iron toxicity in diseases of aging: Alzheimer's disease, Parkinson's disease and atherosclerosis. Journal of Alzheimer's disease : JAD. 2009;16(4):879-95.

169. Atamna H, Killilea DW, Killilea AN, Ames BN. Heme deficiency may be a factor in the mitochondrial and neuronal decay of aging. Proc Natl Acad Sci U S A. 2002;99(23):14807-12.

170. Atamna H, Liu J, Ames BN. Heme deficiency selectively interrupts assembly of mitochondrial complex IV in human fibroblasts: revelance to aging. The Journal of biological chemistry. 2001;276(51):48410-6.

171. Atamna H, Frey WH, 2nd. A role for heme in Alzheimer's disease: heme binds amyloid beta and has altered metabolism. Proc Natl Acad Sci U S A. 2004;101(30):11153-8.

172. Scheuermann S, Hambsch B, Hesse L, Stumm J, Schmidt C, Beher D, et al. Homodimerization of amyloid precursor protein and its implication in the amyloidogenic pathway of Alzheimer's disease. The Journal of biological chemistry. 2001;276(36):33923-9.

173. Letarte PB, Lieberman K, Nagatani K, Haworth RA, Odell GB, Duff TA. Hemin: levels in experimental subarachnoid hematoma and effects on dissociated vascular smooth-muscle cells. Journal of neurosurgery. 1993;79(2):252-5.

174. Atamna H, Boyle K. Amyloid-β peptide binds with heme to form a peroxidase: Relationship to the cytopathologies of Alzheimer’s disease. Proceedings of the National Academy of Sciences of the United States of America. 2006;103(9):3381-6.

175. Atamna H. Heme binding to Amyloid-beta peptide: mechanistic role in Alzheimer's disease. Journal of Alzheimer's disease : JAD. 2006;10(2-3):255-66.

176. Wang Y, Hamasaki K, Rando RR. Specificity of aminoglycoside binding to RNA constructs derived from the 16S rRNA decoding region and the HIV-RRE activator region. Biochemistry. 1997;36(4):768-79.

177. Kong DM, Cai LL, Guo JH, Wu J, Shen HX. Characterization of the G-quadruplex structure of a catalytic DNA with peroxidase activity. Biopolymers. 2009;91(5):331-9.

178. Li T, Dong S, Wang E. G-quadruplex aptamers with peroxidase-like DNAzyme functions: which is the best and how does it work? Chemistry, an Asian journal. 2009;4(6):918-22.

179. Qi C, Zhang N, Yan J, Liu X, Bing T, Mei H, et al. Activity enhancement of G-quadruplex/hemin DNAzyme by spermine. RSC Advances. 2014;4(3):1441-8.

180. Park HJ, Reiser CO, Kondruweit S, Erdmann H, Schmid RD, Sprinzl M. Purification and characterization of a NADH oxidase from the thermophile Thermus thermophilus HB8. European journal of biochemistry. 1992;205(3):881-5.

181. Floyd RA, Hensley K. Oxidative stress in brain aging. Implications for therapeutics of neurodegenerative diseases. Neurobiol Aging. 2002;23(5):795-807.

182. Uttara B, Singh AV, Zamboni P, Mahajan RT. Oxidative Stress and Neurodegenerative Diseases: A Review of Upstream and Downstream Antioxidant Therapeutic Options. Current Neuropharmacology. 2009;7(1):65-74.

183. Maizels N. G4 motifs in human genes. Annals of the New York Academy of Sciences. 2012;1267:53-60.

184. Sadrzadeh SM, Saffari Y. Iron and brain disorders. American journal of clinical pathology. 2004;121 Suppl:S64-70.

185. Jeong SY, Rathore KI, Schulz K, Ponka P, Arosio P, David S. Dysregulation of iron homeostasis in the CNS contributes to disease progression in a mouse model of amyotrophic lateral sclerosis. The Journal of neuroscience : the official journal of the Society for Neuroscience. 2009;29(3):610-9.

186. Gunther MR, Vangilder R, Fang J, Beattie DS. Expression of a familial amyotrophic lateral sclerosis-associated mutant human superoxide dismutase in yeast leads to decreased mitochondrial electron transport. Archives of biochemistry and biophysics. 2004;431(2):207-14.

187. Ferrante RJ, Browne SE, Shinobu LA, Bowling AC, Baik MJ, MacGarvey U, et al. Evidence of increased oxidative damage in both sporadic and familial amyotrophic lateral sclerosis. Journal of neurochemistry. 1997;69(5):2064-74.

188. Liu D, Wen J, Liu J, Li L. The roles of free radicals in amyotrophic lateral sclerosis: reactive oxygen species and elevated oxidation of protein, DNA, and membrane phospholipids. FASEB journal : official publication of the Federation of American Societies for Experimental Biology. 1999;13(15):2318-28.

189. Smith AG, Raven EL, Chernova T. The regulatory role of heme in neurons. Metallomics : integrated biometal science. 2011;3(10):955-62.

190. Zhou Y, Wang J, Liu L, Wang R, Lai X, Xu M. Interaction between amyloid-beta peptide and heme probed by electrochemistry and atomic force microscopy. ACS chemical neuroscience. 2013;4(4):535-9.

191. Zamiri B, Reddy K, Macgregor RB, Jr., Pearson CE. TMPyP4 porphyrin distorts RNA G-quadruplex structures of the disease-associated r(GGGGCC)n repeat of the C9orf72 gene and blocks interaction of RNA-binding proteins. The Journal of biological chemistry. 2014;289(8):4653-9.

192. Luedtke NW. Targeting G-Quadruplex DNA with Small Molecules. CHIMIA International Journal for Chemistry. 2009;63(3):134-9.

193. Bryan TM, Baumann P. G-quadruplexes: from guanine gels to chemotherapeutics. Molecular biotechnology. 2011;49(2):198-208.

194. Campbell NH, Neidle S. G-quadruplexes and metal ions. Metal ions in life sciences. 2012;10:119-34.

195. Kamiya H. Mutagenic potentials of damaged nucleic acids produced by reactive oxygen/nitrogen species: approaches using synthetic oligonucleotides and nucleotidesSURVEY AND SUMMARY. Nucleic Acids Research. 2003;31(2):517-31.

196. Chaput JC, Switzer C. A DNA pentaplex incorporating nucleobase quintets. Proc Natl Acad Sci U S A. 1999;96(19):10614-9.

197. Cai M, Marlow AL, Fettinger JC, Fabris D, Haverlock TJ, Moyer BA, et al. Binding Cesium Ions with Nucleosides: Templated Self-Assembly of Isoguanosine Pentamers This research was supported by the Separations and Analysis Program, Division of Chemical Sciences, Office of Basic Energy Sciences, U.S. Department of Energy. J.T.D. thanks the Dreyfus Foundation for a Teacher-Scholar Award. We thank Drs. Bryan Eichhorn, Steve Rokita, and Lyle Isaacs for advice. Angew Chem Int Ed Engl. 2000;39(7):1283-5.

198. Meyer M, Sühnel J. Self-Association of Isoguanine Nucleobases and Molecular Recognition of Alkaline Ions: Tetrad vs Pentad Structures. The Journal of Physical Chemistry A. 2003;107(7):1025-31.

199. Seela F. 7-Deazaisoguanine quartets: self-assembled oligonucleotides lacking the Hoogsteen motif. Chemical Communications. 1997(19):1869-70.

200. Seela F, Wei C, Melenewski A. Isoguanine quartets formed by d(T4isoG4T4): tetraplex identification and stability. Nucleic Acids Research. 1996;24(24):4940-5.

201. van Leeuwen FWB, Davis JT, Verboom W, Reinhoudt DN. Non-covalent (iso)guanosine-based ionophores for alkali(ne earth) cations. Inorganica Chimica Acta. 2006;359(6):1779-85.

202. Pierce SE, Wang J, Jayawickramarajah J, Hamilton AD, Brodbelt JS. Examination of the effect of the annealing cation on higher order structures containing guanine or isoguanine repeats. Chemistry. 2009;15(42):11244-55.

203. Saito K, Tai H, Hemmi H, Kobayashi N, Yamamoto Y. Interaction between the heme and a G-quartet in a heme-DNA complex. Inorg Chem. 2012;51(15):8168-76.

204. Seela F, Wei C, Melenewski A. Four-stranded DNA formed by isoguanine quartets: complex stoichiometry, thermal stability and resistance against exonucleases. Orig Life Evol Biosph. 1997;27(5-6):597-608.

205. Pavlov V, Xiao Y, Gill R, Dishon A, Kotler M, Willner I. Amplified chemiluminescence surface detection of DNA and telomerase activity using catalytic nucleic acid labels. Analytical chemistry. 2004;76(7):2152-6.

206. Xiao Y, Pavlov V, Gill R, Bourenko T, Willner I. Lighting up biochemiluminescence by the surface self-assembly of DNA-hemin complexes. Chembiochem : a European journal of chemical biology. 2004;5(3):374-9.

207. Niazov T, Pavlov V, Xiao Y, Gill R, Willner I. DNAzyme-Functionalized Au Nanoparticles for the Amplified Detection of DNA or Telomerase Activity. Nano Letters. 2004;4(9):1683-7.

208. Li T, Wang E, Dong S. Potassium−Lead-Switched G-Quadruplexes: A New Class of DNA Logic Gates. Journal of the American Chemical Society. 2009;131(42):15082-3.

209. Li T, Wang E, Dong S. Lead(II)-Induced Allosteric G-Quadruplex DNAzyme as a Colorimetric and Chemiluminescence Sensor for Highly Sensitive and Selective Pb2+ Detection. Analytical chemistry. 2010;82(4):1515-20.

210. Lu N, Shao C, Deng Z. Rational design of an optical adenosine sensor by conjugating a DNA aptamer with split DNAzyme halves. Chemical Communications. 2008(46):6161-3.

211. Elbaz J, Shlyahovsky B, Li D, Willner I. Parallel analysis of two analytes in solutions or on surfaces by using a bifunctional aptamer: applications for biosensing and logic gate operations. Chembiochem : a European journal of chemical biology. 2008;9(2):232-9.

212. Li D, Shlyahovsky B, Elbaz J, Willner I. Amplified Analysis of Low-Molecular-Weight Substrates or Proteins by the Self-Assembly of DNAzyme−Aptamer Conjugates. Journal of the American Chemical Society. 2007;129(18):5804-5.

213. Li T, Wang E, Dong S. G-quadruplex-based DNAzyme for facile colorimetric detection of thrombin. Chemical Communications. 2008(31):3654-6.

214. Li W, Liu Z, Lin H, Nie Z, Chen J, Xu X, et al. Label-Free Colorimetric Assay for Methyltransferase Activity Based on a Novel Methylation-Responsive DNAzyme Strategy. Analytical chemistry. 2010;82(5):1935-41.

215. Freeman R, Sharon E, Teller C, Henning A, Tzfati Y, Willner I. DNAzyme-like activity of hemin-telomeric G-quadruplexes for the optical analysis of telomerase and its inhibitors. Chembiochem : a European journal of chemical biology. 2010;11(17):2362-7.

216. Cotton ML, Dunford HB. Studies on Horseradish Peroxidase. XI. On the Nature of Compounds I and II as Determined from the Kinetics of the Oxidation of Ferrocyanide. Canadian Journal of Chemistry. 1973;51(4):582-7.

217. Goral VN, Ryabov AD. Reactivity of the horseradish peroxidase compounds I and II toward organometallic substrates. A stopped-flow kinetic study of oxidation of ferrocenes. IUBMB Life. 1998;45(1):61-71.

218. English AM, Tsaprailis G. Catalytic Structure–Function Relationships in Heme Peroxidases. Advances in Inorganic Chemistry. 1995;43:79-125.

219. Erman JE, Vitello LB, Mauro JM, Kraut J. Detection of an oxyferryl porphyrin pi-cation-radical intermediate in the reaction between hydrogen peroxide and a mutant yeast cytochrome c peroxidase. Evidence for tryptophan-191 involvement in the radical site of compound I. Biochemistry. 1989;28(20):7992-5.

220. Huyett JE, Doan PE, Gurbiel R, Houseman ALP, Sivaraja M, Goodin DB, et al. Compound ES of Cytochrome c Peroxidase Contains a Trp .pi.-Cation Radical: Characterization by Continuous Wave and Pulsed Q-Band External Nuclear Double Resonance Spectroscopy. Journal of the American Chemical Society. 1995;117(35):9033-41.

221. Gunther MR, Sturgeon BE, Mason RP. A long-lived tyrosyl radical from the reaction between horse metmyoglobin and hydrogen peroxide. Free radical biology & medicine. 2000;28(5):709-19.

222. Ivancich A, Jouve HM, Sartor B, Gaillard J. EPR investigation of compound I in Proteus mirabilis and bovine liver catalases: formation of porphyrin and tyrosyl radical intermediates. Biochemistry. 1997;36(31):9356-64.

223. Ivancich A, Mazza G, Desbois A. Comparative electron paramagnetic resonance study of radical intermediates in turnip peroxidase isozymes. Biochemistry. 2001;40(23):6860-6.

224. Dietz R, Nastainczyk W, Ruf HH. Higher oxidation states of prostaglandin H synthase. Rapid electronic spectroscopy detected two spectral intermediates during the peroxidase reaction with prostaglandin G2. European journal of biochemistry. 1988;171(1-2):321-8.

225. Dorlet P, Seibold SA, Babcock GT, Gerfen GJ, Smith WL, Tsai AL, et al. High-field EPR study of tyrosyl radicals in prostaglandin H(2) synthase-1. Biochemistry. 2002;41(19):6107-14.

226. Karthein R, Dietz R, Nastainczyk W, Ruf HH. Higher oxidation states of prostaglandin H synthase. EPR study of a transient tyrosyl radical in the enzyme during the peroxidase reaction. European journal of biochemistry. 1988;171(1-2):313-20.

227. Tsai A, Kulmacz RJ. Tyrosyl radicals in prostaglandin H synthase-1 and -2. Prostaglandins & other lipid mediators. 2000;62(3):231-54.

228. Tsai A, Wu G, Palmer G, Bambai B, Koehn JA, Marshall PJ, et al. Rapid kinetics of tyrosyl radical formation and heme redox state changes in prostaglandin H synthase-1 and -2. The Journal of biological chemistry. 1999;274(31):21695-700.

229. Chouchane S, Girotto S, Yu S, Magliozzo RS. Identification and characterization of tyrosyl radical formation in Mycobacterium tuberculosis catalase-peroxidase (KatG). The Journal of biological chemistry. 2002;277(45):42633-8.

230. Ivancich A, Jakopitsch C, Auer M, Un S, Obinger C. Protein-based radicals in the catalase-peroxidase of synechocystis PCC6803: a multifrequency EPR investigation of wild-type and variants on the environment of the heme active site. J Am Chem Soc. 2003;125(46):14093-102.

231. Singh R, Switala J, Loewen PC, Ivancich A. Two [Fe(IV)=O Trp*] intermediates in M. tuberculosis catalase-peroxidase discriminated by multifrequency (9-285 GHz) EPR spectroscopy: reactivity toward isoniazid. J Am Chem Soc. 2007;129(51):15954-63.

232. Miller VP, Goodin DB, Friedman AE, Hartmann C, Ortiz de Montellano PR. Horseradish peroxidase Phe172-->Tyr mutant. Sequential formation of compound I with a porphyrin radical cation and a protein radical. The Journal of biological chemistry. 1995;270(31):18413-9.

233. Goodin DB, Mauk AG, Smith M. Studies of the radical species in compound ES of cytochrome c peroxidase altered by site-directed mutagenesis. Proceedings of the National Academy of Sciences of the United States of America. 1986;83(5):1295-9.

234. Yang X, Fang C, Mei H, Chang T, Cao Z, Shangguan D. Characterization of G-Quadruplex/Hemin Peroxidase: Substrate Specificity and Inactivation Kinetics. Chemistry–A European Journal. 2011;17(51):14475-84.

235. Canale TD, Sen D. Hemin-utilizing G-quadruplex DNAzymes are strongly active in organic co-solvents. Biochim Biophys Acta. 2016.

236. Henry E, Hofrichter J. [8] Singular value decomposition: Application to analysis of experimental data. Methods in enzymology. 1992;210:129-92.

237. Maeder M, Zuberbuehler AD. Nonlinear least-squares fitting of multivariate absorption data. Analytical chemistry. 1990;62(20):2220-4.

238. Kanzow C, Fukushima M, Yamashita N. Levenberg-Marquardt methods for constrained nonlinear equations with strong local convergence properties: Inst. of Applied Math. and Statistics; 2002.

239. Grigg JC, Shumayrikh N, Sen D. G-quadruplex structures formed by expanded hexanucleotide repeat RNA and DNA from the neurodegenerative disease-linked C9orf72 gene efficiently sequester and activate heme. PLoS One. 2014;9(9):e106449.

240. BRITTAIN T, BAKER AR, BUTLER CS, LITTLE RH, GREENWOOD C, WATMOUGH NJ. Reaction of variant sperm-whale myoglobins with hydrogen peroxide: the effects of mutating a histidine residue in the haem distal pocket. Biochemical Journal. 1997;326(1):109-15.

241. Catalano CE, Choe YS, de Montellano PO. Reactions of the protein radical in peroxide-treated myoglobin. Formation of a heme-protein cross-link. Journal of Biological Chemistry. 1989;264(18):10534-41.

242. He K, Bornheim LM, Falick AM, Maltby D, Yin H, Correia MA. Identification of the heme-modified peptides from cumene hydroperoxide-inactivated cytochrome P450 3A4. Biochemistry. 1998;37(50):17448-57.

243. HINER AN, RODRÍGUEZ-LÓPEZ JN, ARNAO MB, RAVEN EL, GARCÍA-CÁNOVAS F, ACOSTA M. Kinetic study of the inactivation of ascorbate peroxidase by hydrogen peroxide. Biochemical Journal. 2000;348(2):321-8.

244. LAMBEIR AM, DUNFORD HB. Oxygen binding to dithionite-reduced chloroperoxidase. European journal of biochemistry. 1985;147(1):93-6.

245. Nagababu E, Rifkind JM. Heme degradation during autoxidation of oxyhemoglobin. Biochemical and biophysical research communications. 2000;273(3):839-45.

246. Nakajima R, Yamazaki I. The conversion of horseradish peroxidase C to a verdohemoprotein by a hydroperoxide derived enzymatically from indole-3-acetic acid and by m-nitroperoxybenzoic acid. Journal of Biological Chemistry. 1980;255(5):2067-71.

247. Spector A, Zhou W, Ma W, Chignell CF, Reszka KJ. Investigation of the mechanism of action of microperoxidase-11,(MP11), a potential anti-cataract agent, with hydrogen peroxide and ascorbate. Experimental eye research. 2000;71(2):183-94.

248. Wilks A, de Montellano PO. Rat liver heme oxygenase. High level expression of a truncated soluble form and nature of the meso-hydroxylating species. Journal of Biological Chemistry. 1993;268(30):22357-62.

249. Adediran S. Kinetics of the formation of p-670 and of the decay of compound III of horseradish peroxidase. Archives of biochemistry and biophysics. 1996;327(2):279-84.

250. ADEDIRAN SA, LAMBEIR AM. Kinetics of the reaction of compound II of horseradish peroxidase with hydrogen peroxide to form compound III. The FEBS journal. 1989;186(3):571-6.

251. Schonbaum GR, Lo S. Interaction of peroxidases with aromatic peracids and alkyl peroxides product analysis. Journal of Biological Chemistry. 1972;247(10):3353-60.

252. Davies DM, Jones P, Mantle D. The kinetics of formation of horseradish peroxidase compound I by reaction with peroxobenzoic acids. pH and peroxo acid substituent effects. Biochemical Journal. 1976;157(1):247-53.

253. Wu S, Lin J, Chan SI. Oxidation of dibenzothiophene catalyzed by heme-containing enzymes encapsulated in sol-gel glass. Applied biochemistry and biotechnology. 1994;47(1):11-20.

254. Stachyra T, Guillochom D, Pulvin S, Thomas D. Hemoglobin, horseradish peroxidase, and heme-bovine serum albumin as biocatalyst for the oxidation of dibenzothiophene. Applied biochemistry and biotechnology. 1996;59(3):231-43.

255. Vazquez-Duhalt R, Westlake DW, Fedorak PM. Lignin peroxidase oxidation of aromatic compounds in systems containing organic solvents. Applied and environmental microbiology. 1994;60(2):459-66.

256. Mondelli R, Scaglioni L, Mazzini S, Bolis G, Ranghino G. 3D structure of microperoxidase-11 by NMR and molecular dynamic studies. Magnetic Resonance in Chemistry. 2000;38(4):229-40.

257. da Silva Madeira L, Ferreira-Leitão VS, da Silva Bon EP. Dibenzothiophene oxidation by horseradish peroxidase in organic media: effect of the DBT: H 2 O 2 molar ratio and H 2 O 2 addition mode. Chemosphere. 2008;71(1):189-94.

258. Rodriguez-Lopez JN, Hernandez-Ruiz J, Garcia-Canovas F, Thorneley RN, Acosta M, Arnao MB. The inactivation and catalytic pathways of horseradish peroxidase with m-chloroperoxybenzoic acid. A spectrophotometric and transient kinetic study. The Journal of biological chemistry. 1997;272(9):5469-76.

259. Arnao M, Acosta M, Del Rio J, Varon R, Garcia-Canovas F. A kinetic study on the suicide inactivation of peroxidase by hydrogen peroxide. Biochimica et Biophysica Acta (BBA)-Protein Structure and Molecular Enzymology. 1990;1041(1):43-7.

260. Valderrama B, Vazquez-Duhalt R. Electron-balance during the oxidative self-inactivation of cytochrome c. Journal of Molecular Catalysis B: Enzymatic. 2005;35(1):41-4.

261. Martins D, Bakas I, McIntosh K, English AM. Peroxynitrite and hydrogen peroxide elicit similar cellular stress responses mediated by the Ccp1 sensor protein. Free Radical Biology and Medicine. 2015;85:138-47.

262. Gumiero A, Metcalfe CL, Pearson AR, Raven EL, Moody PC. Nature of the ferryl heme in compounds I and II. Journal of Biological Chemistry. 2011;286(2):1260-8.

263. Svistunenko DA. An EPR study of the peroxyl radicals induced by hydrogen peroxide in the haem proteins. Biochimica et Biophysica Acta (BBA)-Protein Structure and Molecular Enzymology. 2001;1546(2):365-78.

264. Fleming AM, Burrows CJ. G-quadruplex folds of the human telomere sequence alter the site reactivity and reaction pathway of guanine oxidation compared to duplex DNA. Chemical research in toxicology. 2013;26(4):593-607.

265. Clore GM, Hollaway MR, Orengo C, Peterson J, Wilson MT. The kinetics of the reactions of low spin ferric haem undecapeptide with hydrogen peroxide. Inorganica Chimica Acta. 1981;56:143-8.

266. Adams PA. The peroxidasic activity of the haem octapeptide microperoxidase-8 (MP-8): the kinetic mechanism of the catalytic reduction of H 2 O 2 by MP-8 using 2, 2′-azinobis-(3-ethylbenzothiazoline-6-sulphonate)(ABTS) as reducing substrate. Journal of the Chemical Society, Perkin Transactions 2. 1990(8):1407-14.

267. Cunningham ID, Snare GR. Identification of catalytic pathways in the peroxidatic reactions of the haem octapeptide microperoxidase-8. Journal of the Chemical Society, Perkin Transactions 2. 1992(11):2019-23.

268. Yeh H-C, Wang J-S, Su OY, Lin W-Y. Stopped-flow kinetic study of the H 2 O 2 oxidation of substrates catalyzed by microperoxidase-8. Journal of Biological Inorganic Chemistry. 2001;6(8):770-7.

269. Ohlsson P, Yonetani T, Wold S. The formation of ES of cytochrome-c peroxidase: a comparison with lactoperoxidase and horseradish peroxidase. Biochimica et Biophysica Acta (BBA)-Protein Structure and Molecular Enzymology. 1986;874(2):160-6.

270. Loo S, Erman JE. Kinetic study of the reaction between cytochrome c peroxidase and hydrogen peroxide. Dependence on pH and ionic strength. Biochemistry. 1975;14(15):3467-70.

271. Nicholls P, Mochan E. Complex-formation between cytochrome c and cytochrome c peroxidase. Kinetic studies. Biochemical Journal. 1971;121(1):55-67.

272. Allentoff AJ, Bolton JL, Wilks A, Thompson JA, Ortiz de Montellano PR. Heterolytic versus homolytic peroxide bond cleavage by sperm whale myoglobin and myoglobin mutants. Journal of the American Chemical Society. 1992;114(25):9744-9.

273. Schünemann V, Jung C, Trautwein A, Mandon D, Weiss R. Intermediates in the reaction of substrate-free cytochrome P450cam with peroxy acetic acid. FEBS letters. 2000;479(3):149-54.

274. Schünemann V, Jung C, Terner J, Trautwein A, Weiss R. Spectroscopic studies of peroxyacetic acid reaction intermediates of cytochrome P450cam and chloroperoxidase. Journal of inorganic biochemistry. 2002;91(4):586-96.

275. Schünemann V, Lendzian F, Jung C, Contzen J, Barra A-L, Sligar SG, et al. Tyrosine radical formation in the reaction of wild type and mutant cytochrome P450cam with peroxy acids A multifrequency EPR study of intermediates on the millisecond time scale. Journal of Biological Chemistry. 2004;279(12):10919-30.

276. Jung C, Schünemann V, Lendzian F. Freeze-quenched iron-oxo intermediates in cytochromes P450. Biochemical and biophysical research communications. 2005;338(1):355-64.

277. Jung C, Schünemann V, Lendzian F, Trautwein AX, Contzen J, Galander M, et al. Spectroscopic characterization of the iron-oxo intermediate in cytochrome P450. Biological chemistry. 2005;386(10):1043-53.

278. Kellner DG, Hung S-C, Weiss KE, Sligar SG. Kinetic characterization of compound I formation in the thermostable cytochrome P450 CYP119. Journal of Biological Chemistry. 2002;277(12):9641-4.

279. Rittle J, Green MT. Cytochrome P450 Compound I: Capture, Characterization, and C-H Bond Activation Kinetics. Science (New York, NY). 2010;330(6006):933-7.

280. Raner GM, Thompson JI, Haddy A, Tangham V, Bynum N, Reddy GR, et al. Spectroscopic investigations of intermediates in the reaction of cytochrome P450 BM3–F87G with surrogate oxygen atom donors. Journal of inorganic biochemistry. 2006;100(12):2045-53.

281. Spolitak T, Dawson JH, Ballou DP. Replacement of tyrosine residues by phenylalanine in cytochrome P450cam alters the formation of Cpd II-like species in reactions with artificial oxidants. JBIC Journal of Biological Inorganic Chemistry. 2008;13(4):599-611.

282. Witting PK, Travascio P, Sen D, Mauk AG. A DNA Oligonucleotide−Hemin Complex Cleaves t-Butyl Hydroperoxide through a Homolytic Mechanism. Inorganic Chemistry. 2001;40(19):5017-23.

283. Nam W, Han HJ, Oh S-Y, Lee YJ, Choi M-H, Han S-Y, et al. New Insights into the mechanisms of O− O bond cleavage of hydrogen peroxide and tert-alkyl hydroperoxides by iron (III) porphyrin complexes. Journal of the American Chemical Society. 2000;122(36):8677-84.

284. Zucca P, Rescigno A, Rinaldi AC, Sanjust E. Biomimetic metalloporphines and metalloporphyrins as potential tools for delignification: Molecular mechanisms and application perspectives. Journal of Molecular Catalysis A: Chemical. 2014;388:2-34.

285. Chouchane S, Lippai I, Magliozzo RS. Catalase-peroxidase (Mycobacterium tuberculosis KatG) catalysis and isoniazid activation. Biochemistry. 2000;39(32):9975-83.

286. Keilin D, Mann T. On the haematin compound of peroxidase. Proceedings of the Royal Society of London Series B, Biological Sciences. 1937;122(827):119-33.

287. Villegas JA, Mauk AG, Vazquez-Duhalt R. A cytochrome c variant resistant to heme degradation by hydrogen peroxide. Chemistry & biology. 2000;7(4):237-44.

288. Barr DP, Mason RP. Mechanism of radical production from the reaction of cytochrome c with organic hydroperoxides. An ESR spin trapping investigation. Journal of Biological Chemistry. 1995;270(21):12709-16.

289. Peisach J, Blumberg W, Wittenberg BA, Wittenberg JB. The electronic structure of protoheme proteins III. Configuration of the heme and its ligands. Journal of Biological Chemistry. 1968;243(8):1871-80.

290. Wariishi H, Gold MH. Lignin peroxidase compound III. Mechanism of formation and decomposition. Journal of Biological Chemistry. 1990;265(4):2070-7.

291. Lardinois OM. Reactions of bovine liver catalase with superoxide radicals and hydrogen peroxide. Free radical research. 1995;22(3):251-74.

292. Wariishi H, Akileswaran L, Gold MH. Manganese peroxidase from the basidiomycete Phanerochaete chrysosporium: spectral characterization of the oxidized states and the catalytic cycle. Biochemistry. 1988;27(14):5365-70.

293. Valderrama B. Deactivation of hemeperoxidases by hydrogen peroxide: focus on Compound III. Biocatalysis Based on Heme Peroxidases: Springer; 2010. p. 291-314.

294. Sivaraja M, Goodin DB, Smith M, Hoffman BM. Identifaction by ENDOR of Trp191 as the Free-Radical Site in Cytochrome c Peroxidase Compound ES. Science (New York, NY). 1989;245(4919):738.

295. Roe JA, Goodin DB. Enhanced oxidation of aniline derivatives by two mutants of cytochrome c peroxidase at tryptophan 51. Journal of Biological Chemistry. 1993;268(27):20037-45.

296. Hori H, Yonetani T. Powder and single-crystal electron paramagnetic resonance studies of yeast cytochrome c peroxidase and its peroxide and its peroxide compound, Compound ES. Journal of Biological Chemistry. 1985;260(1):349-55.

297. Pond AE, Bruce GS, English AM, Sono M, Dawson JH. Spectroscopic study of the compound ES and the oxoferryl compound II states of cytochrome c peroxidase: Comparison with the compound II of horseradish peroxidase. Inorganica chimica acta. 1998;275:250-5.

298. Erman JE, Vitello LB. Yeast cytochrome c peroxidase: mechanistic studies via protein engineering. Biochimica Et Biophysica Acta (BBA)-Protein Structure and Molecular Enzymology. 2002;1597(2):193-220.

299. Vitello LB, Erman JE, Mauro JM, Kraut J. Characterization of the hydrogen peroxide-enzyme reaction for two cytochrome c peroxidase mutants. Biochimica et Biophysica Acta (BBA)-Protein Structure and Molecular Enzymology. 1990;1038(1):90-7.

300. Neidle S. Principles of nucleic acid structure: Academic Press; 2010.

301. Leung EK, Sen D. The use of charge flow and quenching (CFQ) to probe nucleic acid folds and folding. Methods. 2010;52(2):141-9.

302. Huang YC, Cheng AK, Yu H-Z, Sen D. Charge conduction properties of a parallel-stranded DNA G-quadruplex: Implications for chromosomal oxidative damage. Biochemistry. 2009;48(29):6794-804.

303. Huang YC, Sen D. A contractile electronic switch made of DNA. Journal of the American Chemical Society. 2010;132(8):2663-71.

304. Huang YC, Sen D. A twisting electronic nanoswitch made of DNA. Angewandte Chemie. 2014;126(51):14279-83.

305. Zhou J, Fleming AM, Averill AM, Burrows CJ, Wallace SS. The NEIL glycosylases remove oxidized guanine lesions from telomeric and promoter quadruplex DNA structures. Nucleic acids research. 2015:gkv252.

306. Miller VP, DePillis G, Ferrer J, Mauk AG, De Montellano PO. Monooxygenase activity of cytochrome c peroxidase. Journal of Biological Chemistry. 1992;267(13):8936-42.

307. Choe YS, Rao SI, Demontellano PO. Requirement of a second oxidation equivalent for ferryl oxygen transfer to styrene in the epoxidation catalyzed by myoglobin-H2O2. Archives of biochemistry and biophysics. 1994;314(1):126-31.

308. Einarson OJ, Sen D. Self-biotinylation of DNA G-quadruplexes via intrinsic peroxidase activity. Nucleic Acids Research. 2017;45(17):9813-22.